

FAST ORBIT FEEDBACK FOR DIAMOND-II

I. Kempf*, M. Abbott, L. Bobb, G. B. Christian, Diamond Light Source, Oxfordshire, UK
G. Rehm, Helmholtz-Zentrum für Materialien und Energie, Berlin, Germany
S. Duncan, University of Oxford, Oxford, UK

Abstract

The electron beam stability is critical for 4th generation light sources. As opposed to 10 % of beam size up to 140 Hz at Diamond, advances in detector speed and resolution at Diamond-II increase the stability requirements to 3 % up to 1 kHz. This paper presents a novel control methodology for the fast orbit feedback at Diamond-II, which will stabilise the beam using two arrays of 252 slow and 144 fast correctors and 252 beam position monitors at 100 kHz. In contrast to existing approaches that separate slow and fast feedback loops, our approach is based on a two-matrix factorisation called the generalised singular value decomposition (GSVD), which decouples the system into 144 two-input modes controlled by slow and fast magnets and 108 modes controlled by slow magnets only. The GSVD-based controller is implemented in the existing Diamond storage ring using a centralised communication architecture, such as planned for Diamond-II. We present results from the Diamond storage ring and simulation, which confirm that the proposed approach meets the target specification for Diamond-II.

INTRODUCTION

The fast orbit feedback (FOFB) at Diamond Light Source (Diamond) attenuates disturbances of the electron beam in the storage ring. Disturbance sources include ground and girder vibrations, power supply and RF noise, and transients induced by insertion device (ID) gap changes. At Diamond, the FOFB uses 173 electron beam position monitors (BPMs) measuring both horizontal and vertical positions, and 172 vertical and 172 horizontal correctors to perform global orbit correction of the electron beam at 10 kHz. The FOFB reduces the root-mean square (RMS) deviation of the electron beam to within 10 % of the beam size up to a closed-loop bandwidth of 140 Hz, i.e. the frequency at which disturbances are attenuated by 3 dB. For Diamond-II, advances in beamline technology require the closed-loop bandwidth to be increased to 1 kHz, while the new multi-bend achromat lattice will reduce the beam size [1], resulting in the increased beam stability requirements summarised in Table 1 (top).

To meet these requirements, the FOFB hardware and software for Diamond-II have been redesigned, increasing the specifications as shown in Table 1 (bottom). Firstly, the sampling frequency is increased to 100 kHz and the overall latency reduced to 100 μ s. Secondly, the number of BPMs

Table 1: Top: Beam size, relative and absolute orbit stability requirements at standard straight source points. Bottom: FOFB specifications. Tables adapted from Ref. [1].

Parameter	Diamond	Diamond-II
Beam size H/V	123 μ m/3.5 μ m	30 μ m/4 μ m
Rel. stability	10 % up to 100 Hz	3 % up to 1 kHz
Abs. stability H/V	12 μ m/0.35 μ m	0.9 μ m/0.12 μ m
Closed-loop BW	140 Hz	\geq 1 kHz
Latency	700 μ s	\leq 100 μ s
BPMs	173	252
Correctors	172	252 slow/144 fast

H: horizontal, V: vertical, BW: bandwidth

is increased to 252. Finally, to achieve the 1 kHz closed-loop bandwidth, the open-loop bandwidth, i.e. the overall corrector bandwidth, is increased from 500 Hz to \geq 5 kHz by introducing two types of correctors: 252 slow correctors producing a deflection of 1 mrad, and 144 fast correctors producing a deflection of 20 μ rad [1].

While using two types of correctors allows the closed-loop bandwidth to be increased, it prohibits the existing FOFB control algorithm to be reused, which is based on diagonalising the dynamics using the modal decomposition and controlling the single-input single-output (SISO) modal dynamics. Although extensions of modal decomposition have been proposed in [2, 3], they leave the decoupling process unspecified for systems with fewer fast than slow correctors. For Diamond-II, we propose a joint design method based on the generalised singular value decomposition (GSVD) [4] to decouple the system into sets of two-input single-output (TISO) and SISO systems. It can be shown that the generalised modal decomposition of a system with two corrector types is closely related to the modal decomposition of a system with one corrector type, which allows techniques to be carried over to the system with two corrector types, including regularisation gains that account for a large condition number of the orbit response matrix (ORM).

Based on the assumption that the bandwidths of the slow and fast correctors differ significantly, other approaches split the control problem into two separate feedback loops: one feedback loop for the slow correctors that may be operated at a lower sampling/actuation frequency, and a separate feedback loop for the fast correctors. Such a separation is implemented in most synchrotrons that use separate sets of slow and fast correctors [5–7], but interactions at intermediate frequencies can require the introduction of a frequency deadband between the slow and fast loops [8]. Depending on the disturbance spectrum, this approach can lead to significant performance degradation [6]. One common way

* Corresponding author: idris.kempf@eng.ox.ac.uk. Also at University of Oxford. This work was supported in part by Diamond Light Source and in part by the Engineering and Physical Sciences Research Council (EPSRC) with a Collaborative Awards in Science and Engineering (CASE) studentship.

COUPLED BUNCH MODE ZERO CORRECTION WITHIN THE ORBIT FEEDBACK BANDWIDTH *

P. Kallakuri[†], A. Brill, J. Carwardine, L. Emery and N. Sereno
Argonne National Lab, Lemont, USA

Abstract

The fast orbit feedback (FOFB) bandwidth for Advanced photon source upgrade (APS-U) will be DC-1 kHz and the synchrotron frequency will be between 100-560 Hz. This frequency overlap places coupled bunch mode 0 (CBM0) induced horizontal orbit motion inside the orbit feedback bandwidth, potentially affecting our ability to achieve beam stability goals. Longitudinal feedback kicker is not strong enough to damp CBM0 oscillations. We developed new beam-based feedback method to suppress CBM0 oscillations with low level RF phase as actuator. It uses existent FOFB framework with no changes to the feedback algorithm. Effectiveness of this method is verified using present APS operations lattice where synchrotron frequency is outside orbit feedback bandwidth. In the present work, low alpha lattice is created to emulate APS-U setting where synchrotron frequency is inside the orbit feedback bandwidth. Experiments with this lattice successfully demonstrated CBM0 correction within orbit feedback bandwidth. Combined operation of orbit feedback and CBM0 correction is stable, and CBM0 oscillations are damped. We achieved better orbit motion suppression and corrector drive efforts are reduced as well.

INTRODUCTION

The target bandwidth of the Advanced Photon Source Upgrade (APS-U) Fast Orbit Feedback (FOFB) is DC-1000 Hz where the synchrotron tune will be between 100-560 Hz. This overlap places Coupled Bunch Mode 0 (CBM0) induced horizontal position offsets within the FOFB bandwidth range, affecting APS-U goals for beam stability. Large storage-rings such as APS would need longitudinal feedback system with high kick voltage capability for CBM0 suppression. APS-U longitudinal feedback kicker is not strong enough to damp CBM0 oscillations. We developed new orbit to RF phase feedback method using existent orbit feedback framework with no additional processing hardware requirements [1]. It operates at the Low Level RF (LLRF) signal level of the main RF system and does not require high kick voltages. Based on synchrotron oscillation theory [2,3], we derived relationship between beam position deviation at dispersive BPMs and RF phase noise that represents the open loop dynamics of our feedback configuration. An analytical model is devised for the coupling mechanism of synchrotron oscillations to transverse orbit through dispersion. It allows an energy-induced component to be extracted

from the measured orbit which is derivative of the RF phase error. Using this the orbit feedback controller generates a RF phase control signal as another drive signal in the orbit feedback algorithm. Experiments conducted at the present APS storage ring using 7 GeV operations lattice and APS-U prototype fast orbit feedback controller [4,5] demonstrated the effectiveness of this method at damping coupled bunch mode zero oscillations.

In the above experiments [1] the synchrotron frequency (2.2 kHz) and orbit feedback bandwidth (920 Hz) are well separated. We continued our study using low-alpha lattice configuration developed to mimic APS-U setting where, synchrotron frequency (60 Hz) is within the orbit feedback bandwidth (90 Hz). We would be able to study the interaction of both feedbacks more clearly in this setup. The storage-ring energy is set to 6 GeV and low momentum compaction factor of $3.6 \cdot 10^{-6}$ is used to get synchrotron frequency to around 60 Hz. Orbit feedback with 1.5 kHz sampling rate used for APS operations is termed as Real Time Feedback (RTFB) [6]. Experiments with low-alpha lattice are conducted using RTFB system so that we would be able to use 38 fast correctors and 154 BPMs around the ring. With the prototype system we could only use 3 fast correctors and 12 BPMs in 2 sectors that is not adequate to deal with larger noise seen in low-alpha lattice. Details of our experimental setup with RTFB controller, closed loop performance of orbit to RF phase feedback, and results from the simultaneous operation of RTFB and CBM0 correction with low alpha lattice are presented in next sections.

EXPERIMENTAL SETUP

Closed loop schematic of RTFB together with orbit to RF phase feedback is shown in Figure 1. RTFB controller hardware only allows use of total 160 BPMs (4 per sector) for orbit feedback computations. We used 154 BPMs for beam position measurements. Orbit feedback uses 38 horizontal fast correctors, and orbit to RF phase feedback is integrated into RTFB framework by repurposing fast corrector (S40A:H3) analog drive signal as phase drive. DAC output channel of S40A:H3 is connected to LLRF system [7] phase input. The cavity phase loop bandwidth is adequately greater than the synchrotron oscillation frequency. So the RF system is considered as simple gain term in the feedback model. PID_rtfb controller is used orbit correction and PID_rfPh controller is used for CBM0 correction. Same feedback algorithm that generates corrector power supply set-points is used for phase drive. Phase computations are incorporated as additional row in Inverse Response Matrix (IRM) dot product. Horizontal BPM position vector \mathbf{x} is

* Work supported by the U.S. Department of Energy, Office of Science, under Contract No. DE-ACO2-O6CH11357.

[†] pkallakuri@anl.gov

SOLEIL NEW PLATFORM FOR FAST ORBIT FEEDBACK

R. Bronès[†], A. Bence, J. Bisou, N. Hubert, D. Pédeau, G. Pichon
 Synchrotron SOLEIL, Gif-sur-Yvette, France

Abstract

SOLEIL is upgrading its Fast Orbit Feedback platform to withstand coming obsolescence of electronic BPM and future evolutions of the machine. This new platform has to be compatible with current boundary devices such as BPM electronics or corrector power supplies, but it also shall evolve to interface future versions of these systems. A MTCA based platform was designed and installed. It is integrated in the control system by mean of a OPCUA server, and care has been taken to seamlessly toggle the closing of the feedback loop on the former or new FOFB platform. This paper will present the first tests and results conducted to commission this new system.

CONTEXT AND SPECIFICATIONS

SOLEIL is working on upgrading its accelerators to the fourth generation of synchrotron. SOLEIL II will bring outstanding performances, with a new beam lattice, renewed systems and cutting-edge technics. As presented in [1], the renewal of BPM electronics will be conducted prior to the long shutdown and machine upgrade. The current Fast Orbit FeedBack (FOFB) system, which is strongly embedded in these electronics, is to be ported on a new platform.

The evolution of the FOFB spreads on several years and must follow the numerous modifications and improvements that will bring SOLEIL II. The roadmap for this system can be summarized in Table 1, while evolutions of key points are underlined in Table 2.

Table 1: FOFB Roadmap

	Evolution	Impact
2024	FOFB running on new platform	Same performances
2025	Added features	Faster lattice identification.
2026	New BPM electronics	Loop latency reduced, data rate increased, correction bandwidth increased
2028	SOLEIL II, new PSC	Loop latency reduction, dimension reduction, SOLEIL II performances
2028 +	New correction algorithm	Increased performances

Table 2: FOFB Performances Evolution

	Actual FOFB	Future FOFB
# BPM	122	180~200
# Corrector	50 H & V	44~60 H & V
Data rate	10 kHz	100 kHz
Correction BW	200 Hz	1 kHz
Loop Latency	350 μ s	100 μ s
Stability	10 % of beam size 20 μ m H ; 0.8 μ m V	2-3% of beam size 50 nm H & V

[†] romain.brones@synchrotron-soleil.fr

FOFB NEW PLATFORM INSTALLATION

A versatile platform was elaborated and is presented in [1]. We will detail last additions and comment on the installations.

Hardware Platform

The basis of the platform is a MTCA chassis, equipped with a SOC-FPGA board that host a SFP-FMC. The overall system is composed of five of these chassis, connected in a star topology. For denomination: a Central Node connected to four Cell Nodes. Communication between these nodes is a simple custom packet protocol, encapsulated in Ethernet frames and transported over optical fibers at 10 Gbps. This network was installed in the first months of 2023. Three full duplex fiber pairs are layed between Central and Cell Nodes, with one used and two as spare links.

The Cell Nodes are installed near BPM electronics in four different cells. For now they are connected as data spy to the running communication ring transporting the position data. After the upgrade of the BPM electronics, each Cell Node will be connected directly to a subset of them. Position data are grabbed, before being packeted and forwarded to the Central Node.

Correction packets are received back and transmitted to Power Supply Controller (PSC). A 1.25 Mbps RS422 UART link connects a Cell Node to each PSC. This limits the link length to 80 m and great care has been taken to position the Cell Nodes, each one serving PSCs in its own cell cabinet and to three neighbour cells. Current PSC can only receive command from one driver. We selected and installed very simple RJ45-CAT6 cables, each one transporting 4 differential pairs. To ease commutation from actual drivers (BPM electronics) to Cell Nodes, electromechanical relays were temporarily installed to toggle the differential lines from one driver to the other. Each relay can toggle 2 differential pairs. All relays are powered from a central location, activated by a single switch lever. Switched off relays connect the PSC to the BPM electronics. For the new platform tests, we simply have to toggle the lever to switch on all relays and connect PSC to the Cell Nodes. This feature was well received and shortened greatly the set-up times for dedicated machine shifts. Ultimately, relays will be removed.

To provide the RS422 UART commands to each PSC, Cell Nodes are equipped with a custom made RTM board named CACTUS. These very simple boards receive LVCMOS single-ended signals from the AMC FPGA and translate it to RS422 pairs, transported to RJ45 outlets, allowing us to put eight outlets on the RTM, hence providing signals to eight groups of four PSCs. Except from the MTCA management, no other functionality is

DEVELOPMENT OF THE SLS 2.0 BPM SYSTEM

B. Keil, R. Ditter, F. Marcellini, G. Marinkovic, J. Purtschert, M. Rizzi,
 M. Roggli, D. Stephan, X. Wang, Paul Scherrer Institut, Villigen, Switzerland

Abstract

After more than 20 years of operation, the storage ring of the Swiss Light Source (SLS) will be replaced. The new ring called SLS 2.0 will have 40 times higher brilliance, thanks to an innovative low-emittance magnet lattice and a beam pipe with smaller aperture. For SLS 2.0, the ageing SLS RF beam position monitor (BPM) electronics will be incrementally replaced for the whole accelerator, including linac, booster, transfer lines and storage ring. This contribution presents the development status and latest prototype test results of the SLS 2.0 BPM system, including pickups, mechanics, and electronics.

INTRODUCTION

Machine and Beam Parameters

Table 1 shows the parameters of the SLS 2.0 [1] compared to the present SLS (“1.0”) ring. The nominal beam energy for user operation will be slightly increased from 2.4 GeV to 2.7 GeV, which is already supported by the SLS 1.0 full energy booster synchrotron that is re-used for SLS 2.0, as well as the linac and linac-to-booster transfer line. The booster-to-ring transfer lines will be modified, including a new magnet lattice and additional BPMs for improved control of the more critical injection process.

Table 1: SLS Storage Ring Beam Parameters

Parameter	Units	SLS 1.0	SLS 2.0
Circumference	m	288	
Beam Current	mA	400	
Injection Charge	nC	~0.15	
Beam Energy	GeV	2.4	2.7
Main RF	MHz	499.637	499.654
Harmonic No.	#	480	
Hor. Emittance	pm	5030	131-158
Vert. Emittance	pm	5-10	10
Ring BPMs	#	75	136

BPM REQUIREMENTS AND TYPES

Table 2 shows the BPM requirements for the SLS 2.0 storage ring, with an expected minimal beam size of $\sigma \geq 5 \mu\text{m}$ at the BPMs, where $<0.05 \mu\text{m}$ desired electronics RMS noise from 0.1 Hz to 1 kHz translates to 1% of this beam size. Like SLS 1.0, SLS 2.0 will operate in top-up injection mode at 400 mA with typ. 2-3 mA (max. 4 mA) periodic current variation within a few minutes. 430-460 of 480 successive RF buckets are typically filled with approximately the same charge, with ~10% charge variation between buckets, excluding an optional so-called “cam-shaft” bunch in the bunch gap with ~3-5 times higher charge. For the linac, booster and transfer lines operated with single

bunches of ~0.15 nC at 3 Hz injection rate, the position resolution requirement is also $<50 \mu\text{m}$, aiming at $<10 \mu\text{m}/\text{week}$ long-term drift of the averaged position readings in the booster-to-ring transfer line for negligible variations of bunch charge transfer efficiency to the ring.

Table 2: SLS 2.0 Storage Ring BPM Position Measurement Requirements

Parameter	Goal
RMS Noise, 0.1 Hz-1 kHz, 400 mA	0.05 μm
RMS Noise, 0.1 Hz-0.5 MHz, 400 mA	1 μm
RMS Noise, 1 Bunch, 0.15 nC	50 μm
Electronics Drift (400 mA Top-Up)	0.1 $\mu\text{m}/\text{h}$ 0.4 $\mu\text{m}/\text{week}$ 1 $\mu\text{m}/\text{year}$
Overall Drift (incl. Cables/Mechan.)	0.25 $\mu\text{m}/\text{h}$ 1 $\mu\text{m}/\text{week}$ 2.5 $\mu\text{m}/\text{year}$
Beam Current Dependence	0.02 $\mu\text{m}/\text{mA}$

Table 3: SLS 1.0 / 2.0 BPM Types

Location	Type	geom. factors kx/ky [mm]
Linac & Transfer Lines	Resonant Stripline	various
Booster	Button	8.3/7.7
SLS 1.0 Ring	Button	16.7/14.3
SLS 2.0 Ring	Button	7.1/7.2

Table 3 shows a list of BPM types used in SLS. Booster and storage ring have button BPMs with four diagonal electrodes. Linac and transfer lines have so-called resonant stripline BPMs, generating a decaying 500 MHz sine signal which can be processed by the normal storage ring BPM electronics also working at 500 MHz. The beam position is calculated by the BPM electronics from the button/stripline signal voltage amplitudes A, B, C and D (upper outer, upper inner, lower inner and lower outer button/stripline) for the horizontal (X) and vertical (Y) plane with the common approximation formulas

$$X = k_x * (A-B-C+D)/(A+B+C+D)$$

$$Y = k_y * (A+B-C-D)/(A+B+C+D)$$

Storage Ring Beam Pipe

Figure 1 shows the cross section of the SLS 1.0 storage ring beam pipe in blue and the smaller SLS 2.0 pipe in orange. The latter has an octagonal shape, usually with 18 mm aperture. While the SLS 1.0 pipe is made of stainless steel, SLS 2.0 uses a NEG-coated copper pipe. However, at the BPMs and their adjacent horizontal and vertical orbit corrector dipole magnets, the pipe is made of stainless

A MTCA BASED BPM-SYSTEM FOR PETRA IV

G. Kube, H.-T. Duhme, J. Lamaack, F. Schmidt-Föhre, K. Wittenburg
Deutsches Elektronen-Synchrotron DESY, Germany

A. Bardorfer, L. Bogataj, M. Cargnelutti, P. Leban, M. Oblak, P. Paglovec, B. Repič
I-Tech, Solkan, Slovenia

Abstract

The PETRA IV project at DESY aims to upgrade the present PETRA III synchrotron into an ultra low-emittance source. The small emittances translate directly into much smaller beam sizes, thus imposing stringent requirements on the machine stability. In order to measure beam positions and control orbit stability to the level of 10% of beam size and divergence, a high resolution BPM system will be installed which consists of 788 individual monitors with the readout electronics based on MTCA.4. In order to fulfil the long-term drift requirement ($< 1 \mu\text{m}$ over 7 days), several analog, digital and SW parts were taken from the Libera Brilliance+ and a new RTM module has been developed to be used as BPM electronics RF frontend (RFFE). In addition, its analogue RF switch matrix used for long-term stabilization was separated and placed close to the BPM pickup, hence enabling an additional drift stabilization of the acquired RF input signals against environmental and other impact along the RFFE cables. At present, a fully populated MTCA crate with 6 AMC boards for the readout of 12 BPMs is installed at PETRA III and is extensively being tested. This contribution summarizes the latest beam measurements, showing the achieved performance of the BPM system.

INTRODUCTION

The PETRA IV project at DESY (Hamburg, Germany) aims at the construction of a diffraction limited ultra-low emittance light source operating at 6 GeV [1, 2]. The PETRA IV storage ring will be built in the existing PETRA III tunnel, thus inheriting the original 8-fold symmetry of the former PETRA collider. The accelerator lattice is based on a modified hybrid six-bend achromat (H6BA) cell and, taking advantage of the 2.3 km circumference, it provides electron beams with 20 pm rad emittance. The facility layout is shown in Fig. 1, the PETRA IV design operational parameters are summarized in Table 1.

Table 1: PETRA IV Main Parameters

Parameter	Value
energy	6 GeV
circumference	2304 m
emittance	20 pm rad
rel. energy spread	0.91×10^{-3}
momentum compaction	3.3×10^{-5}
$\beta_{x,y}$ at IDs	2.2 m, 2.2 m

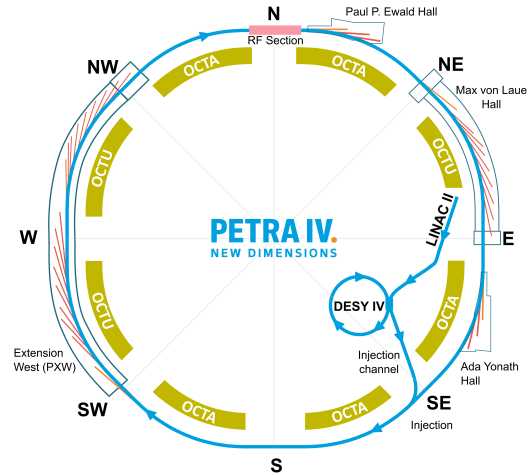


Figure 1: Layout of the PETRA IV facility.

The small beam emittances translate directly into much smaller beam sizes of about $7 \mu\text{m}$ horizontally and $3 \mu\text{m}$ vertically at the insertion device source points, thus imposing stringent requirements on the machine stability. In order to measure beam positions and control orbit stability to the level of 10% of beam size and divergence, a high resolution BPM system will be installed which consists of 788 individual monitors with the readout electronics based on MTCA.4 as technical platform.

In the beam commissioning phase of a storage ring, the BPM accuracy is essential. Before any beam accumulation in the ring will be possible, the BPM measurement accuracy must satisfy the requirements for the beam-based alignment (BBA) procedure, i.e. offset errors between the magnetic axes of the nearby quadrupoles and the electric centers of the BPMs must be identified. These offsets comprise alignment tolerances as well as electric and electro-mechanical offsets

Table 2: Readout electronics specifications. The single bunch / turn resolution holds for 0.5 mA bunch current, the closed orbit one for 1 kHz bandwidth, the beam current dependency for a 60 dB range with centered beam, and the long term stability should be measured over 6 days and a temperature span of $\pm 1^\circ\text{C}$ within a stabilized rack.

Requirement	Value
single bunch / single turn	$< 10 \mu\text{m}$
closed orbit resolution	$< 100 \text{ nm (rms)}$
beam current dependence	$\pm 2 \mu\text{m}$
long term stability	$< 1 \mu\text{m}$

CANADIAN LIGHT SOURCE BEAM POSITION VISUALIZATION TOOL

M. A. Bree*, T. D. Batten, C. W. Stevens, J. M. Vogt
Canadian Light Source, Saskatoon, Canada

Abstract

The Canadian Light Source orbit correction system acquires, collates, and publishes storage ring beam centroid position information from 48 beam position monitors (BPMs) at a rate of 1000 samples per second. We present a "Beam Position Visualization Tool" that computes and displays dynamic Fast Fourier Transforms (FFTs) and Cumulative Power Spectral Densities (CPSDs) for all BPMs in real-time using full resolution data. The computed FFTs and CPSDs can be plotted in various combinations and in waterfall plots that allow visualization of changes over long periods of time. In addition, correlations between all BPM channel combinations are computed and ranked. Data from any two BPM channels can be selected for plotting in two dimensions wherein correlations are visually apparent. Computed CPSDs are further binned and archived for further analysis. Preliminary results from the Beam Position Visualization Tool have proven useful in identifying storage ring beam position noise at the Canadian Light Source.

INTRODUCTION

The Canadian Light Source (CLS) is a third generation synchrotron commissioned in 2005 that now supports 22 operational beamlines. The storage ring orbit correction (OC) system was upgraded in November 2021 to replace obsolete hardware and support new diagnostic capabilities [1]. The original Beam Position Monitors (BPMs) and associated Bergoz electronics are unchanged but new high speed D-tAcq analog-to-digital converters (ADCs) [2] feed beam position data via fiber optic cables to an OC host computer running Scientific Linux 7. The OC host uses the BPM data as input to the orbit correction algorithm to compute and send setpoints to the orbit corrector magnets (OCMs) over dedicated private Ethernet networks. The OC system uses the Experimental Physics and Industrial Control System (EPICS) [3] for configuration and control.

Many new features were built into the new OC system to facilitate specific diagnostic requirements such as hardware status. One such feature, called "beam position broadcast", publishes a data stream consisting of the beam positions read at all OC BPMs. Since the data stream protocol is connectionless and static, its usage by clients is completely decoupled from the OC system. Future diagnostic tools can be implemented using the data stream without modifying, interrupting, or otherwise interacting with the running OC system in any way.

* michael.bree@lightsource.ca

This paper covers two general topics:

- *Beam Position Broadcast*, which publishes BPM data.
- *Beam Position Visualization Tool*, which is an example of a client that consumes the published BPM data.

BEAM POSITION BROADCAST

The new OC system uses four D-tAcq ACQ435ELF ADCs to read BPM values of the X (horizontal) and Y (vertical) beam centroid positions at 48 locations around the CLS storage ring. The BPMs are read at 1000 Hz, and each reading (sample) is three bytes. Using four bytes per sample results in a data rate of 384,000 bytes/s (plus protocol overhead) to transmit all 96 channels.

Publishing the beam position data in some form allows clients external to the OC system to process the information as they see fit, independently of OC operation. The CLS uses the EPICS control system and one possible mechanism for publishing beam position data is via EPICS Process Variables (PVs). EPICS clients can connect to PVs via a TCP-based protocol and can receive (and transmit) data via PVs over the control system network. However, the 1000 Hz update rate is high for EPICS (although there are techniques to mitigate this). More important, though, was the desire to not burden the real-time OC host computer that publishes the BPM data stream with hosting EPICS PVs for full resolution BPM data; and to not require data consumers (clients) to support EPICS. Therefore, EPICS was not used to publish the BPM data stream.

System Architecture

The User Datagram Protocol (UDP) [4] was chosen to publish the BPM data stream. UDP is a lightweight, connectionless protocol that minimizes the burden on the OC host computer which has as its primary task running the orbit correction algorithm and sending updates to the OCMs. A dedicated CPU core on the OC host was assigned to transmit the data stream on a configurable network interface. The data stream is transmitted on a private network to keep it off the control system network. It is sent to the broadcast address which allows any number of clients to independently receive it with no impact on the transmitting OC host. For example, the beam visualization tool described later in this paper is a data stream client that runs on a separate computer which is connected to the private network. The tool is a pure Python program that receives the BPM data stream directly, processes it, and publishes its results as EPICS PVs. The overall system architecture is illustrated in Fig. 1.

CURRENT STATUS OF THE HESR BEAM INSTRUMENTATION

C. Böhme, Forschungszentrum Jülich, Germany
 A. Halama, V. Kamerdzhev, G. Koch, K. Laihem, K. Reimers
 GSI Helmholtzzentrum für Schwerionenforschung, Darmstadt, Germany

Abstract

The High Energy Storage Ring (HESR), within the FAIR project, will according to current planning, provide anti-proton beams for PANDA and heavy ion beams for i.a. the SPARC experiment. Manufacturing for most of the envisaged beam instrumentation devices in vacuum is completed and testing is well underway. The overall status update of the beam instrumentation devices is presented, with a focus on the test-bench results of the BPMs. In addition, the planned future timeline of the HESR beam instrumentation is briefly reported.

INTRODUCTION

The HESR, part of the Facility of Antiproton and Ion Research in Europe (FAIR) in Darmstadt, Germany, is dedicated to the field of antiproton and heavy ion physics. The envisaged energy range is 0.8 GeV to 14 GeV for antiprotons and 0.17 GeV/a to 5 GeV/a for heavy ions [1]. The ring will be a racetrack design with a length of 574 m. The foreseen beam instrumentation within the modularized start version is:

- 63 Diagonally Cut Beam Position Monitors (BPM)
- 118 Beam Loss Monitors (BLM)
- 2 Beam Current Transformers (BCT)
- 2 Ionization Beam Profile Monitors (IPM)
- 1 In-gap particle measurement
- 1 Schottky Pick-up
- 1 Phase Pick-up
- 1 Dynamical Tune-meter
- 5 Viewer
- 2 Scraper

BPM SYSTEM

The pick-up design is based upon the diagonally cut shoe-box design of the COSY BPMs [2]. The design was shown in detail in [3]. While 62 BPMs will have the inner diameter of 89 mm, one is designated to be located closely after the injection septum, where the beam pipe has a diameter of 150 mm. Therefore, this BPM has to have a larger diameter to not limit the aperture at this place. This one has still to be designed and the production is not planned for the near future.

In the bend sections of the synchrotron, between the dipole magnets, different configurations of quadrupole, sextupole and steering magnets are foreseen, with at least one quadrupole magnet but a different secondary magnet being in place. In order to save as much longitudinal space as possible, the BPM is build in the single vacuum chamber

servicing through all these devices. But for each configuration a different length of the vacuum chamber, 1585 mm, 1249 mm, or 1180 mm, is needed. In addition, in the straight sections, these restrictions do not apply, therefore a 450 mm long vacuum chamber is used there. But the BPM pick-ups itself are identical in each configuration. All these different length vacuum chamber have to fit on the test stand.

Signal Chain

Within the FAIR project, the standard signal chain consists of the A110 pre-amplifier [4], which features an amplification range of +60 dB to -60 dB. For the readout and calculation of the beam position the LIBERA Hadron [5] was chosen. It features an extension for orbit control, which has been adapted to the FAIR magnet control units (ACU). As an extension to the original plan, the orbit control extension units have been ordered for the HESR as well. As an addition to the FAIR standard, taking the low expected signal for the HESR into account, an additional low-noise head amplifier of 20 dB, will be used directly on the vacuum feedthroughs in front of the A110 pre-amplifiers. It is foreseen to use the same head-on amplifiers in other parts of FAIR with expected low signal, e.g. the high energy beam transport (HEBT) beamlines.

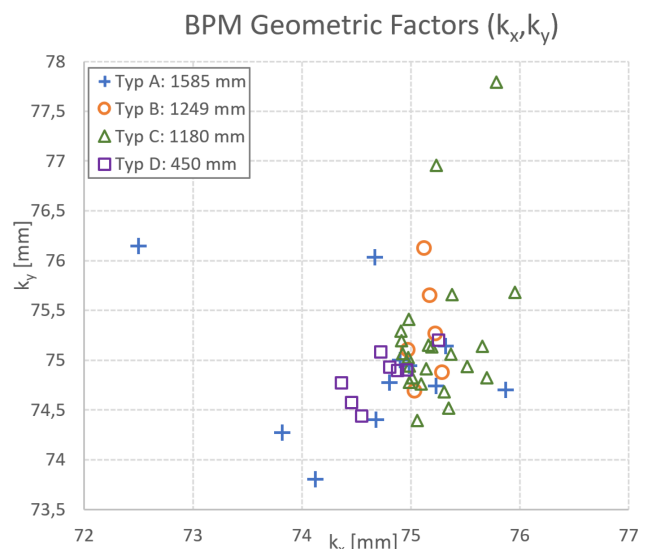


Figure 1: Overview of the measured geometric factors of the HESR BPMs. Notable spread and outliers result from the real statistical characteristic of the individual BPM, systematic errors on the test bench as well as measurement uncertainties. The standard deviations of the geometrical factors are $k_x = 0.55$ mm and $k_y = 0.66$ mm.

MiniBEE - MINIBEAM BEAMLINE FOR PRECLINICAL EXPERIMENTS*

J. Reindl[†], A. Rousseti, J. Neubauer, G. Datzmann¹, G. Dollinger
Universität der Bundeswehr München, Neubiberg, Germany

G. Kourkafas, J. Bundesmann, A. Dittwald, A. Denker², Helmholtzzentrum Berlin, Berlin, Germany

¹also at Datzmann Interact & Innovate GmbH, Munich, Germany

²also at Berliner Hochschule für Technik, Berlin, Germany

Abstract

Spatial fractionated radiotherapy using protons, so-called proton minibeam radiotherapy (pMBT) was developed for better sparing of normal tissue in the entrance channel of radiation. Progressing towards clinical use, pMBT should overcome current technical and biomedical limitations. This work discusses a preclinical pMBT facility, currently built at the 68.5 MeV cyclotron at the Helmholtz Zentrum Berlin. The goal is to irradiate small animals using focused pMBT with a sigma of 50 μm , a high peak-to-valley dose ratio at center-to-center distance as small as 1 mm and beam current of 1 nA. A first degrader defines the maximum energy of the beam. Dipole magnets and quadrupole triplets transport the beam to the treatment room while multiple slits properly form the transverse beam profiles. A high magnetic field gradient triplet lens forms the minibeam in front of the target station and, scanning magnets are used for a raster scan at the target. An additional degrader, positioned close before the focusing spot and the target, further reduces the energy, forming a spread-out Bragg peak. A small animal radiation research platform will be used for imaging and positioning of the target.

INTRODUCTION

Radiation therapy (RT) aims to maximize the delivered dose in the tumor while minimizing the dose to the normal tissues [1]. Proton beams can contribute to that goal due to their advantageous physical properties [2]. They deposit low dose at the entrance and the maximum dose is deposited in a well-defined range, based on their initial energy. Additional methods of protecting the healthy tissues are the temporal and spatial fractionation. The concept of Spatially Fractionated Radiation Therapy (SFRT) is the fragmentation of dose in space creating at the entrance a periodical pattern of regions with high (peak) and low (valley) doses [3]. Proton minibeam radiation therapy (pMBT) is an innovative treatment method which exploits the advantages of proton beams and spatial fractionation [4, 5]. Minibeams have a transverse beam size (σ) in the submillimeter range and they are delivered with an interdistance, which is called center-to-center (ctc) distance, in the millimeter range in order to cover the tumor laterally. In this way, the created alternated pattern of peaks and valleys in the entrance spares the healthy tissues. When proton beams transverse the matter they broaden due to multiple

Coulomb scattering (MCS) ending up to cover the tumor homogeneously (see Fig. 1).

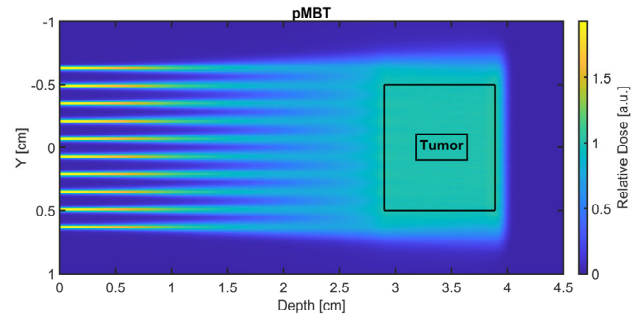


Figure 1: Simulated dose distribution of pMBT applying 68 MeV proton minibeam ($\sigma = 98 \mu\text{m}$ and ctc = 1.4 mm) in a water phantom assuming a tumor in 2.9 - 3.9 cm depth. The spread-out Bragg peak (SOBP) was obtained by positioning a range shifter close to the phantom.

The in-vivo studies conducted so far have highlighted the superiority of pMBT over conventional RT. One of the first proof-of-principle experiments, in which the right ear of the mice were irradiated with a broad proton beam or with an array of 16 minibeam ($\sigma = 180 \mu\text{m}$ and with ctc = 1.8 mm), showed that the acute side effects can be bypassed [6]. Another important in-vivo experiment investigated the dependence of side effects to the σ of the beam [7]. Also in this case, the right ear of the mice were irradiated with an array pattern of proton minibeam with different σ and the same ctc. The results showed that better sparing can be achieved with smaller beam sizes. Furthermore, a study in which rats with RG2 glioma were irradiated with pMBT or conventional RT schemes showed that rats irradiated with minibeam had better survival rate and less side effects [8]. All the aforementioned results gave a prominence to pMBT over conventional RT due to the better sparing of healthy tissue. However, the biological mechanisms underlying that phenomenon are not clear yet. A preclinical pMBT facility can contribute to intense and systematic research and tissue sparing effects have to be demonstrated on various tissues and beam settings in order to fully investigate the aspects and prospects of pMBT. In this paper we describe the concept of a preclinical proton minibeam radiotherapy facility for small animal irradiation at the Helmholtz-Zentrum in Berlin (HZB) [9].

BEAMLINE DESIGN

The proposed beamline concept should fulfill some constraints related to the beam energy, the beam energy degra-

* Work supported by German Ministry of Defence BMVg

[†] Judith.reindl@unibw.de

DESIGN AND STUDY OF CAVITY QUADRUPOLE MOMENT AND ENERGY SPREAD MONITOR*

Q. Wang, Q.Y. Dong, L.T. Huang

Dalian Institute of Chemical Physics, Chinese Academy of Sciences, Dalian, China

Q. Luo[†]

NSRL, University of Science and Technology of China, Hefei, China

Abstract

A nondestructive method to measure beam energy spread using the quadrupole modes within a microwave cavity is proposed. Compared with a button beam position monitor (BBPM) or a stripline beam position monitor (SBPM), the cavity monitor is a narrow band pickup and therefore has better signal-to-noise ratio (SNR) and resolution. In this study, a rectangular cavity monitor is designed. TM₂₂₀ mode operating at 4.76 GHz in the cavity reflects the quadrupole moment of the beam. The cavity plans to be installed behind a bending magnet in Dalian Coherent Light Source (DCLS), an extreme ultraviolet FEL facility. In this position, the beam has a larger dispersion, which is beneficial to measure the energy spread. A quadrupole magnet, a fluorescent screen, and a SBPM with eight electrodes is installed near the cavity for calibration and comparison. The systematic framework and simulation results are also discussed in this paper.

INTRODUCTION

Energy spread is an important parameter that reflects the quality of the beam. Especially in linear accelerators used as storage rings and collider injectors, ensuring a good energy spread of the beam can improve injection efficiency and maintain beam stability. Therefore, real-time and high-resolution measurement of energy spread needs to be achieved.

The most widely used method for energy spread measurement at present is to insert a fluorescent screen or an OTR after bending magnets. By measuring the generated light spot, the transverse distribution of the beam can be determined, and the energy spread is capable to be obtained based on the principle that different energy electrons have different turning radius [1]. However, this intercepting method is unsuitable for real-time measurement or feedback control. Therefore, a nonintercepting energy spread monitor is required.

A feasible nondestructive method is using stripline beam position monitor (SBPM) [2–4]. SBPM is installed at positions with high value of dispersion function, allowing extraction of the beam's quadrupole moment to obtain the energy spread. The sensitivity of this method is influenced by the angle of electrodes.

* Work supported by the National Key Research and Development Program of China No.2022YFA1602201, the International Partnership Program of the Chinese Academy of Sciences Grant No. 211134KYSB20200057 and the STCF Key Technology Research Project.

[†] email address: luoqueing@ustc.edu.cn

In order to achieve the energy spread measurement with high-resolution, this paper proposes the method of RF resonant cavity. Similar to SBPMs, cavities can also measure the quadrupole moment, thus obtaining the energy spread. Compared to SBPMs, cavities have higher signal-to-noise ratio (SNR), enabling better quadrupole moment resolution, which can also be confirmed in the position measurement. Additionally, in the direction of the beam, cavities can realize a more compact layout.

This paper introduces a design of cavity-based quadrupole moment and energy spread monitor for the Dalian Coherent Light Source (DCLS), an extreme ultra-violet FEL facility with a length of 100 m, and provides simulation results to verify the feasibility of the proposed approach.

THEORETICAL BASIS

While passing through the cavity, the bunch will excite different eigenmodes. The signal amplitude of an eigenmode can be written as

$$V = k_n q \int_{-T}^T f(t) \exp(i\omega t) dt, \quad (1)$$

where q is bunch charge, the final integral is related to the longitudinal distribution of the bunch, and k_n is the loss factor, which is related to the mode type. As shown in Fig. 1, for a rectangular cavity rotated 45° about the axis, its TM₂₂₀ mode amplitude is proportional to the beam quadrupole moment [5, 6].

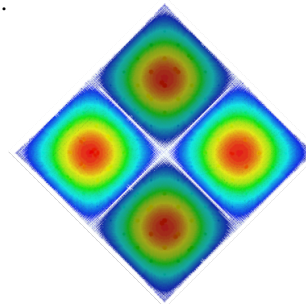


Figure 1: Electric field of TM₂₂₀ mode in rectangular cavity. Warmer colors represent stronger electric fields.

$$V_{TM220} \propto x^2 - y^2 + \sigma_x^2 - \sigma_y^2, \quad (2)$$

where x and y are the beam positions in the two directions. σ_x and σ_y are the beam rms sizes in the two directions. When the bunch length is short and does not change significantly, the quadrupole moment $x^2 - y^2 + \sigma_x^2 - \sigma_y^2$ can be obtained by extracting the charge and the amplitude of the TM₂₂₀ mode.

EXPERIMENTAL VERIFICATION OF THE COHERENT DIFFRACTION RADIATION MEASUREMENT METHOD FOR LONGITUDINAL ELECTRON BEAM CHARACTERISTICS

R. Panaś*, A. I. Wawrzyniak, NSRC SOLARIS, Kraków, Poland
K. Lasocha, CERN, Geneva, Switzerland
A. Curcio, INFN LNF, Frascati, Italy

Abstract

This paper presents a natural extension of prior theoretical investigations regarding the utilization of coherent diffraction radiation for assessing longitudinal characteristics of electron beams. The study focuses on the measurement results obtained at the SOLARIS synchrotron and their analysis through a theoretical model. The findings are compared with previous estimates of the electron beam's longitudinal profile.

COHERENT DIFFRACTION RADIATION

Electromagnetic radiation is emitted when a beam of charged particles accelerates or changes medium of propagation (abruptly or continuously in terms of the local electromagnetic susceptibility) [1, 2]. If wavelength of the emitted radiation is comparable or greater than the bunch length, the radiation is said to be "coherent" because the contributions from the distinct particles within the beam interfere constructively, and the bunch radiates as a whole. In the low frequency limit the emitted radiation power is proportional to the square of the bunch intensity, while for intermediate frequency ranges the power decreases with increasing bunch length. For bunch lengths of the picosecond scale, variations in the radiation intensity can be easily monitored by GHz-THz detectors like Schottky diodes [3, 4]. For shorter bunches, far-infrared diagnostics are needed, such as spectrometers [5].

Coherent radiation can be coupled out of the beamlines through suitable transparent windows, eventually transported in air into power detectors. For the diagnostic purposes of the PoFEL project [6], application of the Coherent Diffraction Radiation (CDR) was investigated at SOLARIS [7]. Diffraction radiation is a type of radiation that a bunch of particles emits while passing close to the boundary of two media with different indices of refraction, which allows for non-destructive bunch length measurements [8].

In the experimental setup at SOLARIS, the beam passes through a hollow aluminium disk. The radiation is emitted from localized layers of that surface, imprinting the beam properties into the emitted radiation at the transition plane and enabling diagnostics. The fact that the disk is hollow allows the beam not to be scattered, preserving the emittance even if the particles do not propagate inside it.

The spectral angular distribution of energy emitted backward in the form of diffraction radiation from a perfectly

conducting round disk, with an internal and external radius equal to respectively a and b , can be described with the following formula [9, 10]:

$$\frac{d^2 I}{d\omega d\Omega} = |F(\omega)|^2 \times \frac{Q^2}{(4\pi^3 \epsilon_0 c^5 \beta^4 \gamma^2)} \times \left| \int_a^b d\rho \rho K_1 \left(\frac{\omega \rho}{\beta \gamma c} \right) J_1 \left(\frac{\omega \rho}{c \sin \theta} \right) e^{\frac{j\omega^2 \rho^2}{2c^2}} \right|^2, \quad (1)$$

where Q denotes the bunch charge, ϵ_0 is the vacuum permittivity, c is the velocity of light, β is the ratio of particle velocity to the velocity of light, and γ is the Lorentz factor. The quantity $F(\omega)$ is called the *bunch form factor* and strictly depends on the shape of the electron bunch. The theoretical prediction of the spectral-angular distribution of CDR emitted with the experimental setup at SOLARIS is shown in Fig. 1.

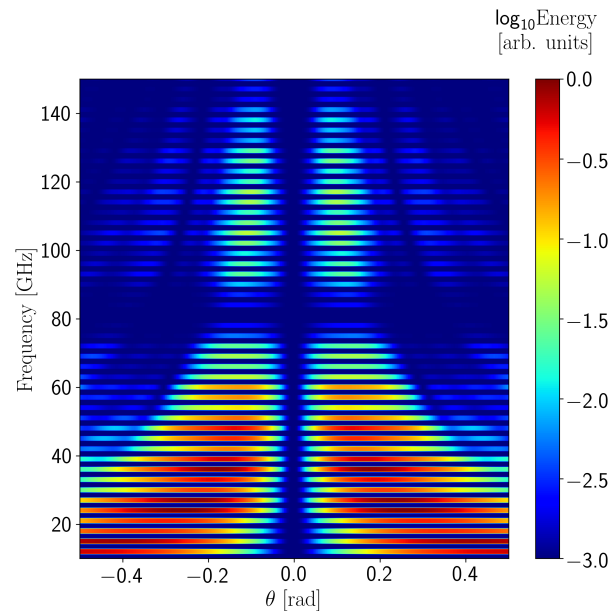


Figure 1: CDR spectral-angular distribution for the SOLARIS injector bunch repetition pattern and beam energy of 550 MeV.

BUNCH LENGTH MEASUREMENT

The diagnostic technique considered for PoFEL is based on the power balance of CDR radiation collected by Schottky

* roman.panas@uj.edu.pl

CONSIDERATION OF BEAM INSTRUMENTATION FOR SOLARIS LINAC UPGRADE

A. Curcio, INFN LNF, Frascati, Italy

R. Panaś, J. Biernat, M. Ūnal, J. Wiechecki, A.I. Wawrzyniak*, NSRC SOLARIS, Kraków, Poland

Abstract

SOLARIS linac currently operates at 540 MeV and is used as an injector to the storage ring, where after the accumulation the energy is ramped up to 1.5 GeV via two active RF cavities. Top-up injection would be of extreme benefits for user operation, therefore a new 1.5 GeV linac is being designed. The idea is to replace the current machine without infrastructural interventions in terms of tunnel expansion. Performed studies demonstrate that the best solution is provided by a Hybrid S-band/C-band LINAC. One of the main goals is to achieve bunch compression below the picosecond level and low-emittance beams for a future short-pulse facility or a Free Electron Laser. Within this presentation the results of performed simulations will be presented together with the concept of different diagnostics as BPMs, current transformers, YAG screens, coherent diffraction radiation monitor distribution.

INTRODUCTION

SOLARIS National Synchrotron Radiation Centre (NSRC) is first light source infrastructure built in Krakow, Poland. Currently it consists of 600 MeV linac with thermionic gun, 1.5 GeV storage ring and 5 operating beam-lines serving for the users community. The storage ring operates in the decay mode with 2 injections during the day. An optimal perspective for the future operations at SOLARIS [1] would be the beam injection from the LINAC [2] into the storage ring at full energy, i.e. 1.5 GeV. There are several advantages related to this approach. The most intuitive is the possibility to keep the stored current at a constant level. This would favor the user operation requiring a constant level of brilliance of the synchrotron source and/or of the sources associated to insertion devices. The radiation source, therefore, can operate continuously, avoiding injection downtime and energy ramp. Additionally, from an operational point of view, all the machine settings, which are normally current-dependent, could be kept at the same value. Avoiding invasive feedbacks meant to follow the electron current's decay, would allow the establishment of fine feedbacks working around equilibrium conditions for the beam parameters (like emittance, optics and orbit stability). Fine feedbacks could efficiently maintain optimal performances for days.

Furthermore, having a 1.5 GeV LINAC machine would open up a wide range of new possibilities for the facility, solely related to the LINAC as independent module. It's worth specifying that in a top-up injection system the LINAC

is permanently serving the storage ring, nevertheless a beam-splitter system might be thought in order to save a fraction of charge for diverse applications, bypassing the transfer line to the ring. It has been already demonstrated the interest of doing electron irradiations with the LINAC [3]. Currently, a diagnostic station placed before the LINAC dump is already under development for tests/experiments on novel concepts of beam diagnostics [4]. A futuristic view of the same area would foresee a Free Electron Laser (FEL). Indeed, such a FEL source would be pulsed on a much shorter scale length than the pulses provided by the storage ring, and it would be designed to cover a different frequency range.

OPTICS DESIGN AND BEAM DYNAMICS

There were several considerations for the new linac design. However due to space constraints in the linac tunnel the decision was made to change the technology from S-band to C-band allowing for higher accelerating gradient. The layout of the new LINAC placed in the existing tunnel is reported in Fig. 1. The schematics of the lattice elements is, instead, reported in Fig. 5. Such schematics will be discussed later on in this paper, specifically regarding the beam instrumentation used for beam diagnostics. The start-to-end simulations studies, from the cathode to the injection point for a Hybrid S-band/C-band LINAC were done by using the ASTRA and elegant [5] codes. The start-to-end simulation has been conducted for several different beam charges [6].

For the case of 100 pC the resulting beam optics in terms of rms beam sizes (Σ_x and Σ_y) is reported in Fig. 2. It is possible to notice that the beam size is maintained within the range of a few hundreds microns all along the LINAC, corresponding to a normalized emittance $\epsilon_{Nx} \approx \epsilon_{Ny} \lesssim 5 \text{ mm} \cdot \text{mrad}$. The emittance at the gun is around $1 \text{ mm} \cdot \text{mrad}$ but it reaches such a value in the magnetic compressor due to space charge [6]. The final rms bunch length St is in fact $\approx 500 \text{ fs}$ rms, as depicted in Fig. 3. Such a short bunch length may be used in the future to drive radiation sources or to perform ultra-fast irradiations for different applications.

ERROR STUDIES

Once the start-to-end simulation studies have been finalized, spanning over beam parameters, and beam optics solutions have been found to efficiently transport low-emittance, compressed beams, to the end of the full-energy LINAC, investigation of the errors in the lattice elements has been performed. The goal has been to evaluate if the selected focusing elements and their positioning is suitable for preserving the beam optics even for non-ideal elements, and

* adriana.wawrzyniak@uj.edu.pl

A SNAPSHOT OF CERN BEAM INSTRUMENTATION R&D ACTIVITIES

T. Lefevre*, A. Boccardi, S. Jackson, D. Louro Alves, F. Roncarolo,
J. Storey, R. Veness, C. Zamantzas
CERN, Geneva, Switzerland

Abstract

The CERN accelerator complex stands out as unique scientific tool, distinguished by its scale and remarkable diversity. Its capacity to explore a vast range of beam parameters is truly unparalleled, spanning from the minute energies of around a few keV and microampere antiproton beams, decelerated within the CERN antimatter factory, to the 6.8 TeV high-intensity proton beams that race through the Large Hadron Collider (LHC). The Super Proton Synchrotron (SPS) ring plays also a crucial role by slowly extracting protons at 400 GeV. These proton currents are then directed toward various targets, generating all sorts of secondary particle beams. These beams, in turn, become the foundation of a diverse fixed-target research program, enabling scientific exploration across a wide spectrum. Moreover, as CERN looks ahead to future studies involving electron-positron colliders, the development of cutting-edge diagnostics for low emittance and short electron pulses is also underway. This contribution serves as a snapshot, shedding light on the main R&D initiatives currently underway at CERN in the field of beam instrumentation.

INTRODUCTION

The CERN accelerator complex is a dynamic and continually evolving system. Over a decade ago, an ambitious global initiative was launched to enhance the collision capabilities of the Large Hadron Collider (LHC). This initiative aims to achieve higher collision rates and is executed in phases. The initial phase focused on the LHC Injector Upgrade program [1], which successfully generated higher brightness beams within the CERN injector complex. Building on this achievement, the subsequent stage of the high Luminosity LHC upgrade (HL-LHC) [2] is scheduled for implementation from 2026 to 2028. This phase aims to further elevate beam intensities and reduce emittance, introducing novel challenges to beam instrumentation. These instruments must adapt to unprecedented beam densities while maintaining the highest reliability and precision.

Beyond its contributions to the LHC and its physics endeavors, CERN has embarked on a comprehensive consolidation of the fixed target physics program in the 'North Area' of the Super Proton Synchrotron (SPS). This undertaking necessitates a complete overhaul of the instrumentation employed for extracting continuous beams from the SPS. These beams are subsequently directed towards various targets and experimental zones.

Anticipating the completion of the LHC's scientific program, the scientific community's aspirations encompass the

exploration of $e^- - e^+$ collisions at up to 380 GeV center of mass energies. While the Compact Linear Collider (CLIC) [3] has been under scrutiny for decades, CERN is currently engaged in assessing the feasibility of the 91-kilometer-long Future Circular Collider (FCC). The FCC would initially focus on lepton collisions [4] and potentially accommodate 100 TeV proton collisions in subsequent phases, using the same infrastructure. Although linear and circular colliders differ in their design and implementation, there are notable similarities in terms of beam properties, beam energy, intensity, transverse and longitudinal sizes, as well as the demand for a high level of radiation tolerance within the tunnel. This suggests the prospect of adapting technologies initially developed for CLIC for use in the FCC-ee.

In this paper, we provide a comprehensive overview of the ongoing R&D endeavors at CERN in the realm of beam instrumentation. This encompasses a spectrum of activities, including the design of innovative electromagnetic pick-ups, the refinement of techniques for measuring transverse profiles of high power density beams, advancements in short longitudinal beam profiling, the optimisation of high dynamic range particle detectors and the latest strides in read-out electronics and digital acquisition systems. By shedding light on these R&D activities, we aim to present the essence of CERN's pursuit of cutting-edge instrumentation techniques.

COMPLEX DESIGN OF ELECTROMAGNETIC PICK-UPS

Within the scope of the HL-LHC program, the demand for large-aperture, high-field quadrupole magnets has surged to compress proton beam sizes during collisions to unprecedentedly minuscule dimensions. This new configuration requires novel cryogenic directional stripline beam position monitors [5], enabling the measurement of counter-propagating beams with a precision surpassing a mere micron. This intricate design encompasses Tungsten alloy inserts, strategically positioned to absorb collision debris and curtail radiation doses to neighboring magnets. Furthermore, these monitors are coated with copper and NEG (Non-Evaporable Getter) coatings, a dual-layer approach that minimizes beam impedance and paves the way for attaining ultra-high vacuum conditions.

Amid recent advancements, beam position monitors (BPMs) with heightened frequency bandwidth have garnered substantial interest. This is not only pertinent to short electron bunches but also to furnish intrabunch monitoring with fast time response for high-intensity proton beams. A range of technologies is presently under exploration, featuring electro-optical (EO) crystals [6] and dielectric pick-ups [7, 8].

* thibaut.lefevre@cern.ch

DIAGNOSTICS FOR A HIGH EMITTANCE AND HIGH ENERGY SPREAD POSITRON SOURCE

N. Vallis^{1*}, F. Marcellini, R. Zennaro, M. Zykova,
 P. Craievich, R. Fortunati, R. Ischebeck, E. Ismaili, P. Juranic, G.L. Orlandi, M. Schaer
 Paul Scherrer Institute, Villigen, Switzerland
¹also at EPFL, Lausanne, Switzerland

Abstract

This paper is an overview of a diagnostics setup for highly spread e+e- beams, to be installed at the PSI Positron Production (P³ or P-cubed) experiment. To be hosted at the Swiss-FEL facility (PSI, Switzerland) in 2026, P³ is e+ source demonstrator designed to generate, capture, separate and detect nano-Coulombs of secondary e+ and e- bunches, in spite of their extreme transverse emittance and energy spread. The experiment will employ an arrangement of broadband pick-ups (BBPs) to detect simultaneously the time structure of secondary e+e- bunches. A spectrometer will follow the BBPs and deflect the e+ and e- onto two unconventional faraday cups that will measure their charge. In addition, the energy spectrum of e+ and e- distribution will be reconstructed through scintillating fibers.

INTRODUCTION

The SwissFEL facility [1] (PSI, Switzerland) will host the PSI Positron Production (P³ or P-cubed) experiment [2] in 2026, a e+ source demonstrator with potential to improve by an order of magnitude the present state-of-the-art e+ yield. The experiment layout is shown in Fig. 1, featuring a e+ source based on a 6 GeV electron (e-) beam and 17.5 mm-thick (or 5 times the radiation length) amorphous Tungsten target. A capture system will follow the target, consisting of a solenoid system and 2 RF accelerating cavities. The remarkable e+ capture capabilities of P³ are enabled to great extent by the usage of high temperature superconducting (HTS) solenoid around the target region, as well as a novel standing wave solution for the RF cavities that provides a large iris aperture to maximize e+ capture.

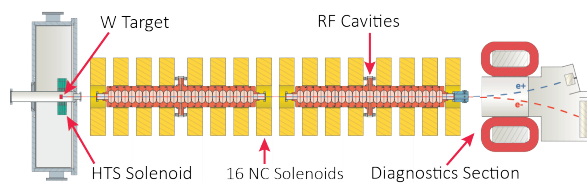


Figure 1: Simplified layout of the P³ [2].

The experiment diagnostics, whose layout is shown in Fig. 2, will be located directly downstream from the 2nd RF cavity, as illustrated in Fig. 1. This setup will measure the e+e- bunches before and after species separation, equipped with an arrangement of broadband pick-ups (BBPs), 2 Faraday Cups (FCs) and a variety of scintillating detectors. The

* nicolas.vallis@psi.ch

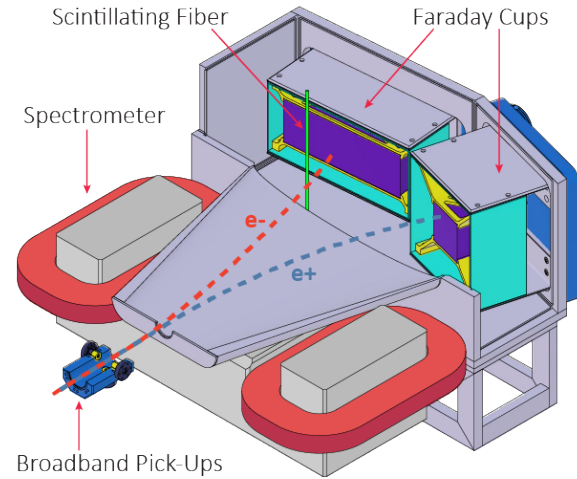


Figure 2: Concept design of the P³ diagnostics.

BBPs will detect, simultaneously for both particle species, the time structure of the captured e+e- bunches. The FCs and scintillators will be installed in the same vacuum chamber, and will measure the charge and energy spectrum of separate e+ and e- streams. Separation will be provided by a spectrometer, a dipole magnet based on four copper coils and an iron yoke, which will be fed at a maximum current of 340 A in order to reach magnetic fields up to 0.25 T. Additional diagnostics such as the arrangement of screens and cameras are still under discussion.

e+e- Dynamics in P³

200 pC e- at 6 GeV will impinge upon the 17 mm-thick Tungsten target, yielding a e+e- beam in the multi-MeV and nano-Coulomb range. Table 1 shows the evolution of the e+ bunches along the P³ capture line. These values clearly indicate that e+ dynamics are heavily dominated by an extremely high transverse emittance. In the transverse plane, e+ collection relies on the so-called Adiabatic Matching [3,4], a well-known e+ capture technique based on transforming the transverse phase space of newly generated e+ (moderate σ_x and large σ_{px}) into the acceptance of the capture line (large σ_x and moderate σ_{px}). Thus, emittance is not damped but matched and transported up to the diagnostics section. As for the longitudinal beam dynamics, RF fields will generate time structures of many consecutive e+ and e- bunches separated by the S-band $\lambda/2$ (167 ps or 50 mm in the ultrarelativistic regime), with the most particle population concentrated over the first two RF buckets. Two RF working points of interest

Content from this work may be used under the terms of the CC-BY-4.0 licence (© 2023). Any distribution of this work must maintain attribution to the author(s), title of the work, publisher, and DOI

SAFETY CONSIDERATIONS FOR SHIELD DOOR CONTROL SYSTEMS*

H.A. Watkins[†], W. Barkley, C. Hatch, D. Martinez, D. Rai, E. Simakov
Los Alamos National Laboratory, Los Alamos, NM, USA

Abstract

The Accelerator Operations and Technology division is upgrading the control system for a 33-ton shield door that will be used when the Cathodes and RF Interactions in Extremes (CARIE) accelerator begins operations. The door was installed in the 1990's but safety standards such as ISO 13849-1 have since emerged which provide safety requirements and guidance on the principles for the design and integration of safety-related parts of a control system. Applying this standard, a safety controller, safety relays and a light curtain barrier have been added to eliminate injury and exposure of personnel to potential hazards during door operations.

OVERVIEW OF CARIE

Los Alamos National Lab (LANL) is starting construction of a new C-band (5.712 GHz) accelerator test facility for cathode, accelerator, and material science studies. The new facility is called Cathode and RF Interactions in Extremes (CARIE). This accelerator will reside in a radiation protection vault on the Los Alamos Neutron Science Center (LANSCE) mesa. This location will house a cryo-cooled copper RF photoinjector with a high quantum efficiency (QE) cathode and a high gradient accelerator section with beam power up to 20 kW [1].

SHIELD VAULT

CARIE will reside in a 12 by 25-foot interior vault that uses 4-foot-thick magnetite blocks to shield the exterior control and operations areas. The vault was originally designed for use with the Advanced Free Electron Laser (AFEL) project which is no longer in operation. A 33-ton moveable shield door separates the vault from the control room. When closed during CARIE operation, the door protects personnel from neutron and bremsstrahlung radiation, activated air, and ozone. The door is constructed of 12 magnetite concrete blocks welded together on their edges and welded to a reinforced concrete base. The door is mounted on four sets of Hilman rollers and guided by tracks on the floor, the door is opened and closed by a hydraulic piston [2]. The shield vault door will need to open and close multiple times a day to support experimentation within the vault. The original control system was decommissioned and removed in the early 2000's. However, the shield blocks, hydraulic piston and roll track system remain intact (see Fig. 1). Attempts to test

the door mechanism and piston were successful and the door is operational from a mechanical perspective. The shield door and existing hydraulic system (see Fig 1).

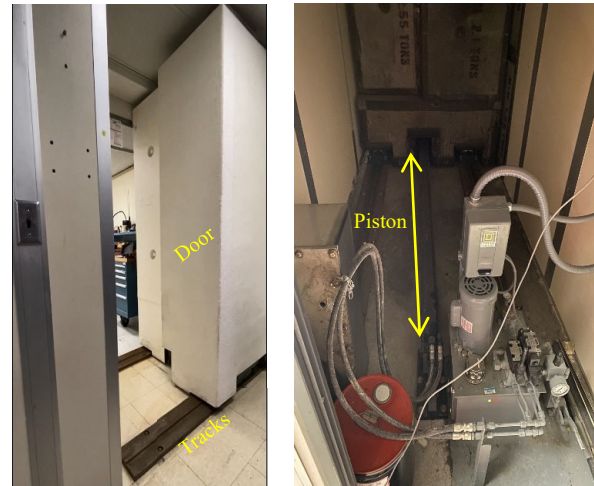


Figure 1: Shield door opening and hydraulic system.

FUNCTIONAL REQUIREMENTS

The purpose of the control system for the shield door is to allow scientists and engineers to easily access the interior vault when CARIE is not in operation and for the door to remain closed when operations commence. The control system requirements are very simple. Open and close buttons mounted exterior to the vault easily meet the functional requirements for operation. Investigation of the mounting points and legacy relay system indicate this is most likely what existed during its operation during the 1990's until decommissioning in early 2000's.

SAFETY REQUIREMENTS

The legacy requirements of safety for the shield door design focused on the radiation shielding that the door provided to the users when the original AFEL was in operation. However, safety of the control system e.g. door operations were not considered or evident in the initial design. ISO 13849-1 is the safety standard that now governs safety requirements for the operation of control systems. This safety standard provides safety requirements and guidance on the principles for the design and integration of safety-related parts of a control system. This standard defines the performance level (PL), which is the discrete level used to specify the ability of safety-related parts of control systems to perform a safety function under foreseeable conditions.

WHAT IS SAFETY? WHAT IS RISK?

Control system engineers must incorporate safety into designs to provide the protective measures needed to insure

* This work was supported by the U.S. Department of Energy through the Los Alamos National Laboratory. Los Alamos National Laboratory is operated by Triad National Security, LLC, for the National Nuclear Security Administration of U.S. Department of Energy (Contract No. 89233218CNA000001).

LA-UR-23-29961

[†] hwatkins@lanl.gov

EXPANSION OF THE MTCA BASED DIRECT SAMPLING LLRF AT MEDAUSTRON FOR HADRON SYNCHROTRON APPLICATIONS

M. Wolf*, M. Cerv, C. Kurfuerst, S. Myalski, M. Repovz, C. Schmitzer
EBG MedAustron GmbH, Wr. Neustadt, Austria
A. Bardorfer, B. Baricevic, P. Leban, P. Paglovec, M. Skabar
Instrumentation Technologies, Solkan, Slovenia

Abstract

The MedAustron Ion Therapy Centre is a synchrotron-based particle therapy facility located in Lower Austria, which delivers proton and carbon ion beams for cancer treatments. Currently the facility treats over 400 patients per year and is expected to double this number in the future. Six years since the start of clinical operation, MedAustron is experiencing end-of-life issues concerning the digital Low Level RF components in the injector and the synchrotron. Replacements for these applications are under development and the chosen hardware is suitable to also update multiple beam diagnostic devices in the facility. Main targets for updates are the Schottky monitors, which were never properly integrated into the MedAustron Control system and the position pickup measurement system, which currently does not support turn by turn measurements. Comparison measurements with other state of the art diagnostic devices are ongoing to demonstrate the capabilities of the generic hardware. Furthermore, these measurements should show the increased usability and diagnostic potential compared to the legacy devices.

INTRODUCTION

MedAustron and Instrumentation Technologies continued to work on a LLRF and beam diagnostic solution to replace all RF applications used at MedAustron and already presented in the last years [1–3]. In the current paper new beam diagnostic usecases in the MedAustron Synchrotron will be shown and measurement results of Schottky detectors and classical Shoebox Pickups will be compared to other off the shelf equipment.

MEASUREMENT SETUP

Position Measurement System

The MedAustron Synchrotron contains multiple beam position monitors in form of Shoebox Pickups. These Pickups are located in different dispersion regions of the Synchrotron and can be used to measure the orbit of the beam circulating in the synchrotron. Head amplifiers are connected to these pickups with short cables to keep the interference and cable influences at a minimum. These head amplifiers generate sum and delta signals out of the pickup plate signals. Afterwards these sum and delta signals are forwarded out of the synchrotron hall and further amplified in distribution

amplifiers. The distribution amplifiers generate multiple copies of the pickups signals. Spare outputs of the distribution amplifiers are used to parasitically measure the two horizontal pickups in high and low dispersion regions.

Digital Data Processing of the Position Measurement

The output of the position measurement system is digitized with off the shelf hardware from Vadatech which was presented in Ref. [1]. For the beam position measurement one AMC560 Carrier card and one FMC231 AD/DA converter card is used. The signals produced by the distribution amplifiers are directly sampled and then demodulated to baseband signals using the revolution frequency of the synchrotron. The resulting amplitude of the delta signal is divided by the amplitude of the sum signal, to calculate position information independent of the beam current. The results of this calculation can then be calibrated to represent absolute position data. This calibration will be finalized in the future.

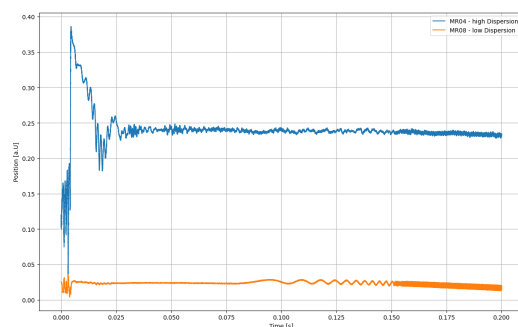


Figure 1: Qualitative position measurement in high and low dispersion regions of the synchrotron.

Schottky Monitors

The Schottky monitors are directly connected to standard low noise amplifiers (FEMTO- HVA-200M-40-F) and afterwards connected to the digitizer hardware outside of the synchrotron hall. In this setup sum and delta signals are calculated after digitizing the signals.

* markus.wolf@medaustron.at

BEAM-DIAGNOSTIC AND T0 SYSTEM FOR THE mCBM AND CBM EXPERIMENTS AT GSI AND FAIR

A. Rost^{1*}, T. Galatyuk^{2,3}, V. Kedych³, M. Kis², W. Krüger³,
 J. Pietraszko², A. Senger¹, J. Thaufelder², F. Ulrich-Pur²

¹FAIR GmbH, Darmstadt, Germany

²GSI Helmholtzzentrum für Schwerionenforschung GmbH, Darmstadt, Germany

³Institut für Kernphysik, TU Darmstadt, Darmstadt, Germany

Abstract

The Compressed Baryonic Matter (CBM) experiment at the Facility for Antiproton and Ion Research (FAIR) in Darmstadt requires a highly accurate beam monitoring and time-zero (T0) system. This system needs to meet the requirements of the CBM time-of-flight (ToF) measurement system for both proton and heavy ion beams, while also serving as part of the fast beam abort system. To achieve these goals, a detector based on chemical vapor deposition (CVD) diamond technology has been proposed. In addition, new developments using Low Gain Avalanche Detectors (LGADs) are currently under evaluation. This contribution presents the current development status of the beam detector concept for the CBM experiment.

INTRODUCTION

The CBM experiment [1] is a fixed-target, multi-purpose detector that will be used to explore the QCD phase diagram of nuclear matter at high net-baryon densities and moderate temperatures. The experiment will be located at the Facility for Antiproton and Ion Research (FAIR) in Darmstadt, Germany.

The CBM detector will be able to detect hadrons, photons, electrons, and muons in elementary and heavy-ion collisions over the entire energy range provided by the SIS100 heavy-ion synchrotron, from 3 to 11 A GeV for heavy ions and 29 GeV for protons. The measurements will be performed at event rates from 100 kHz up to 10 MHz using free-streaming readout electronics and fast online event reconstruction.

The BMON system consists of a high-speed time-zero (T0) and halo detector. The detector must meet the requirements of the time-of-flight (ToF) measurement system for both proton and heavy-ion beams. Specifically, it must achieve a time precision better than 50 ps (sigma), maintain stable long-term operation even at high interaction rates of 10⁷ particles/s, and have a detection efficiency approaching 100%. A summary of the requirements is provided in Table 1.

THE CBM BEAM MONITORING SYSTEM

The CBM BMON system has been already introduced in [2], it will consist of two detector stations located in front of the CBM target chamber. The T0-station is foreseen to measure the start time of the reaction, while the Halo-station

Table 1: Requirements to the CBM BMON System

Max. beam intensity	10 ⁷ particles/s on sensor
Max. read-out rate	5 MHz per channel
Time precision	50 ps
Position resolution	0.5 mm
Beam spot size on sensor	1 cm (2 sigma)
Sensor thickness	70 μm

will be used for beam halo monitoring and as a part of a fast beam abort system (BAS). Both detectors will be mounted inside a beam-pipe using commercially available CF 100 vacuum elements, as schematically shown in Fig. 1.

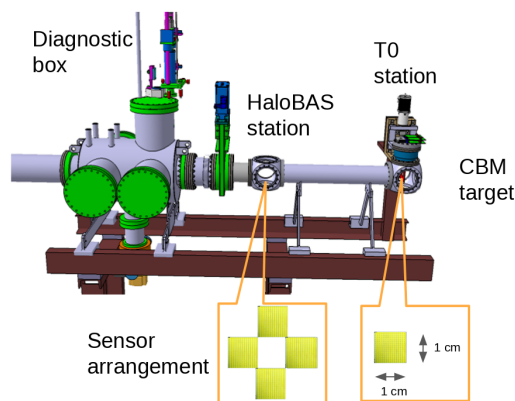


Figure 1: The CBM BMON system consists of two stations for beam halo and T0 measurement. The stations are mounted in standard CF 100 vacuum chambers in front of the CBM target. The T0 station uses a single sensor, while the Halo station uses a mosaic structure of four sensors. The Halo station will also be part of a fast beam abort system (BAS).

The sensor for the T0 station is currently planned to be made using poly-crystal CVD (pcCVD) diamond technology [3]. The sensor will have a thickness of 70 μm and will cover an area of 1 × 1 cm². It will be equipped with a metallization arranged in 16 strips on each side. A detailed description of the sensor and the production and testing of a prototype sensor can be found in [2]. The strip segmentation and orientation, aligned in the *x* and *y*-directions, will allow to extract the position information of the beam particles. We are currently also investigating higher segmen-

* a.rost@gsi.de

FIRST TEST WITH MICROTCA BASED CAVITY BPM ELECTRONICS FOR THE EUROPEAN XFEL AND FLASH

B. Lorbeer*, H. T. Duhme, I. Krouptchenkov, T. Lensch, D. Lipka, M. Werner
 Deutsches Elektronen-Synchrotron DESY, Germany

Abstract

The European X-ray free-electron laser (E-XFEL) and the FLASH2020+ project for the free electron laser Hamburg (FLASH) at DESY in Hamburg, Germany foresee several machine upgrades in the years to come. At FLASH a whole undulator section in a shutdown starting in summer 2024 and finishing in autumn 2025 is going to be rebuild. Existing button beam position monitors installed in this section of the machine do not deliver sufficient signal strength for future required resolution specification and orbit feedback optimization for machine operation. The resolution limitations will be overcome by replacing the button-based beam position monitors with in-house developed cavity beam position monitors and compact microTCA based radio frequency receiver read-out electronics. The measurement system has been tested and evaluated in a test setup at FLASH.

INTRODUCTION

The two international user facilities European X-ray free-electron (E-XFEL) and the free-electron laser of Hamburg (FLASH) are operated by the Deutsches Elektronen-Synchrotron (DESY) in Hamburg, Germany. Both machines are based on the effect of self-amplified spontaneous emission (SASE) which generates ultra-short photon pulses by cascading several undulators. The photon pulses are based on accelerated electron-bunches which originate from a photo injector driven radio frequency (RF) electron gun. The electron bunches are accelerated in a pulsed superconducting linac at a repetition rate of up to 4.5 MHz. More specifications on the different machine parameters can be found here [1]. The high-resolution transversal beam position measurement of the electron beam along the machines is realized with cavity beam position monitors (CAVBPM). The E-XFEL is already equipped with well performing monitors including read-out electronics [2] from in-kind contribution partners. However, future planned upgrades of the machine [3] with additional CAVBPM will be based on in-house developed read-out electronics. Like the E-XFEL the FLASH facility will be upgraded with approximately 20 monitors within the FLASH2020+ project [4]. A CAVBPM electronics read-out system has been developed in the past few years and is already in operation [5]. These electronics have been modified and enhanced to meet the specifications of the E-XFEL and FLASH where the most demanding requirement is a single bunch resolution of better than 1 μm in a charge range from 20 pC up to 1 nC. First tests with these CAVBPMs have been made with a test cavity BPM at FLASH to evaluate the adapted and extended

read-out electronics. The charge has been varied over the specified range and the measurement results demonstrate to fulfill the specified resolution.

CAVITY BEAM POSITION MONITORS AT FLASH AND XFEL

Cavity beam position monitors are composed of a mono-pole and a di-pole resonator from which the electron beam excited modes deliver RF signals from which the charge and the transversal position of the electron beam can be evaluated [6]. The monitors in use at the E-XFEL and in the design procedure for FLASH are also developed in-house [7] and have the characteristics listed in Table 1.

Table 1: Cavity Beam Position Monitor Characteristics E-XFEL and FLASH

Quality	Range
resonance frequency	3.3 GHz
beam pipe diameter	10 – 40.5 mm
mono-pole sensitivity	42.5 – 42.9 Vpk/nC
dipole sensitivity	2.46 – 2.87 Vpk/nC/mm
loaded quality factor	70

ANALOG SIGNAL DYNAMICS

The original developed CAVBPM monitor [8] and corresponding RF front-end electronics [5] have been designed to operate in a charge range from 500 fC up to 100 pC, while the specified charge range in the E-XFEL and at FLASH varies from 20 pC - 1 nC. Due to these different charge ranges and equivalent signal amplitudes modifications in the RF front-end were necessary. For this purpose a typical signal from a mono-pole resonator has been measured at a test cavity at FLASH. The signal is shown in Fig. 1.

Since the signals from the cavity are band-pass filtered in the first place in the RF front-end the signal strength from the band-pass filtered signal has been chosen to determine the necessary front-end dynamics. The derived quantities are summarized in Table 2.

Table 2: Estimation of Expected Signal Powers for the Charge Range From 20 pC–1 nC

Mode/States	Charge	voltage/Vpp	power/dBm
min. charge	20 pC	0.044	-23
max. charge	1 nC	22.25	31

* bastian.lorbeer@desy.de

REPLACEMENT OF THE SINGLE-PASS BPM SYSTEM WITH MicroTCA.4-BASED VERSATILE ELECTRONICS AT SPring-8

H. Maesaka^{*1}, RIKEN SPring-8 Center, Sayo, Hyogo, Japan

H. Dewa, T. Fujita, M. Masaki, N. Hosoda², S. Takano², JASRI, Sayo, Hyogo, Japan

¹also at JASRI, Sayo, Hyogo, Japan

²also at RIKEN SPring-8 Center, Sayo, Hyogo, Japan

Abstract

We have developed a versatile BPM readout electronics based on the MicroTCA.4 (MTCA.4) platform for the SPring-8 upgrade project, SPring-8-II. The new electronics are comprised of an RF frontend rear transition module (RTM) and a high-speed digitizer advance mezzanine card (AMC) having 10-channel, 16-bit, and 370 MSPS ADC. The field-programmable gate array (FPGA) on the AMC calculates both single-pass (SP) and closed-orbit distortion (COD) beam positions. The current BPM system at SPring-8 consists of approximately twenty SP-dedicated BPMs and more than 250 COD-dedicated ones. In advance of SPring-8-II, so far, we replaced half of the old SP BPM electronics with the new MTCA.4 ones and the rest of the old SP BPM electronics are being renewed this summer. The SP resolution of the new BPM electronics was confirmed to be better than 100 μm for a 0.1 nC single bunch, sufficient for SPring-8-II. The new BPM electronics were applied to regular tuning items, such as the adjustment of kicker magnets for pulsed orbit bumps in the beam injection, and the functionalities were confirmed to be compatible with the old SP BPM system. Thus, the MTCA.4-based BPM electronics are ready for SPring-8-II.

INTRODUCTION

The low-emittance upgrade of the SPring-8 storage ring, SPring-8-II [1] was proposed, and many new accelerator components have been developed. The natural emittance will be squeezed from 2.4 nm rad to 100 pm rad by reducing the beam energy from 8 GeV to 6 GeV and by using a 5-bend achromat lattice (5BA).

A new BPM system for SPring-8-II was also developed. The single-pass (SP) BPM resolution is required to be 100 μm std. for a 0.1 nC injected bunch. The error on the electrical center should be within $\pm 100 \mu\text{m}$ before the beam-based calibration. The closed-orbit distortion (COD) BPM is demanded to be sufficiently stable within 5 μm peak-to-peak for 1 month. To fulfill these requirements, we studied the following BPM components:

1. Button BPM electrodes made of molybdenum [2].
2. Radiation-tolerant coaxial cables.
3. BPM readout electronics based on MicroTCA.4 (MTCA.4) [3].

* maesaka@spring8.or.jp

Since the new electronics will benefit the operation of the current SPring-8 storage ring, replacement of the BPM electronics was scheduled in advance of the actual upgrade work. The SPring-8 storage ring has 48 cells (44 double-bend cells and 4 long straight ones). There are typically 6 BPMs in each cell and approximately 280 BPMs in total. Before the development of the new MTCA.4-based electronics, the existing BPM system has two types of readout electronics, COD BPM and SP BPM, and typically one BPM out of 12 (6 BPMs \times 2 cells) is processed by SP BPM and the other 11 are precessed by COD BPM. Contrary to the old electronics, the new MTCA.4-based electronics have both SP BPM and COD BPM functions. Therefore, both SP BPM and COD BPM can be replaced with the MTCA.4 electronics. Since the SP BPM system is more than 25 years old and hard to maintain, we decided to replace the SP BPM electronics with the MTCA.4 ones in advance of the COD BPM. The COD BPM system will be upgraded to MTCA.4 in the actual SPring-8 upgrade work.

The new electronics were first installed into the current SPring-8 ring to implement the adaptive feed-forward correction (AFC) of the error kick from the fast helicity switching beamline [4] in 2019. Old SP BPMs connected to the four BPM heads connected to the four BPM heads selected for the AFC were replaced with the MTCA.4 at that time. Another ten units of SP BPMs were then upgraded to MTCA.4 in 2021 and the rest of the SP BPM units are being replaced in this summer shutdown period (2023).

We describe the design of the MTCA.4-based BPM electronics and introduce the software for data taking. The basic performance of the SP BPM function is presented and compared with the old SP BPMs.

MTCA.4-BASED ELECTRONICS

A block diagram of the MTCA.4-based electronics is illustrated in Fig. 1. The signal from each BPM electrode is fed into the BPM rear transition module (RTM). The signal is filtered by a band-pass filter at the accelerator frequency of 508.58 MHz and the signal level is adjusted by step attenuators and low-noise RF amplifiers. The signal is then converted to a balanced differential signal by a BALUN since the ADC on the digitizer advanced mezzanine card (AMC) receives a differential balanced signal. The digitizer AMC has 10 ADC channels and hence one board can process signals from two BPMs. The ADC has a 16-bit resolution and a maximum sampling rate of 370 MHz. Since the signal frequency is higher than the Nyquist frequency of the ADC,

THE CONCEPTUAL DESIGN STUDY FOR NEW BPM SIGNAL PROCESSING SYSTEM OF J-PARC MAIN RING (MR)*

K. Satou[†], T. Toyama, S. Yamada, J-PARC/KEK, Tokai, Japan

Abstract

The beam position monitor signal processing system, which is a 19-year-old system, has been suffering from gain fluctuation due to contact resistance of the mechanical gain selector and communication disruption caused by an unstable contact of a card edge connector. It also has difficult repairs because some onboard parts have already reached the end of a product-life cycle, and some units have been in an unusable situation. Currently, we are on the beam power upgrade campaign to 1.3 MW by increasing the beam bunch current and shortening the main ring operation cycle, and precise beam tunings would require massive waveform data processing and transfer to a storage system than the present system. For this, we have been developing a system based on the 10 GbE optical link. The ADC board, which is under development, performs direct sampling using the third harmonics of accelerating radio frequency. The digital IQ demodulation technique is used to extract the baseband oscillation from the raw data. The obtained raw waveform and closed orbit data are stored in the data storage system. In the presentation, we will report on the progress of development aimed at operation in 2025 and the conceptual design of the new system.

INTRODUCTION

In the J-PARC main ring (MR), 186 beam position monitors (BPMs) have been used to measure beam orbit and beam optic parameters [1, 2]. Its signal processor, BPM circuit (BPMC), designed 19 years ago, has two modes of position measurement:

- 1) Closed orbit distortion (COD) mode,
- 2) bunch-by-bunch (BxB) mode.

The first mode is a narrowband measurement that performs a fast Fourier transform on the waveforms digitized with 80 MHz to extract the second harmonic component of the accelerating radio frequency (RF) to obtain the COD. Meanwhile, the second mode is a broadband measurement for measuring bunch waveforms to measure the beam center of each bunch. The position measurement error is approximately 30 and 300 μm for the COD and the BxB modes, respectively [3].

At some BPMC, communication disruption was caused by an unstable contact of a card edge connector. However, this BPMC is too old that some circuit parts have already been discontinued. This makes maintenance work difficult and some BPMCs unusable. If this situation progresses, there is a risk that sooner or later stable MR operation will be hindered.

The BPMC shows the beam position shift due to the change in the contact resistance of a relay. To optimize the input signal level, it has a 20 dB fixed attenuator placed just before the input terminal and a variable attenuator in the BPMC. Depending on the beam condition, the attenuation factor is selected by switching a relay element on the circuit, and its switching frequency is approximately several times per year. The contact surfaces are then exposed to atmospheric gas for a long time because the relay is not strictly shielded. The inspection of the relay surface confirmed that the silicon-based compound was layered. This results in surface contamination and consequently resistance changes. A 0.5 Ω change in contact resistance results in an error of 1.3 mm. Moreover, an error of several millimeters—may occur because of individual differences in relays. This resistance can be reduced by applying a voltage [4]. However, there are large individual differences in this effect, and no clear systematicity has been confirmed so far, therefore, calibration is difficult. To examine the impact of this effect, some consistency check methods between the BPM sensors are now proposed [4, 5].

Moreover, beam tuning above 1 MW is supposed to require high-precision measurement of optics parameters [3]. Thus, it is necessary to process a large amount of highly accurate position data. Improvement of the system is also necessary.

NEW BPM SIGNAL PROCESSOR

We are developing a new signal processor as part of the MR beam power upgrade campaign to 1.3 MW. In the new system, we aim to reduce the position error to 1/3 or less in both modes. To achieve this, we will use the following items:

1. Reduction of the reflection coefficient of the attenuator input terminal,
2. reduction of signal distortion and gain temperature coefficient in the attenuator and ADC,
3. improvement of the vertical resolution of the ADC,
4. improved digital signal processing section.

Figure 1 shows a block diagram of the new system installed in four different buildings. It uses the existing BPM sensors and its signal cables, which are 100-300 m depending on the sensor location. An attenuator unit, ADC card, network interface controller unit (NIC unit), and data storage system have been developed.

The attenuator unit is powered by a nuclear instrumentation module (NIM) standard bin power supply and the ADC card is housed in the same NIM case. The digitized waveform data are delivered over a 10 GbE optical private network and forwarded through the NIC unit to the data storage system. This network uses the user datagram protocol (UDP).

* Work supported by Accelerator and Beamline Research and Technology Development for High-Power Neutrino Beams in the U.S.-Japan Science and Technology Cooperation Program in High Energy Physics.

[†] email address: kenichirou.satou@j-parc.jp

A NOVEL BPM MECHANICAL CENTER CALIBRATION METHOD BASED ON LASER RANGING

Xuhui Tang¹, Yanfeng Sui¹, Jun He, Yaoyao Du, Jianshe Cao, Junhui Yue[†]
Institute of High Energy Physics, Chinese Academy of Science, Beijing, China
¹ also at University of Chinese Academy of Science, Beijing, China

Abstract

Determining the mechanical center of the beam position monitor (BPM) has been a difficulty for BPM calibration. To solve this problem, a method of positioning the BPM mechanical center based on laser ranging is proposed. This method uses high-precision antenna support as the core locating datum, and high-precision laser ranging sensor (LRS) as the detection tool. By detecting the distances from the LRSs to the antenna support and the distances from the LRSs to the BPM, the mechanical center of the BPM can be indirectly determined. The theoretical system error of this method is within 20 μm , and the experimental results show that the measurement repeatability is 15 μm . This method has low cost and fast speed, which can be used for large-scale calibration.

INTRODUCTION

The BPM system, as the eyes of the particle accelerator, plays an important role in the stability of the beam orbit. About 600 BPMs are produced during the construction of High Energy Photon Source (HEPS) project [1]. Due to processing errors, the mechanical center and electrical center of BPM do not coincide. Therefore, each BPM is demanded to calibrate before use [2]. For the button-type BPM with 45-degree rotation, as shown in Fig. 1, the relationship between position coordinates and electrode signal amplitudes is defined as Eq. (1) [3].

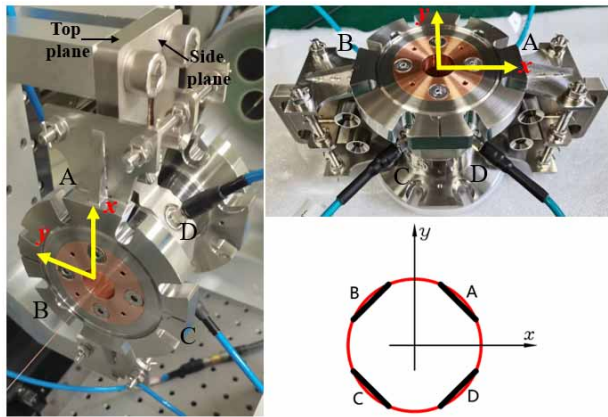


Figure 1: A HEPS BPM and its define of electrode and beam coordinate system.

$$x = K_x \frac{V_a + V_d - V_b - V_c}{V_a + V_b + V_c + V_d} + X_{\text{offset}} = K_x U + X_{\text{offset}} \quad (1)$$

$$y = K_y \frac{V_a + V_b - V_c - V_d}{V_a + V_b + V_c + V_d} + Y_{\text{offset}} = K_y V + Y_{\text{offset}}$$

where K_x, K_y are the BPM sensitivity coefficients, $X_{\text{offset}}, Y_{\text{offset}}$ are the difference between the BPM electrical center and mechanical center. The process of determining $K_x, K_y, X_{\text{offset}}$, and Y_{offset} is called BPM calibration. A BPM automatic calibration system is shown in Fig. 2 and it is composed of an RF signal source, antenna (Goubau line), precision motion stages and their controller, BPM electronics, and the industrial personal computer [4, 5]. The Goubau line emits transverse electromagnetic (TEM) waves with the excitation of the RF signal source, so as to simulate the electromagnetic field of the charged particle beam in the accelerator to enable BPM calibration [5]. The BPM is driven by the precision motion stages to move in horizontal and vertical directions. The industrial computer saves the real BPM position data recorded by the controller and the calculated BPM position data from the BPM electronics. Then, the sensitivity coefficients and offsets are analyzed by the software algorithm.

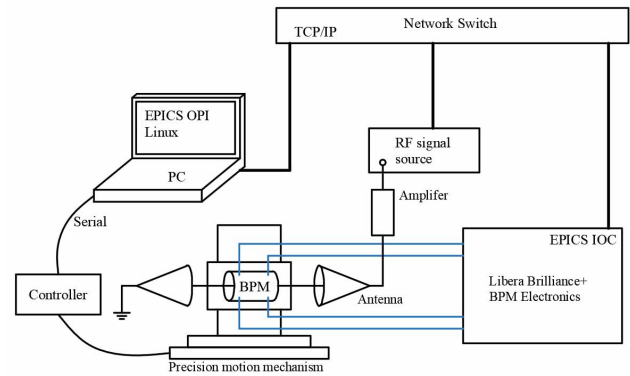


Figure 2: Schematic of BPM automatic calibration system.

In general, it is relatively easy to ascertain the BPM electrical center, as long as the operator observes the four channels of BPM electronics and makes them equal by adjusting the BPM motion stage. To achieve this goal, it is necessary to ensure that the four channels of BPM electronics and the coaxial cables are calibrated. However, finding the mechanical center is extremely difficult, so it is hard to determine X_{offset} and Y_{offset} .

A NEW APPROACH TO DETERMINING BPM MECHANICAL CENTER

The main difficulties in calibrating the mechanical center are as follows: firstly, it is not easy to ensure that the antenna is parallel to the axis of BPM; Secondly, it is almost impossible to directly measure the distance between

DEVELOPMENTS OF 4GSR BPM ELECTRONICS

Si-Won Jang*, Garam Hahn, Jung Yun Huang, Changbum Kim, Dotae Kim, Gyu-jin Kim, Bokkyun Shin, DongCheol Shin, Donghyun Song
 Beam Instrumentation Group, PAL, Pohang, South Korea
 Woojin Song, POSTECH, Pohang, South Korea

Abstract

The emittance of the 4th-generation storage ring (4GSR) to be constructed in Cheongju-Ochang, Korea, is expected to be approximately 100 times smaller than the existing 3rd-generation storage ring. With the decrease in emittance, more precise beam stabilization is required. To meet this requirement, the resolution of the beam position monitor (BPM) system also needs to be further improved. We have conducted research and development on the electronics of the BPM system for the 4GSR storage ring. In order to perform fast orbit feedback in the 4GSR storage ring, we need to acquire turn-by-turn beam position data, with a desired beam position resolution of 1 μm . Additionally, prototypes of the bunch-by-bunch monitoring system are being developed for the transverse feedback system and longitudinal feedback system. The internally developed electronics are intended to be modified for future use as monitors for multi-bunch beam energy measurements at the end of the linear accelerator, by adjusting the logic accordingly. In this presentation, we will describe more details of the current status of the development of the beam position monitor electronics for the 4GSR in Korea.

INTRODUCTION

To achieve precise beam orbit stability in the 4th-generation storage ring with an emittance about 100 times smaller than the existing 3rd-generation storage ring [1], a more precise beam position monitor system with higher resolution is required. Figure 1 shows the construction view map of Korea 4GSR. In addition, the design of the 4GSR BPM electronics should be measure and provides Turn by Turn beam position data for Fast Orbit Feedback (FOFB) system with 375 kHz rate, which is a revolution frequency of 4GSR storage ring.



Figure 1: Construction view map of Korea 4GSR.

DEVELOPMENT STRATEGY OF 4GSR BPM ELECTRONICS

The strategy for developing 4GSR BPM electronics is as follows: First, we aim to develop BBB (Bunch by Bunch) BPM electronics capable of providing the highest performance for bunch-by-bunch beam position measurements. Subsequently, using this technology as a foundation, we will proceed to develop TbT (Turn by Turn) BPM electronics specifically tailored for the 4GSR storage ring. By integrating the front-end and back-end electronics, we will create Transverse & Longitudinal feedback systems (TFS & LFS), referred to as TFS & LFS BPM electronics.

Following this, we plan to adapt the data processing logic of the BBB electronics into a single-pass logic. This adaptation will enable us to install these electronics along the LTB (Linac. to Booster) beamline in the linear accelerator backend. They will serve as multi-bunch beam energy measurement monitors. The diagram below illustrates the development strategy for 4GSR BPM electronics. Figure 2 shows that the development strategy of 4GSR BPM electronics systems.

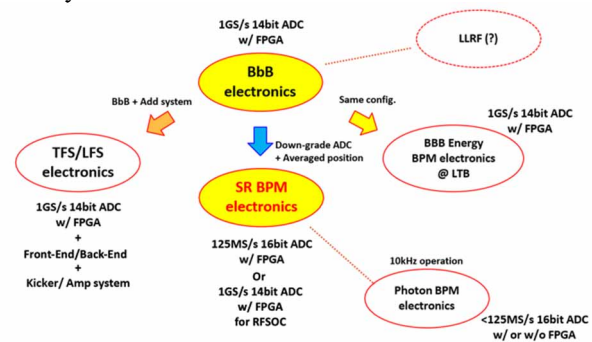


Figure 2: Development strategy of 4GSR BPM electronics.

Development Status of BBB BPM Electronics

The BBB electronics are currently in the prototype development phase [2], and we are undergoing several beam tests to ensure the system's stability. By configuring the desired storage ring parameters and turn counts, we have confirmed the capability of measuring the beam position for all bunches.

Figure 3 shows signal processing logic of BBB electronics. The signal processing procedure of BBB electronics as follows: To obtain a sufficient amount of bunch information, data is collected over several turns. Subsequently, the ADC data from every bunch is rearranged to calculate the beam position information for all bunches in the time domain. However, as previously mentioned, BBB Electronics is also adaptable for use with TbT BPM Electronics.

*siwon@postech.ac.kr

A STUDY INTO THE LONG-TERM STABILITY OF FRONT END X-RAY BEAM POSITION MONITOR SUPPORT COLUMNS AT DIAMOND LIGHT SOURCE

C. Houghton*, C. Bloomer, L. Bobb, D. Crivelli, H. Patel, J. Melton
Diamond Light Source, Oxfordshire, United Kingdom

Abstract

Sand-filled steel columns are used at Diamond Light Source to support front end X-ray beam position monitors. This approach is chosen due to the relatively large thermal mass of the sand being considered useful to reduce the rate at which expansion and contraction of the column occurred as the storage ring tunnel temperature varied, particularly during machine start-up. With the higher requirements for mechanical stability for the upcoming Diamond-II upgrade, there is now a need to assess and quantify the current system's impact on X-ray beam movement. A study of thermal and mechanical stability has been carried out to quantify the stability performance of the front-end X-ray beam position monitor's columns and the impact that column motion may have on the X-ray beam position measurement. Measurements have been made over a range of different timescales, from 250 Hz up to 2 weeks. The measured stability of the support column is presented, showing that it meets our Diamond-II stability requirements. A comparison of the stability of the column with and without a sand filling is presented.

INTRODUCTION

To monitor and improve the stability of the photon beams, Diamond Light Source utilises X-ray beam position monitors (XBPMs) on most insertion device (ID) front ends. Each XBPM is mounted on a steel support column bolted to the synchrotron floor. Currently, the XBPMs are used as a diagnostics tool, monitoring long-term trends and in some cases for slow (0.2 Hz) beam position feedback [1]. After the Diamond-II upgrade, it is proposed that the front end XBPMs could be included in more critical orbit feedback systems. Therefore the mechanical stability of the XBPMs needs to be assessed. Motion of the steel columns arises from various sources, the largest contribution coming from the vertical thermal expansion of the steel over time, correlated with ambient temperature changes in the tunnel.

Each column is constructed from a hollow square tube with external dimensions of 200 mm x 200 mm and a wall thickness of 10 mm. The manufacturer, FMB Berlin GmbH, specifies that the column is produced using S235JR steel, with a coefficient of linear thermal expansion of $12 \times 10^{-6} \text{ K}^{-1}$.

The columns are bolted to the concrete floor using four 50 mm long M12 bolts. One of the open questions this work is intended to answer was whether the steel base of

the XBPM pressed into the floor by the tension of these four bolts is sufficient to thermally couple the column to the thermal mass of the synchrotron floor slab, or if the column temperature is more correlated with ambient air temperature.

Each column is filled with fine sand intended to improve the thermal stability of the column by increasing its thermal mass. Experimental data was first acquired with the column in its original state, filled with sand. Then, during a machine shutdown, the sand was vacuumed out of the column (approximately 30 kg of dry sand), leaving it hollow, and the experiments were repeated.

EXPERIMENTAL SET-UP

Laser Interferometry

In this experiment a laser-interferometry system¹ was utilised to track variations in the height of the XBPM support column. The setup involved positioning one of the detector heads on the top of the XBPM vessel using a mounting bracket. A plane mirror was positioned on the ground and aligned to the laser beam such that the light is reflected back along the incident path. Figure 1 presents a sketch of this system.

Interferometry, the principle underlying this setup, exploits the wave nature of light. When the laser beam splits and travels different paths – one directly to the detector and the other along the length of the column to the mirror and then to the detector – they recombine, forming an interference pattern. By analysing this pattern, a measurement of the column height variation over time periods of 1 s to days is acquired. For background information on the various principles behind modern interferometry measurements, a useful introduction can be found in [2, 3].

Thermal Monitoring

The temperature of the column, the air, and the concrete floor upon which the column was bolted were measured in order to correlate any variation in column height to the temperature of the column and its surroundings.

A total of five temperature sensors, with a thermal resolution of 0.025 °C, were attached to the support column, on different faces of the column and at different heights. The intent of this was to determine if there were any temperature gradients across the column, or if non-uniformity of the column temperature could lead to bending or twisting of the column as different sides of it expanded or contracted at different rates. One temperature sensor was bolted into a

* claire.houghton@diamond.ac.uk

¹ Renishaw RLE10.

ONE DIMENSIONAL BEAM POSITION MONITOR PROTOTYPE USING INCOHERENT CHERENKOV DIFFRACTION RADIATION

A. Clapp*, Royal Holloway University of London, Egham, UK
 also at Diamond Light Source, Didcot, UK
 P. Karataev, Royal Holloway University of London, Egham, UK
 L. Bobb, G. Cook, Diamond Light Source, Didcot, UK

Abstract

This paper proposes a novel advancement in both the studies of Cherenkov diffraction radiation (ChDR) and beam instrumentation. The proposed beam position monitor (BPM) consists of two identical fused Silica prism radiators, with a fibre collimator attached to each one, which in turn are connected to a photodetector via a series of optical fibres. The setup will be implemented into the booster to storage ring transfer line at Diamond Light Source - an electron light source with 3 GeV beam energy. The prototype proposed aims to test the feasibility of a full BPM utilising ChDR. If proven to be fully realisable, optical rather than capacitive BPM pickups could be more widely distributed. The paper will include the complete design and preliminary results of a one-dimensional BPM, utilising the ChDR effect.

INTRODUCTION

Cherenkov radiation (CR) is the emission of electromagnetic radiation when a charged particle travels through a dielectric medium with a speed greater than that of light in that medium. Observed in 1934 by Cherenkov [1], it has since been expanded upon both theoretically and experimentally. Cherenkov radiation is emitted at a well defined angle denoted the Cherenkov angle θ , given by

$$\cos \theta = \frac{1}{\beta n} \quad (1)$$

where $\beta = v/c$ is the ratio of the charged particle velocity v to the speed of light c , and n is the refractive index of the medium the charged particle is travelling through [1]. The emission and directionality of Cherenkov radiation enables this phenomena to be a useful tool in many fields ranging from astrophysics [2] to radiotherapy [3].

The theory of CR has been expanded to account for the situation where the incident relativistic particle is instead travelling close by a medium acting in a manner similar to classical diffraction radiation [4] called Cherenkov Diffraction Radiation [5]. In addition to particle energy and the refractive index of the medium, ChDR is dependent on the impact parameter b which represents the distance between the incident charged particle and the medium. ChDR is produced by a hyper-relativistic particle travelling close to a medium, rather than through it, and given that ChDR is emitted at the well defined Cherenkov angle it is well suited for accelerator diagnostic applications where a non-invasive technique is of paramount importance.

* alec.clapp.2021@live.rhul.ac.uk

The intensity of light emitted increases the closer the particle is to the medium, as such it is necessary to ensure that the incident particle is within the condition

$$b \leq \gamma \lambda \quad (2)$$

where γ refers to the Lorentz factor of the incident particle and λ refers to the wavelength of emitted radiation. The quantity $\gamma \lambda$ refers to the effective electron field radius [6].

For optical wavelengths and an electron beam energy of 3 GeV $b \leq 3$ mm. ChDR has been investigated experimentally and had its applicability to diagnostics examined [7, 8].

BTS TEST STAND

The experiment is located on the Booster To Storage (BTS) transfer line at Diamond Light Source (DLS). The test stand consists of a six-way cross vacuum chamber with a four-dimensional manipulator system which allows for the insertion and removal of experiments. Vertical translation and rotation of the manipulator are automated. It was previously used for another ChDR experiment [9], which tested feasibility of beam position measurements and fundamental ChDR properties.

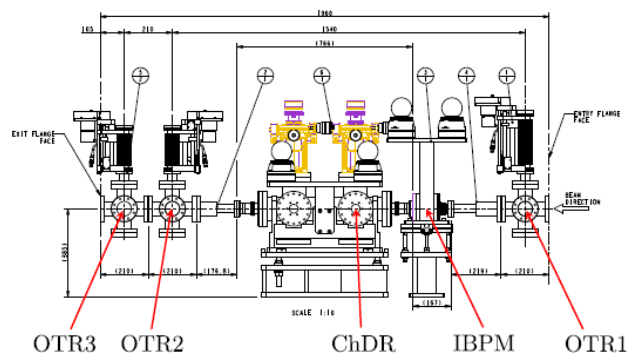


Figure 1: Schematic of BTS test stand.

Figure 1 shows a schematic of the vacuum vessel string on the BTS test stand consisting of three combined Optical Transition Radiation (OTR) and Yttrium Aluminium Garnet (YAG) monitors, and one Inductive Beam Position Monitor (IBPM) developed at CERN [10]. These diagnostic tools are used as references for the beam profile and trajectory through the BTS test stand when taking data with the ChDR BPM. The IBPM provides a reference beam position measurement, which the results from the ChDR BPM are compared against. The first OTR screen is used to measure

Content from this work may be used under the terms of the CC-BY-4.0 licence (© 2023). Any distribution of this work must maintain attribution to the author(s), title of the work, publisher, and DOI

1L TARGET HARP DIAGNOSTIC DISPLAY TOOL*

A. Walker, E. Kerstiens

Los Alamos National Laboratory, Los Alamos, NM, USA

Abstract

The Los Alamos Neutron Science Center (LANSCE) completed upgrades to its 1L Target Facility, which included installing the new Mark IV target assembly. This added a third tungsten target located upstream of the other two targets. Prior to Mark IV, beam centering on target was achieved by using thermocouples mounted to the quadrants and center of the upper target coolant chamber. It is slightly offset from center of the old upper target and it shadows several of the thermocouples previously used to center beam on target. This required adjustments to the diagnostic tools utilized to monitor position of the H- beam that is being delivered to the 1L target. The original display included the thermocouple readouts and displayed a visual beam profile and position taken from an upstream harp. With some of the thermocouples now being shadowed, an image overlay was added to show where the harp's measured beam position is relative to both the upper and middle targets. This gives the beam operations team an additional level of awareness when it comes to thermocouple temperatures, beam steering, and beam tuning. Details of the display tool and its associated upgrades are presented.

INTRODUCTION

1L HARP Purpose

The purpose of the 1L Target [1] HARP is to provide a profile of beam location as it strikes the target stack. The HARP works in tandem with wire scanners to assist the operations team in beam tuning and loss minimization. The HARP is an extremely valuable tool since the new Mark IV target has been installed. The HARP has a similar program to the wire scanners to show beam position.

1L HARP Diagnostic Display Purpose

The 1L Target HARP Display is an aid to the operations team to provide a graphical representation of beam position. The display aggregates the data from the 1L HARP and utilizes a Gaussian distribution algorithm to provide a "heat map" graphical representation. The display also shows a set of thermocouples that are utilized to further analyze the beam position and intensity.

1L HARP CONSTRUCTION

The 1L Target HARP diagnostic is a set of wires spaced out in the beam line in a grid formation to gather a beam profile. An electrical current is induced in them proportional to beam intensity, which shows the beam profile similar to the wire scanners. The upside to the HARP is it is constantly in the beam line and due to that can be provide

constant updates to the beam position. The 1L HARP data can be utilized in a Gaussian fit algorithm to provide a beam position and intensity map. Figure 1 below shows the 1L HARP assembly and wire harness that is part of the 1L Target assembly.

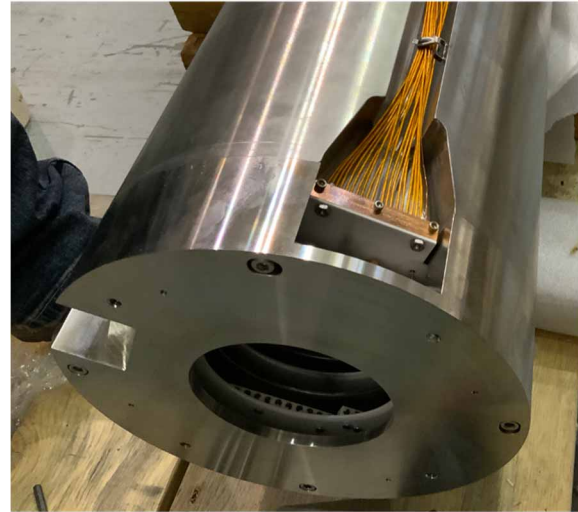


Figure 1: 1L HARP Diagnostic Assembly.

WIRE SCANNERS

1L (Target 1) wire scanner 1, 2, and 3 provides a picture of the beam profile as it is being directed to the target, but don't provide a "live" status of the beam in the event of a tune change. They utilize a single wire inserted in steps in order to get a beam profile. This "live" status is extremely important, and the wire scanners cause significant beam spill making them ineffective for the information needed to visualize. Figure 2 shows a wire scan performed to show beam position in the X and Y axis.

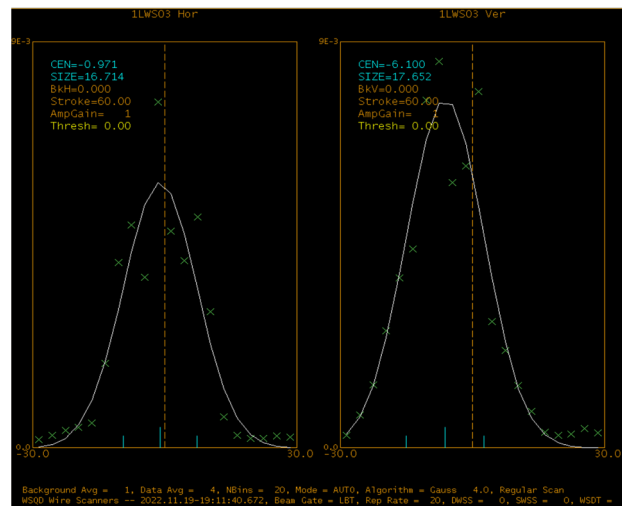


Figure 2: Wire Scanner Diagnostic Tool.

*Work supported by the U.S. Department of Energy, Contract No. DE-AC52-06NA25396

A NEW APPROACH FOR CANADIAN LIGHT SOURCE FUTURE ORBIT CORRECTION SYSTEM DRIVEN BY NEURAL NETWORK

S. Saadat* and M. J. Boland¹, Canadian Light Source, Saskatoon, Canada
¹also at University of Saskatchewan, Saskatoon, Canada

Abstract

The orbit correction system (OCS) of the Canadian Light Source (CLS) comprises of 48 sets of BERGOZ beam position monitors (BPM). Each BPM has the ability to measure the position of the beam in both the X and Y directions and can record data at a rate of 900 Hz times per second. Inverse Response Matrix (IRM) is utilized to determine the optimal strength of the 48 sets of orbit correctors in both the X and Y directions, in order to ensure that the beam follows its desired path. The suggestion in this study is to replace the singular value decomposition (SVD) function with a neural network algorithm, which will act as the central processing unit of the orbit correction system. The training model's design includes three hidden layers, and within each layer, there are 96 nodes. The neural network's outputs for regular operations in CLS exhibit a mean square error (MSE) of 10^{-7} . Various difficult scenarios were created to test the OCS at 8.0 mA, using offsets in different sections of the storage ring. However, the new model was able to produce the necessary orbit correctors (OC) signals without any trouble.

INTRODUCTION

The CLS synchrotron light source storage ring consists of twelve sections and operates at a 2.9 GeV energy level. To maintain the stability of the beam position in the storage ring, an Orbit Correction System is utilized to correct any disturbances.

In 2000, the Motorola single-board computer was the initial implementation of a real-time controller [1]. In 2008, the previous system for correcting the orbit was upgraded and replaced by the current OCS [2]. In 2009, CLS developed and tested a new orbit correction system the CLS Matlab application, known as CLSORB, with a high-speed capability [3]. This system offers an adjustable rate range of 20 Hz to 100 Hz.

The OCS at CLS comprises a computer that runs Matlab, along with four Versa Module Eurocards (VMEs). Each VME corresponds to three sections of the storage ring. Additionally, the system also incorporates a Real-Time Executive for Multiprocessor System (RTEMS). The purpose of this advanced system is to ensure that any disturbances caused by electron perturbations are immediately detected and corrected to maintain beam stability and optimal light quality at the beamlines. Hardware and software of the orbit control systems were developed until the RMS deviation of beam motion was reduced to less than one micrometer in both the X and Y directions. The Accelerator Operations and Development (AOD) team is currently working on upgrading

this system, which suggests that there are new developments underway to enhance its functionality and capabilities. This involves improving its efficiency, increasing its accuracy, or adding new features to meet the evolving needs of users. With technological advancements being made every day, it is important to keep upgrading existing systems to stay relevant and efficient in a rapidly changing landscape. The AOD team has embarked on new research to design a Dynamic Orbit Correction System (DOCS) based on Neural Network (NN) algorithm for the orbit correction system. The NN correction system offers advantages over the IRM algorithm, excelling in dynamic adaptability, flexible programming, and computation speed. Unlike the static IRM, the NN system learns from data, making it accurate in changing conditions. Its adaptable nature handles misalignments effectively. The NN's efficient script allows customization and rapid computations, while IRM's matrix recalculations slow it down. The precision and real-time capabilities of this DOCS have been reported [4]. The aim of this research is to improve the accuracy of the neural network model by incorporating deep learning techniques. To achieve this goal, we will conduct experiments and analyze the data to determine the effects of deep learning methods on accuracy.

NEURAL NETWORK

A neural network is a type of machine-learning model inspired by the structure and function of the human brain. It consists of interconnected nodes or neurons that process information to make predictions or decisions [5]. Also, deep learning is a subfield of machine learning that uses neural networks with multiple layers to extract and learn features from data. It is capable of automatically discovering complex patterns and relationships in large datasets [6].

The following sections will briefly discuss the neural network architecture and parameters utilized in the CLS orbit correction system model, and also provide a definition of deep learning loops.

Network Architecture

Designing a neural network architecture requires a significant amount of information about the real system it will be applied to, as the architecture is highly dependent on the specific characteristics and structure of the system. In brief, the CLS orbit correction system is comprised of 96 Bergoz Beam Position Monitors (BPMs) that transmit the beam's position to the IRM at a frequency of 900 measurements per second. The IRM serves as the central processing unit of the OCS, responsible for computing the strength of the Orbit Correctors. Ultimately, the 96 outputs from the IRM

* shervin.saadat@lightsources.ca

TUNE FEEDBACK AT THE CANADIAN LIGHT SOURCE

W. A. Wurtz*, C. K. Baribeau, A. M. Duffy
 Canadian Light Source, Saskatoon, Saskatchewan, Canada

Abstract

In order to maintain good injection efficiency for top-up operation at the Canadian Light Source, we must keep the betatron tunes constant even as changes in insertion device fields cause the tunes to vary. To meet this requirement, we implemented a tune feedback system. We measure the tunes at a rate of 1 Hz using Dimtel bunch-by-bunch systems. The transverse feedback function of the bunch-by-bunch systems provides tune measurements without disturbing the electron beam. We adjust two quadrupole families at a rate of 0.25 Hz to control the horizontal and vertical tunes. In this article we describe the tune feedback system, its development and its performance. The system has proven to be very robust, enabling reliable top-up operation.

INTRODUCTION

The Canadian Light Source (CLS) began operating in top-up mode for user operations in 2021. In top-up mode, charge is injected into the storage ring every few minutes to maintain a constant current with the present target being between 219 and 220 mA. Top-up requires reliable and efficient injection, and the tune feedback application is an important part of our top-up implementation. We developed the tune feedback application in an iterative manner, incorporating feedback from operators and subject matter experts. Through each iteration we identified operational issues, implemented corrections or new features to resolve the issues, tested the new features and their interactions with existing features and deployed the new version. The resulting product can gracefully handle a variety of situations and provides an alarm and diagnostic information for the operators. The algorithm is adjustable for machine studies outside of user mode, or to implement workarounds while we resolve issues with external systems. Overall, the tune feedback application has been successful and top-up operation has been reliable.

TUNE AND INJECTION

For top-up mode, we desire that >90% of the charge injected into the storage ring be captured. We measure the stage 2 injection efficiency using an integrating current transformer (ICT) at the end of the transfer line and the parametric current transformer (PCT) in the storage ring. Because there is some uncertainty in the ICT calibration, we give the stage 2 injection efficiency in arbitrary units (a.u.) with a stage 2 efficiency of 97 a.u. meaning that somewhere between 94 and 100% of the electrons were captured.

We have previously reported on injection efficiency issues caused by a superconducting wiggler, BMIT SCW4 [1], and an elliptically polarizing undulator, SM EPU75 [2]. We show

* ward.wurtz@lightsources.ca

updated injection efficiency tune scans for these devices in Fig. 1. The nominal tunes, represented by a diamond marker, are 10.242 for the horizontal and 4.290 for the vertical. We see that the nominal tunes are on a small island of good injection efficiency, and if the tunes were to shift, the stage 2 efficiency would quickly become unacceptable. Tune shifts are mostly caused by insertion device field changes.

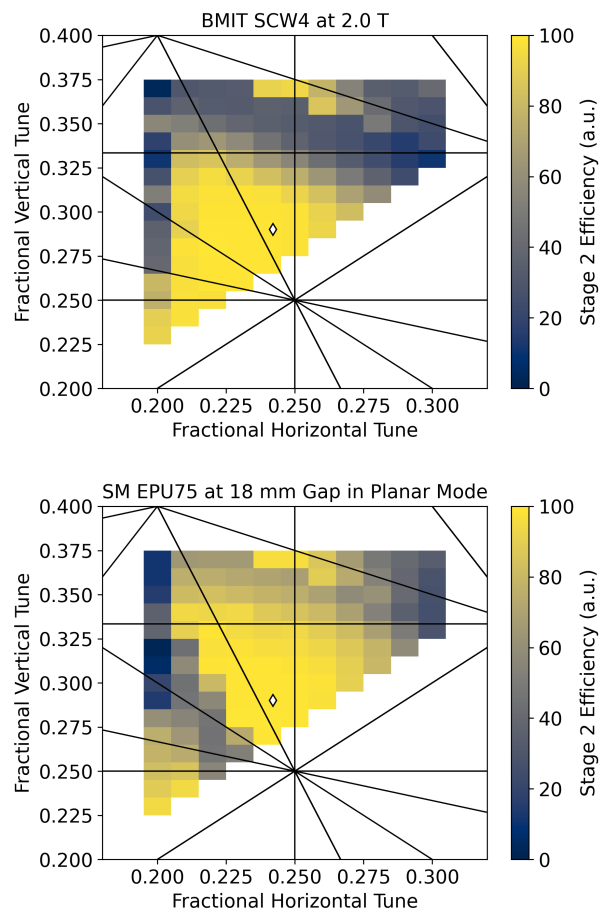


Figure 1: Measurements of injection efficiency as a function of the fractional tunes for two insertion devices with all other insertion devices forced open or turned off. We operated the BMIT SCW4 at approximately half its maximum field in order to avoid quenching the device during the measurement.

We do not measure the integer portions of the tunes during normal operations and obtain the fractional portions by performing a Fourier transform of position data. In this work, if we say that the horizontal tune is 0.242, the integer portion is understood to be 10, and similar for the vertical with an integer portion of 4.

Content from this work may be used under the terms of the CC-BY-4.0 licence (© 2023). Any distribution of this work must maintain attribution to the author(s), title of the work, publisher, and DOI

DEVELOPMENT OF AN ACTIVE BEAM-STABILIZATION SYSTEM FOR ELECTROFISSION EXPERIMENTS AT S-DALINAC*

D. Schneider[†], M. Arnold, U. Bonnes, A. Brauch, M. Dutine, R. Grewe,
L. E. Jürgensen, N. Pietralla, F. Schließmann, G. Steinhilber

Technische Universität Darmstadt, Institute for Nuclear Physics, Darmstadt, Germany

Abstract

The r-process fission cycle terminates the natural synthesis of heavy elements in binary neutron-star mergers. Fission processes of transuranium nuclides will be studied in electrofission reactions at the S-DALINAC. Due to the minuscule fissile target, the experimental setup requires an active electron-beam-stabilization system with high accuracy and a beam position resolution in the submillimeter range. In this contribution, requirements and concepts for this system regarding beam diagnostics elements, feedback control and readout electronics are presented. The usage of a beam position monitor cavity and optical transition radiation targets to monitor the required beam parameters will be discussed in detail. Additionally, various measurements performed at the S-DALINAC to assess requirements and limits for the beam-stabilization system will be presented. Finally, the option to use advanced machine learning methods, such as neural networks and agent-based reinforcement learning, will be discussed.

INTRODUCTION

The superconducting Darmstadt linear electron accelerator (S-DALINAC) at the institute for nuclear physics at the Technische Universität Darmstadt is used for scientific research in nuclear spectroscopy and meteorology, nuclear astrophysics and accelerator science [1] and can be operated in energy-recovery modes [2, 3]. The current layout of the S-DALINAC is shown in Fig. 1. Due to its superconducting design the accelerator is able to provide a continuous-wave electron beam at a frequency of 2.997 GHz with a kinetic design energy of up to 130 MeV. The beam quality can be further improved using the scraper systems located in both the low and high energy sections to reach its minimum design energy spread of 10^{-4} with bunch lengths of smaller than 2 ps [4]. The electron beam can be utilized at various experimental setups including the QCLAM magnet spectrometer. Multiple high-resolution (e, e') and (e, e', γ) coincidence experiments have been conducted successfully at the QCLAM [5, 6].

Within the cluster project ELEMENTS a new series of measurements based on electron-induced fission at S-DALINAC is proposed to aim at a better understanding of the natural synthesis of heavy elements in our universe. While the details of the proposed experiment are provided

in the following chapter, the requirements for the accelerator facility are challenging due to the minuscule radioactive target of 1 mm, the request of ultra-short bunch lengths in the order of 1 ps and the demand for stable beam conditions for several hundreds of hours of measurement. In particular, the monitoring and control of the beam spot size and position are of importance.

Therefore, a new active beam-stabilization system is being designed for electrofission experiments at the QCLAM spectrometer at the S-DALINAC. This project includes the commissioning of beam diagnostics elements and correction magnets including an in-house developed beam position and phase monitor. Additionally, the electronics layout for signal readout and processing will be designed. The focus is on utilizing existing in-house developed electronics and commercially available solutions. As feedback control algorithm both the performance of traditional PID (Proportional–integral–derivative) controllers and machine learning methods will be assessed. To test and optimize the control mechanism beforehand, the creation of a virtual test environment based on neural networks and beam dynamics simulations are planned.

ELECTROFISSION AT S-DALINAC

In order to investigate fission reactions of actinides and their dependence of the excitation energy of the nucleus, electron-induced fission will be employed at the S-DALINAC. It allows the determination of the excitation energy of the actinide target nucleus. Additionally, higher multipoles can be excited and studied.

A schematic representation of the proposed electrofission setup is shown in Fig. 2. The electron beam will be delivered by S-DALINAC with a beam current of 3 μ A, electron energies of the order of 100 MeV and a 3σ beam spot size smaller than 1 mm at the electrofission interaction point. The electrofission target has a diameter of 1 mm and a target thickness of approximately 350 μ g/cm². After its interaction with an electron the target nuclei can decay via fission. An accurate description of this process, which is not available up to date, requires the measurement of both fission fragments in coincidence. While e.g. photon-induced fission primarily excites E1 transitions, in electrofission higher multipole orders such as E2 and E3 can be excited. As electron scattering experiments allow the decoupling of excitation energy and momentum transfer, a model-independent multipole decomposition using the electrofission cross section [7]

* Work supported by DFG (GRK2128), BMBF, the state of Hesse within Research Cluster Project ELEMENTS and the LOEWE Research Group Nuclear Photonics

[†] dschneider@ikp.tu-darmstadt.de

TRANSVERSE MULTI-BUNCH FEEDBACK DETECTOR ELECTRONICS USING DIRECT SAMPLING ANALOG-TO-DIGITAL CONVERTERS FOR THE SYNCHROTRON RADIATION SOURCE PETRA IV

S. Jablonski*, H.-T. Duhme, U. Mavrič, S. Pfeiffer, H. Schlarb
Deutsches Elektronen-Synchrotron, Hamburg, Germany

Abstract

PETRA IV, a new fourth generation synchrotron radiation source planned at DESY, will require a transverse multi-bunch feedback (T-MBFB) system to damp transverse instabilities and keep the beam emittance low. The critical part of the T-MBFB is a detector that must measure bunch-by-bunch, i.e. every 2 ns, position variations with the resolution not worse than 1 μm for the beam dynamic range of ± 1 mm. In this paper, we present the conceptual design of the T-MBFB detector from the beam position pickups to the direct sampling ADCs. We analyze noise sources limiting the detector resolution and present measurement results based on the evaluation modules.

INTRODUCTION

PETRA IV will operate in two modes, i.e. the brightness and timing mode. The requirements for the T-MBFB are summarized in Table 1. Due to short bunch spacing of 2 ns and low bunch charge of 0.4 nC in the brightness mode, it is more challenging to fulfill the resolution requirement of 1 μm in this mode than in the timing mode. Therefore, all performance calculations in this paper are done for the brightness mode. It is expected that in the timing mode the results are similar or better.

T-MBFB DETECTOR SCHEME

Figure 1 presents a simplified block diagram of the vertical T-MBFB detector electronics. The horizontal detector differs only in the connection of the stripline electrodes to the combiners in such a way that the detector is sensitive to horizontal bunch variations. Hence, it will not be discussed further in the text.

The stripline BPM is composed of four electrodes equally distributed around the beam pipe, i.e. every 90°, with a characteristic impedance Z_o of 50 Ω . For the vertical beam position measurement, electrical pulses from the upper and lower pick-ups are combined together, creating signals V_{AB} and V_{CD} , respectively. The signals are doubled in the pulse multiplier, and further, they are subtracted from each other in the bunch offset compensation. The difference signal ΔV is fed to the front-end electronics (DRTM-MBFB-FE) and the digitizer (DAMC-DS5014RT), which are implemented in the MicroTCA.4 form factor. The above mentioned hardware is described in more detail in the following sections.

* szymon.jablonski@desy.de

Table 1: PETRA IV design parameters in the brightness (B) and timing (T) mode and the requirements for the T-MBFB.

Design Parameter	Value
Energy E	6 GeV
Revolution freq. f_{rev}	130.12 kHz
Emittance ϵ_x/ϵ_y	< 20/4 pm rad (B) < 50/10 pm rad (T)
Total current I	200 mA (B), 80 mA (T)
Number of bunches	max. 3840 (B), 80 (T)
Bunch charge q_b	~ 0.4 nC (B), ~ 7.7 nC (T)
Bunch spacing T_{rep}	2 or 4 ns (B), 96 ns (T)
Bunch length σ_t	~ 45 ps (B), ~ 64 ps (T)
Betatron freq. f_x/f_y	23.4 kHz, 35.2 kHz
T-MBFB det. bandwidth	750 – 1250 MHz
Max. bunch offset r_{dc}	± 1 mm (from vacuum chamber center)
Max. betatron osc. amplitude r_{ac}	± 1 mm
T-MBFB det. resolution	< 1 μm (SNR > 60 dB)
T-MBFB damping time	< 40 turns (for $r_{ac} < 200 \mu\text{m}$)

MODEL OF THE PICKUPS AND ANALOG ELECTRONICS

Electron Bunch in the Vacuum Chamber Center

The frequency-domain transfer impedance of a stripline cylindrical electrode can be modelled as [1]:

$$Z(\omega) = j \frac{\alpha}{2\pi} Z_o \exp \left[-j\omega \left(\frac{L}{c_0} + \Delta t \right) \right] \frac{\sin(\omega\Delta t)}{\omega\Delta t} \sin \left(\omega \frac{L}{c_0} \right), \quad (1)$$

where c_0 is the speed of light in vacuum, L is the length of the electrode, R is the radius of the vacuum chamber, α is the electrode width in rad (geometric coverage factor), Δt is a time delay given by $\Delta t = R\alpha/c_0$. Assuming the electron bunch traveling in the middle of the vacuum chamber is a point charge in the transverse direction and has a Gaussian shape in the longitudinal direction with the rms bunch length of σ_t , the stripline coupler output voltage is

$$V(\omega) = Z(\omega)q_b \exp \left[\frac{-(\omega\sigma_t)^2}{2} \right], \quad (2)$$

where q_b is the bunch charge.

Figure 2 presents amplitude spectrum at the stripline coupler output for the brightness mode (3840 bunches, rep. rate

MODIFIED FAST ORBIT FEEDBACK CONTROLLER FOR DISTURBANCE ATTENUATION IN LONG STRAIGHTS FOR DIAMOND-II *

S. Banerjee^{1,†}, I. Kempf^{1,2}, M. Abbott¹, L. Bobb¹,
¹ Diamond Light Source, Didcot, United Kingdom
² University of Oxford, Oxford, United Kingdom

Abstract

At Diamond Light Source, the fast orbit feedback (FOFB) uses one array of correctors and the controller is designed using the internal model control (IMC) structure. The Diamond-II upgrade will introduce an additional array of fast correctors and a new controller that is designed using the generalised modal decomposition, increasing the overall closed-loop bandwidth from 140 Hz to 1 kHz. Although simulation results have shown that the resulting beam displacement is within specification in all straights, they have also shown that the performance on long straights is limited, particularly in the vertical plane. In this paper, the controller is tuned in order to increase the FOFB performance in long straights by introducing a mode-by-mode regularisation parameter. The performance of the controller beyond 1 kHz is assessed using new disturbance data and a new measurement noise model, showing that the Diamond-II performance criteria are met, even in the presence of measurement noise.

INTRODUCTION

At Diamond Light Source (Diamond), the fast orbit feedback (FOFB) attenuates disturbances in the storage ring and reduces the root-mean square deviation of the electron beam to $\leq 10\%$ of the beam size up to 140 Hz in both planes. The FOFB uses 173 beam position monitors (BPMs) and 172 identical corrector magnets, and the control algorithm is based on the internal model control (IMC) structure, which is naturally amenable to systems with large time delays. The controller is designed using the modal decomposition, which decouples the multi-input multi-output (MIMO) systems into sets of single-input single-output systems using the singular value decomposition (SVD) of the orbit response matrix (ORM) [1].

Due to advances in detector speed and resolution at Diamond-II [2], the beam stability requirements are raised to 3% of the beam size up to 1 kHz, such as shown in Table 1. The increased closed-loop bandwidth in turn requires to introduce an additional corrector type. The FOFB at Diamond-II will use 252 slow correctors with a bandwidth of ~ 200 Hz and 144 fast correctors with a bandwidth of ~ 8 kHz. To accommodate the fast correctors, the Diamond FOFB controller has been extended and adapted to the Diamond-II configuration [3]. Analogous to Diamond, the MIMO system is decoupled into sets of two-input single-output (TISO) and SISO systems using the generalised singular value decomposition (GSVD), which is a two-matrix factorisation

Table 1: Beam Size, Relative and Absolute Orbit Stability Requirements at Standard Straight Source Points [2].

Parameter	Diamond	Diamond-II
Beam size H/V	123 μm /3.5 μm	30 μm /4 μm
Rel. stability	10 % up to 100 Hz	3 % up to 1 kHz
Abs. stability H/V	12 μm /0.35 μm	0.9 μm /0.12 μm

H: horizontal, V: vertical, BW: bandwidth

technique [4]. The decoupled systems are then embedded in the IMC structure and the controllers designed using mid-ranging control [5]. In addition, a tunable regularisation matrix is included in the feedback loop to avoid large control inputs and increase the robustness of the controller.

As part of the Diamond-II design, the performance of the new control algorithm has been assessed using estimates of the Diamond-II disturbance [6]. Although this has shown that the Diamond-II controller meets the beam stability requirements, it has also shown that the performance for primary BPMs on the long straights of the new multi-bend achromat (MBA) lattice is worse than on the standard straights and mid straights. To reduce this performance difference, this paper extends the approach presented in [3] by introducing mode-based weights for the regularisation matrix, increasing the control effort for primary BPMs on long straights. The performance of the FOFB is then reassessed, considering both disturbance and a new measurement noise model.

DISTURBANCE

The Diamond-II disturbance data presented in Ref. [6] has been extended from 1 kHz to 2.44 kHz. The data includes power spectral density (PSD) estimates of ground and girder vibrations, RF and power supply noise, and is scaled using the local beta function to obtain the disturbance profile at each BPM, such as shown in Fig. 1 for the upstream primary BPM of the first standard straight, which is comparable to primary BPMs in other straight.

Note that the PSDs from Fig. 1 lack phase information, which complicates the analysis of the MIMO system. Since the ORMs are ill-conditioned, most of the measured disturbance is concentrated in the modes associated with large singular values of the ORMs. However, this is not reflected in the PSDs from Fig. 1, and therefore impacts the performance estimation of the MIMO system.

* Work supported by Diamond Light Source

† Corresponding author: shohan.banerjee@diamond.ac.uk.

USING LAG COMPENSATOR IN ORBIT FEEDBACK*

Igor Pinayev†, Brookhaven National Laboratory, Upton, NY, USA

Abstract

Growing demand on the beam orbit stability requires higher loop gain within the operational bandwidth. Increasing the gain leads to the increase of the unity gain frequency and creates problems with systems stability due to the additional phase shifts caused by the trims (power supplies, eddy currents in vacuum chambers, etc.) and filtering of beam position data. Conventionally employed systems have 20 dB/decade slope near the unity gain providing 90° phase shift which is sufficient for stability. Utilizing one or more lag compensators allows to increase the gain at low frequencies while keeping phase margin acceptable. The paper provides more details on the proposed solution as well as simulations of how the transients will be modified.

INTRODUCTION

Rejection of the disturbance in the linear system feedback is proportional to the gain of the open loop. If the open loop gain is described by a transfer function $G(s)$ the suppression of the disturbance is given by formula:

$$P(s) = \frac{1}{1+G(s)} \quad (1)$$

Increase of the slope to 40 dB/decade by adding additional pole into the signal chain increases the phase shift to 180° and makes system unstable. Increase of the implemented gain is limited by the requirement of the system stability. The phase shift caused by different elements of orbit feedback (trims with power supplies [1], eddy currents in vacuum chamber [1], filters implemented in the beam position monitors [2], latency in the signal propagation chain [3]) can turn negative feedback into positive one and make system unstable. Typically, the transfer function of the orbit feedback system is described by few poles. The lowest frequency pole is user defined and might be at zero frequency if integrator is utilized. The second pole is defined by hardware and is the main limiting factor in the system bandwidth. Therefore, at high frequencies the loop gain is inversely proportional to the frequency

$$|G(f)| \cong \frac{f_c}{f} \quad (2)$$

where f_c is crossover frequency where gain is unity. Since the slope of the Bode plot is usually fixed (-20 dB/decade for single pole), increase in suppression of the high-frequency disturbances requires increase of the crossover frequency.

* Work supported by Brookhaven Science Associates, LLC under Contract No. DE-SC0012704 with the U.S. Department of Energy

† pinayev@bn.gov

LAG COMPENASTOR

Usage of lag compensation provides higher low-frequency gain [4]. The transfer function of lag compensator is

$$D(s) = \alpha \frac{Ts+1}{\alpha Ts+1}, \quad \alpha > 1 \quad (3)$$

where α is the ratio between zero/pole breakpoint frequencies and T is time constant. At DC the lag compensator provides additional gain $\alpha > 1$. But it also creates negative phase shift. For $\alpha=10$ phase shift is almost 60° and can create a long ringing response or even cause instability. This drawback can be overcome by using more compensators with different time constants. This will increase the slope of the Bode diagram above 20 dB/decade but keep phase margin acceptable as it can be seen in Fig. 1.

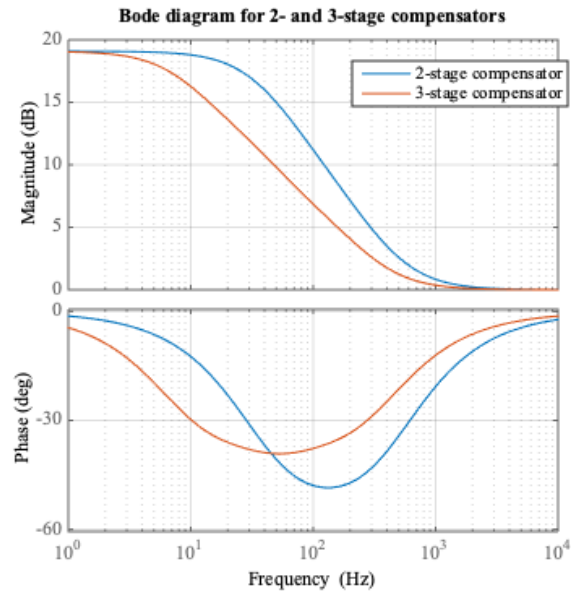


Figure 1: Bode plot of the open loop with two and three lag compensators. Total gain increase is the same but maximal phase shift different for three-stage it is 40° and for two-stage it is 50°.

IMPLEMENTATION IN ORBIT FEEDBACK

Figure 2 shows implementation of stages lag compensator the single input – single output (SISO) system with integrator in error amplifier and single pole at 800 Hz. Three stages providing 20 dB gain at DC were used. Figure 3 shows noise suppression and phase of the residuals.

“INSTANTANEOUS” LIFETIME MEASUREMENT IN STORAGE RING WITH TOP-UP INJECTION*

Igor Pinayev†, Brookhaven National Laboratory, Upton, NY, USA

Abstract

Top-up operation becomes routine in the light sources. The goal of the top-up operation is to keep the current of the circulating beam stable to avoid variations of the heat load on the beamline optics. It is also considered for the electron-ion collider to maintain the polarization of the electron beam. Frequent re-injection makes measurement of the beam lifetime very difficult if possible. Since, only part of the bunch train is refreshed during the injection cycle then the distribution of the bunch charges in the train has a characteristic saw-tooth distribution. The slope of saw tooth is defined by the lifetime and filling frequency and can be used for the measurements. The data for processing can be obtained either from fast current transformer or from the raw ADC signal from beam position monitor. In this paper we present the theoretical considerations as well as experimental data from NSLS-II storage ring.

TOP-UP OPERATION OF THE NSLS-II

To satisfy requirements of the beam stability NSLS-II storage ring operates with top-up. Presently, around 1200 buckets out of 1320 are filled. The stored current is 400 mA, and lifetime is around 12 hours as shown in Fig. 1. Each 200 seconds approximately 100 bunches are injected into the ring to maintain current level [1, 2]. Therefore, top-up cycle takes 40 minutes. In the electron-ion collider being built at Brookhaven National Laboratory the re-fill is expected each two seconds making conventional lifetime measurement harder.

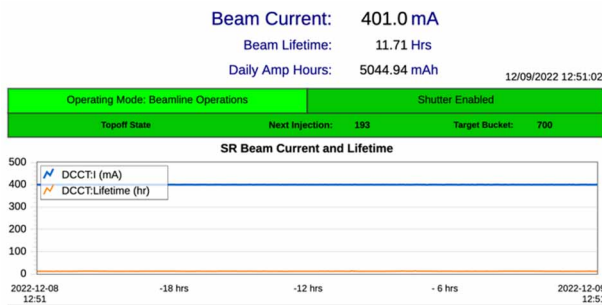


Figure 1: Screenshot of NSLS-II status showing stored beam current and beam lifetime of 11.7 hours from the DCCT data between injections.

NSLS-II BEAM POSITION MONITORS

NSLS-II BPMs are processing 500 MHz signal induced by the circulating beam. The parameters of the bandpass

filters define the rising and falling of the induced train as well as ringing down as one can see in Fig. 2. After amplification the signal is sampled with analog-to-digital converter [3]. The ADC sampling rate is chosen so that there are 310 readings per turn. The clock is phased locked to the RF frequency. The down sampling results in the 500 MHz signal being converted into the 80 periods per turn. There is possibility to extract buffer of 100000 consecutive ADC readings per channel (more than 322 turns) for the offline analysis.

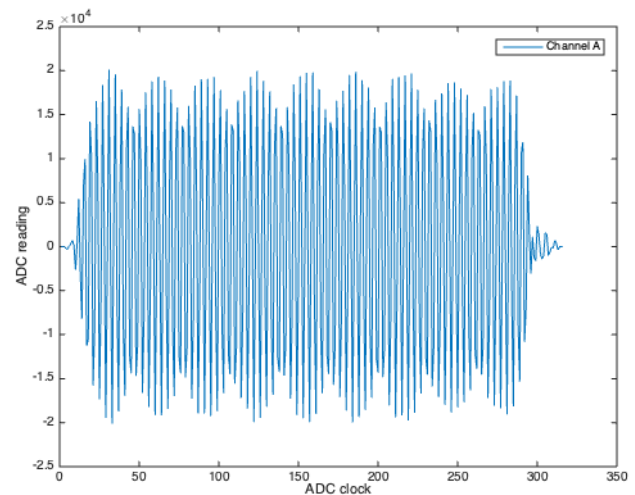


Figure 2: Raw ADC signal from NSLS-II beam position monitor. The visible modulation is due to the limited sampling rate (just below four readings per period).

To evaluate the signal level evolution along the train the sliding window was used. The user defined number of data samples around the current ADC clock were used to perform sine wave fit and the amplitude of the wave was used as signal strength. The 310 samples were padded with zeros on both sides for these calculations. The result is shown in Figs. 3 and 4. The sliding fit was using 11 points to smear the modulation caused by artefacts in the NSLS-II injection complex. The step down is clearly visible near ADC clock 236. The amplitude of the step as well as average amplitude can be used for the evaluation of the beam lifetime (in assumption that injection is stable in time) from the period of the top-up:

$$\tau_{lifetime} = T_{top-up} \frac{\langle amplitude \rangle}{step} \quad (1)$$

The step was calculated as difference between two linear fits on the left and on the right sides shown in Fig. 4. The modulation of the intensity is caused by modulation of charge trains in the NSLS-II injection system.

* Work supported by Brookhaven Science Associates, LLC under Contract No. DE-SC0012704 with the U.S. Department of Energy
† pinayev@bn.gov

ROBUST EMITTANCE MEASUREMENTS*

I. Pinayev†, Brookhaven National Laboratory, Upton, NY, USA

Abstract

The quadrupole scan is commonly used for measurement of beam emittance. The found dependence of the beam size vs. quadrupole strength is fitted with parabola, which coefficients are used for emittance calculations. The measurement errors can cause substantial variations in the emittance value. Sometimes the fitted parabola has negative minimum value, making impossible emittance calculation. We propose more robust data processing modifying the quadrupole scan procedure using or weighted fit for parabola. The experimental results are presented.

INTRODUCTION

Emittance serves as measure of the transverse phase space occupied by the beam as well as a measure of beam quality in many applications. By definition [1] emittance is

$$\varepsilon_x^2 = \sigma_x^2 \sigma_{x'}^2 - \sigma_{xx'}^2 \quad (1)$$

where σ_x^2 and $\sigma_{x'}^2$ are variances, and $\sigma_{xx'}$ is covariance of beam distribution.

Commonly used technique is scanning of a focusing element such as a quadrupole or a solenoid and measuring dependence of the transverse beam size on a profile monitor [2, 3]. The obtained data are fit with a parabola which coefficients are used for calculating emittance. In some cases, even slight changes in the data can cause substantial variation of the emittance value. This is due to that we are subtracting two large numbers. Example of such measurement is shown in Fig. 1.

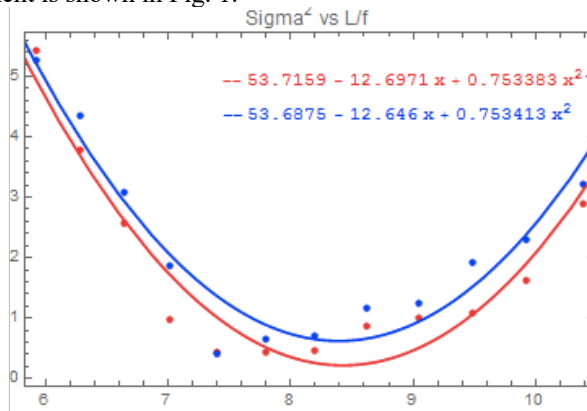


Figure 1: The horizontal axis shows ratio of distance from the solenoid center to the profile monitor and solenoid's focal length. Vertical axis shows the square of the r.m.s. beam size in mm^2 .

The maximal difference between the parabolic fit coefficients is 0.2%. Distance from the solenoid to the profile

monitor is 3.63 m. Emittance for the blue curve is 0.19 mm mrad, and for the red curve it is 0.11 mm mrad, difference is factor of 2.

Moreover, due to the statistical variations the value of the fitted parabola minimum can be less than zero making the data set unusable for obtaining value of the emittance.

MODIFICATION OF SCAN

We are going to modify the procedure to avoid such subtracting. We can present beam angular distribution as sum of correlated and uncorrelated parts, so that for each particle $x' = \alpha x + \tilde{x}'$, where α is correlation factor and \tilde{x}' is uncorrelated angular spread. Correlation factor can be found from the covariance:

$$\alpha = \sigma_{xx'} / \sigma_x^2 \quad (2)$$

Beam emittance can be found from Eq. (1)

$$\varepsilon_x^2 = \sigma_{x0}^2 \sigma_{\tilde{x}'0}^2 \quad (3)$$

where σ_{x0}^2 is r.m.s beam size at focusing element, and $\sigma_{\tilde{x}'0}^2$ is uncorrelated angular spread.

After passing through a focusing element with focal length F and drift with length L the beam size at the observation point can be found

$$\sigma_x^2 = \left(1 - \frac{L}{F}\right)^2 \sigma_{x0}^2 + 2\alpha L \left(1 - \frac{L}{F}\right) \sigma_{x0}^2 + L^2 (\alpha^2 \sigma_{x0}^2 + \sigma_{\tilde{x}'0}^2) \quad (4)$$

The minimum size is observed when $1 - L/F = -\alpha L$ and minimal size is:

$$\sigma_{x\min}^2 = L^2 \sigma_{\tilde{x}'0}^2 \quad (5)$$

So, from $1 - L/F_{\min}$ corresponding to the minimal beam size one can find the first order correlation factor α between transverse positions and angles of the particles in the bunch, and the uncorrelated angular spread can be calculated using the minimal beam size.

Now we need to find beam size at focusing element to calculate beam emittance. For this purpose, we can measure the beam size when focusing element is off ($1/F = 0$):

$$\sigma_x^2 = \sigma_{x0}^2 + 2\alpha L \sigma_{x0}^2 + \alpha^2 L^2 \sigma_{x0}^2 + \sigma_{x\min}^2 \quad (6)$$

and

$$\sigma_{x0}^2 = \frac{\sigma_x^2 - \sigma_{x\min}^2}{(1 + \alpha L)^2} = \frac{\sigma_x^2 - \sigma_{x\min}^2}{(L/F_{\min})^2} \quad (7)$$

Emittance can be found using formula below:

$$\varepsilon^2 = \frac{\sigma_x^2 - \sigma_{x\min}^2}{(L/F_{\min})^2} \frac{\sigma_{x\min}^2}{L^2} \quad (8)$$

If the beam is converging to the minimal size with focusing element off or close to such condition, then there can be significant error in determination of the beam size at the

* Work supported by Brookhaven Science Associates, LLC under Contract No. DE-SC0012704 with the U.S. Department of Energy

† pinayev@bnl.gov

MEASUREMENT OF SLICE EMITTANCE WITH DEFLECTING CAVITY AND SLIT*

I. Pinayev†, Brookhaven National Laboratory, Upton, NY, U.S.A.

Abstract

In this paper we describe the system for the of measurement slice emittance utilizing transverse deflecting cavity and slit. The image of the beam passing through the slit is used to measure slice intensity and uncorrelated angular divergence. Beam size at slit location is measured by scan of the beam across the slit with calibrated trim. The angular kick by the trim is taken into the account during calculations. Data processing and the experimental results are presented.

INTRODUCTION

Coherent Electron Cooling experiment carried out at RHIC [1] requires small slice emittance of 15 MeV electron beam with high peak current.

Many applications require knowledge of the local properties of the beam distribution. These properties include slice emittance and/or slice energy spread. In most cases the emittance is measured by a quadrupole scan when beam is streaked with transverse deflecting cavity [2, 3]. For a low-energy beam with high peak current the measurements are affected by space charge forces. If beam is not centered with quadrupole, then it will be steered during the scan what can mix different slices.

To overcome these difficulties slit scan be used [4]. The slit is moved across the beam and image is observed on a downstream profile monitor. The angular distribution is estimated from the spatial distribution observed on the screen, and the transverse beam size at the location of the slit is found from the dependence of image intensity from slit position. In our experiment we utilize a fixed slit, and we are scanning the beam with help of calibrated trim.

EXPERIMENTAL SET UP

Beam parameters are measured in the dedicated beam-line shown in Fig. 1 [5].

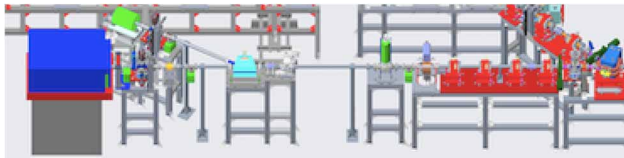


Figure 1: Layout of the diagnostics line. There are four quadrupoles to adjust the beam optics for measurement, followed by a transverse deflecting cavity. Beam can be observed on three profile monitors.

The beam is matched with four quadrupoles. The transverse deflecting cavity tuned to 1.3 MHz provides vertical

streak of the beam [6]. Beam can be observed with three profile monitors. The first profile monitor is placed before the 45-degree dipole and used for measurement of the longitudinal profile of the beam. This screen is also used for slice emittance measurement using quadrupole scan. Second profile monitor is placed before the high-power dump and is preceded by a vertical slit. This combination is used for slice emittance measurement described in this paper. The third profile monitor is placed after the 45-degree dipole and is used for measurement of the energy slew and slice energy spread.

The scan of the beam across the slit is performed with two calibrated horizontal trims. The first trim changes position of the beam on the slit and the second trim is restoring initial beam angle (it has the same kick of opposite sign) thus performing parallel scan of the beam over the slit.

Beamlet intensity w_i is estimated from the image brightness inside of the region of interest (ROI). The beamlet angle α_i is found from its center of gravity on the profile monitor and uncorrelated divergence $\sigma_{x'i}$ from the beamlet width. The measured beam size is corrected for the final resolution of the system defined by point spread function of the optical system and slit width. The result of the scan is shown in Fig. 2.

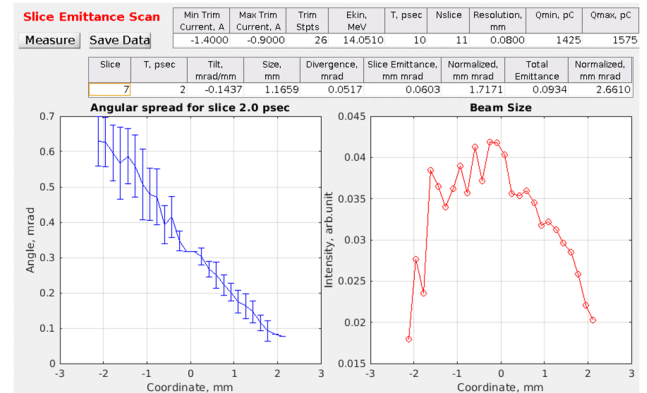


Figure 2: The result of scan of the beam parameters. On the left side one can see phase space plot for the slice at 2 ps from the beam center. Negative sign of the correlated angular spread indicates the beam convergence. R.m.s. beam size is calculated from the right plot, the uncorrelated angular divergence from the left plot. Both values are used for calculation of the slice emittance.

The slice emittance is calculated using conventional formula:

$$\varepsilon_{slice}^2 = \langle x^2 \rangle \langle x'^2 \rangle - \langle x x' \rangle^2 \quad (1)$$

* Work supported by Brookhaven Science Associates, LLC under Contract No. DE-SC0012704 with the U.S. Department of Energy

† pinayev@bnl.gov

BEAM INSTRUMENTATION CHALLENGES FOR HIGH-ENERGY AND LOW-EMITTANCE BEAM AT SuperKEKB

G. Mitsuka*, KEK, 1-1 Oho, Tsukuba, Ibaraki, Japan

Abstract

The SuperKEKB electron–positron collider, which started the commissioning in February 2016, is a luminosity frontier machine for the search for new physics. In this presentation, we review the main challenges we face for the high-energy and low-emittance beam at SuperKEKB, fast and low-noise beam-orbit feedback system, X-ray beam-profile monitors for measurements for the beam size of 10 μm , novel diamond mirrors with extremely high thermal conductivity for extracting synchrotron radiation, and various type’s beam loss diagnostics for the identification or possibly early detection of sudden beam losses. This presentation includes future directions of the R&D—X-ray interferometry for micron-level beam size measurements and fast optics measurements with the gated turn-by-turn BPMs—towards next-generation light source facilities and high-energy colliders.

OVERVIEW OF SuperKEKB

SuperKEKB is a positron–electron collider with a nanobeam scheme [1], which currently achieves the world’s highest luminosity for producing B meson pairs. SuperKEKB consists of a 4 GeV positron ring (LER) and a 7 GeV electron ring (HER) [2]. The nanobeam scheme allows the vertical beta function at the interaction point to be much smaller than the bunch length. The vertical beta function and the beam size at the interaction point are the smallest in the world among colliders. The machine operation started in March 2018 with a test run to verify a nano-beam scheme, and then the physics run began in March 2019. The vertical beta function at the interaction point, β_y^* , has been squeezed down to 1.0 mm during 2019. We tested for further squeezing in β_y^* down to 0.8 mm for approximately one week in 2020 and 2022. Adopting a crab-waist scheme for both rings since the 2020 spring run has increased the luminosity. The crab-waist ratio is 80 % and 40 % in LER and HER, respectively. The crab-waist scheme at SuperKEKB is combined with the local chromaticity correction in the interaction region. We achieved a peak luminosity of $4.65 \times 10^{34} \text{ cm}^{-2}\text{s}^{-1}$ with $\beta_y^* = 1.0 \text{ mm}$ in the physics run and the highest luminosity of $4.71 \times 10^{34} \text{ cm}^{-2}\text{s}^{-1}$ without data acquisition by the Belle-II detector. The machine parameters that accomplished the peak luminosity and those for the target luminosity in 2028 are presented in Table 1.

As of September 2023, we are in a long shutdown to upgrade the Belle-II detector and SuperKEKB. SuperKEKB is scheduled to resume operations in December 2023.

* gaku.mitsuka@kek.jp

Table 1: SuperKEKB Machine Parameters Achieved on 8 June 2022 and Expected in 2028

Parameters		8 June 2022		2028	
		LER	HER	LER	HER
I	[A]	1.321	1.099	2.75	2.20
n_b		2249		2345	
I_b	[mA]	0.587	0.489	1.17	0.938
β_x^*	[mm]	80.0	60.0		
β_y^*	[mm]	1.0	1.0	0.6	0.6
ξ_y		0.0407	0.0279	0.0604	0.0431
ε_y	[pm]	31.7		21	
Σ_y^*	[μm]	0.252		0.160	
σ_z	[mm]	5.69	6.02	7.23	7.05
Crab-waist ratio [%]		80	40		
L	[$\text{cm}^{-2}\text{s}^{-1}$]	4.65×10^{34}		2.4×10^{35}	

BEAM PROFILE MONITORS

The realization of a low-emittance beam is essential for high luminosity in SuperKEKB. Accordingly, accurately measuring small beam sizes and short bunch lengths is entrusted to beam diagnostic systems.

SuperKEKB operates synchrotron radiation monitors in the X-ray and visible light regions to measure the beam profile, say, beam size and bunch length. Here, we report the recent updates of the X-ray beam size monitors and visible-light beam profile monitors.

X-ray Beam Size Monitors

The X-ray beam size monitor (XRM) is dedicated to measuring the electron and positron vertical beam size using X-ray synchrotron radiation and will be capable of single-shot (single bunch, single turn) measurements [3]. The XRM is installed one to each main ring. Since the fast silicon-strip detectors and the fast readout systems developed under the US-Japan collaboration were not in time, we have measured the vertical beam sizes by analyzing the X-ray-induced images projected on the scintillator screens. X-rays produced by the bending magnet pass through the coded aperture optical mask about 10 m downstream and enter a detector box 30 m further downstream, where the scintillator screen and CMOS camera are housed.

The beam study results, which commenced in May–July 2018, suggest the point spread function $\sigma_s = 6.6 \mu\text{m}$, consistent with the simulation-estimated spatial resolution of the imaging system and scattering in the beamline. The overall performances of XRM in LER and HER are accurate and satisfy the measurement accuracy presently required by SuperKEKB.

BEAM INSTRUMENTATION PERFORMANCE DURING COMMISSIONING OF THE ESS NORMAL CONDUCTING LINAC

I. Dolenc Kittelmann*, R. Baron, E. Bergman, E. Donegani, V. Grishin,
H. Hassanzadegan, H. Kocevar, N. Milas, R. Miyamoto, M. Mohammednezhad,
F. Nilen, D. Noll, K. Rosengren, T. Shea, R. Tarkeshian, C. Thomas
European Spallation Source ERIC, Lund, Sweden

Abstract

Once constructed, the European Spallation Source (ESS) will be a 5 MW pulsed neutron source based on a 2 GeV proton linac delivering 2.86 ms long pulses at a 14 Hz repetition rate. This paper focuses on the beam instrumentation performance during the recent linac beam commissioning up to drift tube linac (DTL) tank 4 with 74 MeV output energy. Instrumentation and measurement results will be presented for beam parameters such as current, position, energy, emittance and beam loss.

INTRODUCTION

The European Spallation Source (ESS) is a neutron-based research facility, currently under construction and designed to deliver the world's brightest neutron beams [1, 2]. The neutron production will be based on the bombardment of a tungsten target with a proton beam generated by a pulsed linac. The linac will accelerate and transport the protons towards the target through a normal-conducting (NCL) and superconducting (SCL) linac (Fig. 1) resulting in a beam with a peak current of 62.5 mA, 2.86 ms pulse length, 14 Hz repetition rate, and energy of 2 GeV once the linac design average power of 5 MW is reached.

For a high-power machine like the ESS linac, one of the biggest challenges during its commissioning and operations is to minimize beam losses and protect its components by adequately adjusting the electromagnetic elements and achieving ideal beam parameters. A comprehensive set of proton beam instrumentation has been developed to provide detailed beam property measurements throughout the linac and thus to support achieving the required beam parameters. The set comprises instruments for beam characterisation along the linac to provide beam profile, position, energy, current and loss measurements [3].

The ESS linac commissioning is performed in phases. Each commissioning phase is focused on the linac parts up to the selected beam destination. In parallel, the linac installation downstream of the end-destination continues. Three commissioning phases have been completed successfully with low power beam and end-destinations in LEBT (2018-2019) [4, 5], in MEBT (2021-2022) [6] and at the end of DTL1 reaching 21 MeV (2022) [7-9]. From April to July 2023, the commissioning has advanced to the fourth phase, reaching the end of the DTL4 tank with an output energy of 74 MeV. Towards the end of 2024, the beam commissioning

will continue to the Dump, while the first beam on target is planned to be achieved at the end of 2025 followed by the start of the user program in 2026.

This paper focuses on ESS beam instrumentation deployed for the DTL4 commissioning phase and highlights their key features and contributions during this phase.

BEAM INSTRUMENTATION FOR THE NCL COMMISSIONING

The ESS beam instrumentation is being deployed in a staged approach. Systems that are critical for meeting commissioning goals proceed through a formal verification process beginning with unit testing in the laboratory followed by integrated system testing, and finally, formal testing with beam to achieve operational status. Figure 1 summarises the instrumentation systems installed for the DTL4 commissioning run. The Faraday Cups (FCs), Beam Current Monitor (BCM), and Beam Position Monitor (BPM) have all gone through the aforementioned formal verification workflow. In addition, several other systems, at an intermediate stage of their development were deployed for diagnostic beam studies to gain early operational experience. The Wire Scanners (WSs) [10], Emittance Measurement Unit (EMU) [7] and two types of Beam Loss Monitors (BLMs) were deployed at this level. Beam studies with the neutron-sensitive BLM (nBLM) and horizontal EMU station offered valuable data for system development as well as beam characterisation and the results are presented here together with results with the FCs, BPM and BCM systems. In addition, some limited beam studies were performed with WSs, the vertical EMU station and the Ionisation Chamber based BLM [11] system. Results from these systems will be covered in future publications.

Faraday Cups

Three Faraday cups were operational during the DTL4 commissioning. Once inserted, each FC is a beam end-destination and measures the transported beam current at the destination. The FC locations were in the LEBT [5, 12], in the MEBT [12, 13] and in a dedicated shielding at the (foreseen) position of DTL5 [12, 14] tank. All FCs are water-cooled and rely on a pneumatic actuator to move in or out of the beamline.

The LEBT FC is designed to withstand full power at the ion source exit, namely 75 keV proton beam pulses with up to 100 mA current, 6 ms pulse length at 14 Hz repetition rate. However, MEBT and DTL4 FC can cope with only

* Irena.DolencKittelmann@ess.eu

AN EXPERIMENTAL SETUP FOR PIXE ANALYSIS IN A MEDICAL CYCLOTRON AT TENMAK-NUKEN

G. Turemen*, S. Bulut, U. Kaya, D. Porsuk, N. O. Serin, E. Yeltepe
TENMAK-NUKEN, Ankara, Türkiye

Abstract

A 30 MeV cyclotron is operated at TENMAK-NUKEN for producing medical radioisotopes with three beamlines and a fourth beamline is dedicated for research purposes. The minimum energy of extracted proton beam from cyclotron is 15 MeV. There is no facility in Türkiye for applying ion beam analysis techniques (IBA) currently. These techniques generally require 1-5 MeV proton beam energy. An energy degrader system was designed and installed on the R&D beamline for this purpose. The degrader system is capable of decreasing the energy down to 1 MeV with pA to μ A current levels. A high vacuum irradiation chamber is designed and installed at the end of the beamline. The chamber has ports to install several types of detectors for different IBA techniques. This work includes the description of the setup and preliminary PIXE measurements.

INTRODUCTION

Cyclotrons are compact particle accelerator systems used for scientific research, medical and industrial applications. Turkish Energy, Nuclear and Minerals Research Agency (former Turkish Atomic Energy Authority) acquired a 30 MeV energy proton cyclotron with associated systems dedicated to the production of medical radioisotopes and scientific research purposes in 2011. The accelerator facility (TENMAK-PAF) has three beamlines for production of medical isotopes and another beamline for scientific research purposes. The research vault comprises a five-port electromagnet which can deflect the proton beam up to an angle of $\pm 40^\circ$ with respect to the beam axis. The minimum beam energy and current provided by the cyclotron is 15 MeV and 0.1 μ A respectively. This constraint on energy and current excludes certain applications. One of these applications is ion beam analysis (IBA) which finds use in a wide range of disciplines such as chemistry, biology, solid state physics, materials science, archaeology, anthropology etc. Non-destructive IBA techniques in general and certain irradiation requests from internal/external researchers require relatively low particle energies and low beam currents, i.e. 1-5 MeV energy with pA-nA current levels. A way to decrease the energy and the current is to let the beam pass through a thin foil during which the particles interact with the foil medium causing a decrease in energy and current. In this work, development and tests of the irradiation system and preliminary studies with PIXE method are described.

* gorkem.turemen@tenmak.gov.tr

IRRADIATION SETUP

Low-energy and low-current irradiations for the required absorbed doses demand additional effort and equipment in medical cyclotrons due to the design priorities for this type of accelerators. Therefore an energy degrader system is developed to decrease the energy of the cyclotron extracted beam. The cyclotron's original beam current measurement system is capable of measuring the current down to 0.1 μ A which is convenient for radioisotope production purposes but not suitable for material irradiations and non-destructive analysis. Thus, a beam current measurement system is designed to measure the beam current down to tens of pA levels. Also, an irradiation chamber, an energy degrader system and various collimators were manufactured to irradiate assorted types of samples while controlling the beam energy, size and position (see [1] for details). The irradiation system requires additional conditions for shielding, positioning of the particle/radiation detectors and data acquisition systems to perform non-destructive analysis (Fig. 1). The secondary gamma and neutron radiation generated from the energy degraders is the primary concern due to increased background radiation in X-ray and gamma analysis. A water-cooled degrader system is installed in the cyclotron room, just after the extraction of the beam, to decrease the radiation background in the R&D room.



Figure 1: Irradiation system and detector placement.

Energy Degradation System

A water-cooled degrader (Fig. 2) system degrades the beam energy down to 3 MeV from 15.6 MeV using three stacked pyrolytic graphite foils with a total thickness of 1.3 mm. The foil stack is sandwiched between copper blocks and aluminum flanges for adequate cooling and collimation. The cooling system of the degrader assembly utilizes deionized water from the cyclotron cooling loop with a flow of

FIRST DIRECT MEASUREMENT OF ELECTRON AND POSITRON BUNCH CHARACTERISTICS DURING POSITRON CAPTURE PROCESS AT THE POSITRON SOURCE OF THE SuperKEKB B-FACTORY

T. Suwada*, High Energy Accelerator Research Organization (KEK),
also at SOKENDAI (The Graduate University for Advanced Studies), Tsukuba, Japan

Abstract

Electron (e^-) and positron (e^+) bunch characteristics were directly measured for the first time using wideband beam monitors (WBMs) and a detection system at the e^+ source of the SuperKEKB B-factory. Both secondarily generated e^- and e^+ bunches after the e^+ -production target were clearly identified during their dynamical capture process at locations of the WBMs under a two-bunch acceleration scheme. Not only the longitudinal but also transverse bunch characteristics, the time intervals between the e^- and e^+ bunches, bunch lengths, transverse bunch positions, and bunch charges were simultaneously and separately measured for each bunch as a function of the capture phase to investigate their dynamical capture process. The results show that quite symmetric dynamical behaviors for both the bunch characteristics were observed. The new WBMs open up a new window for direct measurements of both bunches during their dynamical capture process.

INTRODUCTION

High-intensity e^+ sources are indispensable and challenging in high-energy e^+e^- colliders to achieve the high luminosity required for high-energy physics experiments. In general, conventional e^+ sources [1] comprise a e^+ -production target and a e^+ capture section subsequently located. Positrons are produced by impinging high-energy primary e^- beams with high intensity to a target of a high-Z material through a e^+e^- pair-production process in an electromagnetic cascade shower. The total amount of produced positrons is principally dominated by two main factors. One is the primary e^- beam power, the product of the e^- beam intensity and energy, and the other is the target characteristics of material and thickness. The resulting transverse emittances of positrons secondarily generated from the target are very large owing to the large momentum and angular spreads through an electromagnetic cascade shower process and multiple scattering in the target.

Only some parts of the positrons ejected forward are immediately captured in the e^+ capture section, in which they are focused in the transverse plane with strong axial magnetic fields, and they are captured in radio-frequency (RF) buckets of multiple accelerating structures (ACCs) in the longitudinal direction. Note that in the e^+ capture section, not only positrons but also secondarily generated electrons with approximately equivalent amounts of bunch charges simultaneously emerge from the target through this process.

* tsuyoshi.suwada@kek.jp

They are immediately and simultaneously captured in the subsequent capture section. While the e^- bunch is stopped by a beam stopper after passing the capture section, the e^+ bunch is separated from the e^- bunch and it is further accelerated by subsequent accelerating structures. After the capture section, the e^+ intensity can be measured using a beam position monitor (BPM) (or a beam intensity monitor).

An essential role of the e^+ capture section is to increase the e^+ capture efficiency as much as possible. The capture efficiency is generally simulated and optimized on the basis of beam dynamics in multidimensional transverse and longitudinal parameter spaces, which are related to electromagnetic fields of accelerating structures and magnetic fields in the capture section. Moreover, the transverse parameters of primary electrons, namely, transverse positions, injection angles, and impinging radii at the target, are also those in multidimensional parameter spaces. It is generally difficult to fully optimize the capture efficiency only by simulations. The optimization procedure should also be experimentally investigated to optimize it in multidimensional parameter spaces under realistic operation conditions.

An objective function to be optimized is only the e^+ intensity obtained after passing the e^+ capture section because no instrumentation devices are installed in it. It is generally difficult to determine not the local optimum but the global optimum in terms of the e^+ intensity with one objective function in multidimensional parameter spaces. This is because it is difficult to separately measure the e^+ and e^- bunches in the capture section by a conventional technique.

It is challenging to simultaneously and separately measure the e^+ and e^- bunch characteristics to directly verify complicated beam dynamics in the capture section and to optimize the e^+ intensity under the realistic operation condition. This is the main reason why the WBMs and detection system were developed at the e^+ source of the SuperKEKB B-factory.

HISTORICAL BACKGROUND

The purpose of introducing WBMs is to simultaneously and separately measure not only longitudinal but also transverse bunch characteristics for both e^- and e^+ bunches in the capture section. Here, I mention the background for introducing WBMs in 2018, in which preliminary investigations were started. One of the preconditions for installing any monitor in the capture section is the use of simple electromagnetic detection monitors because no advanced optical devices can be applied owing to limited installation spaces.

SUB-20 fs SYNCHRONIZATION BETWEEN MODE-LOCKED LASER AND RADIO-FREQUENCY SIGNAL *

J.G. Wang¹, B.W. Wu^{2,3}, B. Liu^{1,†}

¹ Shanghai Advanced Research Institute, Chinese Academy of Science, Shanghai, China

² Shanghai Institute of Applied Physics, Chinese Academy of Sciences, Shanghai, China

³ University of Chinese Academy of Sciences, Beijing, China

Abstract

The femtosecond synchronization and distribution system of the Shanghai soft X-ray free-electron laser facility (SXFEL) and Shanghai high repetition rate XFEL and extreme light facility (SHINE) are based on the optical pulse trains generated by passively mode-locked lasers. The passively mode-locked laser has ultralow noise in the high offset frequency (<5 fs, [1 kHz- 1 MHz]). In this paper, we report precise synchronization of the low-noise passively mode-locked laser to the radio frequency (RF) master oscillator. RF-based phase-locked loop scheme, the absolute jitter of the phase-locked passively mode-locked laser is less than 20 fs integrated from 10 Hz up to 1 MHz.

INTRODUCTION

Large-scale femtosecond stability has become an urgent requirement in modern free-electron lasers (FELs) facilities. At SXFEL [1] and for the SHINE, a pulsed optical synchronization has been used. The central component of the pulsed optical synchronization is the low-noise mode-locked laser which operates at telecommunication wavelength (~1550 nm). The use of low noise mode-locked laser as the optical master oscillator has become an excellent way to achieve an effectively synchronized network by distributing the optical master oscillator output to the individual end stations by length stabilized and dispersion compensated fiber links. The fiber links are based on a balanced optical cross-correlation method [2-4].

The optical synchronized network composed of fiber links distribute high-purity pulsed reference signals to three different types of end stations along the complete FEL facility to achieve femtosecond synchronization.

The bunch arrival time monitor based on the electro-optical modulator (EOM) scheme [5] is used to measure the arrival time of electron bunch with femtosecond accuracy at some special positions along the accelerator and undulator.

The remote lasers synchronization using two-color balanced optical cross-correlation [6, 7] is used to synchronize remote lasers, such as the photocathode lasers in the injector, the seed lasers near the undulator, and the pump-probe lasers in the experiment stations, to the output of fiber links

The laser-RF synchronization using a balanced optical microwave phase detector enables timing detection between the output fiber link and radio frequency signal zero-crossing for stable RF signal re-generation which is needed in the SRF cavities and beam-diagnostics devices.

Being the heart of the optical synchronized network, the low-noise performance of the optical master oscillator is of tremendous importance. Due to the inherent characteristic of the optical master oscillator, the cavity length is easily affected by environmental fluctuations. The optical master oscillator is stabilized by the phase-locked loop against the radio frequency master oscillator to ensure long-term stability.

RF-BASED OPTICAL MASTER OSCILLATOR SYNCHRONIZATION

A common microwave phase-locking technique is used for synchronization between the optical master oscillator and RF master oscillator.

Figure 1 describes the RF-based experimental setup of synchronization between the optical master oscillator and RF master oscillator. For this test setup a commercial mode-locked laser from Menhir Photonics, which operates at 238-MHz repetition rate with 1558-nm center wavelength and 170-fs pulse duration, was used as the optical master oscillator. The RF reference signal at 1428-MHz is supplied by a 1428-MHz RF master oscillator (Rohde & Schwarz).

In order to achieve phase detection for synchronization purposes, it is necessary to convert pulsed optical signals into electrical signals. The photodetector generates electrical signals with high spectral purity harmonics of the laser repetition rate. A power splitter is used to split the electrical signal from the photodetector into two parts. A sixth harmonic of the photodetected electronic spectrum is filtered out using an RF bandpass filter and a low noise amplifier in combination with an RF phase detector. Meanwhile, another frequency comb with the same repetition rate as the optical master oscillator is filtered out using another bandpass filter and a low noise amplifier in combination with an RF phase frequency detector. The fundamental frequency is used for coarse tuning for the setting phase point. The sixth harmonic frequency is used for fine-tuning for precise synchronization. The lock on the higher harmonic improves the performance. The phase error signal between the RF reference signal from the RF master oscillator and optical master oscillator signal is fed to the digital controller. Once the phase-locked loop (PLL) was established using the RF-based laser-to-RF synchronization setup, a traditional method of measuring the timing jitter of the optical master oscillator was used. The scheme has been widely adopted by the current state-of-the-art signal source analyzers (SSAs). The phase noise of the obtained RF signal from the optical master oscillator is converted to ampli-

* This work is supported by the National Natural Science Foundation of China (12105348 and 12275341)

† bo.liu@sari.ac.cn

COMMISSIONING OF THE LCLS-II MACHINE PROTECTION SYSTEM FOR MHz CW BEAMS*

J. A. Mock[†], A. S. Fisher, R. T. Herbst, P. Krejcik, L. Sapozhnikov
SLAC National Accelerator Laboratory, Menlo Park, United States

Abstract

Beam power at the LCLS-II linac and FEL can be as high as several hundred kW with CW beam rates up to 1 MHz. The new MPS has a latency of less than 100 μ s to prevent damage when a fault or beam loss is detected. The MPS architecture encompasses the multiple FEL beamlines served by the SC linac and can mitigate a fault in one beamline without impacting the beam rate in a neighboring beamline. The MPS receives inputs from various devices including loss monitors and charge monitors as well as magnet power supplies and BPMs to pre-emptively turn off the beam if a fault condition is detected. Link nodes distributed around the facility gather the input data and stream it back to a central processor that signals other link nodes connected to beam rate control devices. The system design and some experience during initial commissioning are discussed.

INTRODUCTION

The Linear Accelerator Facility at the SLAC National Accelerator Laboratory (SLAC) has seen a significant upgrade to the Linac Coherent Light Source (LCLS) facility with the installation of LCLS-II. This new accelerator and undulator complex was designed to increase capacity at SLAC for photon science using the free electron lasers. A high level diagram of the new facility is shown in Figure 1.

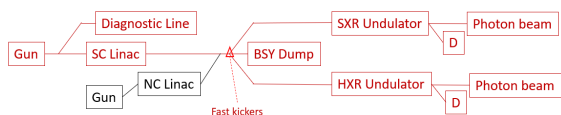


Figure 1: A high level map of the new LCLS-II facility (red), alongside the old NC linac. The new LCLS-II MPS has mitigation devices to inhibit beam or reduce beam rate at either the gun or the fast kickers, to each of the destinations shown.

Because it uses superconducting RF cavities, the LCLS-II accelerator is capable of delivering electrons with a minimum bunch spacing of 1 μ s and maximum electron energy of 4 GeV, leading to a maximum overall beam power of 120 kW. An upgrade is also in progress to raise the energy to 8 GeV which will further double this power. The high rate and high power potential of these beams requires safety systems capable of reacting to beam events such that operations remain safe. The personnel protection and beam containment

systems (PPS and BCS) are safety systems designed to protect people from radiation-based hazards, and the Machine Protection System (MPS) is designed to protect the accelerator from damaging itself. The MPS is not a credited safety system, so it is designed to be more agile to allow a variety of operating conditions while still protecting the accelerator.

SYSTEM REQUIREMENTS

The scope of the MPS is confined exclusively to shutting off the electron beam when a fault condition occurs that can potentially damage beam line hardware. Other systems that protect high power devices such as power supplies, RF power sources, vacuum systems, or cryogenic systems are handled separately as equipment protection.

Response Time

A key driving parameter of the MPS is the maximum allowable time interval in which the beam must be shut off before damage can occur. The MPS requirement for the original LCLS dictated that the electron beam be shut off within one beam pulse at the full repetition rate of 120 Hz. This is not possible in LCLS-II where the minimum bunch spacing is only 1 μ s and propagation delay for a signal in a cable from one end of the accelerator to the other can be as long as 20 μ s, not including additional processing delays incurred from electronics. The MPS baseline beam shutoff time, defined as the time between detection of fault and suppression of the electron beam, is required to not exceed 100 μ s to avoid catastrophic damage to the beam line, though in principle the MPS physics requirement is as low as reasonable achievable. Not every fault condition requires the fast shutoff time of 100 μ s. For example, a slow change in some state, such as a temperature rising, allows ample time for the control system to warn of the impending change. Therefore, MPS responses to prompt events such as beam loss mitigate within the fast response window, and other, slower events and more complicated logic process within a 360 Hz window, equal to the processing time of the legacy LCLS-I MPS.

As shown in Figure 1, the LCLS-II accelerator can deliver to some combination of an injector diagnostic line, one of two undulator beamlines, or through the linac to a high power dump in the SLAC Beam Switchyard (BSY). The default destination for the electron beam is this high power dump. Pulsed kicker magnets are used to kick the beam into one of the other beamlines, which means if the pulser does not kick, the beam will need to travel to the BSY beam dump. Therefore, the MPS uses this high power dump as its primary mitigation device for downstream faults. It grants

* SLAC is supported by the U.S. Department of Energy, Office of Science, under contract DE-AC02-76SF00515

[†] jmock@slac.stanford.edu

FPGA ARCHITECTURES FOR DISTRIBUTED ML SYSTEMS FOR REAL-TIME BEAM LOSS DE-BLENDING

M.A. Ibrahim*, M.R. Austin, J.M. Arnold, J.R. Berlioz, P. Hanlet,
 K.J. Hazelwood, J. Mitrevski, V.P. Nagaslaev, D.J. Nicklaus, G. Pradhan, A.L. Saewert,
 B.A. Schupbach, K. Seiya, R.M. Thurman-Keup, N.V. Tran, A. Narayanan¹
 Fermi National Accelerator Laboratory[†], Batavia, IL USA
 J.YC. Hu, C. Xu, J. Jiang, H. Liu, S. Memik, R. Shi, A.M. Shuping, M. Thieme
 Northwestern University[‡], Evanston, IL USA
¹also at Northern Illinois University, DeKalb, IL USA

Abstract

The Accelerator Real-time Edge AI for Distributed Systems (READS) project's goal is to create a Artificial Intelligence (AI) system for real-time beam loss de-blending within the accelerator enclosure, which houses two accelerators: the Main Injector (MI) and the Recycler Ring (RR).

In periods of joint operation, when both machines contain high intensity beam, radioactive beam losses from MI and RR overlap on the enclosure's beam loss monitoring Beam Loss Monitor (BLM) system, making it difficult to attribute those losses to a single machine. Incorrect diagnoses result in unnecessary downtime that incurs both financial and experimental cost. The ML system will automatically disentangle each machine's contributions to those measured losses, while not disrupting the existing operations-critical functions of the BLM system.

This paper will focus on the evolution of the architectures, which provided the high-frequency, low-latency collection of synchronized data streams to make real-time inferences. The ML models, used for learning both local and global machine signatures and producing high quality inferences based on raw BLM loss measurements, will only be discussed at a high-level.

INTRODUCTION

Accelerator Complex

After the Collider Physics program [1] ended in 2011, RR was re-purposed as a proton stacker for Main Injector, delivering 8-120 GeV beam to multiple experiments and facilities. The RR is directly installed above MI, such that their beam lines' centers are physically separated by only about 120 cm. As a result, when high intensity beams are in both machines simultaneously, understanding beam losses becomes a significant concern during normal operation of the accelerator complex (Fig. 1).

* Equal contribution

[†] Operated by Fermi Research Alliance, LLC under Contract No.De-AC02-07CH11359 with the United States Department of Energy. Additional funding provided by Grant Award No. LAB 20-2261

[‡] Performed at Northwestern with support from the Departments of Computer Science and Electrical and Computer Engineering

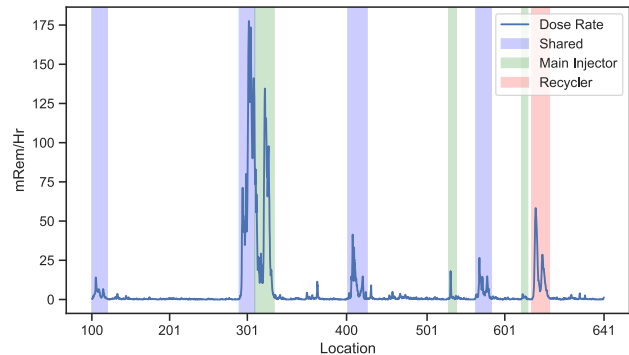


Figure 1: Plot of localized beam losses based on tunnel residual dose rates.

Beam Loss Monitoring

Real-time localized beam losses for both the MI and RR are monitored by over 250 argon gas ionization chamber-type BLM detectors. These signals are received, processed, and instrumented within a Versa Module Eurocard (VME)-based architecture, forming a distributed network of 7 VME "front-end nodes" around the 2.2 mile complex. Together, they capture and report spatially-identifiable and time-correlated integrated beam loss measurements on all BLM detectors within the enclosure for display and analysis [2].

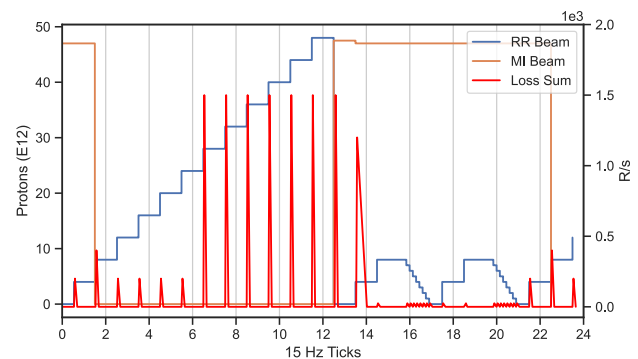


Figure 2: Example to overlay beam events and expected losses during a machine cycle.

Although the origin of radioactive losses measured on any operational BLM can be difficult to attribute to a single machine, experts can often manually decipher and attribute losses to either MI or RR, based on timing, machine state, and physical location within the ring (Fig. 2).

Content from this work may be used under the terms of the CC-BY-4.0 licence (© 2023). Any distribution of this work must maintain attribution to the author(s), title of the work, publisher, and DOI

COLLIMATOR SCAN BASED BEAM HALO MEASUREMENTS IN LHC AND HL-LHC*

P. Hermes[†], M. Giovannozzi, C. E. Montanari¹, S. Morales Vigo^{2,3}, M. Rakic⁴, S. Redaelli,
B. Salvachua, CERN, Geneva, Switzerland, ¹also at University of Manchester, UK,
²also at Cockcroft Inst. Accel. Sci. Tech., Warrington, Cheshire, UK,
³also at University of Liverpool, UK, ⁴also at EPFL, Lausanne, Switzerland

Abstract

Measurements in the CERN Large Hadron Collider (LHC) have indicated that the population of the transverse beam halos is greater than that of a Gaussian distribution. With the upcoming High-Luminosity project (HL-LHC), the stored beam energy in the beam halo could become large enough to threaten the integrity of the collimation system. Given the unprecedented stored beam energies of about 400 MJ, currently achieved at the LHC, and roughly 700 MJ planned at the HL-LHC, conventional measurements are difficult. Considerable efforts in the ongoing LHC Run 3 are dedicated to characterising experimentally the transverse beam halos, and its diffusion properties, after the LHC Injector Upgrade (LIU) in preparation for HL-LHC operation. Halo and diffusion measurements are currently based on collimator scans, where robust collimators are inserted in steps into the circulating beam halo. In this contribution, we present techniques for halo characterisation employed in LHC and compare results obtained from such measurements in LHC Run 2 and the ongoing LHC Run 3. We present plans for measurements in the remainder of LHC Run 3 and describe the expected challenges for halo characterization in HL-LHC.

INTRODUCTION

The Large Hadron Collider (LHC) at CERN is a 27 km long circular collider for protons and heavy ions [1]. LHC design beam intensities are so high that even small amounts of beam loss can generate beam dumps, triggered by the interlock system, magnet quenches, or even damage to machine equipment. To preserve the integrity of the machine hardware and avert potential hazards arising from uncontrolled beam losses, the LHC is equipped with a multi-stage collimation system, predominantly located in the betatron collimation insertion region IR7 [1, 2]. Additional details on the collimation system are provided in the following section.

While methods of active and non-destructive monitoring of beam halos are currently under study [3], the current state-of-the-art method for studying the beam halo is scraping with the LHC collimators. In LHC Run 1 (2009–2013) and Run 2 (2015–2018) measurements, up to 5% of the total stored beam energy was found at transverse amplitudes greater than $3\sigma_N$ [4] in a given transverse plane (we refer to this subset of beam particles as *halo* in the following). σ_N denotes the nominal beam size using the LHC's nominal

normalised emittance of $3.5\ \mu\text{m rad}$. Measured emittances were typically smaller than this conservative value. With the upcoming High Luminosity upgrade (HL-LHC) [5], stored beam energies in the order of 700 MJ are expected to be reached. The scaling to different beam parameters for the higher-brightness HL-LHC beams is complex. Assuming, for example, that similar fractions of the total stored beam energies were located in the beam halo, the stored beam energy above $3\sigma_N$ would yield 35 MJ. This is enough to damage the LHC collimators in case of sudden orbit shifts, for example, in case of crab-cavity failure [6]. Therefore, measures are needed to mitigate this peril.

Hollow electron lenses (HEL) [7] for active halo removal are considered to be deployed in HL-LHC, but cannot be manufactured in time for Run 4 operation. Understanding the formation and population of the halo in LHC Run 3, the final run before HL-LHC installation, is therefore a critical task. The main goals of these activities are reviewing the expected risk from the halo population in HL-LHC, exploring alternative mitigation strategies, and defining requirements for monitoring the halo in HL-LHC.

In this article, we review the technique used for halo quantification in the LHC and discuss data recorded in LHC Run 2 to compare against measurements performed in Run 3. We will then outline the merits of additional measurements planned for in LHC Run 3 and close the article with an outlook on the challenges of halo quantification for HL-LHC.

COLLIMATOR SCANS FOR HALO MEASUREMENTS

LHC collimators are equipped with one or two movable jaws of a robust material used to scatter and/or absorb beam particles. Different collimator types are used, following a defined hierarchy [8]. Primary collimators (TCP) are the only LHC components designed to be directly exposed to the main beam. They are built with two 60 cm long jaws made of a low-density material [9]. This assures robustness against high loads of particle fluxes while providing scattering toward larger amplitudes, where the particles can be intercepted by the secondary collimators and their shower absorbers. Each jaw can be moved independently by two stepper motors, with a step size of $5\ \mu\text{m}$ [10].

Each collimator is equipped with a beam loss monitor (BLM) [11] downstream, as illustrated in Fig. 1. BLMs are ionisation chambers, measuring local secondary particle showers created when particles leave the beam vacuum and interact with surrounding matter. More than 3000 BLMs

* Work supported by the HL-LHC project.

[†] pascal.hermes@cern.ch

COMPARISON OF DIFFERENT BUNCH CHARGE MONITORS USED AT THE ARES ACCELERATOR AT DESY

T. Lensch*, D. Lipka, R. Neumann, M. Werner
Deutsches Elektronen-Synchrotron DESY, Germany

Abstract

The SINBAD (Short and INnovative Bunches and Accelerators at DESY) facility, also called ARES (Accelerator Research Experiment at SINBAD), is a conventional S-band linear RF accelerator allowing the production of low charge ultra-short electron bunches within a range of currently 0.01 pC to 250 pC. The R&D accelerator also hosts various experiments. Especially for the medical eFLASH experiment an absolute, non-destructive charge measurement is needed. Therefore different types of monitors are installed along the 45 m long machine: A new Faraday Cup design had been simulated and realized. Further two resonant cavities (Dark Current monitors) and two Beam Charge Transformers (Toroids) are installed. Both, Dark Current Monitors and Toroids are calibrated independently with laboratory setups. At the end of the accelerator a Bergoz Turbo-ICT is installed. This paper will give an overview of the current installations of charge monitors at ARES and compare their measured linearity and resolution.

INTRODUCTION

The SINBAD facility (Short and INnovative Bunches and Accelerators at DESY) hosts various experiments in the field of production of ultra-short electron bunches and novel high gradient acceleration techniques. ARES (Accelerator Research Experiment at SINBAD), is a conventional, 45 m long S-band linear RF accelerator allowing the production ultra-short electron bunches (fs to sub-fs) with high stability. The machine is operated with a repetition rate of 10 Hz with a charge range of 0.01 pC up to 250 pC. ARES is used for applications related to accelerator R&D in the field of advanced and compact longitudinal diagnostics and accelerating structures development, test of new accelerator components, machine learning and others. In the field of medical application studies an experiment has been set up to perform studies on cancer irradiation techniques with electron beams. For this experiment an absolute, non-destructive charge measurement is essential [1].

As ARES is also related to Accelerator R&D several dedicated charge monitors had been installed: one Faraday Cup and a Dark Current Monitor (DaMon) at the gun section, one DaMon and two Beam Charge Transformers (Toroid) along the machine and one Bergoz Turbo-ICT [2] in-vacuum at the end of the beam line. An additional Bergoz in-air ICT [3] is installed 30 cm next to the T-ICT outside the beamline.

* timmy.lensch@desy.de

CHARGE MONITORS AT ARES

Faraday Cup

Simulations of at DESY existing Faraday Cup geometries showed 4 % to 22 % of primary and secondary charged particles escaping from the cup. This does not fulfill the ARES demand for an absolute charge measurement at the Gun. Due to this, a new Faraday Cup geometry had been simulated for an energy of 5 MeV. This geometry of a copper cup with an inner diameter of 15 mm, inner depth of 24 mm and an Aluminum plate inlay shows only 0.6 % of charged particles escaping from the Faraday Cup in the simulation. Also different beam configurations (pencil beam, out of center, angled beam) had been taken into account. None of them showed more than 1 % loss of charged particles [4]. Figure 1 shows the final design of the simulated Faraday Cup for ARES prior vacuum installation.

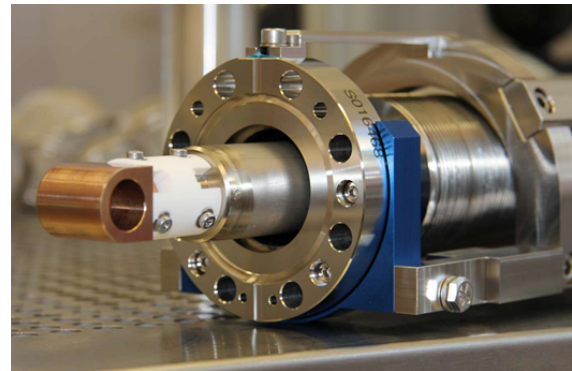


Figure 1: New Faraday Cup mounted with ceramic spacer on a mover rod.

The signal from the Faraday Cup is connected to an MicroTCA system [5] via a 15 MHz low pass and a pre amplifier. A Struck SIS8300-L2D [6] ADC board samples the pulse with 125 MS/s. The charge is reconstructed using a *pulse form fit* with three samples as described in Ref. [7]. For calibration of the electronics and cables an electrical pulse which corresponds to 1 nC is fed into the front end box input. An appropriate scaling factor is set in the software.

Beam Charge Transformers (Toroids)

Different types of in-house developed charge monitors based on transformers (Toroids) had been used at DESY machines since the 1980s. Beginning in 2010 an optimization of existing Toroids for the E-XFEL and FLASH accelerator had been started. These new monitors are based on one or two ferrite cores with four pickup coils, each consisting of a single winding. These four coils are combined outside the Toroid housing. The read out procedure is the same as with

LOW INTENSITY BEAM CURRENT MEASUREMENT OF THE ASSOCIATED PROTON BEAM LINE AT CSNS

R.Y. Qiu, W.L. Huang, F. Li, L. Zeng, Muhammad Abdul Rehman, M.Y. Liu, Q.R. Liu, R.J. Yang, T. Yang, Z.H. Xu, Z.X. Tan

Institute of High Energy Physics, Chinese Academy of Sciences, Beijing, China
Spallation Neutron Source Science Center, Dongguan, China

Abstract

The Associated Proton beam Experiment Platform (APEP) beamline is the first proton irradiation facility to use naturally-stripped protons which come from H⁻ beams interacting with the residual gas in the linac beampipe at CSNS. The stripped beam current, which is in the order of

then injected into the Rapid Cycling Synchrotron (RCS) by charge-exchange stripping. The proton beam is then accelerated to 1.6 GeV and finally extracted to bombard the tungsten target for neutron production with a repetition rate of 25 Hz [3]. In the linac of CSNS, a portion of H⁻ beam interacts with the residual gas. As a result, in the beampipe

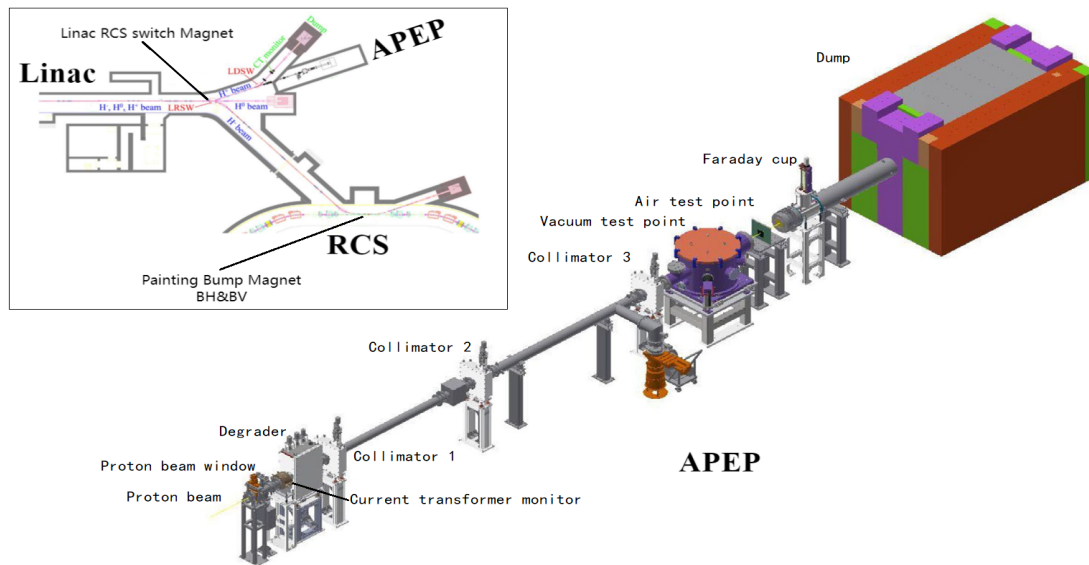


Figure 1: Layout of the APEP beam line. [2].

0.1% of the original H⁻ beam and approximately 10 microamperes, should be measured precisely to provide the proton number for irradiation experiments. Therefore, a low-intensity beam current measurement system was developed with considerations to eliminate the external interferences. An anti-interference design is adopted in this system with an elaboration of probes, cables and electronic low-noise technology to minimize the impact of environmental noise and interferences. This improves the signal-to-noise ratio and enables a more precise measurement of the microampere-level pulsed beam current. The system was installed and tested during the summer maintenance in 2021 and 2022. It shows a good agreement with the measurement of the Faraday cup.

INTRODUCTION

The linear accelerator of China Spallation Neutron Source (CSNS) consists of a negative hydrogen ion source, a 3 MeV radio frequency quadrupole accelerator (RFQ), and a 4-tank drift tube linear accelerator (DTL) [1]. The negative hydrogen ion beam is accelerated to 80 MeV and

there are three types of particles with different charge states: H⁻ (~15 mA, 100~500 μ s), hydrogen atom (H⁰), and proton (H⁺). The associated proton beam current is about 0.1% of the original H⁻ beam. Therefore, the APEP beam line is established from the bending magnet at the end of linac. The number of protons in the beam is a crucial parameter for irradiation experiments.

Figure 1 shows the layout diagram of the APEP area. There are three devices used for measuring beam intensity. The first one is the current transformer measurement system located at the entrance of APEP. In order to precisely measure this microampere-level beam intensity, a low-intensity beam current measurement system was developed in 2021. It achieved stable measurements by addressing external interferences in September 2022. The second device, located behind collimator3, is the beam intensity measurement system based on the secondary electron emission method. The third device is the Faraday cup beam intensity measurement device located in front of the DUMP. The two devices behind are currently undergoing debugging.

To obtain the final version of the work, please refer to the original work published in the proceedings of the 12th International Beam Instrumentation Conference (IBIC2023) at Saskatoon, Canada, 2023. Any distribution of this work must maintain attribution to the author(s), title of the work, publisher, and DOI.

DEVELOPMENT OF BUNCH POSITION MONITORS TO OBSERVE SUDDEN BEAM LOSS OF SuperKEKB RINGS

Makoto Tobiyama, Hitomi Ikeda, Gaku Mitsuka
 KEK Accelerator Laboratory, 1-1 Oho, Tsukuba, Japan
 also Department of Accelerator Science, SOKENDAI, Tsukuba, Japan

Abstract

In the SuperKEKB rings, we have encountered extremely fast beam losses occurring primarily within one to two turns in some parts of the bunch train. Such sudden beam loss induced severe failure in the vertical collimator heads, quenches on the superconducting final quadrupoles, and damage on the Belle II detector in some cases. It is essential to investigate the cause and take countermeasures. This paper presents the phenomena clarified by the bunch current and position monitor of the bunch feedback system. The upgrade plan for the existing monitor, and recently developed simple monitors installed in the suspected area is also introduced.

INTRODUCTION

The SuperKEKB collider consists of 7 GeV electrons (HER) and 4 GeV positron (LER) rings with the circumference of 3 km. To achieve much higher luminosity than previous KEKB collider, the nanobeam collision method was adopted with low emittance and low x-y coupling. Up to 2022b runs, new world record of highest luminosity of $4.7 \times 10^{34} \text{ cm}^{-2} \text{ s}^{-1}$ has been achieved with lower beam current than KEKB, with $\beta_y^* = 1 \text{ mm}$ which is much shorter than the natural bunch length of $\sim 6 \text{ mm}$ [1]. The beam currents were 1.3 A for LER and 1.1 A for HER with the stored number of bunches of 2249, which corresponds to almost 2 RF bucket filling pattern. The next target of the luminosity after the long shutdown 1 (LS1) from Jun 2022 to Dec 2023 is to increase the luminosity more than $10^{35} \text{ cm}^{-2} \text{ s}^{-1}$ as soon as possible. During luminosity runs, we have encountered many so-called sudden beam loss (SBL) events on both ring which losses some part of bunch train within one or two turns when we have exceeded the bunch current of some threshold value ($\sim 0.65 \text{ mA}$ for LER) [2]. The SBL usually damages the head of vertical beam collimators (and other accelerator components), quenches the final focusing superconducting magnets (QCSs), and causes huge backgrounds to Belle-II detector. Since the luminosity will be proportional to the bunch current product, those limitations on the bunch current are a big obstacle to achieve target luminosity. To understand the cause of SBL, and to take countermeasure to it, it is essential to monitor the beam behavior just before the SBL event, such as the bunch-by-bunch position and currents, the fastest beam loss points along the ring, vacuum burst if exist, etc.

We have used the bunch oscillation recorders (BORs) and bunch current monitors (BCMs) as the by-products of the bunch feedback systems installed in the ring to observe the SBL. Though the BORs and BCMs can separate the

bunch information with the minimum bunch space of 2 ns, they have large limitations on such very quick event because of the location of the monitor is only one position per ring: it is impossible to estimate the cause point.

We have developed the simplified, low-cost BOR to place it in the suspicious point to observe the rough bunch oscillations and intensities. We are also trying to collect more detailed data by effectively using the existing system. The main parameters of the SuperKEKB rings on 2022b is shown in Table 1.

Table 1: Main Parameters of SuperKEKB in 2022b Runs

	HER	LER
Energy (GeV)	7	4
Circumference (m)	3016	
Maximum beam current (mA)	1099	1321
Max. bunch current (mA)	1	1.5
Natural bunch length (mm)	5	6
RF frequency (MHz)	508.886	
Harmonic number	5120	
Synchrotron Tune	0.028	0.024
Momentum compaction	0.00045	0.00032
L. damping time (ms)	29	23
Natural Emittance (nm)	4.6	3.2
Peak luminosity ($\text{cm}^{-2} \text{ s}^{-1}$)	4.7×10^{34}	
Bunch current monitor	1	1
Bunch oscillation monitors	3	3

SUDDEN BEAM LOSS

Monitors to Measure the Sudden Beam Loss

We have post-mortem monitor system to measure the bunch positions (x, y and longitudinal) and bunch intensity just before the beam abort event (BORs and BCM). As we use the same bunch position / intensity detector for the bunch feedback systems that down convert the $4 \times f_{RF} = 2 \text{ GHz}$ components of the bunch signal, the outputs are proportional to both the bunch intensity and the bunch position distortion. The 18k10 digitizing board mainly consists of a fast 8-bit ADC (MAX108), a Spartan6 (XC6SLX45) daughter card with the form for a SO-DIMM card (Mars MX1) and VME-IF CPLDs [3]. They are mounted on a double width, 6U VME card. As we use the

DETECTOR RESPONSE STUDIES OF THE ESS IONIZATION CHAMBER

V. Grishin*, I. Dolenc Kittelmann, ESS ERIC, Lund, Sweden
 E. Effinger, A.T. Lernevall, W. Vigano, C. Zamantzas, CERN, Geneva, Switzerland
 P. Boutachkov, GSI, Darmstadt, Germany

Abstract

The European Spallation Source (ESS), currently under construction in Lund, Sweden, will be a pulsed neutron source based on a proton linac. The ESS linac is designed to deliver a 2 GeV beam with a peak current of 62.5 mA at 14 Hz to a rotating tungsten target for neutron production. One of the most critical elements for protection of an accelerator is a Beam Loss Monitoring (BLM) system. The system is designed to protect the accelerator from beam-induced damage and unnecessary activation of the components.

The main ESS BLM system is based on ionization chamber (IC) detectors. The detector was originally designed for the LHC at CERN resulting in production of 4250 monitors in 2004-2008 (IC-2004). In 2014-2017 a new production of 830 detectors (IC-2016) with a modified design was carried out to replenish spares for LHC and make a new series for ESS and GSI. This contribution focuses on the results from a measurement campaigns performed at the HiRadMat (High-Radiation to Materials) facility at CERN, where response of IC-2016 detectors has been studied. The results may be of interest to other facilities that are using existing or plan to use new generation of IC monitors as BLM detectors.

INTRODUCTION

The European Spallation Source (ESS) is a science facility [1, 2], which is currently being built in Lund, Sweden and will provide neutron beams for neutron-based research. The neutron production will be based on bombardment of a tungsten target with a proton beam of 5 MW average power. A linear accelerator (linac) will accelerate protons up to 2 GeV and transport them towards the target, through a sequence of a normal conducting (NC) and superconducting (SC) accelerating structures (Fig. 1). In 2023 the beam commissioning of Normal Conducting Linac (NCL) has successfully advanced up to including fourth DTL tank.

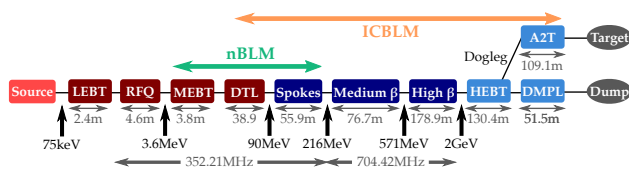


Figure 1: Layout of the ESS linac and BLM system coverage. Red colour represents the NC and blue the SC parts of the linac.

Beam Loss Monitoring (BLM) systems play an important role in machine commissioning, tuning, and operation. By measuring secondary particle rates close to the beam

* Viatcheslav.Grishin@ess.eu

line, these systems provide information about beam loss levels along the machine. The BLM systems are designed to protect the machine from beam-induced damage by detecting unacceptably high beam losses and promptly triggering a request to the Beam Interlock System to stop the beam production. Two types of BLM systems differing in detector technology have been conceived at ESS. The neutron sensitive BLM (nBLM) system [3] is based on 82 neutron detectors primarily covering the lower energy part of the ESS linac. Conversely, the Ionisation Chamber-based BLM (ICBLM) system [4] consists of 266 ionisation chambers (ICs) located almost exclusively along the SC part of the linac.

The ESS ICBLM system is based on parallel plate gas Ionisation Chambers (ICs) originally developed by CERN for LHC (IC-2004) [5] and manufactured and tested in 2004-2008 at the Institute for High Energy Physics (IHEP) in Protvino. IC-2004 type detectors were selected as the ICBLM detectors due to their fast response, no gain variation (with possible exception around the target region) and large dynamic range of 10^8 (pA–mA). In addition to this, they require little maintenance. New production line (IC-2016) [6] was set up in 2014-2017 for ESS, CERN and GSI needs.

When introducing a new detector, it is important to validate its response versus corresponding simulations. In order to validate and fully characterise the new chambers their response in terms of drift time, calibration and saturation was studied at the HiRadMat (High-Radiation to Materials) facility at CERN. The facility offers the opportunity to perform these unique tests due to several reasons, namely, possibility of beam parameters in wide desired range, available beam diagnostics, availability of cables with required grounding, last but not least, having HiRadMat experts around for fast feedback during the test. BLM experiments have been performed at HiRadMat since 2012, starting with experiments BLM19 and BLM2. Currently, the BLM55 experiment is dedicated to focus on three studies:

- Comparison of the IC production lines IC-2004 and IC-2016.
- Comparison of two types of Little Ionization Chambers (LICs), namely, LHC type (LIC-sem) and new LIC with IC ceramics (LIC-ic).
- Testing of the new Proportional Chambers (PCs).

DETECTOR DESIGNS UNDER TESTS

The IC detector active zone consists of 61 parallel electrodes with a 5.75 mm distance between the electrodes in

COMMISSIONING THE BEAM-LOSS MONITORING SYSTEM OF THE LCLS SUPERCONDUCTING LINAC*

Alan S. Fisher[†], Namrata Balakrishnan, Garth Brown, Edward Chin, William G. Cobau,
John E. Dusatko, Bryce T. Jacobson, Sung Kwon, Jeremy Mock, Jino Park, Jeremy Pigula,
Evan Rodriguez, Jacob Rudolph, Daniel Sanchez, Leonid Sapozhnikov, James J. Welch
SLAC National Accelerator Laboratory, Menlo Park, California, USA

Abstract

A 4-GeV superconducting linac has been added to the LCLS x-ray FEL facility at SLAC. Its 120-kW, 1-MHz beam requires new beam-loss monitors (BLMs) for radiation protection, machine protection, and diagnostics. Long radiation-hard optical fibres span the full 4 km from the electron gun of the SC linac to the final beam dump. Diamond detectors at anticipated loss points and other points of concern provide local protection. Detector signals are continuously integrated with a 500-ms time constant and compared to a loss threshold. If crossed, the beam is halted within 0.1 ms. Commissioning began in March 2022 with the 100-MeV injector and with RF processing of the cryomodules. At IBIC 2022 last September, we presented commissioning results from the injector BLMs. In October, the beam accelerated through the full linac, passed through the bypass transport line above the LCLS copper linac, and stopped at an intermediate dump. In August it continued through the soft x-ray undulator and achieved first lasing. Here we present BLM commissioning at energies up to 4 GeV and rates up to 100 kHz. We discuss measurements and software using the fast diagnostic-waveform output to localize beam losses and to detect wire-scanner signals.

INTRODUCTION

Over the past few years, SLAC removed the first km of the 3-km copper normal-conducting (NC) copper linac and replaced it with a superconducting (SC) linac with 35 12-m-long cryomodules operating at $f_{RF} = 1.3$ GHz and two third-harmonic cryomodules. Each has 8 RF cavities and operates at a temperature of 2°K. All have been installed in the first 700 m of the tunnel. The SC linac, driven with continuous-wave (CW) RF power, produces 4-GeV bunches with variable spacing at rates up to 1 MHz ($f_{RF}/1400$). The 750-keV electron gun is also driven by CW RF, but at 186 MHz ($f_{RF}/7$) and followed by a 1.3-GHz buncher. A planned high-energy (HE) upgrade in the remaining 300 m will later double the energy. Before this doubling, the beam power at full rate and at a maximum bunch charge of 300 pC will reach 120 kW. At this time, the full linac has been commissioned to 3.5 GeV and first lasing has been achieved in the soft x-ray (SXR) undulator at 1 kHz.

The risk of damaging beam loss led to the development of a new protection system, including long optical fibres (long beam-loss monitors, LBLMs) that cover the full 4 km from gun to dump in sections of up to 200 m, and diamond

detectors (point beam-loss monitors, PBLMs) that protect small sections or devices such as collimators [1].

At the previous IBIC, in September 2022, only the injector region, the first 50 m through the first cryomodule (80 to 100 MeV), had been commissioned. We reported then [2] on the initial performance of the LBLMs and the one PBLM in this low-energy region. Over the past year, the full beam-loss system has been tested. We now can provide a more complete look at its performance.

LONG BEAM-LOSS MONITORS

Integrated Beam-Loss Signals

Radiation-hard quartz optical fibres (FBP600660710 from Polymicro) run parallel to the beam (z direction, west to east), in lengths of up to 200 m. Beam losses generate showers that pass through the beampipe and fibre, emitting Cherenkov light that travels to the ends of the fibre. At the downstream end, the light is measured by a photomultiplier tube (PMT) outside the tunnel, in a rack-mounted chassis.

The beam can pulse at a steady 1 Hz to 1 MHz, in single shots, or with variable spacings. Consequently, protection is based not on shot-by-shot loss but from the total loss in 500 ms, integrated by an RC circuit. This signal is amplified and compared on the board to the Beam Containment System (BCS) threshold. BCS can stop the beam, the RF cavities and, if necessary, the electron gun. It is analogue, simple, and robust, without awareness of beam rate or the beamline causing the loss. The same integrated signal is buffered and sent to the Machine Protection System (MPS) [3], where it is digitised and compared to a second level below the BCS threshold, to trip the beam first. It is aware of timing and beamline selection. It acts by blocking the photocathode laser or by halting downstream kickers that direct the beam. If dark current causes persistent losses, MPS escalates to BCS, which can halt the gun RF.

The SC linac regions L0B through L3B (here “B” distinguishes these from the LCLS NC linac, in the third km) are separated by warm regions for collimation and bunch compression. Each region is spanned by two fibres, linked for redundant protection in two BCS “chains”, also called “A” and “B”. Linac A-chain fibres are on the north wall at beam height and 90 cm horizontally from the beam. B fibres are on the ceiling and to the south, at a 3-m distance. The different views give the pair similar but not identical responses. Because the thick cryomodule walls require extra gain, fibres span warm or cold regions, but not both. PMT gains for B fibres are somewhat higher to compensate for greater distance. Fibre mounting in transport lines is different; some have only an A fibre.

* SLAC is supported by the U.S. Department of Energy, Office of Science, under contract DE-AC02-76SF00515.

[†] afisher@slac.stanford.edu

SIMULATION AND SHOT-BY-SHOT MONITORING OF LINAC BEAM HALO*

Alan S. Fisher[†], Mei Bai, Thomas Frosio, Alessandro Ratti, John Smedley, Juhao Wu
SLAC National Accelerator Laboratory, Menlo Park, California, USA
Isar Mostafanezhad and Ben Rotter, Nalu Scientific, Honolulu, Hawaii, USA

Abstract

FELs require a reproducible distribution of the bunch core at the undulator entrance for robust and reliable lasing. However, various mechanisms drive particles from the core to form a beam halo, which can scrape the beam pipe of the undulator and damage its magnets. Collimators can trim the halo, but at the 1-MHz repetition rate of SLAC's LCLS-II superconducting linac, the collimator jaws can be activated and damaged. The Machine Protection System (MPS) can detect excessive radiation and halt the beam, but repeated MPS trips lead to significant downtime. Halo control begins by studying its structure, formation, and evolution, using a sensitive halo monitor. To that end, we are developing a pixellated diamond sensor. Diamond offers a dynamic range of up to 7 orders of magnitude, extending from the edge of the core to the faint halo expected at greater distances. Nalu Scientific has developed fast electronics for high-rate shot-by-shot readout. Initial tests are starting with a prototype 16-pixel sensor at the beam dump of SLAC's FACET-II test facility. The tests and simulations will guide more elaborate sensor designs.

INTRODUCTION

Generating a beam with the desired particle distribution in the core of each bunch and maintaining this distribution as the beam travels is a critical requirement for accelerators. However, various mechanisms drive particles from the core into a beam halo. At x-ray free-electron laser (XFEL) facilities, the shape of the bunch core at the entrance of the undulator is crucial for lasing. Reproducibility of this shape is necessary for robust and reliable performance. If a halo surrounds the core, it could scrape on the undulator beam pipe, generating a radiation shower that damages the undulator's permanent magnets. Our numerical simulation of LCLS-II with a start-to-end electron beam-dynamics model finds that collective effects will cause an electron beam—4 GeV, repeating at 300 kHz, 180 pC, plus both dark current and halo electrons—to scrape 1 to 10 W at the undulator entrance. Collimators are commonly used to trim the halo, but at the 1-MHz repetition rate of LCLS-II, the resulting radiation could activate and damage the collimator jaws, making this approach problematic. Moreover, the Machine Protection System (MPS) detects excessive radiation and halts the beam, but repeated MPS trips creates significant downtime for users.

Advanced techniques to detect and mitigate halo are necessary. Non-destructive characterization of the halo

distribution is crucial for understanding in detail the mechanisms behind its formation and for identifying countermeasures. We are developing pixellated diamond sensors surrounding the beam core, to monitor halo noninvasively (“parasitically”), shot by shot, with high spatial and temporal resolution. Diamond offers several orders of magnitude of dynamic range, allowing measurements from the edge of the core to the faint halo expected at greater distances. Below we describe an initial test using a diamond chip with 16 pixels, by the beam dump of FACET-II [1], the test-beam facility at SLAC. Fast electronics built by Nalu Scientific [2] provide shot-by-shot pixel readout.

PIXELLATED DIAMOND DETECTORS

Diamond Sensors

The diamond sensor used in this monitor is based on more than a decade of experience using diamond as an x-ray beam diagnostic [3-5]. In effect, these devices form a solid-state ionization chamber: a photon or electron excites an energetic electron within the material, which then loses energy via electron-electron scattering, producing one electron-hole pair for each 13.3 eV [6] of deposited energy. The FACET electron beam is near the minimum of the dE/dx curve, with an expected collisional energy loss of 35 keV/electron for a 50- μm -thick diamond. With the current electronics, we anticipate being sensitive to 10 electrons per pixel.

These devices have demonstrated a linear dynamic range spanning 11 orders of magnitude with photons [3, 4], due to the lack of recombination in the bulk, and are very radiation tolerant. We anticipate at least 7 orders of magnitude when used with electrons. The device can be read in pulsed or current mode. The goal is to resolve the halo in space—by dividing the chip's surface into pixels using lithographic patterning of the electrodes—and in time—by using pulse-mode readout for shot-by-shot data. In addition to its radiation hardness, diamond is an attractive medium for halo monitoring because its low Z makes it significantly less sensitive than other semiconductors to bremsstrahlung photons, which create background for direct halo detection.

Figure 1 shows the relatively simple patterned diamond in the FACET-II test. The chip is a square single crystal, 4 mm on each side and 50 μm -thick. Four parallel electrode strips, each platinum with a width of 750 μm and a thickness of 25 nm, cross one face with a 1-mm period. The second face has four similar strips, but orthogonal to those on the first. Their intersections form a 4 \times 4 grid of pixels. Figure 2 shows a microscope photograph of the diamond.

Future detectors are envisioned with many more pixels, spread over several chips. Each detector will surround the

* SLAC is supported by the U.S. Department of Energy, Office of Science, under contract DE-AC02-76SF00515.

[†] afisher@slac.stanford.edu

USE OF THE ISAC-II FLIGHT TIME MONITORS TOWARD AUTOMATED TUNING

S. Kiy*, P. Jung, T. Planche, O. Shelbaya, V. Verzilov, TRIUMF, Vancouver, BC, Canada

Abstract

A time-of-flight measurement system has been in use at ISAC-II since 2006 for the phasing of cavities and accurate ion beam velocity measurements across the nuclear chart. This system is heavily relied upon as the primary energy-time domain diagnostic downstream of the ISAC-II linac. Ongoing High Level Applications (HLA) development at TRIUMF has enabled the use of methods that are being applied to these measurements - both for processing and automation of data acquisition. An update will be provided on operational experience with the system over the past 10 years including its recent re-calibration and error analysis. A brief summary of the current HLA framework will be given, including a database for beam measurements and the ability to carry out sequential measurement processes. Finally, the way in which these developments enable beam-based calibration of cavity parameters and a shift to model-based tuning methods is discussed.

INTRODUCTION

The present configuration of the ISAC-II linac was installed in two phases, in 2006 [1] and 2010 [2]. Each phase consists of 20 superconducting quarter wave resonators designed to provide a total effective voltage of 40 MV for the full linac. Phase-I houses two cavity types ($\beta = 0.057$ and $\beta = 0.071$) and consists of 5 cryomodules, while phase-II has a single cavity design ($\beta = 0.110$) and consists of 3 cryomodules. Each of the eight cryomodules houses a single superconducting solenoid which provides transverse focusing to the beam. The primary diagnostic devices for measurements of beam velocity and phasing of cavities are three flight time monitors (FTMs) downstream of the ISAC-II linac. The FTMs were originally installed in 2006 [3] and later upgraded in 2011 [4] to have allow their positions to be adjustable with respect to the ion beam.

Shown in Fig. 1, these diagnostics are composed of a $50\ \mu\text{m}$ wire aligned along the axis of a grounded cylinder, with a negative bias of $\sim 2\ \text{kV}$ applied to the wire. The full cylinder is actuated at 45 degrees from horizontal into the beam, and the ions induce emission of secondary electrons from the wire. These secondary electrons move away in the electric field and are detected by a micro channel plate (MCP) detector with a time resolution of better than 100 ps.

* spencerkiy@triumf.ca

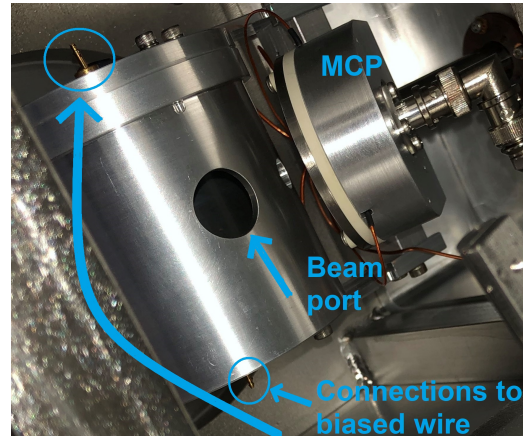


Figure 1: ISAC-II Flight Time Monitor Canister showing beam port and MCP.

OPERATIONAL EXPERIENCE

Maintenance

The FTMs have been regularly used since they were last upgraded in 2011. During this time they have been regularly used both for time of flight (TOF) measurements for calculating the beam velocity, as well as for setting cavity phases during setup to experiments (phase-TOF scans). The latter technique can be a fairly time consuming way to set cavity phases, and with ISAC-II typically serving between 5 and 10 experiments per calendar year, the FTMs can often end up being used for a total of 100 hours or more per year.

These monitors have proven to be very reliable over the past 12 years. The only major repairs required over this time has been the replacement of two of the three MCPs in 2016, and the replacement of the tungsten wires due to increased signs of field emission which can cause damage the MCPs.

Calibration

A calibration laser was installed in 2011 to measure and correct for small discrepancies of delays in cables of the three separate monitors [4]. While it was initially envisioned routinely re-check the calibration, the process was only repeated just recently during the first half of 2023. The same procedure described in Ref. [4] was carried out to measure the arrival time of the laser at each of the three monitors, with the resulting TOF spectrum shown in Fig. 2. Shown below in Table 1, the recent calibration indeed showed small changes in the timing offsets relative to the typical flight times between the monitors.

The change in calibrations in Table 1 is attributable to 2016 maintenance of the system, during which monitors were removed and MCPs replaced. Plotting the relative

BUNCH LENGTH MEASUREMENT SYSTEM DOWNSTREAM THE INJECTOR OF THE S-DALINAC*

A. Brauch[†], M. Arnold, M. Dutine, J. Enders, R. Grewe, L. E. Jürgensen,
 N. Pietralla, F. Schliessmann, D. Schneider
 Technische Universität Darmstadt, Dept. of Physics, Institute for Nuclear Physics,
 Schlossgartenstr. 9, Darmstadt, Germany

Abstract

The S-DALINAC is a thrice recirculating electron accelerator with a continuous-wave beam at a frequency of 2.9972(1) GHz. Short bunches are crucial to enable tuning of the machine for operation as an energy-recovery linear accelerator. Currently, measurements of the bunch length are accomplished by using the radio-frequency zero-crossing method. Since this method is time consuming, a new setup for these measurements using a streak camera is developed. Optical transition radiation emitted from an aluminum-coated Kapton screen is used to map the bunch length information to a light pulse which enables an accurate measurement compared to a scintillating screen. The light pulse can then be evaluated with the streak camera. This contribution will present the current status of the measurement setup as well as its design and properties.

INTRODUCTION

The superconducting Darmstadt electron linear accelerator S-DALINAC was originally established as a twice-recirculating accelerator in 1991 operating at a radio frequency of 2.9972(1) GHz. An upgrade of the machine adding a third recirculation beamline in 2015/16 was performed. This beamline also features an adjustment system for the path length of the electrons in the second recirculation beamline with a range of 10 cm which is identical to the wavelength of the operation frequency (see Fig. 1). It is possible to recover the energy of this beam by passing the main accelerator a second time if this system is set to an 180° phase shift and the beam passing the main accelerator for the first time is led to the respective beamline. This operation mode called 1×ERL (1× Energy-Recovery Linear accelerator) was achieved in 2017 for the first time at the S-DALINAC [1]. Four years later a 2×ERL mode was demonstrated by accelerating and decelerating the beam twice [2]. More than 87 % of the beam energy were recovered in this mode. The efficiency was observed to decrease with the increase of the initial current at the electron gun. The effect is partly caused by the greater bunch length in high current operation. Therefore, the minimization of this parameter is important for reaching higher currents and efficiencies in ERL operation. This requires a setup for measuring the bunch length.

* Work supported by the State of Hesse within the Cluster Project ELEMENTS (Project ID 500/10.006) and by DFG (GRK 2128 AccelenceE).

[†] abrauch@ikp.tu-darmstadt.de

BUNCH LENGTH MEASUREMENTS DOWNSTREAM THE INJECTOR

The current method for bunch length measurements is based on the radio-frequency zero-crossing method [3]. An RF (radio-frequency) cavity is used to impose a momentum chirp on a bunch.

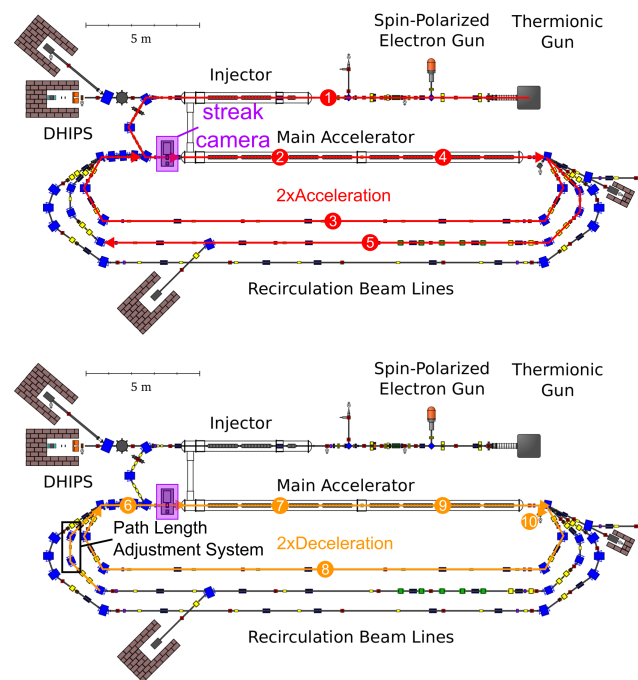


Figure 1: The layout of S-DALINAC including the beam path for operation in 2×ERL mode (following [2]). The top image shows the acceleration in this mode. After passing the injector in (1) the beam is led to its main acceleration in (2). Following the first recirculation beamline (3) the beam is accelerated a second time in the main accelerator (4). The beam then enters the second recirculation beamline (5). The bottom image shows the deceleration of the beam in 2×ERL mode. Because of the path length adjustment system the beam receives a phase shift of 180° in (6). The first deceleration takes place in (7) and the beam is again led through the first recirculation beamline in (8). The second deceleration stage (9) reduces the beam energy to the energy that was originally provided by the injector linac. At this energy, the beam is dumped (10). The intended bunch length measurement setup location for commissioning is also shown in purple.

Content from this work may be used under the terms of the CC-BY-4.0 licence (© 2023). Any distribution of this work must maintain attribution to the author(s), title of the work, publisher, and DOI

INTERMEDIATE FREQUENCY CIRCUIT COMPONENTS FOR INTEGRATION OF ON-CHIP AMPLIFIER WITH THz DETECTORS

R. Yadav^{1,*}, S. Preu, Terahertz Devices and Systems, TU Darmstadt, Darmstadt, Germany

A. Penirschke, High Frequency Tech., Mittelhessen Univ. of Appl. Sci., Friedberg (Hesse), Germany

¹also at High Frequency Tech., Mittelhessen Univ. of Appl. Sci., Friedberg (Hesse), Germany

Abstract

The demand for THz detectors for beam diagnosis and alignment at THz generating accelerator facilities increases continuously especially for room temperature applications. The Zero-Bias Schottky Diode (ZBSD) and field effect transistor (TeraFET) based Terahertz (THz) detectors are well suited for both, signal power detection at DC as well as Pulse shape diagnostics by down-conversion at intermediate frequencies (IF). The limited signal strength due to the roll-off factor of the low pass filter characteristic of the detectors at higher THz frequencies requires wide-band amplifiers to enhance the IF signal from a few μW to nW well above the noise floor of the subsequent post detection electronics. Using external amplifiers would enhance the signal losses even further due to additional connectors and rf-cable losses and degrade the signal to noise ratio (SNR). In order to maximize the SNR, we propose to have an on-chip amplifier integrated in the detectors intermediate frequency (IF) circuit in the same housing. In this work, we present the design and parametric analysis of components for transition to an IF circuit, which will be integrated in the ZBSD and TeraFET on chip with amplifier. A rigorous design analysis has been done to find the optimal parameters for wide-band operation in order to enhance the detector's resolution to capture pulses in the pico-second range with the help of fast post detection electronics.

INTRODUCTION

Research and development of materials and components in the Terahertz (THz) domain has been done rigorously since last couple of decades in order to explore this part of electromagnetic spectrum [1–3]. Due its excellent characteristics, the THz domain has numerous applications such as in imaging, spectroscopy, quality control, security, medical industry, astronomy, communications, energy and matter research, beam diagnostics and alignment at accelerator facilities, etc. [3]. The increasing demand for using this frequency spectrum has led the scientists to develop THz sources and detectors in this operable range. Room-temperature THz detectors developed in Refs. [4–6] are proved to be a cutting-edge technology for detector applications in THz domain. The detector itself is composed of both active and passive part. The active part consists of a semiconductor device such as Field Effect Transistors (TeraFET), Zero-Bias Schottky Diode (ZBSD), etc. The passive part is composed of all passive components which are used for connecting active to

RF connector and later on post-detection electronics. The TeraFET or ZBSD rectifies the THz signal coupled through a silicon lens and is further down-converted from THz to millimeter frequency range [1]. The received signal is typically feed to the post detection electronics by using the intermediate frequency circuit (IF). For the detection of pico-second range pulses, it is necessary to increase the IF bandwidth components in the IF circuit as well as impedance matched circuitry to harness the full potential of the detectors [7]. Considering the important requirement for the optimization of the detector IF circuitry, in this paper we present the transition and ultra-broadband planar power divider (UBPPD) components which will be used for integrating the amplifier on-chip together with active devices in a same housing. The transition structures and UBPPD are investigated using 3D electromagnetic field simulation software (CST).

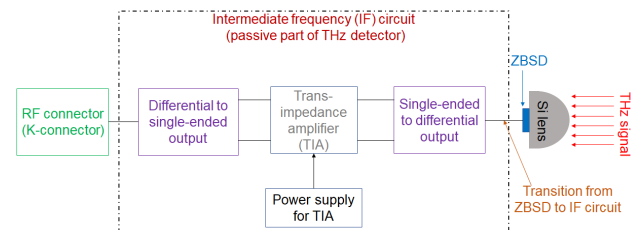


Figure 1: Block diagram of the THz detector.

TRANSMISSION LINES AS TRANSITION STRUCTURES

The block diagram of THz detector circuit is shown in Fig. 1. The blocks inside the dotted box represents the intermediate frequency (IF) circuit. The THz signal incident on the silicon lens is coupled to Zero-Bias Schottky Diode (ZBSD), which is mounted on the back side of the silicon lens (depicted as blue colour in Fig. 1.). A planar power divider along with a broadband phase shifter will be used to convert the rectified signal from single-ended to the differential input of the Trans-impedance amplifier (TIA). The output of the IF circuit is fetched to the read-out electronics via an RF connector (K-connector in this case as our target is to optimize detector initially until 40 GHz).

Figure 2 shows the transmission lines from TeraFET or ZBSD to the IF circuit. The dimensions of these structures are calculated according to Refs. [8,9]. Four different types of transmission lines such as coupled micro-strip lines (Fig. 2 (a)), co-planar wave-guide with only signal on top (Fig. 2 (b)), co-planar wave-guide (Fig. 2 (c)) and micro-strip line (Fig. 2 (d)) is investigated. All transmission line structures are simulated on a thin-film substrate with a thickness

* rahul.yadav@iem.thm.de

GEOMETRY STUDY OF AN RF-WINDOW FOR A GHz TRANSITION RADIATION MONITOR FOR LONGITUDINAL BUNCH SHAPE MEASUREMENTS

S. Klaproth*¹, A. Penirschke, Technische Hochschule Mittelhessen, Friedberg, Germany
R. Singh, GSI Helmholtzzentrum für Schwerionenforschung, Darmstadt, Germany
H. De Gersem, Technische Universität Darmstadt, Darmstadt, Germany
¹also at Technische Universität Darmstadt, Darmstadt, Germany

Abstract

GHz Transition Radiation Monitors (GTRs) can be used to measure longitudinal beam profiles even for low β beams. In contrast to traditional methods e.g., Fast Faraday Cups (FFCs) and Feschenko monitors, GTRs are a non-destructive measurement method and are able to resolve bunch-by-bunch longitudinal profiles at the same time. It is planned to measure the transition radiation outside the beam line through a custom-design RF window within a frequency range up to 8 GHz using broadband antenna structures. The material and the shape of the RF-window is crucial in order to minimize the fraction of the transition radiation that is not propagating in the direction of the antenna. In this contribution, we show a study of different geometries to suppress reflections generated at the transition to the RF-window. For higher permittivity the reflections becomes stronger, simultaneously reducing the measured signal strength at the position of the antenna. Secondly the RF-window's material must be UHV compatible and should be durable.

INTRODUCTION

The longitudinal bunch shape is important for conditioning and verifying the beam dynamics of LINACs. In the case of the GSI UNILAC, the bunch velocities β typically range from 0.05 to 0.15. For these slow bunches, the self-field widens significantly alongside the beam axis, rendering direct measurement of the longitudinal bunch shape inherently ambiguous [1]. This applies to devices such as phase probes and other pick-ups. Therefore, more common tools for longitudinal bunch shape measurements of low-beta beams are FFCs and Feschenko monitors.

FFCs measure the profile by collecting the bunch charge in a $50\ \Omega$ optimized cup. Typically, the beam's self-fields are shielded to suppress signal widening caused by early arriving fields on the collector. This enables FFCs to detect the bunch shape with high precision on a bunch-by-bunch basis. Additional considerations must be taken on the emission of secondaries during the design phase and later on while interpreting the measured signals. Nevertheless, the destructive measurement makes a further usage of the beam impossible [2–4].

Feschenko monitors, on the other hand, measure the average bunch shape. The beam passes by a thin wire generating secondary electrons. The longitudinal structure of the beam

is coherently transformed to the transversal distribution of these secondaries using an RF-deflector [2, 5]. The interaction of the beam and the wire is minimal, allowing the bunches to remain suitable for further acceleration.

A new candidate for bunch shape measurements is the GTR. This type of device is still under investigation, but has the potential to combine the advantages of both FFCs and Feschenko monitors, enabling bunch-by-bunch measurements without beam destruction. The GTR comprises three major components: a metal target plate with an aperture to generate transition radiation while the beam passes through, an RF-window for decoupling the transition radiation from the inner beam line to the outside simultaneously maintaining the vacuum, and an antenna/coupler structure to observe the radiation as seen in Fig. 1. This promising concept has

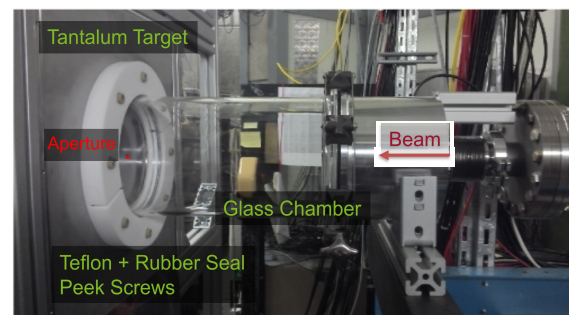


Figure 1: Experimental Setup of the proof-of-concept measurements [6].

been tested successfully at GSI [6]. Consequently, further investigations were made to optimize the RF window in the current setup. Simulations were carried out using different possible materials for the RF window, both ideal [7] and realistic [8], to examine their influence on the expected transition radiation signal. Thereby, a cylindrical RF-window with a wall thickness of 10 mm analog to the proof-of-concept measurement has been used. In Fig. 2a,b, we illustrate the expected maximum peak field (E_{\max}) for two different typical β values at GSI UNILAC. It becomes evident, that a low relative permittivity ϵ_r is advantageous for maximizing the expected signal amplitude. The antenna should be positioned at an angle θ at least above 40° . As a rule of thumb for high β beams, $\theta = \frac{1}{\gamma}$ provides a good approximation for the angle at which the transition radiation peak power is emitted [10]. In case of GSI UNILAC this corresponds to approximately 55° to 60° . But actually at these low β values the maximum intensity rises continuously towards

* Stephan.Klaproth@iem.thm.de

FIRST MEASUREMENTS OF AN ELECTRO-OPTICAL BUNCH ARRIVAL-TIME MONITOR PROTOTYPE WITH PCB-BASED PICKUPS FOR ELBE

B. E. J. Scheible^{1*}, A. Penirschke, Technische Hochschule Mittelhessen, Germany
M. K. Czwalinna, N. T. A. Nazer, H. Schlarb, S. Vilcins-Czvitkovits

Deutsches Elektronen-Synchrotron DESY, Germany

M. Freitag, M. Kuntzsch, Helmholtz-Zentrum Dresden Rossendorf HZDR, Germany

W. Ackermann, H. De Gersem, Technische Universität Darmstadt, Germany

¹also at Technische Universität Darmstadt, Germany

Abstract

A vacuum-sealed prototype of an electro-optical bunch-arrival-time monitor has been commissioned in 2023. It consists of a pickup structure and a low- π -voltage ultra-wideband traveling-wave electro-optical modulator. The stainless-steel body of the pickup structure is partially produced by additive manufacturing and includes four pickups as well as an integrated combination network on a printed circuit board. This novel design aims to enable single-shot bunch-arrival-time measurements for electron beams in free-electron lasers with single-digit fs precision for low bunch charges down to 1 pC. The theoretical jitter-charge-product has been estimated by simulation and modeling to be in the order of 9 fs pC. The new prototype is tailored for validation experiments at the ELBE accelerator beamline. In this contribution first measurement results are presented.

INTRODUCTION

For synchronizing many subsystems and for stabilizing the arrival time of electron bunches an all-optical approach is used in several large free-electron-laser (FEL) facilities [1], where the arrival time is particularly critical for applications like pump-probe experiments [2]. The system requires a master laser oscillator phase-locked to the main RF oscillator, which emits picosecond laser pulses as timing reference [1, 3]. Furthermore, an actively stabilized distribution system must be established to transfer these pulses along the facility with minimal drift [1]. The electro-optical (EO) bunch arrival-time monitor (BAM) [1] is one of various end-stations in the all-optical synchronization system.

EO-BAM Operating Principle

In contrast to cavity-based BAM in radio-frequency (RF) synchronization [4], where the electron bunch excites a rather slowly decaying resonance, the EO-BAM detects an evanescent bipolar voltage signal [1]. The voltage is induced by the co-moving electric field of a bunch as the surface currents are disturbed by the pickup. The transient voltage leads to a current, which is transmitted via coaxial cables to a Mach-Zehnder-type electro-optical modulator (EOM) [1]. Usually the signals of two or more angular distributed pickups are

combined to compensate for orbit variations [5]. The voltage signal serves as input for the EOM, where the intensity of the reference laser pulse is modulated accordingly [1]. The EOM bias voltage is set to a value such that the laser pulse amplitude is reduced to 50 % of the maximum value in order to make use of the bipolar pickup signal. By adjustable delay lines the system is tuned to perfect timing, so that the reference pulse and the zero crossing (ZC) of the voltage signal coincide at nominal bunch arrival time without additional modulation [6]. Early or late bunches result in a positive or negative signal, which causes an intensity modulation [1]. The laser-intensity modulation is processed by dedicated receiver electronics [3, 6]. A calibration curve is used to deduce the arrival time for every electron bunch [3, 6].

For future applications it is desirable to reach lower bunch charges, while at the same time the demands for synchronization accuracy rise as well. The current BAMs are equipped with 40 GHz cone-shaped pickups designed for bunch charges down to 20 pC [5], which achieve an overall resolution of 3.5 fs with 250 pC nominal bunch charge in the synchronization system of the European XFEL [7]. For low charges the signal strength and therefore also the BAM sensitivity decreases rapidly.

EO-BAM Upgrade

To pave the way for 1 pC operation of the European XFEL, an upgrade of the arrival-time diagnostics is mandatory. To reach the goal of maintaining a resolution below 10 fs even at this low-charge operation, an upgrade of the main BAM components is necessary. First the RF part, comprising of the pickup structure and the signal transmission, and second, the EOM must be redesigned. The bandwidth of both components should be increased up to 100 GHz and the length of the transmission line has to be reduced [8].

The EOM's half-wave voltage V_{π} needs to be lowered in order to reach a high modulation with the low expected signal strength. To reduce cable losses especially at high frequencies, the EOM will be placed closer to the beamline and thus the radiation hardness has been examined. In a future upgrade it might even be integrated in the RF structure.

For the pickup system, it was proposed to have pickups and combination network integrated on a printed circuit board (PCB) [8, 9]. This idea was first combined with rod-shaped

* bernhard.scheible@iem.thm.de

DESIGN AND TEST OF A PROTOTYPE 324 MHz RF DEFLECTOR IN THE BUNCH SHAPE MONITOR FOR CSNS-II LINAC UPGRADE*

W.L. Huang^{†,1}, X.Y. Liu, Y.F. Sui, X.J. Nie

Institute of High Energy Physics, CAS, Beijing, China

Q.R. Liu, M.Y. Liu, University of Chinese Academy of Sciences, Beijing, China

¹also at China Spallation Neutron Source, Dongguan, China

Abstract

During the upgrade of linac in CSNS-II, the beam injection energy will increase from 80.1 MeV to 300 MeV and the beam power from 100 kW to 500 kW. A combined layout of superconducting spoke cavities and elliptical cavities is adopted to accelerate H- beam to 300 MeV. Due to a ~ 10 ps short bunch width at the exit of the spoke SC section, the longitudinal beam density distribution will be measured by bunch shape monitors using low energy secondary emission electrons. As the most important part of a bunch shape monitor, a prototype 324 MHz RF deflector is designed and tuned on the basis of a quasi-symmetric $\lambda/2$ 325 MHz coaxial resonator, which was fabricated for the C-ADS proton accelerator project. Preliminary parameters of the bunch shape monitor are presented. Simulation of the RF deflector and test results in the laboratory are described and analysed.

INTRODUCTION

China Spallation Neutron Source (CSNS) is the first pulsed neutron source built in China [1]. It consists of an 80 MeV H- linac, a 1.6 GeV proton rapid cycling synchrotron (RCS), two beam transport lines and a target station. We achieved the design goal of phase I with protons bombarding the target at a beam power of 100 kW in Feb. 2022, and now begins the upgrade project to 500 kW. During the linac upgrade, the DTL section will be followed by a section of 324 MHz double-spoke superconducting cavities and a section of 648 MHz elliptical superconducting cavities [2], as shown in Fig. 1. The proton beam will be accelerated to 300 MeV at the exit of the 8th cryomodule in the second SC section.

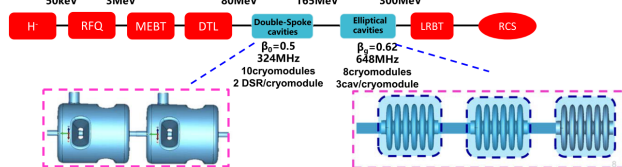


Figure 1: Superconducting cavities in CSNS-II [2].

Longitudinal bunch density distribution in ion linac is one of the main characteristics of accelerated beam. Bunch shape information is extremely important for medium energy accelerators consisting as a rule of two main parts with different rf frequencies. Results of bunch shape measurement after accelerating tank may be used to set rf phase and

amplitude. What's more, longitudinal bunch density may be used to calculate energy spectrum and longitudinal beam emittance [3-6]. In the CSNS-II linac upgrade plan, two bunch shape monitors will be installed. The transverse and longitudinal beam parameters at the BSM installation point are listed in Table 1.

Table 1: Micro Bunch Parameters in the Linac of CSNS-II

Micro Bunch	Spoke 1	ELL7
Energy (MeV)	86.97	300.1
RF Freq. (MHz)	324	648
$\Phi_{rms}(\circ)$	2.77	1.05
$X_{rms}(\text{mm})$	2.27	2.38
$Y_{rms}(\text{mm})$	4.1	2.28
$Z_{rms}(\text{mm})$	2.86	1.75

Due to the ultrahigh bandwidth requirement and long cable attenuation, the normal phase detectors, such as fast current transformers and wall current monitors, are not suitable to measure the bunch shape in ion linacs. The technique of a coherent transformation of a temporal bunch structure into a spatial charge distribution of secondary electrons through RF-modulation was initially implemented by R. Witkover for BNL linac [7]. An energy (longitudinal) RF-modulation of low energy secondary electrons was used. In the Feschenko type Bunch Shape Monitor (BSM), developed in INR RAS, a transverse RF-scanning is used [8]. Thus a similar BSM is adopted in the linac upgrade project of CSNS-II, as shown in Fig. 2.

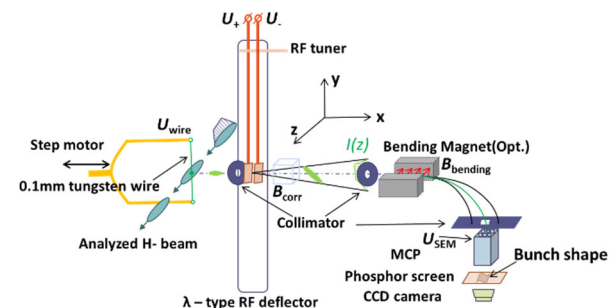


Figure 2: Configuration of bunch shape monitors in CSNS-II.

As the most important part of a bunch shape monitor, a prototype 325 MHz RF deflector was fabricated for the longitudinal bunch shape measurement in C-ADS. Due to the limitation of installing space, it was assumed to be tested at the CSNS linac. This paper will illustrate its design parameters and test results in the laboratory.

* Work supported by Natural Science Foundation of Guangdong Province, 2021A1515010269, National Natural Science Foundation, 11475204

[†] huangwei@ihep.ac.cn

DEVELOPMENT OF THE RF PHASE SHIFTER WITH FEMTOSECOND TIME DELAY RESOLUTION FOR THE PAL-XFEL LASER SYSTEM*

D.C. Shin[†], G.J. Kim, H. -S. Kang, G. Mun, C.-K. Min
Pohang Accelerator Laboratory, Pohang, South Korea

Abstract

We introduce the RF Phase Shifter (RPS) developed in the Pohang Accelerator Laboratory X-ray Free-Electron Laser (PAL-XFEL) to control the timing of optical laser system. This equipment is designed to finely adjust the timing of laser pulses with femtosecond scale by manipulating the phase of the RF reference using a couple of Direct Digital Synthesizer (DDS) devices. Furthermore, it is designed with low phase noise and low phase drift features in order to minimize the impact on the system in an open-loop operation.

Currently these units are installed at the Injection site, Hard X-ray and Soft X-ray Beamline. They are implemented for the feedback control of the photocathode gun phase at the Injector and for the use in pump-probe experiments at the Beamlines. This paper describes the design, fabrication, and experimental results of the RPS, as well as its usage status at PAL-XFEL.

INTRODUCTION

Optical Laser systems have been established in the Injector and Beamlines at PAL-XFEL for generating a highly stable electron beam and ultrafast X-ray sciences.

Time delay is a critical function in laser systems. In the Injector section of PAL-XFEL, laser time delay is utilized to compensate for drift of the electron beam. In the Beamline, it is employed to control the time delay of the pump laser in pump-probe experiments. The time delay of lasers can typically be adjusted by altering the physical length of the laser path using mirrors and delay stages. The PAL-XFEL laser system has employed this method since its early operational stages [1].

However, the approach involving delay stages can lead to degradation in laser quality due to vibration and shift in laser focus. Additionally, the difficulty in adjusting the time delay at pulse-to-pulse speed (60 Hz) results in the waste of the probe laser in pump-probe experiments.

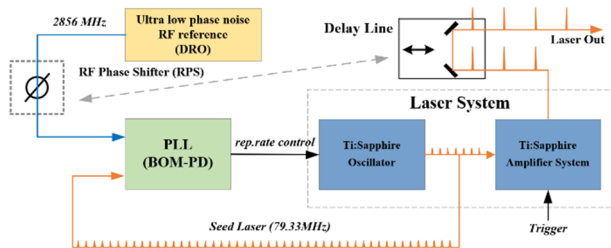


Figure 1: RPS and delay stage in the injector laser.

To address these aspects, we believed that a digital time delay control device would be more effective than mechanical time delay methods. As shown in Fig. 1, we considered installing an RF phase shifter between the REF and PLL to modify the phase. By adjusting the phase in this manner, we expected that a corresponding time delay proportional to the phase change would naturally occur during the Lock Tracking process of the PLL. Additionally, we fabricated a prototype device and confirmed its operation to be as expected.

We manufactured and installed a total of six devices in both the Injector laser and Beamline laser systems. In the following section, we will introduce the fabrication process and outcomes of the RF Phase Shifter.

DESIGN OF THE RPS

Key Specifications

Considering the requirements from the laser team and the limitations of electronic devices, we have defined the specifications as follows:

- Phase Control Resolution: 0.0055 degrees
- Control Range: $(-2^{30} \sim 2^{30}) \times \text{resolution}$
- Linearity (0~360 degrees): $\leq \pm 0.05$ degrees
- Update Rate: ≥ 10 kHz
- Stability degrees/day: ≤ 0.1 degrees
- Phase Noise: ≤ -150 dBc@100 kHz~1 MHz

Determination of Phase Shifting Methods

We explored various phase shifting methods to develop a unit that satisfies the specifications at a reasonable cost. Initially, we considered Digital/Voltage Controlled Phase Shifter components due to their affordability and straightforward control mechanisms. However, after reviewing the datasheets, we determined that they would not meet the required resolution and linearity specifications [2, 3].

The vector modulation approach allows for high resolution implementation, but due to hardware issues such as phase unbalance in Hybrid and Combiner, as well as I/Q DC offset, the linearity of the output phase deteriorates. Therefore, meticulous calibration efforts are required to meet the linearity specifications. However, even with such calibration, we had determined that achieving the less than ± 0.05 degrees linearity is very challenging [4].

Next, we examined the DDS device. The DDS enables precise frequency/phase control and fast response characteristics by converting digital values obtained through the 'Phase Accumulator' and 'Amplitude/Sine Converter' into RF signals via the DAC (Digital-to-Analog Converter) [5].

* Work supported by Ministry of Science and ICT of Korea

[†] dcshin@postech.ac.kr

CHARACTERISATION OF CHERENKOV DIFFRACTION RADIATION USING ELECTRO-OPTICAL METHODS

A. Schlögelhofer^{1,*}, T. Lefèvre, S. Mazzoni, E. Senes, CERN, Geneva, Switzerland
 L. Duvillaret, KAPTEOS, Saint-Helene-du-Lac, France
¹ also at TU Wien, Vienna, Austria

Abstract

The properties of Cherenkov diffraction radiation (ChDR) have been studied extensively during the recent years to be exploited for non-invasive beam diagnostic devices for short bunches. The dependence of charge and the influence of the bunch form factor on the coherent part of the radiated spectrum have been demonstrated and studied in the past. However, the actual field strength of coherent ChDR as well as its study in time domain need further investigation. In this contribution we are using electro-optical techniques to investigate and quantify these parameters. The electro-optical read-out brings the advantage of high bandwidth acquisition and insensitivity to electromagnetic interference, whereas at the same time a large fraction of the acquisition setup can be installed and operated outside of the radiation controlled areas. We will present experimental results from the CLEAR facility at CERN as well as simulations of the peak field of the temporal profile of beam-generated ChDR pulses.

INTRODUCTION

Cherenkov diffraction radiation (ChDR) describes the radiation produced at the surface of a dielectric by the electric field of a relativistic charged particle passing by in the vicinity of the dielectric. This mechanism is illustrated in Fig. 1, where the ChDR is emitted at the well-defined Cherenkov angle $\cos(\theta_{Ch}) = 1/(n_1 \beta)$ with n_1 denoting the refractive index of the dielectric medium and $\beta = v/c$ the normalized velocity of the charged particle. The produced ChDR can be analysed to measure critical properties of a beam of charged particles, e.g. its length or position [1]. While previous work focused on studying the qualitative behaviour of ChDR and measuring the frequency spectrum to reconstruct beam properties [2-4], this contribution shows the measurement of the electric field strength generated by coherent ChDR in terms of absolute numbers by sampling its temporal profile.

METHODOLOGY

An electro-optical probe (eo-probe) [5] was used to obtain a real-time high bandwidth measurement insensitive to electromagnetic interference.

Working Principle of the Eo-Probe

The eo-probe is fully dielectric and, amongst other optical elements, contains a sensing crystal made out of BSO ($\text{Bi}_{12}\text{SiO}_{20}$). It utilizes the Pockels effect, which describes

* andreas.schloegelhofer@cern.ch

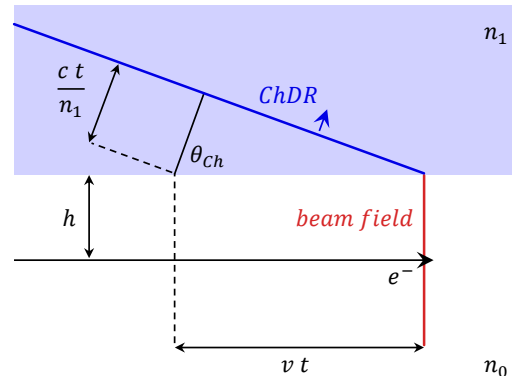


Figure 1: Schematic of the ChDR principle in a dielectric medium ($n_1 \approx 3$). The Cherenkov condition $n_1 \cdot v/c > 1$ must be satisfied to produce ChDR.

the linear change of the refractive index of a medium exposed to an external electric field. This induced refractive index change introduces a birefringence in the BSO crystal. A continuous-wave sensing laser of known polarization is sent through the crystal. During exposure to an external electric field, the BSO crystal alters the polarization state of the sensing laser. The modulated laser light passes through polarizers, and its changed polarization state is then analyzed with fast photodiodes. Using this principle, the eo-probe measures the electric field vector up to field strengths of MV/m.

The eo-probe (with a bandwidth ≤ 10 GHz) was placed in the accelerator hall. All the other parts of the detection system were placed outside the radiation-controlled area. The sensing laser was transported to the probe via 20-metre-long optical fibres. The signal was measured with a high-bandwidth oscilloscope (10 GHz, 256 GSa/s, 10-bit) and then corrected for the change of insertion loss during the measurement as well as converted according to the antenna factor of the probe to obtain an absolute electric field measurement. As the electric field strength scales linearly with the bunch charge, the bunch charge was also independently recorded. All the data presented in this contribution are normalized to a bunch charge of 300 pC.

CALIBRATION

To calibrate the system's response, a first measurement campaign was performed on the direct beam field of an electron bunch propagating in air.

The bandwidth of the data acquisition system is limited to 10 GHz. Therefore, as electron bunches at the CLEAR

APPLICATION OF A CAMERA ARRAY FOR THE UPGRADE OF THE AWAKE SPECTROMETER

Eugenio Senes*¹, F. Pannell², D.A. Cooke², S. Mazzoni¹,
M. Turner¹, M. Wing², G. Zevi Della Porta^{1,3}
¹ CERN, Geneva, Switzerland

² University College London, London, United Kingdom

³ Max Planck Institute for Physics, Munich, Germany

Abstract

The first run of the AWAKE experiment successfully demonstrated the acceleration of an electron beam in the plasma wakefields of a relativistic proton beam. The planned second run will focus on the control of the emittance of accelerated electrons, requiring an upgrade of the existing spectrometer. Preliminary measurements showed that this might be achieved by improving the resolution of the scintillator and with a new design of the optical system. This contribution discusses the application of a digital camera array in close proximity of the spectrometer scintillator, to enable the accelerated electron beam emittance measurement.

INTRODUCTION

In the AWAKE experiment, a 19 MeV electron bunch gets accelerated in the wakefield of a rubidium plasma [1]. The plasma wake is driven by a 400 GeV proton bunch produced in the CERN Super Proton Synchrotron.

In order to measure the characteristics of the accelerated electron beam, a magnetic spectrometer was installed downstream of the plasma cell. The development of the magnetic spectrometer is reported in [2–4].

The core functions of the electron spectrometer are to measure on the accelerated electron beam:

1. The beam peak energy and energy profile
2. The beam charge
3. The beam emittance

In AWAKE Run 1 the resolution proved to be too limited to measure the beam emittance; a study was launched to improve the spectrometer system for AWAKE Run 2. This paper discusses possible technical implementations to improve the spectrometer resolution, focusing on a high resolution optical system. Possible modifications of the spectrometer magnetic lattice to transport the accelerated beam will be discussed elsewhere, and go beyond the scope of this work.

SPECTROMETER DESIGN

Beamline Components

The magnetic components of the spectrometer have not changed since AWAKE Run 1 [5, 6]. The electron and proton

beams exit the plasma, pass through a quadrupole doublet and then through a dipole magnet. A dipole field up to 1.5 T separates the electron and proton beams, introducing a spatial dependence for the electron beam energy in the range 30 MeV–8.5 GeV. After the dipole, the accelerated electrons traverse a 2 mm thick vacuum window, and impact on a 1 m-long plastic scintillator. The scintillator currently in use is a 0.5 mm thick DRZ-High, a terbium-doped, gadolinium oxysulfide (Gd₂O₂S:Tb) screen produced by Mitsubishi Chemical. The particle transport through the spectrometer was simulated and validated through measurements with partially stripped ions [7, 8]. A layout of the spectrometer system is shown in Fig. 1.

Optical System

Information on the electron beam structure is reconstructed from the emitted light pattern produced by the scintillator. An accurate imaging of the scintillator emission is essential for a correct measurement of the electron beam parameters.

During AWAKE Run 1, the scintillation light was propagated through a 17 m-long optical line, to reach an intensified camera in a dedicated dark room outside the high radiation area [9, 10]. The camera is equipped with a 400 mm photographic lens, in order to resolve the whole scintillator. Although this system worked, the optical resolution proved to be too limited for emittance measurements.

Recent developments in the CMOS camera infrastructure for AWAKE allowed for placing cameras inside the experimental hall. A camera array was installed within 1.5 m of the scintillator, to record its light. This system is described in detail later on.

Beam Charge Measurement

In order to measure the total accelerated charge, the scintillator light yield is calibrated against a known electron charge. In the past, the calibration was performed by installing the scintillator and the camera in the CLEAR test accelerator [11], and using electron beams with known charge. To allow for the in-situ calibration, a commercial Integrating Current Transformer (ICT) from Bergoz [12] was installed in the beamline upstream of the dipole. The charge signal is detected with custom electronics within a range of 750 pC.

* eugenio.senes@cern.ch

BUNCH COMPRESSOR MONITORS FOR THE CHARACTERIZATION OF THE ELECTRON BUNCH LENGTH IN A LINAC-DRIVEN FEL

G. L. Orlandi*

Paul Scherrer Institut, Villigen, Switzerland

Abstract

The lasing performance of a Free Electron Laser (FEL) strongly relies on a precise characterization of the electron bunch length and on the control and stabilization of the bunch compression settings of the machine under normal user operations. In a FEL driver linac, the so-called Bunch Compressor Monitors (BCMs) normally ensure the non-invasive monitoring of the electron bunch length. BCMs, being sensitive to the temporal coherent threshold of the radiation energy emitted by the electron beam crossing the last dipole of a magnetic chicane or a holed diffraction screen just downstream, can provide a bunch length dependent signal resulting from the integration of the detected radiation pulse energy over the acceptance frequency band of the detector. Thanks to the non-invasiveness, BCMs are primary diagnostics in a FEL to stabilize the bunch compression by feeding back the RF settings of the accelerating structure. In this contribution, we present a formal method to determine an absolute measurement of the electron bunch length from the analysis of a BCM signal.

INTRODUCTION

The lasing performance of a linac driven x-ray Free Electron Laser (FEL) strongly depends on the beam quality and capability to preserve it all along the entire acceleration and compression stages of the electron beam. Electron beams with a small emittance and a smooth longitudinal profile are typically generated in a FEL by photocathode guns. In order to counteract the effects of beam emittance dilution due space charge at the early stage of the acceleration, relatively long bunch lengths are generated at the cathode. Hence the necessity to longitudinally compress the electron bunch-length at higher energy stages of the acceleration. Besides a characterization and optimization of the beam emittance, the machine set up for FEL users' operations requires an optimization of the compression scheme by means of precise measurements of the electron bunch length that represents the upper limit for the laser pulse duration. In a linac driven FEL, absolute and precise measurements of the electron bunch length are normally carried out by means of rf Transverse Deflecting Structures (TDSs). The rf field resonating in a TDS structure induces a chirp of the transverse momentum of the electrons in the bunch vs the electron arrival time. The imaging and the analysis of the spatial trace produced by the electron beam impinging on a downstream view-screen permits to estimate the electron bunch length provided that a calibration of the image centroid vs TDS phase is known [1-5]. Main drawback of a TDS based

measurement of the electron bunch length is the fully beam invasiveness as well as possible machine protection issues due to beam losses. After the initial machine set-up, the monitoring of the electron bunch-length during FEL users' operations is normally ensured by Bunch Compressor Monitors (BCMs) [6-13] also called Bunch Length Monitors. In a linac-driven FEL, a BCM is normally designed to detect the synchrotron radiation (SR) emitted by the electron beam while crossing the fourth dipole of a magnetic chicane or the diffraction radiation produced by the electron beam passing through a holed diffraction screen placed just downstream of the magnetic chicane. The wavelength acceptance of a BCM detector is designed to match with the temporal coherent enhancement of the radiation spectral energy emitted by the electron beam at the given compression stage. BCMs in a linac-driven FEL such as, for instance, SwissFEL [14, 15] are typically designed not to perform a spectral reconstruction of the detected radiation energy distribution by means of a spectrometer. Main goal of a BCM is to provide - in a real-time - a bunch-length dependent signal to the machine compression feedback rather than an off-line reconstruction of the absolute value of the electron bunch length from a cumbersome analysis of a spectrogram. In most of the cases, the BCM output signal is hence the result of the integration of the detected radiation energy over the full acceptance wavelength band of the detector. The bunch-length dependent output signal of a BCM can be so fruitfully exploited for a fully non-invasive and shot-sequential monitoring of the electron beam during a FEL users' session and for a stabilization of the bunch compression by means of a feedback loop of the rf parameters (field phase and amplitude) of the accelerating structures.

In the present work, we will present a formal method of analysis of the BCM signals that permits an absolute determination of the electron bunch length. The implementation of the aforementioned formal method will be presented for two different scenarios: the simple case of a BCM equipped with a single detector; the more advanced case of a BCM equipped with two detectors with a different wavelength band of acceptance which are simultaneously illuminated by the same light pulse emitted by the electron beam thanks to a beam splitter and a suitable optics. In the case of a BCM with a single detector, the presented method permits to track the relative variation of the electron bunch length with respect to a reference value - either the mean value over a sequence of data acquisition or the shot-sequential value - as a function of the corresponding statistical fluctuations of the measured relative variations of the beam charge and BCM signal. In the case of a BCM equipped with two independent detectors having a different acceptance wavelength

* gianluca.orlandi@psi.ch

MICROBUNCHING OF THERMIONIC CATHODE RF GUN BEAMS IN THE ADVANCED PHOTON SOURCE S-BAND LINAC *

J. Dooling[†], A. Brill, N. Kuklev, I. Lobach, A. Lumpkin, N. Sereno, Y. Sun
Argonne National Laboratory, Lemont, IL, USA

Abstract

We report on measurements of beams from thermionic cathode (TC) rf guns in the Advanced Photon Source S-Band Linac. These measurements include the macropulse out of both new and existing TC guns as well as the observation of microbunching within the micropulses of these beams. A gun chopper limits the macropulse FWHM duration to the 10 ns range. Our objectives were to analyse the new TC gun and investigate microbunching within a TC-rf-gun-generated beam. Our diagnostics elucidated longitudinal beam structures from the ns to the fs time scales. Coherent transition radiation (CTR) interferometers responding to far-infrared wavelengths were employed after each compression stage to provide the autocorrelations of the sub-ps micropulse durations. The first compression stage is an alpha magnet and the second a chicane. A CCD camera was used to image the beam via optical transition radiation from an Al screen at the end of the linac and also employed to measure coherent optical transition radiation (COTR) in the visible range. The COTR diagnostic observations, implying microbunching on a fs time scale, are presented and compared with a longitudinal space-charge impedance model.

INTRODUCTION

The injection system of the Advanced Photon Source (APS) has relied on thermionic cathode (TC) rf guns as electron-beam sources since 2001 [1]. This will continue to be the case for the APS Upgrade with the multi-bend achromatic magnet lattice installation in the 6 GeV storage ring currently in progress [2]. There are two such S-Band TC rf guns installed in the linac so that one is a "hot" spare. We report the basic testing of the beams from new generation TC rf guns manufactured by RadiaBeam Technologies (RBT) [3] in terms of the ≈ 10 ns long macropulse composed of micropulses with an S-Band repetition frequency (2856 MHz). We obtained basic macropulse data for a newly installed RBT gun to comparison with one of a set of three TC rf guns purchased from AET Associates (AET) in 2001. The AET guns have been the primary electron source for the APS since that time.

Our interest was to measure the charge of each micropulse within the macropulse structure from the chopper-gated [4], TC-rf gun [5–7]. The extraction of charge from the TC rf gun involves high-power rf applied to the cathode; thus, the extracted charge comes in a series of micropulses. With the macropulse temporal distribution, we can then determine

the charge per micropulse. Only the AET gun was employed for the bunch compression experiment discussed below.

In the APS linac, the micropulse duration after the alpha magnet is sub-ps. After further compression in the chicane, longitudinal space charge (LSC) induced microbunching within the micropulses generates coherent optical transition radiation (COTR) when striking the downstream intercepting Al screen. The COTR (visible wavelengths, fs temporal scale) was transported out of the tunnel to a CCD camera, and the images were recorded. We present a comparison of the observed COTR enhancements with the predictions of a LSC-impedance model.

EXPERIMENTAL DESCRIPTION

A schematic of the linac with components relevant for the present discussion is presented in Fig. 1. Compression is provided by the alpha magnet at the end of the gun beam line and the L3 chicane after the first four accelerating structures in L2. Coherent Transition Radiation far-infrared (CTR FIR) interferometers, positioned in the L2 section (L2:CTR) and after the chicane (L3:CTR), provide longitudinal pulse length data [8]. Average current is monitored immediately after the gun and macropulse charge is measured after the alpha magnet in the linac beamline. Optical transition radiation (OTR) and COTR are generated by an Al screen (S5:OTR, as shown in Fig. 1) when struck by the electron beam. An optical transport line guides the light to a camera system outside of the tunnel.

A block diagram of the macropulse duration measurement is presented in Fig. 2. Raw beam signals from the four button pickups are input to 20 dB directional couplers (Mini-Circuits ZGDC20-33HP+). The coupled signals ("c") are combined to form the sum output (Mini-Circuits ZN4PD-642W-S+) which is fed into one channel of a fast oscilloscope with 50 Ω input impedance. The main, uncoupled signals continue on to the analog conditioning electronics associated with the rest of the S-band linac BPMs [9–11]. Because of capacitive coupling, the DC component of the macropulse is not present. Alternatively, the summing unit can be bypassed to provide coupled input to the oscilloscope from all four of the BPM channels. Four channel input allows for observation of beam position within the macropulse. The BPM rf signals are digitally undersampled by the oscilloscope's analog-to-digital converter following the discussion in Ref. [12].

A new 1.5-cell, TC rf gun developed by RBT was installed at the RG1 location in the linac during the December 2022-January 2023 APS maintenance period. We wished to measure the macropulse waveform of this gun to compare with that of the operating TC gun. Further tests with the RBT

* Work supported by the U.S. D.O.E., Office of Science, Office of Basic Energy Sciences, under contract number DE-AC02-06CH11357.

[†] dooling@aps.anl.gov

COLLIMATOR IRRADIATION STUDIES AT THE ADVANCED PHOTON SOURCE*

J. Dooling[†], W. Berg, M. Borland, J. Calvey, L. Emery, A. Grannan, K. Harkay, Y. Lee,
 R. Lindberg, G. Navrotski, V. Sajaev, N. Sereno, J. Stevens, Y. Sun, K. P. Wootton
 Argonne National Laboratory, Lemont, Illinois, USA
 N. Cook, RadiaSoft LLC, Boulder, Colorado, USA
 D. Lee, S. Riedel, University of California, Santa Cruz, Santa Cruz, California, USA

Abstract

We present results from a recent collimator irradiation experiment conducted in the Advanced Photon Source (APS) storage ring. This experiment is the third in a series of studies to examine the effects of high-intensity electron beams on potential collimator material for the APS-Upgrade (APS-U). The intent here is to determine if a fan-out kicker can sufficiently reduce e-beam power density to protect horizontal collimators planned for installation in the APS-U storage ring. The fan-out kicker (FOK) spreads the bunched-beam vertically allowing it to grow in transverse dimensions prior to striking the collimator. In the present experiment, one of the two collimator test pieces is fabricated from oxygen-free copper; and the other is from 6061-T6 aluminum. As in past studies, diagnostics include turn-by-turn BPMs, a diagnostic image system, fast beam loss monitors, a pin-hole camera, and a current monitor. Post-irradiation analyses employ microscopy and metallurgy. To avoid confusion from multiple strikes, only three beam aborts are carried out on each of the collimator pieces; two with the FOK on and the other with it off. Observed hydrodynamic behavior will be compared with coupled codes.

INTRODUCTION

Previous whole-beam-loss experiments carried out in 2019 and 2020 in the Advanced Photon Source (APS) storage ring (SR) studied effects in aluminum and titanium collimator test pieces [1–3]. No steps were taken to mitigate damage caused by the high intensity electron beam during these earlier studies. In the present experiment, a vertically-deflecting fan-out kicker (FOK) was employed to spread the beam bunch train transversely on both aluminum and copper targets. The action of the FOK spreads both the bunch train as well as individual bunches; in the latter case, by forcing them into regions of non-linear focusing.

Unlike earlier collimator experiments, where studies were carried out at the beginning of a user run, this study took place during the final Machine Studies period at the end of APS SR operations. The collimator test pieces were installed for the entire final run and thus were well conditioned for the experiment.

* Work supported by the U.S. D.O.E., Office of Science, Office of Basic Energy Sciences, under contract number DE-AC02-06CH11357.

[†] dooling@anl.gov

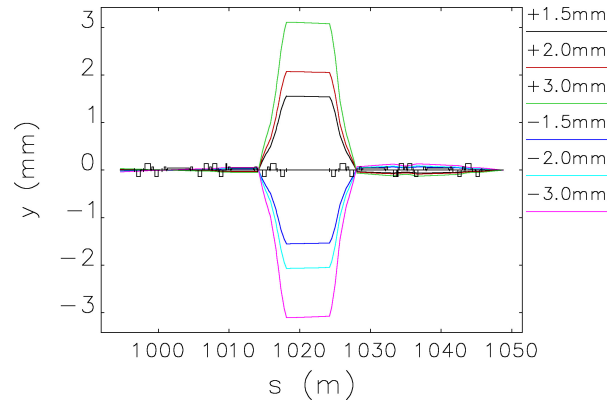


Figure 1: Vertical bumps in the Sector 37 region modeled with elegant.

Table 1: Beam Abort Case List Parameters

Case No.	Vertical Offset (mm)	Mat'l	FOK Voltage (kV)	Vertical Defl. Angle y' (μ rad)
0	+1.5	Cu	2	245.0
1	-1.5	Al	2	245.0
2	-2.0	Al	1	122.5
3	+3.0	Cu	0	0
4	-3.0	Al	0	0
5	+2.0	Cu	3	367.5

EXPERIMENTAL DESCRIPTION

As in previous experiments, the collimator test piece targets were placed in the Sector 37 (S37) straight section approximately 2 m downstream of the fourth S37 rf cavity. Vertical orbit bumps in the S37 region used to separate the strike regions on the targets were simulated with eLlegant [4, 5] and shown in Fig. 1. With positive y -bumps, the beam strikes copper and with negative bumps, the beam intercepts aluminum.

Six separate whole-beam aborts with 200 mA, 6 GeV beam were employed to strike the collimator test pieces; three on the copper and three on the aluminum. The six cases are summarized in Table 1.

A HYBRID APPROACH TO UPGRADE HARDWARE FOR THE PROTON STORAGE RING FAST KICKER

T. Ramakrishnan, J. Duran, H. Watkins
Los Alamos National Laboratory, Los Alamos, USA

Abstract

The Los Alamos Neutron Science Center (LANSCE) Proton Storage Ring (PSR) needs precise timing to ensure successful extraction of the bunched protons. The current control system's hardware is obsolete and unmaintainable. The task was to replace the 1980's era CAMAC control and timing system for the PSR extraction kickers. This included a system which halts charging of the kickers after a duration without firing to prevent equipment damage. A hybrid approach was taken to integrate a Berkeley Nuclear Electronics Corporation (BNC) pulse generator that was controlled by a soft input/output controller (IOC) and National Instrument (NI) compact Reconfigurable Input/Output (cRIO) IOC. This allowed for flexibility and modularity of the software and hardware development. This approach built the framework to streamline robust deployment of hybrid systems and develop a solution for upgrades of other LANSCE kickers.

INTRODUCTION

Proton Storage Ring

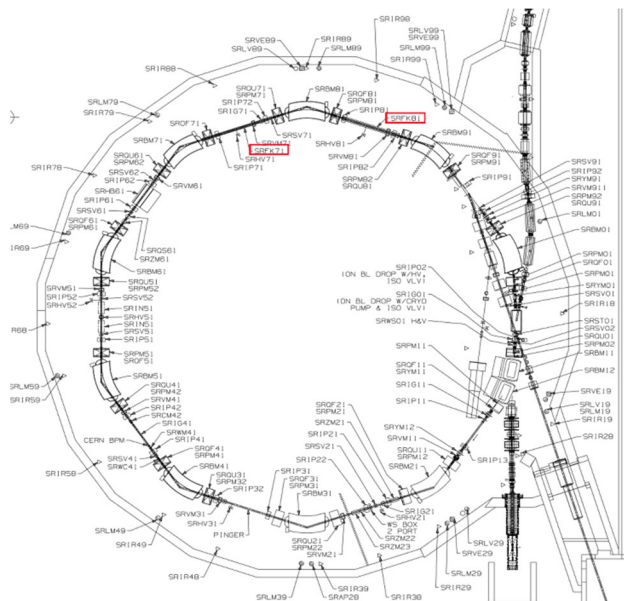
The LANSCE proton storage ring (PSR) [1], Fig. 1, is used to collect and bunch protons. The alignment and frequency of the protons are changed continuously to keep them inside the ring for multiple cycles which are then ejected to the Lujan Mark IV target [2] to produce neutrons which are used in several experiments.

Fast Kicker Purpose & Controls Upgrade

The storage fast kicker (SRFK) [3] system consists of a DC power supply, a Blumelein [4] that acts as a capacitor, and two plates (SRFK71 and SRFK81) as well as a control system that directs and monitors certain functionality. The fast kicker system is responsible for extracting the bunched protons from the PSR and sending them down the beam line towards the neutron producing target.

The control system that was upgraded used an obsolete, 1980's, CAMAC form factor. It is worth mentioning that it had no safety mechanisms in place for over charging the fast kicker Blumelein which is holding the charge that is being provided in a pulsed fashion by a DC power supply. The newly deployed and functionality advanced control system utilizes a hybrid approach by using two commercial of the shelf systems (a) BNC 577 pulse generator [5] for generating delayed pulses and (b) cRIO [6] for reading back the status of an RF switch and keeps track of charging

pulses to the Blumelein. The hybrid approach also extends to the controls software implementing (a) soft IOC to control the BNC 577 and (b) NI cRIO based IOC that has a field programmable gate architecture (FPGA) [7] backplane interacting with the modules for high-speed data acquisition.



BEAM TEST OF A HARMONIC KICKER CAVITY*

M. W. Bruker[†], J. Grames, J. Guo, J. Musson, S. A. Overstreet, G. T. Park,
 T. Plawski, M. Poelker, R. Rimmer, H. Wang, C. Wilson, S. Zhang
 Thomas Jefferson National Accelerator Facility, Newport News, VA, USA
 M. Pablo, B. Roberts, D. Speirs, Electrodynamic, Albuquerque, NM, USA

Abstract

A harmonically resonant kicker cavity designed for beam exchange in a circulator cooler was built and successfully tested at the Upgraded Injector Test Facility (UITF) at Jefferson Lab. This type of cavity is being considered for the injection scheme of the Rapid Cycling Synchrotron at the Electron-Ion Collider, where the spacing of neighboring bunches demands very short kicks. Operating with five transversely deflecting modes simultaneously that resonate at 86.6 MHz and consecutive odd harmonics thereof, the prototype cavity selectively deflects 1 of 11 electron bunches while leaving the others unperturbed. An RF driver was developed to synthesize phase- and amplitude-controlled harmonic signals and combine them to drive the cavity while also separating the modes from a field-probe antenna for RF feedback and dynamic tuning. Beam deflection was measured by sweeping the cavity phase; the deflection waveform agrees with expectations, having sub-nanosecond rise and fall times. No emittance increase is observed. Harmonically resonant cavities like the one described provide a new capability for injection and extraction at circulators and rings.

INTRODUCTION

In circulating accelerators, the minimum bunch spacing needed to accommodate the rise/fall time of a kicker can limit the design options for the bunch train. Originally developed for the Circulating Cooler Ring, a hypothetical ring with 11 revolutions driven by an energy-recovery linac that was intended to be part of the Jefferson Lab Electron-Ion Collider [1], the harmonic kicker cavity offers a new option for applications where every n th bunch must be deflected [2]. One such application is the injection into the Rapid Cycling Synchrotron at the Electron-Ion Collider [3], where one out of four consecutive bunches is injected at a time; here, the bunch spacing is 1.6 ns, and each set of four bunches is followed by a gap of 12 μ s, encouraging the use of a pulsed device but out of reach for a stripline due to the short bunch spacing.

A harmonic kicker is a transversely deflecting cavity that can be excited at multiple harmonic frequencies at the same time, allowing one to Fourier-synthesize any deflection waveform containing only these frequencies; the high Q of the modes compared to a stripline makes the drive power manageable, while pulsed drive is still possible if the gap between

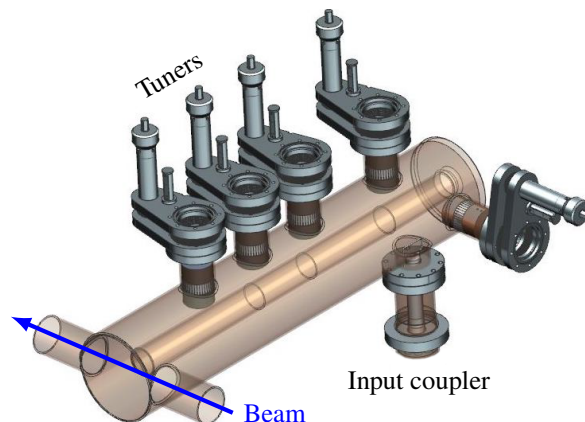


Figure 1: CAD model of a 5-mode harmonic kicker cavity. Five stub tuners are needed to tune all modes. The RF signal is coupled in through a single port; another port serves as the field probe (not shown here).

sets of bunches is sufficiently long. Figure 1 shows a model of the prototype reduced to the most important parts.

An example waveform providing a kick to 1 out of 11 bunches is shown in Fig. 2. The usefulness of this type of waveform is not characterized by its absolute flatness outside of the main peak but by the locations of its zero crossings or minor peaks, depending on design. While conceptually flexible, the mode structure of such cavities must be chosen according to the bunch timing of the intended application.

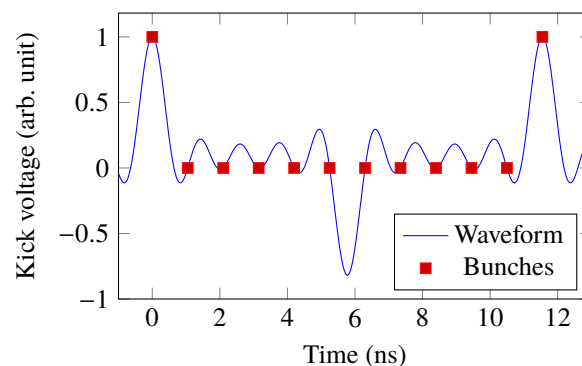


Figure 2: Kick action only on bunches at a bunch frequency equal to the fundamental of the kick waveform, $f_{HK} = 86.6$ MHz; in this example, all 11 buckets are filled at a bunch frequency of $11 f_{HK} = 952.6$ MHz.

Compared to placing multiple cavities with different resonant frequencies in series, combining the modes in one cavity has the upside of providing all the deflection in the

* Work supported by the U.S. Department of Energy, Office of Science, Office of Nuclear Physics under contract DE-AC05-06OR23177. Multi-Harmonic driver development has been supported by DOE's NP SBIR program (DE-SC0020566).

[†] bruker@jlab.org

AXIAL CRYOGENIC CURRENT COMPARATOR (CCC) FOR FAIR

L. Crescimbeni^{†1}, F. Schmid¹, Friedrich-Schiller-University Jena, Jena, Germany
 D. M. Haider, A. Reiter, M. Schwickert, T. Sieber
 GSI Helmholtz Centre for Heavy Ion Research, Darmstadt, Germany
 M. Schmelz, R. Stolz³, V. Zakosarenko⁴, Leibniz IPHT, Jena, Germany
 T. Stoehlker^{1,2}, V. Tympel¹, Helmholtz Institute Jena, Jena, Germany
¹also at GSI Helmholtz Centre for Heavy Ion Research, Darmstadt, Germany
²also at Institute for Optics and Quantum Electronics, Jena, Germany
³also at Technical University Ilmenau, Ilmenau, Germany
⁴also at supracon AG, Jena, Germany

Abstract

The Cryogenic Current Comparator (CCC) is a superconducting device based on an ultrasensitive SQUID (superconductive quantum interference device) magnetometer (fT range). Measuring the beam azimuthal magnetic field, it provides a calibrated non-destructive measurement of beam current with a resolution of 10 nA or better, independent from ion species and without tedious calibrations procedure. The non-interceptive absolute intensity measurement of weak ion beams (< 1 μ A) is essential in heavy ion storage rings and in transfer lines at FAIR. With standard diagnostics, this measurement is challenging for bunched beams and virtually impossible for coasting beams. To improve the performance of the CCC detector several upgrades are under study and development: One is the investigation of a new type of CCC using an alternative magnetic shield geometry. The so-called “axial” geometry will allow for much higher magnetic shielding factor, an increased pick-up area, and a reduced low frequencies noise component. Further improvements and optimizations of the detector will be presented. The CCC will be tested on the beamline at the end of 2023 allowing to define the best possible version for FAIR.

INTRODUCTION

After proof of principle with an earlier CCC version [1], the first prototype of CCC for GSI and FAIR is the FAIR-Nb-CCC-xD (Fig. 1) that is part of the family of CCC-XD that has been developed for the use with the beamline dimensions at FAIR HEBT (\varnothing 150 mm).

The CCC is installed in a beam-line cryostat [2] equipped with a helium reliquifier[†] that provides stable operating conditions.

The CCC has been tested in CRYRING@ESR [3] confirming the viability of the detector and its current resolution in the order of nA. The test in CRYRING@ESR has shown some limitation of the system like the limited slew rate and the low magnetic shielding. The CCC prototype is

built out of niobium, causing high costs and several mechanical difficulties in the construction process (for example the needing of electron beam welding). Other than this, the FAIR-Nb-CCC-xD is equipped with a high permeability core, that produces low frequencies noise (due to trapped magnetic field) and introduces the need of a low pass circuit to avoid resonances, reducing the maximum bandwidth of the system.

To improve these aspects of the detector a new version of the CCC, with an axial geometry, has been developed.

NEW AXIAL CORELESS CCC

A new type of CCC, developed together with IPHT Jena, will be built out of lead with an axial shield geometry and without a high permeability core (Fig. 1).

Radial CCC with Core Axial Coreless CCC

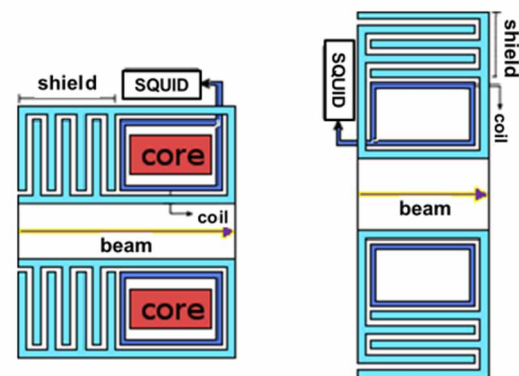


Figure 1: Left: Radial Geometry, like the FAIR-Nb-CCC-xD, with high permeability core. Right: Axial geometry coreless CCC, made of lead, the pickup coil is filled only with non magnetic foam for structural support.

The axial CCC is expected to be less sensitive to external perturbations, in particular very low-frequency noise (<1 Hz), caused by magnetic field caught inside the core material [4], and less sensitive to mechanical perturbation.

The new coreless lead CCC will have a much higher screening factor due to the axial magnetic shield composed of 10 layers of lead sheet [5]. The simulation shows a theoretical screening factor higher than 200 dB, reducing the effect of a magnetic perturbation in the order of 10 μ T

*Work supported by AVA – Accelerators Validating Antimatter the EU H2020 Marie-Curie Action No. 721559 and by the BMBF under contract No 05P21SJRB1.

[†]l.crescimbeni@gsi.de

[†]Model PT415 from Cryomech Inc, Syracuse, NY, USA

MULTI-TILE ZINC-OXIDE-BASED RADIATION-HARD FAST SCINTILLATION COUNTER FOR RELATIVISTIC HEAVY-ION BEAM DIAGNOSTICS: PROTOTYPE DESIGN AND TEST^{*†}

M. Saifulin^{1,‡}, P. Boutachkov, C. Trautmann¹, B. Walasek-Höhne
GSI Helmholtz Center for Heavy Ion Research, Darmstadt, Germany
P. Rodnyi, I. Venevtsev, Peter the Great Polytechnic University, St. Petersburg, Russia
E. Gorokhova, JSC S.I. Vavilov State Optical Institute, St. Petersburg, Russia
¹also at Technical University Darmstadt, Darmstadt, Germany

Abstract

This contribution summarizes the design and performance test of a prototype radiation-hard fast scintillation detector based on the indium-doped zinc oxide ceramic scintillator, ZnO(In). The prototype detector has been developed for use as a beam diagnostics tool for high-energy beam lines of the SIS18 synchrotron at the GSI Helmholtz Center for Heavy Ion Research GmbH. The new detector consists of multiple ZnO(In) scintillating ceramics tiles stacked on the front and back sides of a borosilicate light guide. The performance of the detector was tested in comparison to a standard plastic scintillation detector with 300 MeV/u energy ⁴⁰Ar, ¹⁹⁷Au, ²⁰⁸Pb, and ²³⁸U ion beams.

The investigated prototype exhibits 100% counting efficiency and radiation hardness of a few orders of magnitude higher than the standard plastic scintillation counter. Therefore, it provides an improved beam diagnostics tool for relativistic heavy-ion beam measurements.

INTRODUCTION

The heavy-ion accelerator facility at the GSI Helmholtz Center for Heavy Ion Research (Darmstadt, Germany) and other similar ion-beam facilities worldwide provide energetic heavy-ion beams for a wide range of research purposes, including fundamental nuclear and particle physics, atomic and plasma physics, material sciences, radiation biology, and cancer therapy research.

Various diagnostics systems are used to measure heavy-ion beam parameters to ensure the safety and reliability of the accelerator facility operation, as well as to optimize the beam delivery to the experimental locations. For example, this includes beam position, profile, intensity, energy, and emittance measurements.

The information provided by the beam diagnostics tools is used by the operating team for the online feedback controls of the accelerator and beam transfer lines. This helps to maintain the desired quality and stability of the beam. The beam diagnostics systems are also used by experimental users directly for the characterization and calibration of the

experimental setups, which require precise knowledge of the incoming beam parameters.

In particular, at the high-energy beam transfer lines (HEST) of the GSI facility, the intensity of heavy-ion beams slowly extracted from the SIS18 synchrotron is measured using three different detector types (particle detector combination, PDC): scintillation counter (SC), ionization chamber (IC) and secondary electron monitor (SEM). Each detector type is used to cover a specific range of beam intensity [1].

Plastic scintillation counters based on BC-400 (Saint Gobain), or EJ-212 (Eljen Technology) scintillators are currently used as a part of the HEST ion beam intensity diagnostics, covering counting rates in the range up to 1×10^6 ions/s. The heavy-ion beams induce a large amount of radiation damage when passing through the plastic scintillator. This leads to frequent detector services where plastic scintillators are exchanged, which is highly undesirable from an operational point of view.

In this work, we investigated an alternative to the plastic scintillation counter, that could provide less frequent detector maintenance through the use of a more radiation-hard scintillator. We developed a new detector prototype based on indium-doped zinc oxide (ZnO(In)) ceramic scintillator. We report on the new prototype design and performance, which was evaluated experimentally through in-beam tests and simulations using the OpenGATE [2].

ZINC OXIDE CERAMIC SCINTILLATOR

Zinc oxide (ZnO) is a well-known inorganic compound used in various applications [3–5]. In particular, it has been used for the detection of X-rays and α -particles [6–9].

ZnO exhibits two luminescence bands when excited by light or ionizing radiation: (1) emission in the ultraviolet (UV) spectral range (~ 390 nm) with a short scintillation decay time (< 1 ns), and (2) emission in a broad-band with a maximum around 550 nm wavelength (green luminescence) with a longer decay time (> 1 μ s). The green luminescence is unsuitable for fast-counting applications. Therefore, it is avoided either by annealing in a reducing environment or doping with a group 3A element impurities, such as Al, Ga, or In [3, 10, 11].

In-doped and Ga-doped ZnO ceramics prepared by uniaxial hot pressing in vacuum have been investigated as promising scintillators for fast heavy ion counting appli-

* The results presented in this contribution are based on the work performed before the 24th of February 2022.

† DLR funded this work within the ERA.Net RUS Plus Project RUS_ST2017-051.

‡ m.saifulin@gsi.de (corresponding author)

CRYOGENIC CURRENT COMPARATORS (CCC) AS LOW INTENSITY DIAGNOSTICS FOR ION BEAMS*

T. Sieber[†], D. M. Haider, M. Schwickert, GSI, Darmstadt, Germany
L. Crescimbeni¹, F. Schmidl, Friedrich-Schiller-University Jena, Jena, Germany
M. Schmelz, R. Stolz³, V. Zakosarenko⁴, Leibniz IPHT, Jena, Germany
T. Stoehlker^{1,2}, V. Tympel, Helmholtz Institute Jena, Jena, Germany
N. Marsic

TEMF, Institute for Theory of Electromagnetic Fields, Technical University, Darmstadt, Germany

J. Tan, CERN European Organization for Nuclear Research, Geneva, Switzerland

¹also at GSI Helmholtz Centre for Heavy Ion Research, Darmstadt, Germany

²also at Institute for Optics and Quantum Electronics, Jena, Germany

³also at Technical University Ilmenau, Ilmenau, Germany

⁴also at supracon AG, Jena, Germany

Abstract

The Cryogenic Current Comparator (CCC) is a SQUID based superconducting device for intensity measurement. It was firstly proposed as a beam diagnostics instrument in the mid '90s at GSI. After prove of principle the CCC was introduced into other facilities, showing great potential for high resolution measurements as well as raising considerable mechanical and cryogenics challenges and costs.

In the course of planning for FAIR the CCC has been revitalized. Systematic investigations started - also involving now commercially available SQUID systems - which led to improvements of detector and cryostat. The developments resulted in nA spill measurements at GSI (2014) followed by the installation of a CCC in CERN Antiproton Decelerator (AD), which has become a key instrument.

Since then optimization of the device is ongoing, with respect to various operating conditions, system robustness, current resolution and last but not least system costs. Alternative CCC versions with improved magnetic shielding have been developed as well as 'Dual Core' versions for background noise reduction. We give an overview of CCC optimization and development steps, with focus on applications at GSI and FAIR.

INTRODUCTION

The Cryogenic Current Comparator measures the beam intensity via the beam azimuthal magnetic field, which is for nA currents in the fT range. The device consists of a superconducting shielding, which provides an attenuation of non-azimuthal external fields in the range -70 dB to -140 dB, depending on the shield geometry (see below). The shielding guides the superconducting Meissner-Current (compensation current for the beam magnetic field) to the internal pickup loop, which allows for DC measurements

as a matter of principle. The pickup loop is basically a one-winding coil around a high permeability ring core, acting as a flux concentrator. The latter is used in the 'classical' CCC shown in Fig. 1 to ensure efficient coupling of the beam magnetic field to the SQUID circuit. The arrangement can be regarded as a transformer with the particle beam being the primary winding and the pickup coil the secondary winding. The signal from the pickup coil is fed (via a matching transformer for impedance matching) to a DC SQUID (Superconducting Quantum Interference Device) magnetometer, which is operated in a compensation circuit, using a so called Flux Locked Loop (FLL) electronics [1]. Figure 1 shows the currently used arrangement, originally developed at the PTB (Physikalisch-Technische Bundesanstalt) [2] and adapted to the accelerator application at GSI [3].

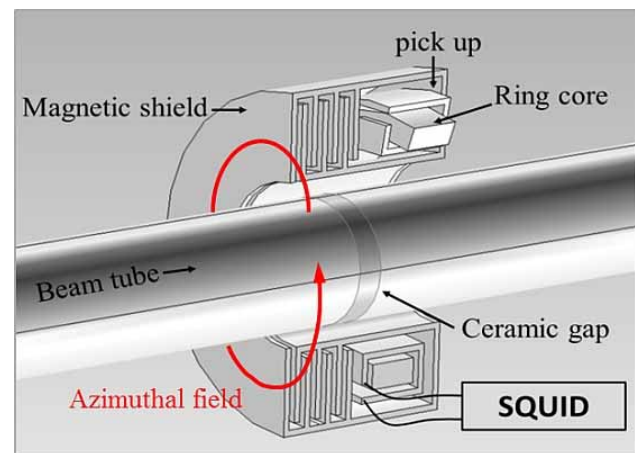


Figure 1: Classical CCC, shielding geometry with radial meanders and high permeability ring core.

Recent developments at IPHT Jena have shown that it is possible to build a CCC without toroidal core, using a shielding with axial meander geometry [4], consequently the device is called coreless or axial CCC (see Fig. 2). This

* supported by BMBF under contracts 05P18RDRB1 and 05P18SJRBI

[†]T.Sieber@gsi.de

CHARGE MEASUREMENT WITH RESONATORS AT ARES

T. Lensch, D. Lipka*, R. Neumann, M. Werner
Deutsches Elektronen-Synchrotron DESY, Notkestr. 85, Hamburg, Germany

Abstract

The ARES facility (Accelerator Research Experiment at SINBAD) is an accelerator to produce low charge ultra-short electron bunches within a range of currently 0.5 pC to 200 pC. Especially for eFLASH experiments at ARES an absolute, non-destructive charge measurement is required. To measure an absolute charge of individual bunches different types of monitors are installed. A destructive Faraday Cup is used as reference charge measurement device. To measure the charge non-destructively 2 Toroids, 1 Turbo-ICT and 2 cavity monitors are installed. The latter system consists of the cavity, front-end electronics with logarithmic detectors and μ TCA ADCs. The laboratory calibration of the cavity system is performed by using an arbitrary waveform generator which generate the same waveform like the cavity with beam. This results in a non-linear look-up table used to calculate the ADC amplitude in charge values independent of beam-based calibration. The measured charges from the cavity monitors agree very well within few percent in comparison with the Faraday Cup results.

MOTIVATION

The beam charge determination is one of the most important properties to be measured in all accelerators. For this several monitor systems are developed and installed at every accelerator, but the absolute value of charge is always in discussion. At the Accelerator Research Experiment at SINBAD (ARES) [1–6] we installed different types of charge monitor systems: 2 Toroids, 1 Turbo-ICT and 2 cavity monitors. The charge value results are compared with a Faraday cup who serves as a reference system with good agreement to the other monitors; the expected charge loss of the Faraday Cup due to lost particles is simulated and smaller than 0.6 % [7]. The cavity monitor system consists of a resonator where the first monopole mode at 1.3 GHz carries with the amplitude the charge information. This monitor system is firstly developed to detect the dark current from accelerators with the same accelerator frequency where the single dark current bunches generate superimposed fields within the resonator [8]; for this reason the system is called Dark current Monitor (DaMon). It was found that this resonating system is able to measure very low values of bunch charges. Therefore, the DaMon system is installed at several accelerators at DESY [9–12] to measure the bunch charge from several fC up to few nC. The calibration of the amplitude to the charge from a resonator to get the absolute charge is the issue of this contribution.

* dirk.lipka@desy.de

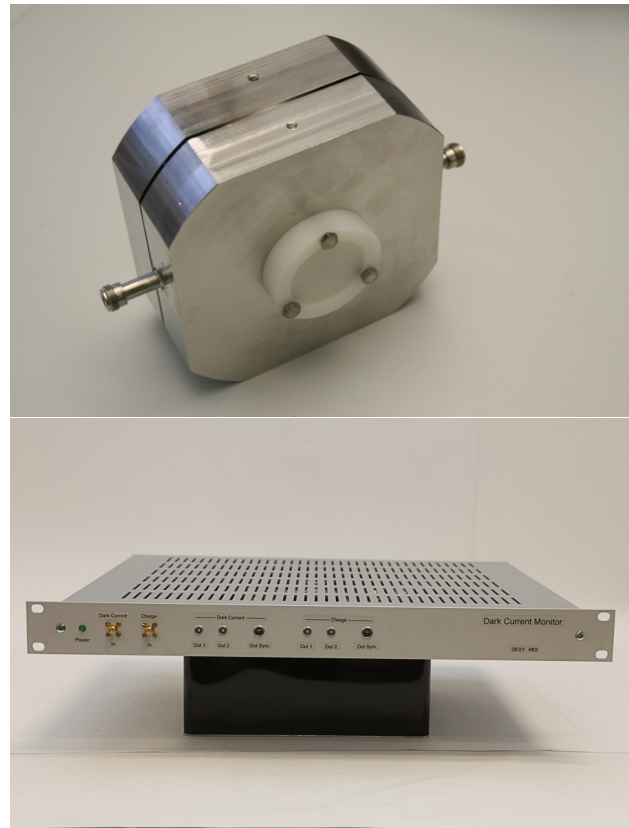


Figure 1: Picture of the resonator and the electronics box with front panel.

SETUP

The DaMon system consists of the resonator integrated into the beamline, a front-end electronics (see an example in Figure 1) and ADCs. One resonator has two identical outputs to ensure symmetry in the resonator, which are connected with low loss coaxial cables to the front-end electronics. Both inputs are processed differently in the electronics. The charge channel (Q) is in most applications attenuated to be able to provide higher charges with band pass filters, logarithmic detectors (for high dynamic range) and followed by gain and offset adjustments to adapt to the 16 bit ADC. The dark current channel (DC) has in addition a down converter in the logarithmic detector with free oscillating reference signal to provide higher sensitivity. This channel was foreseen to superimpose the dark current bunches with acceleration frequency 1.3 GHz but for other accelerators this channel is used for bunch charge measurement too. Therefore, the DC channel provides higher sensitivity and can be used for lower charge values compared to the Q channel.

BCM SYSTEM OPTIMIZATION FOR ESS BEAM COMMISSIONING THROUGH THE DTL TANK 4

H. Hassanzadegan, R. A. Baron, S. Gabourin, H. Kocevar, M. Mohammednezhad, J. Murari, S. Pavinato, K. Rosengren, T. Shea, R. Zeng, European Spallation Source ERIC, Lund, Sweden
K. Czuba, P. K. Jatczak, Warsaw University of Technology, Warsaw, Poland

Abstract

The ESS BCM system is not only used for beam measurement but it also plays an important role for machine protection particularly in the normal-conducting part of the linac. During the previous beam commissionings to the MEBT and DTL1 FCs and before the cavities were fully conditioned, RF breakdowns and other types of discharges in the cavities had a major impact on beam availability due to the Fast machine protection functions of the BCM. Following an investigation on the root cause of the beam trips, the configuration of the machine protection functions was modified to improve beam availability in the more recent beam commissioning to the DTL4 FC. In addition to this, some optimizations were made in the BCM system to improve beam measurement, and a few more functions were added based on new requirements. This paper reports on these improvements and the results obtained during the beam commissioning through the DTL4.

INTRODUCTION

The ESS Beam Current Monitor (BCM) system includes in total nineteen AC Current Transformers (ACCTs) and one Fast Current Transformer (FCT) which are all from Bergoz. Ten of these ACCTs are installed in the normal conducting part of the linac that extends from the Ion Source (ISrc) to the Drift Tube Linac (DTL) tank 5. These sensors overall allow beam measurement at the interface between a section and the following one, and after the temporary beam dumps in the Low Energy Beam Transport (LEBT) and Medium Energy Beam Transport (MEBT) sections. The other nine ACCTs will be installed in the Linac Warm Units (LWUs) in between the cryomodules in the Medium Beta Linac (MBL), High Beta Linac (HBL), High Energy Beam Transport (HEBT) and in the Accelerator To Target (A2T) and Dump Line (DmpL) sections.

The analogue signal from each ACCT is buffered and amplified by a wall-mount Front End (FE) module from Bergoz, and then filtered and further processed in a custom designed Back End (BE) unit in the BCM rack. The signal is then converted to digital and FPGA processed by a Struck SIS8300-KU board in a mTCA crate. The digital signal processing includes baseline restoration, droop compensation, digital filtering, post mortem data buffering as well as a complete suite of machine protection functions that are tailored to meet the ESS beam and machine requirements. Part of these functions are used to measure the amplitude, width and repetition frequency of the beam pulse and send a beam abort request to the Fast Beam Interlock System (FBIS) within 1 μ s if the measured values exceed their thresholds. The BCM firmware configures the

machine protection functions including the levels and activation/deactivation of the thresholds based on a beam mode and a beam destination ID that are distributed over the ESS network before starting with beam. Time windows for the expected beam pulses from the ISrc and LEBT/MEBT choppers are generated by the BCM firmware using some events which are distributed by the ESS Timing System (TS) over an optical fibre network at well-defined times before the arrival of each pulse. These time windows are then used for measuring the beam properties including average beam current over a region of interest and pulse length/charge. The BCM firmware also checks the exact timing of the TS events for any inconsistency with the selected beam mode due to possible bugs in the timing tables, human errors etc. This feature has proven to be very useful to avoid potential damages due to ex. a wrong trigger length/frequency resulting in excessive beam power on a temporary beam dump. Other protection functions include differential beam interlocks with several BCM pairs, errant beam detection and BCM internal checks [1].

Each ACCT includes a calibration winding that is used not only to calibrate the sensor but also to test and verify the system with a test pulse from a waveform generator before starting with beam. A Wetest script is used to sweep the pulse amplitude, width and frequency in multiple steps from a minimum to a maximum, and in each step the full signal chain from the sensor up to the EPICS Process Variables (PVs) including all the protection functions are automatically tested and verified.

BEAM COMMISSIONINGS THROUGH THE LEBT, MEBT AND DTL TANK 1

With the start of the beam commissioning through the LEBT (Sep. 2018) and MEBT (Nov. 2021) [2], a large number of beam trips were initiated by the BCM system and in particular the errant beam interlock. An investigation then showed that part of the trips was due to Electro Magnetic Interference (EMI) issues caused by the safety relay (i.e. ground relay), High Voltage Power Supply (HVPS) and the high power contactors of the ISrc. The issue was then resolved by improving the groundings of both the ISrc cage and the electronics racks, reinforcing the shielding and grounding of the ISrc/LEBT BCM FEs, additional EMI filters, surge protectors, analogue filters on the HVPS current/voltage readouts and digital processing in the BCM FPGA. The tests also showed that a broken insulator around a LEBT repeller ring resulted in some sparks and these occasionally caused some large spikes on the LEBT BCM readout thus adding to the beam trips. The

APS UPGRADE RADIATION SAFETY BEAM CURRENT INTERLOCK*

R. Keane[†], K. Harkay, N. Sereno, Argonne National Laboratory, Lemont, IL, USA
A. Caracappa, C. Danneil, K. Ha, J. Mead, D. Padrazo
Brookhaven National Laboratory, Upton, NY, USA

Abstract

The Advanced Photon Source upgrade (APS-U) replaces the APS storage ring with a new Multi-Bend Acromat (MBA) storage ring utilizing on-axis swap-out injection requiring up to 20 nC charge per injected electron bunch, more than a three-fold increase from the original ring. Enforcement of radiation safety limits for the new storage ring will be accomplished by a new beam charge monitor interlock that acquires the accumulated beam charge in the Booster-to-Storage ring (BTS) transfer line and disables injection when the charge limit over a pre-set time period is exceeded. The new interlock is based on the existing APS Beam Shut-Off Current Monitor (BESOCM) that has been in operation in the APS injector for many years and incorporates significant improvements over the existing system. New features include use of direct digitization and FPGA processing, extensive remote monitoring capabilities, expanded self-test and fail-safe functions, and the ability to adjust settings and monitor status remotely via EPICS. The new device integrates a test pulse (self-check) feature that verifies the integrity of the integrating beam current transformer (ICT) and cable system used to detect the beam signal. This paper describes the new BTS interlock (BESOCM) design and presents results of bench test and in-machine evaluation of the prototype and production units.

INTRODUCTION

The existing APS BESOCM system limits the amount of accelerated charge in the APS Linac over a 1 minute accumulation period in order to enforce radiation safety requirements. If the limit is exceeded, the BESOCM disables the beam by inhibiting several necessary systems. The BESOCM continually tests itself by creating a single test pulse of ~2.5 nC after every beam trigger and sending the pulse through a test winding in the current transformer in the beam line, and has some addition fail-safes that monitor the trigger and integration gate [1,2].

The new BTS BESOCM will function similarly to the legacy system, but with far more adjustments and self-test functions, and will include robust remote monitoring capabilities.

APS ACIS System

The APS Access Control and Interlock System (ACIS) includes both personnel protection and radiation safety interlocks that act to disable accelerated and/or stored

beam for a variety of abnormal conditions. The system uses dual redundant chains denoted A and B, and relies on fault tolerant hardware such as relay contacts and PLCs. The BTS BESOCM electronics chassis contains two redundant sets of electronics that interface to the ACIS system via safety rated relays.

APS Radiation Safety and FPGA Development

APS radiation safety requirements are stated in APS safety assessment documents and specify the risks and consequences of off-normal beam loss events [3]. Since the BTS BESOCM is a layer of protection added as part of the MBA upgrade, the FPGA firmware development process followed a graded approach based on the low specified risk, i.e., identical hardware was used in both chains A & B with separate firmware developers for each chain. Each developer worked independently to implement the FPGA functions as defined in the BESOCM engineering specification document. Independent code reviews were also performed on each FPGA code design.

BTS BESOCM SYSTEM DESIGN

Figure 1 shows a block diagram of the BESOCM system. The electron beam bunch charge is sensed by an Integrating Current Transformer (ICT) in the BTS beam line. The ICT has two independent identical test windings that allow beam to be simulated by passing a test pulse through the winding. One test winding is always in use during BESOCM operation, to provide the self-test pulse to the ICT. The second winding is used only during validation or testing. The ICT connects to the BESOCM electronics chassis, located outside the beam tunnel, via three coax cables.

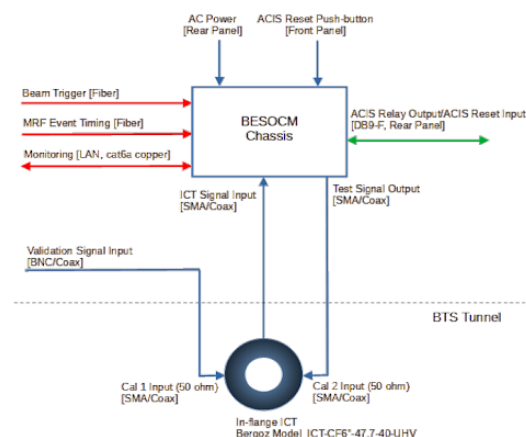


Figure 1: BESOCM system block diagram.

* Work supported by the U.S. Department of Energy, Office of Science, under Contract No. DE-AC02-06CH11357

[†] keane@anl.gov

NANO-AMP BEAM CURRENT DIAGNOSTIC FOR LINAC-TO-ESA (LESA) BEAMLINE*

S.T. Littleton†, A.S. Fisher, T. Raubenheimer, SLAC, Stanford, CA, USA
 C. Huang, Evergreen Valley High School, San Jose, CA, USA

Abstract

The LESA beamline is designed to transport dark current from the LCLS-II and LCLS-II-HE superconducting linacs to the End Station A for various fixed target experiments. The primary experiment is expected to be the Light Dark Matter eXperiment (LDMX) which required beam currents of a few pA. The operation of the beam line must be parasitic to the LCLS-II / LCLS-II-HE FEL operation. The dark current in the LCLS-II is expected to be at the nA-level which will be below the resolution of most of the LCLS-II diagnostics (it will be degraded before the experiments as necessary). This paper will describe a possible non-destructive diagnostic using synchrotron radiation that could be applied at multiple locations along the LCLS-II and the LESA beamline.

INTRODUCTION

The SLAC Linac to End Station A (LESA) beamline is a staged concept to provide a near-CW beam at 186 MHz and sub-harmonics thereof to the SLAC End Station A (ESA) for experiments in particle physics requiring pA to 25 nA electron beams with multi-GeV electron energy [1]. This capability is achieved parasitically by extracting unused bunches from the LCLS-II/LCLS-II-HE superconducting RF (SRF) linac [2, 3].

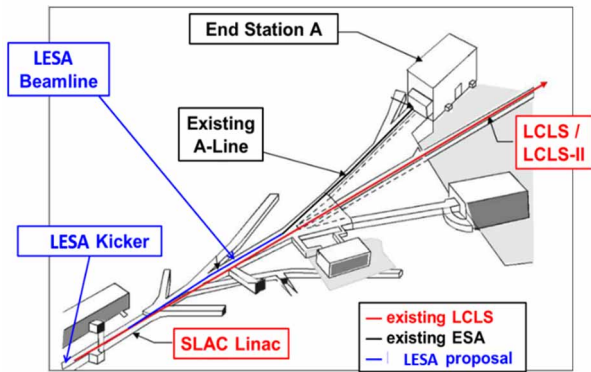


Figure 1: Schematic of LESA beamline starting in SLAC linac and connecting to the A-line.

The LESA beamline begins in Sector 28 of the SLAC linac and continues into the Beam Switchyard, where it connects with the A-line as illustrated in Fig. 1. The beamline consists of (1) a long-pulse kicker and septum magnet to divert low-current bunches off the LCLS-II dump line, (2) a 250m long transfer line from the kicker in Sector 29 to the existing A-line, delivering beam to End Station A, (3) minor improvements in the existing End Station A

* Work supported in part by DOE contract DE-AC02-76-SF00515.

† seantl@stanford.edu.

infrastructure, and (4) an optional laser oscillator that augments the dark current with a well-defined, low-current beam at 46 MHz repetition rate within a ~500 ns macro-pulse between LCLS-II/LCLS-II-HE primary bunches as illustrated in Fig. 2.

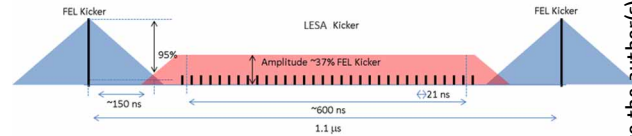


Figure 2: LCLS-II pulse structure showing primary pulses with 10^8 e⁻ and LESA bunches from the gun with 30 e⁻ per bunch. The LESA beam will control the bunch population with an additional seed laser and/or a spoiler/collimation system to deliver final current in the pA to μ A range.

Table 1: LESA Electron Beam Parameters for an Ultra-Low-Current Beam (Baseline) and a Possible Upgrade

Experiment Parameters	Ultra-low-current	Low-current (upgrade)
Energy	4.0 GeV (upgrade to 8.0 GeV in 2027)	4.0 GeV (upgrade to 8.0 GeV in 2027)
Bunch spacing	5.4 – 65 ns	5.4 ns
Bunch charge	0.04 – 10,000 e ⁻	70,000 e ⁻ (10 fC)
Macro pulse beam current	0.1 – 25 nA	2 μ A
Duty cycle	55% (600 ns out of 1.1 μ s)	55% (600 ns out of 1.1 μ s)
Norm. emittance (rms)	~100 μ m; <1000 μ m	~1 μ m
Bunch energy spread	<1%	<1%
IP spot size w/ rastering	4 cm x 4 cm	<250 μ m including jitter
Electrons per year	10 ¹⁵ e ⁻ / year	10 ¹⁹ e ⁻ / year

LESA is being constructed in two stages: the first stage, S30XL, is nearly complete and will demonstrate the dark current extraction from the SRF linac while the 2nd stage, on which construction is just starting, will transport the extracted current to ESA. S30XL will be commissioned in late 2023 while the full LESA beamline is planned to be complete at the end of 2024.

THE DIGITAL SIGNAL PROCESSING CHAIN OF THE CERN LIU BWS

D. Belohrad*, J. Emery, J. C. Felipe,
 A. Goldblatt, A. Guerrero, M. M. Nieto, F. Roncarolo
 European Organisation for the Nuclear Research (CERN), Geneva, Switzerland

Abstract

Between 2019 and 2023, as part of the LHC Injectors Upgrade (LIU), a major renovation of the CERN wire scanners (BWSs) was performed. The main driving force was to prepare the wire scanners for the High-Luminosity LHC (HL-LHC), during which the instantaneous luminosity is expected to double, to around $5 \times 10^{34} \text{cm}^{-2}\text{s}^{-1}$. In 2021 seventeen LIU BWSs were installed in the CERN PS complex and the Super Proton Synchrotron (SPS). Additionally, two BWSs were installed in the LHC, at the end of 2022, to be ready for the 2023 LHC run. The contribution aims to describe in detail the technical implementation of the data acquisition chain (DAQ) and digital signal processing of the photomultipliers of the newly installed BWSs. Particular attention is given to the design of the analogue front-end, signal conversion, and data processing chain — providing data for the profile reconstruction. The synchronisation of the incoming digitised signal with the machine timing is also addressed, as it differs significantly between the PS complex and the LHC and SPS. Finally, the limitations of the system are discussed.

INTRODUCTION

The BWS functional and engineering specifications, as well as commissioning and first operational results, were already documented in the last few years [1–3]. This paper is intended to complement the information about the LIU BWS project with the details about the new DAQ design, development, and implementation.

The previous BWS DAQ, completed in the early 2000s, was based on in-house developed digital acquisition board (DAB), equipped with two individual bunch measurement systems (IBMSs) [4, 5]. They were general-purpose platforms targeting various LHC and SPS instrumentation.

The IBMSs included an analogue integrator ASICs, able to deliver bunch-per-bunch information, e.g. of the secondary particle shower used to reconstruct beam profiles with BWSs. These were converted into digital data streams using 40 MSPS 14-bits ADCs, and then processed by the DAB's FPGA.

As discussed more in detail later in the paper, a new DAQ generation was designed and implemented, as part of the LIU BWS project. The DAQ is based on a modern FPGA VME FMC Carrier [6], equipped with a fast FMC ADC, which allows the bunch-per-bunch signals reconstruction via digital integration.

* david.belohrad@cern.ch

DAQ CHALLENGES AND SOLUTIONS

The LIU BWSs installed in the entire CERN accelerator complex use the same DAQ. This makes maintenance and spares management easier, but implies challenges in the DAQ gate-ware design to adapt to the different accelerators beam parameters. In order to set up the systems, diagnose problems and function during normal operation, the DAQ has to produce bunch-per-bunch integrals together with raw data acquired by the ADC.

The differences between the Proton Synchrotron Complex (CPS) and SPS installations are formalized as follows.

In the CPS the beam can be represented as:

- *bunch pattern* in the Proton Synchrotron (PS), and
- *continuous flow of bunches*, as e.g. in the Proton Synchrotron Booster (PSB), (Fig. 1).

In the CPS the bunches are separated into their respective turns by *Turn tags*. The turn tag is a revolution period signal delivered by the accelerator RF subsystem. The number of bunches in the turn is supplied by SW as a *harmonic number* (H). Knowing the total number of samples in turn (S_{tot}) and H we determine the *integrating window* for each bunch. The bunch-per-bunch integrals $S_{bunch,turn}$ are calculated as the sum of samples over the integrating windows.

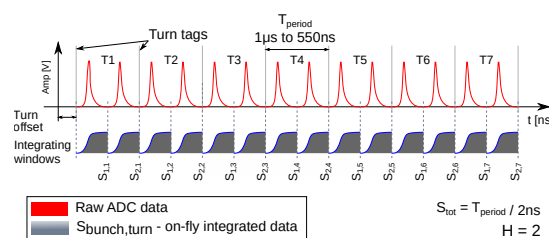


Figure 1: Example of an ideal PSB data acquisition, assuming there are two bunches and the wire passes through a transverse portion of the beam with a constant number of particles during the 7 turns displayed.

In the SPS the integrating windows are not artificially created from the harmonic number. They are identified by the bunch tags delivered together with turn tags via the beam synchronous timing (BST) [7]. The bunch-per-bunch integrals are calculated as the sum of samples between two consecutive bunch tags.

In both cases, a major challenge lies in tracking the tags, since their period changes during the acceleration cycle. In the worst case of the CERN PSB the period changes from $1 \mu\text{s}$ at injection to $\approx 550 \text{ns}$ at extraction. Another difficulty is to find a correct phase relation between the tags delivered to DAQ and the bunches in the sampled data. The tags

REAL TIME MOMENTUM SPREAD MEASUREMENT OF THE CERN ANTIPROTON DECELERATOR BEAM

P. Freyermuth*, B. Dupuy, D. Gamba, CERN, Geneva, Switzerland

Abstract

Constant optimisation and diagnostics of the cooling processes in the CERN antiproton decelerator (AD) relies on a de-bunched beam momentum spread real time measurement. This article will describe the renovation of the acquisition chain of the longitudinal Schottky diagnostics in the AD, using standard CERN hardware and software to maximize reliability, ease maintenance, and meet the requirements for standard operational tools. The whole chain, from the pick-up to the operation software applications will be described with emphasis on the implementation of the data processing running on the front-end computer. Limitations will also be discussed and outlook for further development given.

THE AD LONGITUDINAL PICK-UP

The AD longitudinal pick-up (LPU) consists of two specially designed ultra-low noise ferrite-loaded beam current transformers and amplifiers [1]. They are optimized respectively for high (0.25 – 30 MHz) and low (0.02 – 3 MHz) frequency ranges.

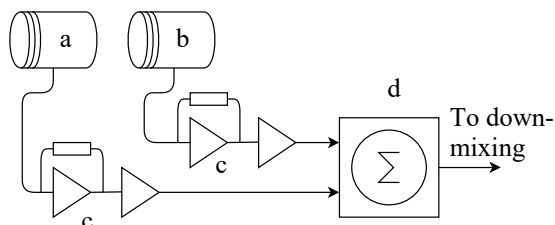


Figure 1: LPU transformers (a & b), amplifiers (c) and summing unit (d).

The output signals of the two transformers are filtered and added together by a summing unit to obtain a flat frequency response over the 0.02-30 MHz bandwidth (Fig. 1). This system is used since the AD went operational in 2001.

SIGNAL DOWN-MIXING

The longitudinal Schottky spectrum of a de-bunched beam consists of bands of frequencies (Schottky bands), located around harmonics (n) of the average revolution frequency. The momentum spread distribution can be derived from these Schottky bands. The power spectral density of these bands decreases with n , but the width of these bands increases by a factor n (Eq. 1) [2].

$$\Delta f = n f_0 \eta \frac{\Delta p}{p}, \quad (1)$$

where Δf is the width of the Schottky band, n is the harmonic number, f_0 is average revolution frequency, η is the slip factor given by the synchrotron parameters and $\Delta p/p$ is the momentum spread.

The band selection, therefore, of the harmonic, is a balance between signal-to-noise ratio, frequency resolution, and LPU and acquisition bandwidth.

To accommodate the different revolution frequencies of the AD cooling plateaus, the signal from the LPU is mixed with a signal generated from a harmonic of the revolution frequency minus 50 kHz (Table 1).

Table 1: Down Mixing Frequencies

Plateau momentum [MeV/c]	Revolution frequency [kHz]	Harmonic	Mixing frequency [kHz]
3574	1589.411	2	3128.822
2000	1487.722	2	2925.445
300	500.465	8	3953.721
100	174.155	8	1343.240

The mixing unit includes filters for image frequency rejection. The result is a transposition of the signal to a fixed centre frequency of 50 kHz, enabling fixed parameters for different cooling plateau energies and modest analogue-to-digital converter (ADC) hardware specifications.

An additional 32 dB amplifier is also placed before the mixer (Fig. 2), pulling the signal strength into the range of the ADC sensitivity.

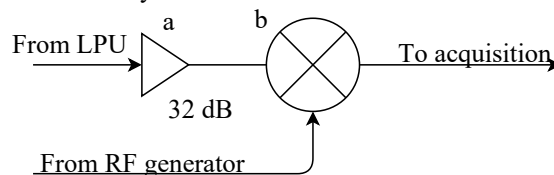


Figure 2: Simplified schematic of the signal down-mixing with a low-noise amplifier (a) and the mixing and filtering unit (b).

* pierre.freyermuth@cern.ch

STATUS OF THE RFSOC-BASED SIGNAL PROCESSING FOR MULTI-BUNCH AND FILLING-PATTERN FEEDBACKS IN THE SLS2.0

P. Baeta, B. Keil, G. Marinkovic, Paul-Scherrer-Institut (PSI), Villigen, Switzerland

Abstract

Having effectively evaluated the RF System-On-Chip (RFSoc) as a suitable technology for the SLS2.0 Filling Pattern Feedback (FPFB) and Multi-bunch Feedback (MBFB), our current focus lies in realizing and expanding the required real-time Digital Signal Processing (DSP) algorithms on an RFSoc evaluation board. This contribution outlines the present status of our feedback systems, including recent outcomes derived from testing prototypes both in the laboratory and with beam signals at the storage ring.

INTRODUCTION

The Swiss Light Source (SLS), a 3rd generation synchrotron light source at Paul Scherrer Institute (PSI), will be upgraded by a cutting-edge storage ring magnet lattice with reverse bends. The new machine, the SLS2.0, will provide a much lower emittance and higher beam energy, ultimately increasing the hard X-ray brightness and making the SLS competitive with other newer facilities [1]. Moreover, upgrading the SLS includes modernizing aging systems, such as the multi-bunch feedback (MBFB) and the filling pattern feedback (FPFB). After we assessed the suitability of RF System-On-Chip (RFSoc) for implementing the MBFB and FPFB of SLS 2.0 [2], we proceeded with deploying the feedback systems on the ZCU111 evaluation board from Xilinx/AMD, which features an RFSoc [3]. In the hardware section of this paper, we present an overview of the set-up installed at the SLS for testing the new MBFB and FPFB designs, which includes an RF-front-end (RFFE) prototype and the RFSoc-based digital back-end. The subsequent Firmware and Software section covers a real-time implementation of bunch-charge and arrival-time measurement for the FPFB, along with DSP firmware upgrades in the MBFB design. Lastly, we report prototype results from testing RFSoc-based systems in the laboratory and at the SLS storage ring, utilizing RF beam position monitor (BPM) signals.

HARDWARE

Figures 1(a) and 1(b) depict a block diagram of the hardware set-up at the SLS storage ring for prototyping our RFSoc-based solution of the FPFB and MBFB systems. The signals from four capacitive electrodes of an SLS beam position monitor (BPM) are connected to an RF hybrid network, yielding the sum signal (S), proportional to the bunch charge, and the difference signals (X and Y), proportional to the bunch charge and the horizontal and vertical bunch position offsets. The RFFE module consists of digital step attenuators (DSAs) and RF amplifiers for conditioning the position signals S, X, and Y. Figure 1(a) presents the signal conditioning path for each of the three

MBFB planes. The RFFE prototype has a bandwidth of approx. 1000 MHz, online user-controllable gain/attenuation adjustments, and on/off switching capabilities for each analog signal conditioning path. The previous MBFB at SLS1.0 used a commercial RFFE that down-converted BPM signals from 1.25-1.5 GHz to the baseband. The new RFFE represents a transition toward direct sampling of S, X, and Y signals. The digital back-end in Figure 1(b) comprises the ZCU111 evaluation board and two interface boards. The ZCU111 is the core of the feedback systems, performing the data acquisition and processing. The Xilinx/AMD FMC-XM500 card breaks out the nets of the RFSoc data converters of the ZCU111. The ADCs acquire the conditioned signals S, X, and Y from the RFFE. The ZCU111 can control the RFFE signal gain and power with a second adapter board. In the context of the MBFB, the DACs generate the correction signals, closing the feedback loop. The correction signals undergo amplification, including upconversion to 1.5 GHz in the longitudinal plane, before driving the MBFB kickers. As for the FPFB, embedded real-time software processes the sum signal (S), calculating bunch charge. This process concludes by providing injection control information across successive top-up cycles, as needed, to close the filling pattern feedback loop.

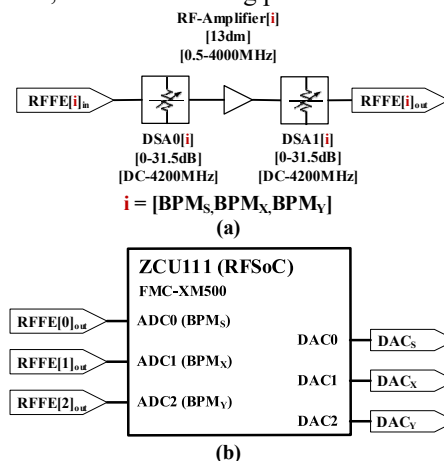


Figure 1: Block diagram of the FPFB and MBFB hardware set-up. (a) RF Front-end (RFFE) module for conditioning position signals from the SLS beam position monitor (BPM). (b) The Digital back-end module incorporates the ZCU111 evaluation board for data acquisition, processing, and communication with the SLS control system.

FIRMWARE AND SOFTWARE

Figures 2 and 3 illustrate the firmware block diagrams for the FPFB and MBFB systems implemented on the RFSoc platform. The Xilinx RF Data Converter is the core IP of the design. This IP configures the ADCs and DACs of the RFSoc and establishes the AXI stream data interface

THz ANTENNA-COUPLED ZERO-BIAS SCHOTTKY DIODE DETECTORS FOR PARTICLE ACCELERATORS

R. Yadav^{1,*}, S. Preu, Terahertz Devices and Systems, TU Darmstadt, Darmstadt, Germany
A. Penirschke, High Frequency Tech., Mittelhessen Univ. of Applied Sciences, Friedberg, Germany
J. Michael Klopff, M. Kuntzsch, Helmholtz-Zentrum Dresden-Rossendorf, Dresden, Germany
¹also at High Frequency Tech., Mittelhessen Univ. of Applied Sciences, Friedberg, Germany

Abstract

Semiconductor-based broadband room-temperature Terahertz (THz) detectors are well suitable for beam diagnosis and alignment at accelerator facilities due to easy handling, compact size, no requirement of cooling, direct detection and robustness. Zero-Bias Schottky Diode (ZBSD) based THz detectors are highly sensitive and extremely fast, enabling the detection of picosecond scale THz pulses. This contribution gives an overview of direct THz detector technologies and applications. The ZBSD detector developed by our group has undergone several tests with table-top THz sources and also characterized with the free-electron laser (FEL) at HZDR Dresden, Germany up to 5.56 THz. In order to understand the rectification mechanism at higher THz frequencies, detector modelling and optimization is essential for a given application. We show parametric analysis of a antenna-coupled ZBSD detector by using 3D electromagnetic field simulation software (CST). The results will be used for optimization and fabrication of next generation ZBSD detectors, which are planned to be commissioned at THz generating FEL accelerator facilities in near future.

INTRODUCTION

The electromagnetic spectrum from 0.1 to 10 THz was commonly known as terahertz (THz) gap until recently as rigorous research and development have led to develop sources, detectors and components which help to bridge the THz gap [1]. Among available tabletop THz sources, accelerator based sources such as free electron lasers (FEL), synchrotrons and linear particle accelerators generate coherent as well as non-coherent THz signals [2]. THz signals can be used for various applications such as spectroscopy, study of matters, medical imaging, etc. [3]. THz detectors plays a crucial role in order to harness the full power of THz signals in various applications. These detectors can be classified into several categories based on their working principles (such as thermal detectors, electrical detectors etc. [1]), operating ranges (frequency of coverage for example narrow or broadband [1]) and operating conditions (room temperature or cryogenic conditions [1, 4–8]). There has been a rigorous work for the development of Schottky diode for THz applications [7, 9–11].

Zero-Bias Schottky Diode (ZBSD) based THz detectors are an end product of combination of ZBSD, antenna, planar electronic components and post detection electronics.

* rahul.yadav@iem.thm.de

Therefore, the overall performance of the ZBSD detector is dependent on all these components. In order to optimize the ZBSD THz detectors, in this paper we focus on the investigation of planar antennas for antenna-coupled ZBSD detector, which is planned to be primarily commissioned at ELBE facility in Helmholtz Zentrum Dresden-Rossendorf (HZDR), Germany and other facilities too.

SIGNAL RECTIFICATION IN ZBSD

For conventional Schottky diodes, the external bias V modifies the Schottky barrier height, which led the electrons to cross the barrier and ultimately led to set the operating point of Schottky diode by reducing differential resistance (R_{diff}) [11, 12]. In case of ZBSD, the material is engineered in such a way that at $V = 0$ sufficient electrons are able to cross the barrier, yet with sufficient non-linearity of the IV characteristics to cause rectification. The ZBSD used for the detector development in our group are fabricated on Indium Gallium Arsenide (InGaAs) substrate which have electron affinity of 4.5 eV. Due to the proprietary reason by ACST GmbH, the in-depth information of Schottky diode itself is out of context of this paper. The ZBSD used here feature a quasi-vertical structure for Schottky and ohmic contact [9], rather than either having only planar or only vertical structure [11].

The signal rectification takes place at the Schottky contact of ZBSD, which can be understand by using Taylor series [13] as follows: The incident (monochromatic) Terahertz wave is transformed to a bias by the antenna as

$$U_0(t) = U_0 \cos(\omega t) \quad (1)$$

where $U_0(t)$ is the signal with amplitude U_0 and angular THz frequency ω . By using the Taylor series expansion of the exponential diode characteristic up-to second order, the diode current I_0 becomes

$$I_0(t) = A_1 U_0 \cos(\omega t) + A_2 U_0^2 \cos^2(\omega t) + \dots \quad (2)$$

$$= A_1 U_0 \cos(\omega t) + \frac{1}{2} A_2 U_0^2 + \frac{1}{2} A_2 U_0 \cos(2\omega t) \quad (3)$$

where the second term in Eq. (3) is the DC term. The first and second terms are derived from diode characteristics [11]:

$$A_1 = \frac{1}{R_{diff}} \quad (4)$$

$$A_2 = \frac{1}{2 \cdot R_{diff} \cdot \eta \cdot U_T} \quad (5)$$

SOFTWARE DEFINED RADIO BASED FEEDBACK SYSTEM FOR TRANSVERSE BEAM EXCITATION*

P. J. Niedermayer**, R. Geißler, R. Singh

GSI Helmholtzzentrum für Schwerionenforschung, Darmstadt, Germany

Abstract

Controlling stored beams in particle accelerators requires specially designed RF signals, such as needed for spill control via transverse excitation. The software-defined radio (SDR) technology is adopted as a low cost, yet highly flexible setup to generate such signals in the kHz to MHz regime. A feedback system is build using a combination of digital signal processing with GNU Radio and RF Network-on-Chip (RFNoC) on a Universal Software Radio Peripheral (USRP). The system enables digitization of signals from particle detectors and direct tuning of the produced RF waveforms via a feedback controller – implemented on a single device. To allow for triggered operation and to reduce the loop delay to a few ms, custom OOT and RFNoC blocks have been implemented. This contribution reports on the implementation and first test results with beam of the developed spill control system.

INTRODUCTION

Radio Frequency Knock Out (RF-KO) extraction [1] is a standard method used to extract stored particle beams from synchrotrons through transverse excitation, providing spills of particles for experiments and medical therapy. It uses a beam optics near a third order resonance driven by sextupole fields [2]. The non-linear amplitude and phase detuning effects create a separatrix in phase space [3]. Transverse electromagnetic RF fields are applied to increase the betatron amplitude of particles in a controlled manner. This process, referred to as excitation, drives the particles into the separatrix. As a result, the motion becomes unbound, and the particles can be extracted at a septum.

The excitation system consists of an RF signal generator, RF amplifiers, and a *stripline kicker* inside which the RF fields act on the beam. Here, the signal generator is the central element by which the extraction process, and thus the spill, can be controlled.

The primary goal is to maintain a constant spill rate, that is, to extract an equal number of particles per unit time. To reach this goal, two complementary strategies exist: On timescales above about 50 ms, the signal amplitude is controlled by a complex function or a feedback system based on measured spill rates [4]. On smaller timescales not accessible by the feedback system, the signal waveform is optimized to reduce statistical fluctuations [5].

* This project has received funding from the European Union's Horizon 2020 Research and Innovation programme under GA No 101004730.

**p.niedermayer@gsi.de

SOFTWARE-DEFINED RADIOS

Software-defined radio (SDR) is an RF transceiver technology where signal processing is implemented in software on computer processors (CPUs) and/or field-programmable gate arrays (FPGAs). It is widely used in radio communication systems, but has potential applications in many fields. An SDR typically consists of a frontend with ADCs and DACs, and a backend performing the digital signal processing (DSP). Here, a Universal Software Radio Peripheral (USRP) is used as off-the-shelf frontend to generate the RF signals. For implementation of the DSP chain, the open source framework GNU Radio [6] is used in combination with the RF Network-on-Chip (RFNoC) technology [7], which enable a flexible, graphical design of signal processing flow graphs by combining predefined and custom blocks. With SDRs being adopted by an increasing number of users in the accelerator community [8–10], collaboration and sharing of algorithms between institutes is easily possible [11].

IMPLEMENTATION

The excitation, feedback and spill control system builds on the development of a beam excitation system with applications in beam diagnostics [12]. The device does not only generate the excitation signals required for RF-KO extraction, but also processes the signals of a spill detector monitoring the extraction process. A feedback controller adjusts the excitation signal amplitude in order to maintain a constant spill rate on the detector. Statistical fluctuations on timescales below about 50 ms down to 10 μ s – which are not accessible by spill feedback systems – are reduced by an automatic optimization of the used excitation signal waveforms. The implementation and realization of the system is described in detail in Refs. [11, 13].

COMMISSIONING

The spill control and feedback system was commissioned at the Cooler Synchrotron (COSY) accelerator in Jülich. For spill detection, a Low Gain Avalanche Detector (LGAD) developed by Ref. [14] for the High Acceptance Di-Electron Spectrometer (HADES) was used, which was being tested by the HADES LGAD group at COSY at the time.

Figure 1 shows a 20 s spill recorded with the developed system. Excitation with a constant signal level shows – as expected for this kind of slow extraction – a significant drift of the achieved spill rate over the course of the extraction. The feedback system, if switched on, is able to adjust the excitation level such as to maintain a constant spill rate on the detector. More details are available in Refs. [11, 13].

BEAM INSTRUMENTATION HARDWARE ARCHITECTURE FOR UPGRADES AT THE BNL COLLIDER-ACCELERATOR COMPLEX AND THE FUTURE ELECTRON ION COLLIDER*

R. Michnoff†, C. Degen, L. DeSanto, D. Gassner, S. Hafeez, R. Hulsart, J. Jamilkowski, J. Mead, K. Mernick, G. Narayan, P. Oddo, M. Paniccia, J. Pomaro, A. Pramberger, J. Renta, F. Severino
Brookhaven National Laboratory, Upton, NY, USA

Abstract

Many beam instrumentation systems at Brookhaven National Laboratory's Collider-Accelerator complex are over 20 years old and in need of upgrading due to obsolete components, old technology and the desire to provide improved performance and enhanced capabilities. In addition, many new beam instrumentation systems will be developed for the future Electron Ion Collider (EIC) that will be housed in the existing Relativistic Heavy Ion Collider (RHIC) tunnel. A new BNL designed custom hardware architecture is planned for both upgrades in the existing facility and new systems for the EIC. A general-purpose carrier board based on the Xilinx Zynq Ultrascale+ System-on-Chip (SoC) will interface with a family of application specific daughter cards to satisfy the requirements for each system. This paper will present the general architecture that is planned, as well as details for some of the application specific daughter cards that will be developed.

EXISTING FACILITY HARDWARE

When RHIC was commissioned in 2000, the majority of instrumentation systems were based on the VME platform. While this has worked very well over the years, options for system upgrades and new systems for the EIC have been carefully considered [1].

A custom-designed Beam Position Monitor (BPM) module (named V301) was developed in 2015 that uses the VME form factor but does not include a VME bus interface [2]. Each module instead includes a direct Ethernet communication interface for higher level control and general data transfer. The V301 is based on the Xilinx Zynq gate array. Four 400 MSPS ADC converters are provided for measurement of BPM pickup signals and onboard filter options are included to process electrons or ions with various bunch repetition rates. The on-board Zynq ARM processor runs Linux with embedded software for processing and communication to higher level systems. Beam synchronous clocks are received by a single board in the chassis and distributed via unused P2 pins to all of the V301 modules. One major benefit of this system is that up to 15 V301 boards can be housed in a single VME chassis, and module replacement is very simple when necessary.

Another VME form factor module (named V340) based on the Zynq Ultrascale+ SoC was also recently developed. This module includes a high pin count FMC connector to enable using both custom and 3rd party FMC modules. The V340 is planned to be used for current transformer data acquisition and processing, as well as other applications.

In 2009 the RHIC RF group developed a Xilinx Virtex-5 based carrier board with custom daughter cards specific for RF applications [3]. This system is housed in a custom developed 3U chassis and runs the VxWorks real-time operating system directly on the Virtex 5 gate array.

OVERVIEW OF THE EIC

The EIC is scheduled to be fully commissioned with beam in 2034 and consists of the following major subsystems as shown in Fig. 1:

- Existing Hadron injector systems
- Hadron Storage Ring (HSR)
- Electron Pre-Injector (Polarized electron source and Linac)
- Rapid Cycling Synchrotron (electron accelerator) (RCS)
- Electron Storage Ring (ESR)

The existing Collider-Accelerator complex injector systems - Tandem, Electron Beam Ion Source (EBIS), Linac with polarized proton source, booster and Alternating Gradient Synchrotron (AGS) - will continue to be used for injection into the new HSR. Therefore, the existing systems need to be maintained and/or upgraded to support the EIC operation. The HSR will reuse significant portions of the existing Relativistic Heavy Ion Collider (RHIC) machine which is scheduled to complete its final beam run in 2025. The electron pre-injector, RCS and ESR will be completely new machines.

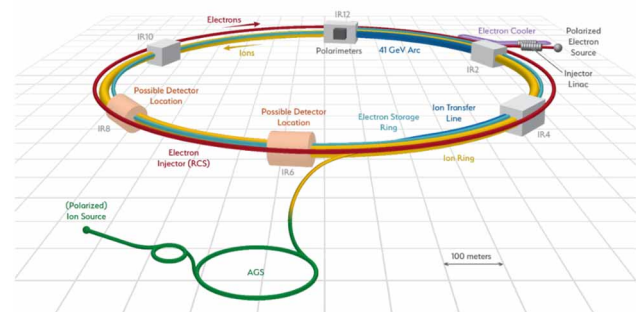


Figure 1: Layout of EIC.

Figure 2 lists the new instrumentation systems planned to be developed for the EIC machine. Note that this list does not include systems that are planned to be upgraded for the existing hadron injector systems.

* Work supported by Brookhaven Science Associates, LLC under Contract No. DE-SC0012704 with the U.S. Department of Energy
† michnoff@bnl.gov

GAS JET BASED FLUORESCENCE PROFILE MONITOR FOR LOW ENERGY ELECTRONS AND HIGH ENERGY PROTONS AT LHC

O. Sedlacek^{*1}, O. Stringer, C. Welsch, A. Webber-Date, H. Zhang
 University of Liverpool and Cockcroft Institute, Daresbury, Warrington, UK
 M. Ady, A. R. Churchman, S. Mazzoni, A. Rossi, M. Sameed, G. Schneider,
 C. C. Sequeiro, K. Sidorowski, R. Veness, CERN, Geneva, Switzerland
 P. Forck, S. Udrea, GSI, Darmstadt, Germany
¹ also at CERN, Geneva, Switzerland

Abstract

The ever-developing accelerator capabilities of increasing beam intensity, e.g. for High Luminosity LHC (HL-LHC), demand novel non-invasive beam diagnostics. As a part of the HL-LHC project a Beam Gas Curtain monitor (BGC), a gas jet-based fluorescence transverse profile monitor, is being developed. The BGC uses a supersonic gas jet sheet that traverses the beam at 45° and visualizes a two-dimensional beam-induced fluorescent image. The principle of observing photons created by fluorescence makes the monitor insensitive to present electric or magnetic fields. Therefore, the monitor is well suited for high-intensity beams such as low-energy electron beam of Hollow Electron Lens (HEL), and HL-LHC proton beam, either as a profile or an overlap monitor. This talk will focus on the first gas jet measured transverse profile of the 7 keV hollow electron beam. The measurements were carried out at the Electron Beam Test Stand at CERN testing up to 5 A beam for HEL. A comparison with Optical Transition Radiation measurements shows consistency with the BGC results. The BGC installation of January 2023 at LHC is shown, including past results from distributed gas fluorescence tests.

INTRODUCTION

The High Luminosity upgrade of the LHC (HL-LHC) aims at extending its operability by a decade by increasing its instantaneous luminosity by a factor of five beyond its present design value [1]. The main feature of HL-LHC is the upgrade of the focusing triplets to allow for a smaller β^* in the interaction region, combined with compact superconducting radio frequency crab cavities for bunch rotation. For these systems to operate safely, a Hollow Electron Lens (HEL) is being studied to improve the cleaning performance of the collimation system. Optimal performance of the HEL requires a means to measure the relative position of the hollow, low-energy electron beam with respect to the LHC proton beam in a non-invasive way. It is in this context, a collaboration between CERN, University of Liverpool and GSI was established to design and produce a Beam Gas Curtain (BGC) as an overlap monitor for the HEL [2–7]. The strategy for commissioning the BGC consists of a parallel validation of its performance in both the Electron Beam Test Stand (EBTS) [8] and the LHC during the present run 3.

* Ondrej.Sedlacek@cern.ch

In this contribution, we report on the recent progress of the BGC at the EBTS and present the configuration of the ongoing LHC installation.

BGC INSTRUMENT

Principle of Detection

The BGC working principle is outlined in Fig. 1. The monitor is based on a flat, supersonic gas jet referred to as a “curtain”, which perpendicularly crosses the beams’ path with the flat edge at 45° with respect to the horizontal plane (see Fig. 1). The beams excite the gas atoms or molecule through collisions. Subsequent radiative deexcitation leads to photon emission (fluorescence). The fluorescence footprint on the gas curtain thus directly relates to the particle beams’ 2D transverse particle distributions, allowing for the observation of the beams’ 2D transverse profiles in a non-invasive way.

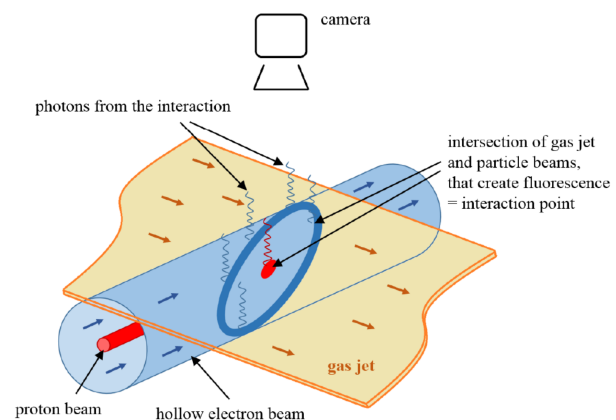
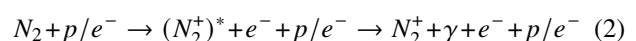
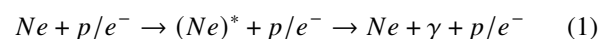


Figure 1: Working principle of the BGC.

Working Gas

Neon, nitrogen, and argon have been selected as working gases for the BGC, each presenting advantages and disadvantages that affect the monitor’s performance. Their fluorescence processes are described in Eqs. (1)–(3):



DEVELOPMENT OF A PRECISE 4D EMITTANCE METER USING DIFFERENTIAL SLIT IMAGE PROCESSING

Bokkyun Shin[†], Chang-Kyu Sung, Garam Hahn, Pohang Accelerator Laboratory, Pohang, Korea
Moses Chung, Ulsan National Institute of Science and Technology, Ulsan, Korea

Abstract

We have developed a highly precise 4D emittance meter for X-Y coupled beams with 4D phase-space ($x-x'$, $y-y'$, $x-y'$, $y-x'$) which utilizes an L-shaped slit and employs novel analysis techniques. Our approach involves two types of slit-screen image processing to generate pepper-pot-like images with great accuracy. One which we call the "differential slit" method, was developed by our group. This approach involves combining two slit-screen images, one at position x and the other at position $x +$ the size of the slit, to create a differential slit image. The other method we use is the "virtual pepper-pot (VPP)" method, which combines x -slit and y -slit images to produce a hole (x , y) image. By combining that hole images, we are able to take extra $x-y'$ and $y-x'$ phase-space. The "differential slit" method is crucial for accurately measuring emittance. Through simulations with 0.1 mm slit width using Geant4, the emittance uncertainties for a 5 nm rad and 0.2 mm size electron beam were 5% and 250% with and without the "differential slit", respectively. In this presentation, we provide a description of the methodology, the design of slit, and the results of the 4D emittance measurements.

INTRODUCTION

In the accelerator the accurate measurement of 4D emittance, the phase space parameters (xx' , yy' , xy' , yx') is important optimizing x - y coupled particle beam properties. This measurement has been accomplished through two primary methods: the pepper-pot and dual slit scanning techniques. However, each of these methods comes with its own set of limitations, such as resolution and time-consuming.

The recently developed 4D emittance measurement is so-called "the Virtual Pepper Pot (VPP)" method, which is image processing to generate a pepper-pot-like image using x and y axis slit scan data [1].

However, it is important to note that both the dual slit scanning and VPP methods have uncertainties related to the width of the slits. To further enhance the capabilities of the VPP method, this paper proposes an additional improvement: the "Differential Slit" method. This method employs image processing is utilized to generate virtual narrower slit images by the positions of the slit at x and $x +$ slit width. This approach aims to minimize the uncertainties associated with slit size, enhancing the accuracy of emittance measurements.

We describe the method of "differential slit" image processing with VPP method and show precision efficiency using the simulation.

[†] bkshin@postech.ac.kr

SLIT DESIGN

The development and application of an L-type slit scanner, which moves to scan X and Y -axis images in a single-axis movement. This slit-scanner design is intended for electron beam testing at PAL-eLABs (or PAL-ITF) [2]. PAL-eLABs utilizes RF photo-cathode guns to generate electron beams with energy up to 70 MeV.

Beam profile imaging is achieved by capturing images through the slit and subsequently viewing them on scintillation screens and/or Optical Transition Radiation (OTR) detectors. These screens and detectors are positioned at distances of 3.5 meters away from the slit.

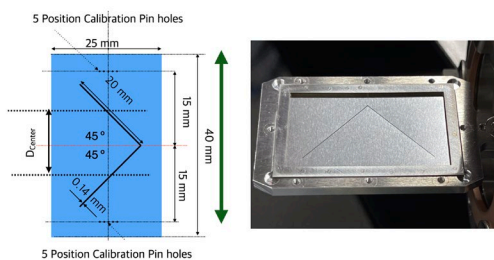


Figure 1: Slit design and manufactured slit scanner.

Two critical aspects of the slit design have been considered: the slit width size and the thickness of the slit plate including its material. Figure 1 shows slit design and manufactured prototype slit. The distance between the X and Y slit centers (D_{center}) is determined considering 15 mm by the beam size to prevent overlapping X and Y slit image in a shot. A thickness and material of slit plate 50 μ m stainless steel has been selected to minimize background from 70 MeV beam scattering with plate and slit punching by etching. And 5 pin holes at bottom and top of slit to get in-site position calibration. The prototype slit was succeeded manufacture with 140 μ m slit width and 100 μ m diameter calibration pinhole.

SIMULATION

The simulation data is generated using the Geant4 [3] and image analyzer OpenCV [4]. Electron interaction with slit and screen are simulated by Geant4. And from energy deposition in the screen to image data by Open CV. The beam condition is used PAL-eLABs [2], 70 MeV and emittance ~ 10 nm rad and beam is artificially rotate for 4D emittance for the 4D phase space study. And Beam Profile screen using the YAG ($Y_3Al_5O_{12}$) is located 3.5 meters away from a slit. The slit is moved every 20 μ m from fully open which is equivalent as 10 Hz beam repetition rate with continuously moving a velocity of 0.2 mm/s. The images vertical resolution is 12 bit which is common resolution of CMOS camera, and they are stored in a scaled 16-bit video format.

RADIATION HARD BEAM PROFILE MONITORS FOR THE NORTH EXPERIMENTAL BEAMLINES CERN

E. Buchanan*, J. Cenede, S. Deschamps, W. Devachelle,
A. Frassier, J. Kearney, R. G. Larsen, I. O. Ruiz
CERN, Geneva, Switzerland

Abstract

A new radiation hard profile monitor is being researched and developed for the North Area Beamlines at CERN. The monitor must have a spatial resolution of 1 mm or less, an active area of 20 x 20 cm, a low material budget (0.3%) and be operational in a beam that has a rate of $\sim 2 \times 10^{11}$ p/s in the full energy range of 0.5 – 450 GeV/c. The current focus is the study of different detection mediums: silica optical fibres (Cherenkov radiation) and glass capillaries filled with liquid scintillator. Prototypes of the different fibre candidates have been tested at different beam facilities at CERN: the M2 beamline and IRRAD. The key properties tested are the light yield and radiation tolerance.

INTRODUCTION

Since the late 1970s, Multi Wire Proportional Chambers, Delay Wire Chambers and Filament Scintillators have been used in the North Area Beamlines to provide the profile and positions of the beams [1]. However, the performance of these detectors is now degrading due to aging effects and there are limitations on the maximum intensity at which they can operate. As part of an upgrade to the beamlines, starting from 2027, the majority of these detectors will be replaced [2]. For the low intensity beamlines ($\sim 10^8$ particles per spill), a scintillating fibre detector called the eXperimental Beam Profile Fibre monitor (XBPF) will be installed [3]. The XBPF consists of a single array of 192 plastic scintillating fibres (SCSF-78) from Kuraray with a square cross-section and 1 mm thickness. Each fibre is individually read-out using si-pm's. A photograph of an XBPF is shown in Fig. 1. For the high intensity beamlines ($\sim 10^{11}$ particles per spill), the XBPF is not expected to have sufficient radiation tolerance, therefore a new radiation hard profile monitor is currently being researched and developed. Ideally the new detector will have a similar silhouette to the XBPF, but the active medium will be replaced with a material that has a higher radiation tolerance. This article describes the different detection mediums that are being studied and presents recent beam test results.

DETECTOR REQUIREMENTS

The new radiation hard profile monitor has the following requirements:

- active area of 20 cm × 20 cm,
- a low as possible material budget ($\sim 0.3\% X_0$),

* emma.buchanan@cern.ch



Figure 1: The XBPF detector.

- a spatial resolution of 1 mm,
- measure particle rates from $\sim 10^4$ to $\sim 10^{11}$ in the full energy range of 0.5 – 450 GeV/c,
- operational up to 2 MGy, equivalent to a minimum of 8 years of operation, and
- operational in vacuum (10^{-3} mbar) and in air.

ACTIVE MEDIUMS

Two different active materials are currently being studied: silica optical fibres and silica capillary fibres filled with liquid scintillator.

Silica Optical Fibres

Silica optical fibres are widely used in the telecommunications industry. They consist of a central silica core surrounded by a cladding layer which has a lower refractive index, enabling the transmission of light via total internal reflection. A well-known phenomenon is the production of Cherenkov light in silica fibres when charged particles pass through them [4]. Often for data transmission in high radiation environments, for example high energy physics experiments, this is an unwanted source of background. However, for some applications, this phenomenon can be exploited as a signal, such as Beam Loss Monitors [5].

The Cherenkov light peaks in the UV wavelengths and is emitted in a cone relative to the impinging particles direction. The angle depends on the refractive index of the

NON-INVASIVE PROFILERS FOR THE COLD PART OF ESS ACCELERATOR

J. Marroncle, P. Abbon, F. Belloni, F. Bénédicti*, B. Bolzon, N. Chauvin, D. Chirpaz-Cerbat, M. Combet, M. Desmons, Y. Gauthier, T. Hamelin, C. Lahonde, P. Legou, O. Leseigneur, Y. Mariette, JP Mols, V. Nadot, M. Oublaïd, G. Perreu, F. Popieul, B. Pottin, Y. Sauce, L. Scola, F. Senée, J. Schwindling, G. Tauzin, O. Tuske, S. Tzvetkov, CEA-Saclay, Gif-sur-Yvette, France
 I. Dolenc Kittelmann, A. Gevorgyan, H. Kocevar, R. Tarkeshian, C. Thomas, ESS Lund, Sweden

Abstract

Several Non-invasive Profile Monitors are being installed along the accelerator to support the commissioning, tuning and operation of the powerful proton based ESS linear accelerator. In the low energy parts of the ESS linac (3.6 MeV to 90 MeV), the residual gas pressure is high enough to measure the transverse beam profile by using fluorescence induced by the beam on the gas molecules. However, in the ESS linac sections above 90 MeV, protons are accelerated by superconductive cavities working at cryogenic temperatures and high vacuum. Therefore, the signal based on the fluorescence process is too weak, while ionization can counteract this drawback.

We have provided five IPM (Ionization Profile Monitors) pairs for energies ranging from 100 to 600 MeV. The design of such monitors is challenging due to weak signal (as a result of high proton energy and low pressure $<10^{-9}$ mbar), tight space constraints inside the vacuum chamber, space charge effect, ISO-5 cleanliness requirement, and electrode polarization at ± 15 kV.

This publication will detail the development we followed to fulfil the ESS requirements.

INTRODUCTION

The European Spallation Source (ESS) [1], presently under construction at Lund (Sweden), will consist of a 537 m long linear proton accelerator delivering a 2 GeV proton beam with a 5 MW power to a tungsten target, equipped with a highly optimized neutron moderator capable of providing a bi-spectral (thermal and cold) neutron beam to 42 beam ports, 22 of which are followed by a flight path leading to faraway measuring stations.

A perfect knowledge of the proton beam is critical for maximizing the number of protons on target and minimizing beam losses. Transverse beam profile monitors are therefore essential to support the tuning of the beam for good operation of the facility, both during its commissioning and in everyday operation.

Due to the high beam power, all beam profilers to be used at nominal operating conditions will be non-invasive type. In the frame of the in-kind contribution agreement signed with ESS, CEA has delivered to the European Spallation Source five Non-invasive Profile Monitors (NPMs) to be installed in the Cold Linac section: one in the Spoke section, 3 in the β -medium section, and one in the β -high

section. These transverse beam profile monitors will cover proton energies ranging between 90 MeV and 600 MeV and are conceived to deliver one profile/pulse at a residual gas pressure of 10^{-9} mbar with an uncertainty on the beam width of less than 10% of its dimension (see Refs. [2] and [3] for a profiler detailed overview).

At such high proton energies and low residual gas pressure, the NPMs located on the superconductive beam line are based on the ionization of the residual gas. In the warm sections, transverse beam profiles are measured by using the fluorescence of the gas molecules induced by the beam.

ESS IPM DESCRIPTION

Two parts can be considered for describing an IPM (Fig. 1): the inner, situated inside the vacuum chamber, and the outer part. The beam traverses the cage approximately at its center.

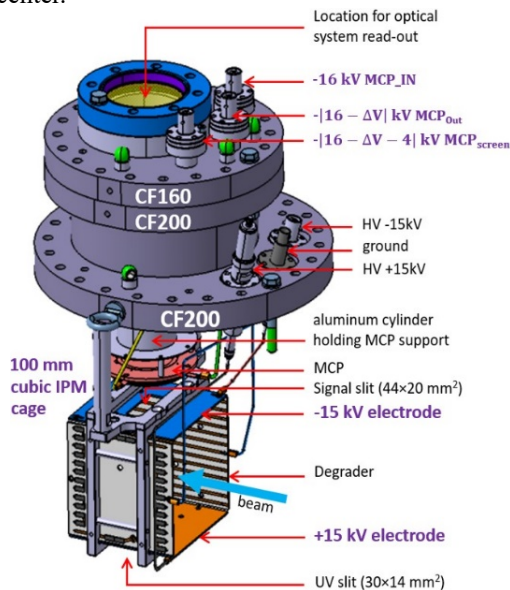


Figure 1: An ESS IPM.

Then, the ions and electrons, by-products of beam-residual gas interactions, drift under the influence of the electric field applied between both electrodes through a slit for ions before collection onto an MCP (Micro-Channel Plate). The MCP is equipped with a phosphorescent screen, allowing electric signal conversion to an optical one. To enhance the electric field uniformity, degraders positioned perpendicular to the electrodes are designed.

* Presently at LIPAc Rokkasho

STUDY OF VISIBLE SYNCHROTRON RADIATION MONITOR ON SOLEIL BOOSTER

A. Moutardier*, G. Cauchon, M. Chevrot, Z. Fan, N. Hubert, S. Kubsy, M. Labat, M. Thomasset
Synchrotron SOLEIL, Gif-Sur-Yvette, France

Abstract

In the scope of SOLEIL II, the booster must also be upgraded to reduce from 130 to $5 \text{ nm} \cdot \text{rad}$ the emittance of the beam delivered to the ring. Control of the emittance in the booster will become crucial to ensure the nominal performance of the storage ring injection. The SOLEIL I booster is already equipped with a Visible Synchrotron Radiation Monitor (MRSV). This equipment, made of an extraction mirror and a simple optical system, was originally planned to be used only for beam presence verification but has not been used routinely for operation since the commissioning in 2005. The control and acquisition systems had to be refreshed to be usable again and allow the beam size measurement along the booster energy ramp. The extraction mirror was replaced due to unexpected degradation leading to a second spot appearing on the camera. This paper traces back the MRSV upgrades from understanding the cause of mirror degradation until mirror replacement and the first proper beam visualisation, achieved at the beginning of 2023.

INTRODUCTION

Fourth-generation synchrotron light sources are presently emerging all around the world. Those machines target ultra-low emittances, below hundred of $\text{pm} \cdot \text{rad}$, enabling the delivery of photon beams with unprecedented brilliance.

In this context, the French synchrotron light source SOLEIL is planning an upgrade for the late 2020s, referred to as SOLEIL-II. The targeted emittance in the storage ring is $88 \text{ pm} \cdot \text{rad}$ in the horizontal plane and $35 \text{ pm} \cdot \text{rad}$ in the vertical plane. To reach such a low emittance, all SOLEIL's accelerators will have to be upgraded, i.e. the storage ring but also the linac and the booster. The requirements on the booster beam quality will be significantly increased, and an emittance measurement along the energy ramp in the booster will be mandatory.

This emittance measurement could be done using a Visible Synchrotron Radiation Monitor (MRSV). In order to confirm this strategy, preliminary tests are ongoing on the present SOLEIL booster, using the MRSV system installed, but barely used, since 2006.

This paper traces back the issues encountered with this diagnostic and presents the solutions considered to achieve an emittance measurement along SOLEIL's booster ramp.

* alexandre.moutardier@synchrotron-soleil.fr

MRSV DESIGN

An MRSV is an electron beam diagnostic which enables to image the synchrotron radiation emitted inside a dipole at its source point. It usually simply consists of an extraction mirror, to collect and deflect the synchrotron radiation out of the accelerator vacuum chamber, an imaging system and a camera. SOLEIL's booster MRSV setup is shown in Fig. 1. The extraction mirror is a simple Pyrex glass, silver-coated, flat mirror, mounted at 45° to deflect the synchrotron radiation in the vertical plane. The imaging system consists of three lenses allowing it to reach a magnification of 0.24. The camera is a CCD camera (Model acA1920-50gm from Basler [1]). A UHV viewport of fused silica between the extraction mirror and the first lens ensures the transition from vacuum to air.

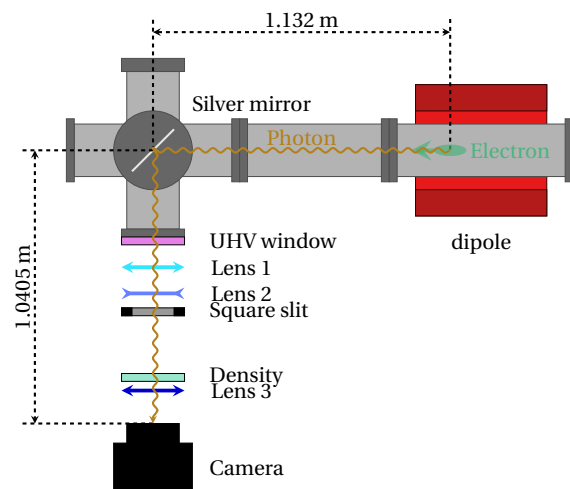


Figure 1: Experimental setup of the MRSV implemented on the booster of SOLEIL.

On many synchrotrons, MRSVs are simply used to check beam presence and its rough stability. But MRSVs can also be used to measure the electron beam size inside the source dipole [2]. In this case, the Point-Spread-Function (PSF) must be accurately considered because dipoles create a longitudinally extended source point. The PSF corresponds to the light distribution of one electron (or zero emittance and energy spread beam) in the image plane which can not be resumed to an infinitesimal point. The light distribution of the real beam (finite emittance and energy spread) results from the convolution of this PSF with the electron beam distribution at the source point magnified by the imaging system. Both the PSF and the light distribution from the whole beam in the image plane can be accurately simulated using SRW [3] as shown in Fig. 2.

EFFECT OF INCOHERENT DEPTH OF FIELD FOR BEAM HALO MEASUREMENT WITH THE CORONAGRAPH IN SuperKEKB

T. Mitsuhashi[†], H. Ikeda and G. Mitsuka, KEK

Abstract

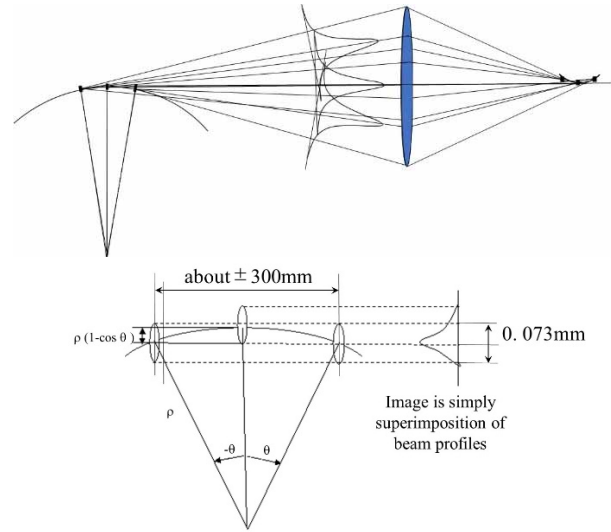
In the case of beam profile measurement by imaging system, observed apparent beam profile will change by the incoherent depth of field. This apparent change of beam profile, especially extra beam tail in one side has certain influence for beam halo measurement using the coronagraph, because it has a large dynamic range of 6-digit contrast. Since the magnitude of asymmetric tail is depending on bending radius, this effect is larger in large high energy physics machine which has a long bending radius. This effect is studied with geometrical optics and coronagraph measurement of beam halo in the SuperKEKB. As a conclusion, the IDF effect has significant effect in the beam halo observation with coronagraph at SuperKEKB.

INTRODUCTION

For the measurement of beam image, the incoherent depth of field (IDF) due to horizontal instantaneous opening of the Synchrotron Radiation will apparently modify the horizontal profile of beam image in asymmetric manner. We have presented this IDF effect for horizontal beam size measurement with interferometry in IBIC2017 [1]. In the interferometry, The IDF effect deduces spatial coherence in horizontal direction, and correction is necessary for the horizontal beam size measurement with interferometry [1]. The IDF effect has not only reducing the spatial coherence, but also modify the apparent horizontal beam profile with asymmetric manner. As a result, observed beam image with focusing system will be deformed. Especially, tis asymmetric deformation of beam profile can introduce extra asymmetric distribution in beam tail (or halo) which is existing surrounding of beam core. We studied this effect using the geometrical optics in the case of beam halo measurement with coronagraph in the SuperKEKB. And compare the measurement result s of beam halo with the coronagraph [2].

EFFECT OF INCOHERENT DEPTH OF FILED FOR APPARENT DEFORMATION OF BEAM PROFILE

In the horizontal plane, the profile of beam is modified apparently by IDF with the instantaneous opening of the SR in the horizontal plane as shown in Fig. 1.



SuperKEKB HER case,

Figure 1: Apparent beam profile with the IDOF effect by the instantaneous opening of the SR in the horizontal plane in the SuperKEKB HER case.

In the geometrical Optics, the intensity distribution in the entrance aperture has no effect for imaging as shown in Fig. 2. Also, due to small emittance of the source beam, opening angle and source size is very smaller than opening of SR in the visible light region, this effect will be negligible small for IODF.

In the geometrical optics

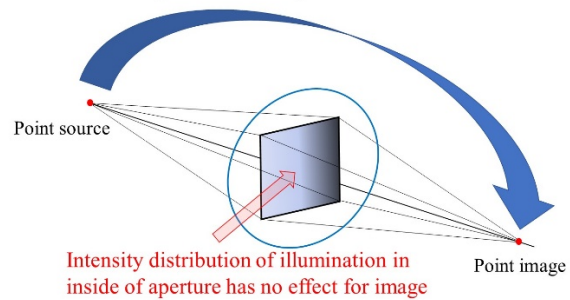


Figure 2: Point to point transfer of source point into imaging point in the geometrical optics.

Denote the total intensity of SR inside of the entrance aperture in horizontal plane by $I(\theta)$ as a function of horizontal observation angle θ , the apparent beam shape $\sigma_a(x)$ is given by,

$$\sigma_a(x) = \int I(\theta) \cdot \frac{\exp\left[-\frac{[x - \rho\{1 - \cos(\theta)\}]^2}{2\sigma^2}\right]}{\sigma \cdot \sqrt{2\pi}} d\theta \quad (1)$$

where the original beam profile is assumed to be a Gaussian distribution.

For the discussion of horizontal IODF, we need knowledge of instantaneous intensity distribution of SR in horizontal plane to evaluate $I(\theta)$.

[†]email address: toshiyuki.mitsuhashi@kek.jp

DEVELOPMENT OF PEPPER-POT EMITTANCE MONITOR FOR HIGH-INTENSITY ION BEAM ACCELERATED BY RIKEN AVF CYCLOTRON

Y. Kotaka*, K. Kamakura, H. Yamaguchi, N. Imai, Y. Sakemi
 Center for Nuclear Study, University of Tokyo, Wako, Japan
 J. Ohnishi, Riken Nishina Center, Wako, Japan

K. Hatanaka†, Research Center for Nuclear Physics, Osaka University, Ibaraki, Japan

Abstract

At the Center for Nuclear Study of the University of Tokyo, the measurement of Electric Dipole Moment of Francium (Fr) is underway with the world highest precision. Fr is generated by nuclear fusion reaction by irradiating gold with oxygen ion beam accelerated by RIKEN AVF Cyclotron. The required beam intensity is 18 μA or more. However, the average beam transport efficiency drops to be around 66% as the beam intensity exceeds 10 μA . To solve the problem, a pepper-pot emittance monitor (PEM) for high-intensity beams has been developed. Referencing the PEM used for the injection beams of AVF Cyclotron, we have developed three additional items. The first is reducing the radiation damage to a camera, which is placed away from the beamline. The distance between the camera and PEM is 2.2 m, and the average image position accuracy of 0.15 mm is achieved. The second is the angular accuracy suitable for the accelerated beam. The required angular accuracy is estimated to be less than 0.3 mrad. A beam test for the first and second items is planned. The third is a beam shutter system to prevent PEM from heating due to beam. The measurement time by the system reaches 0.27 seconds now.

INTRODUCTION

At the Center for Nuclear Study of the University of Tokyo (CNS), the measurement of Electric Dipole Moment (EDM) of Francium (Fr) is underway with the world highest precision [1]. Fr is generated by nuclear fusion reaction by irradiating the gold target of EDM experiment device (EDM target) with $^{18}\text{O}^{6+}$ ion beam of 7 MeV/u accelerated by RIKEN AVF Cyclotron. Our goal is transporting $^{18}\text{O}^{6+}$ ion beam of more than 18 μA (400 W), without loss and converging beam to be 1 mm of standard deviation (SD) of the beam distribution on the EDM target shown in Fig. 1.

CNS performs experiments in the three courses of C12 for EDM, CRIB [2], and E7B for students of the University of Tokyo in the E7 experiment room of RIKEN Nishina Center shown in Fig. 1. Figure 2 shows the beam transport efficiencies from AVF Cyclotron to C12, CRIB, and E7B as a function of beam intensities. As beam intensities are larger than 10 μA , the average beam transport efficiency is 0.66. The stronger beam intensity tends to lower the beam transport efficiency. Figure 3 shows beam emittances mea-

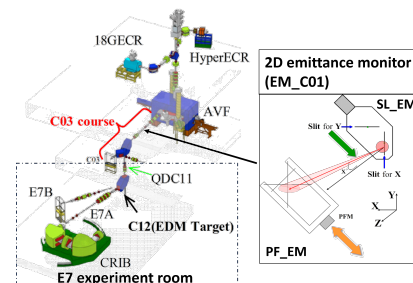


Figure 1: AVF Cyclotron and beamlines to the experiment devices. EM_C01 is shown in the right.

sured by 2D emittance monitor (EM_C01) shown in Fig. 1 tend to expand as beam intensities increase. We think beam transport efficiencies decrease as beam emittances expand as a function of beam intensities. However, we cannot measure a high intensity beam emittance because the cooling ability of EM_C01 is suitable for less than 130 W beam power [3].

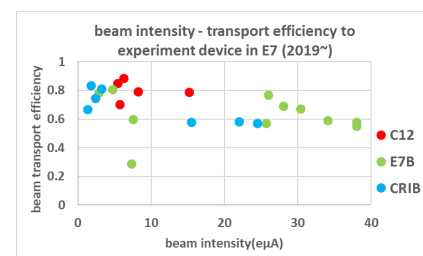


Figure 2: The relationship between beam intensity and transport efficiency to C12(red), E7B(green), and CRIB(blue)

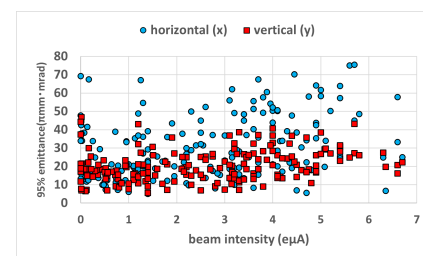


Figure 3: The relationship between beam intensity and 95% horizontal (blue) and vertical (red) beam emittance.

To solve the problem, a pepper-pot emittance monitor (PEM) [4, 5] for high-intensity beams has been developed.

* kotaka@cns.s.u-tokyo.ac.jp
 † Deceased.

BEAM PROFILE MEASUREMENT USING HELIUM GAS LIGHT EMISSION AND BEPM FOR SUPERHEAVY ELEMENT SEARCH EXPERIMENT

T. Watanabe*, T. Adachi, P. Brionnet, O. Kamigaito,
K. Morimoto, T. Nishi, A. Uchiyama, RIKEN, Wako, Japan
A. Kamoshida, National Instruments Japan Corporation, Tokyo, Japan
K. Kaneko, R. Koyama, SHI Accelerator Service Ltd., Wako, Japan

Abstract

The newly constructed superconducting linear accelerator (SRILAC) is now in operation with the aim of discovering new superheavy elements and advancing the production of medical radiation isotopes. Because it is crucial to extend the durability of the expensive Cm target for as long as possible, these experiments require the accelerated V beam to be sufficiently widened. To this end, a helium gas light emission monitor (HeLM) has been introduced to measure the beam profile. Because He gas flows within the target chamber, by capturing the light emitted from He gas with a CCD camera, the beam profile can be obtained nondestructively and continuously. These measurements are handled through programming in LabVIEW, with analyzed data integrated into an EPICS control system. A method to estimate the beam envelope has been recently developed by leveraging the measured quadrupole moments with beam energy position monitors (BEPMs), and incorporating calculations of the transfer matrix. The synergistic use of HeLM and BEPM plays a useful role in accurately controlling the beam size at the Cm target.

INTRODUCTION

To upgrade the RIKEN Heavy-ion Linac (RILAC), the Superconducting RILAC (SRILAC) has been constructed, and successful commissioning has been completed [1]. These accelerators are being operated to advance research into even heavier synthetic elements [2]; build on the discovery of element 113, Nihonium [3]; and enhance the production capability of the short-lived radioisotope ²¹¹At, which is anticipated to have applications in cancer therapy [4]. Over the past three years, the V beam, accelerated by both the RILAC and SRILAC, has been irradiated onto the Cm target for superheavy elements research.

BEAM PROFILE MEASUREMENT USING He GAS LIGHT EMISSION

RILAC, SRILAC, and GARIS III

A schematic drawing of the RILAC, SRILAC, GARIS III, and production apparatus for medical RIs is shown in Fig. 1. The V beam, accelerated by both RILAC and SRILAC, is irradiated onto the Cm targets inside a target chamber. To

prevent the Cm targets from melting due to the beam irradiation, several thin Cm targets are mounted on a 30-cm radius wheel, which rotates at 2000 rpm. GARIS III separates the superheavy elements from the unwanted particles, achieving high background noise reduction, by using dipole and quadrupole magnets. Furthermore, helium gas is introduced so that the electron charges of the superheavy elements converge to a certain value. Even if superheavy elements with different charges are ejected from the target, because the charges of superheavy elements become equal while they are passing through the helium gas, it is possible to collect the desired superheavy elements.

Target Chamber and HeLM for GARIS III

To protect the Cm target, it is essential to extend its durability for as long as possible. Therefore, the accelerated V beam must not only hit the Cm target but also be adequately widened. A schematic drawing of the beam line with a differential pumping system and the target chamber for GARIS III is shown in Fig. 2. Baffle electrodes are installed at the top, bottom, left, and right to detect the edge of the beam, and a carbon slit is installed in front of the target to cut the edge of the beam. CCD cameras monitor how the beam irradiates the target through view ports located upstream and downstream of the target. In Fig. 2, the beam comes from the left side, hits the Cm targets, and then proceeds to GARIS III. Since He gas flows within the target chamber,

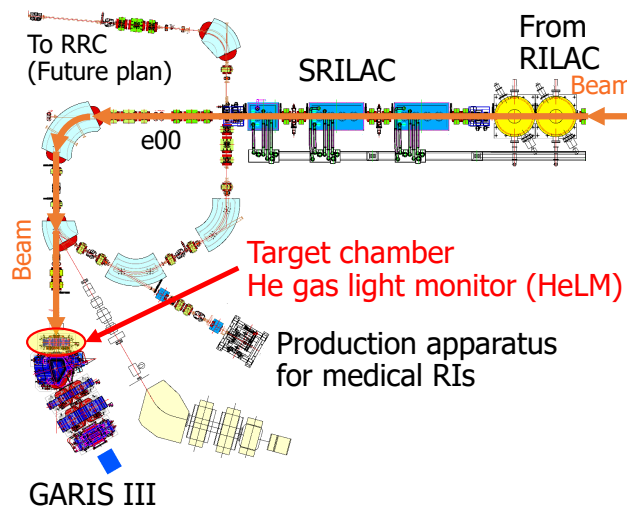


Figure 1: Schematic drawing of the RILAC, SRILAC, GARIS III, and production apparatus for medical RIs.

* wtamaki@riken.jp

A PRELIMINARY DESIGN OF BUNCH-BY-BUNCH 3D POSITIONS MEASUREMENT

Ruizhe Wu, Yunkun Zhao, Dongyu Wang, Ping Lu, Leilei Tang, Baogen Sun*
 University of Science and Technology of China (USTC),
 No. 96, JinZhai Road Baohe District, Hefei, Anhui, China

Abstract

The decrease of beam emittance in the 4th generation light source greatly increases the electron density, thus the wakefields and beam impedance in the storage ring are significantly enhanced, resulting in various beam instabilities. Therefore, it is necessary to observe the transient state of beams using the bunch-by-bunch technique, so as to dig into these instabilities. Here a three-dimensional (3D) positions measurement instrument is designed based on data synchronization module (DSM) to acquire the transverse positions and longitudinal phases of beams in real-time.

INTRODUCTION

Compared with the 3th generation light sources, the 4th generation light sources are generally built with compact MBA structures, so that the horizontal emittance of the beam is reduced by 1 to 2 orders, close to the X-ray diffraction limit. Consequently, the strong nonlinear elements in the MBA structures make the dynamic aperture significantly smaller, causing the beam dynamics to be extremely sensitive to the effects of instabilities, and even affecting the maximum beam current during operation time. Hence, it is essential to observe the beam characteristics on fine time scales using bunch-by-bunch technique, figuring out the instabilities induced by wakefields, and even eliminating these instabilities.

Generally, bunch-by-bunch technique covers bunch length, longitudinal phase, bunch charge, transverse positions and bunch profiles [1–5]. However, it is obvious that these measurements are limited by the number of sampling channels on a single acquisition board, and only one single beam parameter can be obtained, rather than multiple parameters simultaneously. In order to break through the limitation of the number of sampling channels, a bunch-by-bunch 3D positions measurement instrument is designed with DSM [6], as shown in Fig. 1.

The instrument is mainly composed of microwave components and digital logic components, in which the microwave components are divided into signal part and timing part. For the signal part, it duplicates the four-channel signal sensed from the BPM in the storage ring and sends the two duplicated four-channel signals to data acquisition boards. For the timing part, the synchronous signal generated from the storage ring timing system is frequency quadrupled and then divided into two channels to data acquisition boards, between which there is a certain phase difference due to the delay

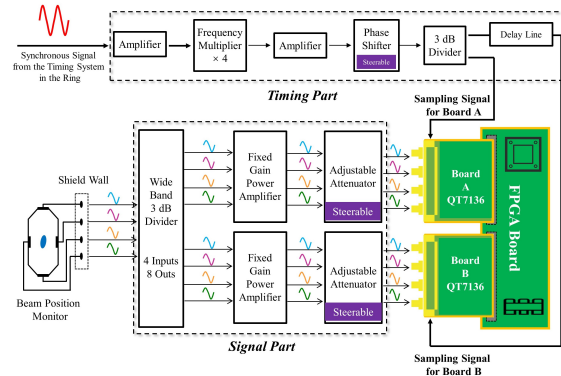


Figure 1: The layout of bunch-by-bunch 3D positions measurement instrument.

line. As for the digital logic components, two four-channel signals are digitized by the acquisition boards, then these digitized signals are synchronized by the DSM in FPGA, and finally the 3D positions of each bunch are calculated. Since these microwave components are at the factory, an evaluation system based on oscilloscope is set up to research the 3D positions measurement processes in the designed instrument.

EVALUATION SYSTEM SETUP

In order to determine the measurement performance in the 3D positions, an oscilloscope-based performance evaluation system was constructed, as shown in Fig. 2. With the help of the low-pass filter, the bandwidth of the oscilloscope is equivalent to that of the acquisition board, so that the data obtained by the oscilloscope and the data acquisition board are consistent. After the acquisition, these data will be sent to the computer for processing, and finally obtain the signals of each bunch during the bunch interval [7]. Finally, the corresponding measurement performance can be obtained by analyzing the signals in the bunch interval.

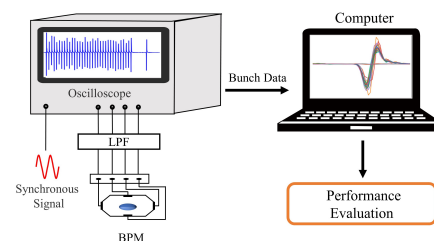


Figure 2: Evaluation system based on oscilloscope.

* bgsun@ustc.edu.cn

QUALITY ASSURANCE OF PROTON BEAM PROFILE USING PHOSPHOR SCREEN AND TE-COOLED CMOS CAMERA*

Gwangil Jung[†], Young-Seok Hwang, Young Jun Yoon
Korea Atomic Energy Research Institute, Gyeongju-si, Republic of Korea

Abstract

The Korea Multi-Purpose Accelerator Complex (KOMAC) operates a 100 MeV proton linear accelerator, providing a high flux proton beam at the TR103, a general-purpose irradiation facility. Ensuring uniform irradiation of sample with protons is critical, necessitating confirmation of beam profile uniformity through the quality assurance (QA) process. To address this, a real-time and in-situ proton beam profile monitoring system was recently introduced and tested at the TR103. This system includes a P43 phosphor screen and TE-cooled CMOS camera, which captures images of the emitted light from protons with energies of 20, 50, and 100 MeV incident on the screen. Subsequent post-processing, such as background subtraction, image smoothing, geometrical correction, was performed on the image data. The measured beam profiles using the phosphor screen and cooled camera were then compared to those obtained using Gafchromic filmTM, a widely used dosimeter in radiation measurements. Additionally, the linearity between light output and beam flux was measured to establish a quantitative relationship. This study presents the test results of the proton beam profile measurement using the phosphor screen and TE-cooled CMOS camera, demonstrating its potential as an effective tool for quality assurance in proton beam irradiation experiments at the TR103 facility.

INTRODUCTION

Since 2013, KOMAC has operated a 100 MeV proton linear accelerator, facilitating various proton beam irradiation experiments. To ensure optimal experimental conditions and minimize irradiation errors, a rigorous quality assurance (QA) process for proton beam profiling is essential to achieve uniform proton irradiation within the sample. The uniformity criteria, defined as the difference between the maximum and minimum intensity divided by the mean intensity, must meet a threshold of 10% within the target diameter.

The TR103, a general-purpose irradiation facility at KOMAC, has used film dosimetry for beam profile QA. However, film dosimetry lacks real-time and in-situ monitoring capabilities due to the need for scanning to acquire beam profile data and its susceptibility to saturation under continuous irradiation of high-flux proton. To address these limitations, a recent advancement introduced the use of a P43 phosphor screen and TE-cooled CMOS camera for real-time and in-situ proton beam profile monitoring.

This study aimed to verify the accuracy of the P43 phosphor screen and CMOS camera system and integrated it into the quality assurance process. An experiment was conducted to capture the light response of the phosphor screen.

EXPERIMENTS AND DISCUSSTION

Phosphor Screen and Cooled Camera

Proton irradiation tests were performed at TR103 with a flux of approximately 10^{10} to 10^{11} particle/(cm²·pulse). The pulsed proton beam was accelerated to energies of 20, 45, and 102 MeV, and its energy was attenuated by 15, 42, and 100 MeV, respectively, as it passed through the beam window and air before reaching the target point. The beam profile monitoring system primarily consisted of a phosphor screen, where light is emitted as protons deposit energy, and a real-time capturing camera. The phosphor screen was positioned 1.5 m away from the beam window, tilted at a 45-degree angle relative to the beam path, while the camera was placed 1 m perpendicular to the screen for real-time imaging of the emitted light (Fig. 1).

The phosphor screen used in this study consisted of a P43 (Gd₂O₂S:Tb) layer on an Al substrate, providing a detection area of 310 mm × 310 mm and a peak wavelength of 545 nm [1]. With a decay time of 1 ms to 10% and high light efficiency, the phosphor screen proved suitable for real-time light emission detection. The TE-cooled CMOS camera (ASI183MC Pro, ZWO) utilized in the setup had a sensor size of 13.2 mm × 8.8 mm and a thermoelectric cooler capable of cooling sensors down to -10°C [2]. Figure 2 illustrates the arrangement of the P43 phosphor screen and the camera. To minimize image noise and avoid saturation at high light outputs, the camera

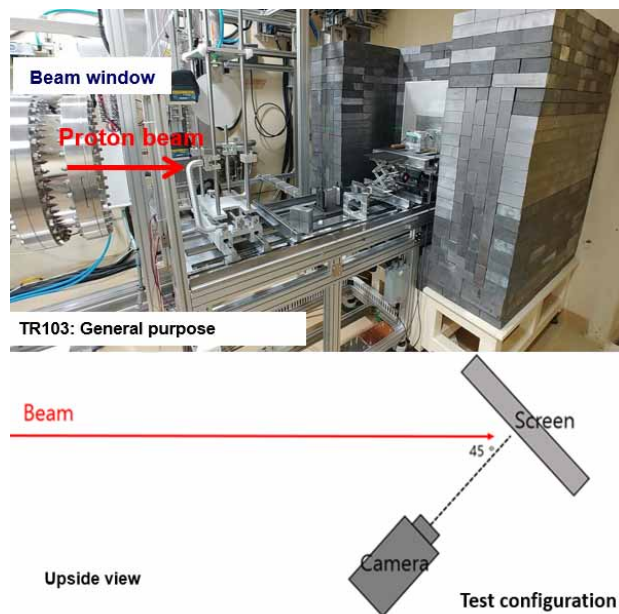


Figure 1: View of general-purpose irradiation facility, TR103 (top) and configuration of device layout (bottom).

MEASURING ELECTROMAGNET POLARITY USING MAGNETIC REMANENCE*

K. P. Wootton[†], Argonne National Laboratory, Lemont, IL, USA

Abstract

Large accelerator systems typically include many individually powered electromagnets. An important activity prior to commissioning with beam is verifying that the polarity of the installed magnets matches the design lattice. In the present work, we motivate the measurement of magnet polarity in a manner that is electrically safe, by measuring the magnetic remanence of iron yokes of normal conducting electromagnets. This has been used to confirm the polarities of iron-dominated dipole and quadrupole electromagnets at the Linac Extension Area at the Advanced Photon Source.

INTRODUCTION

During installation and commissioning of accelerator systems, a common quality assurance task associated with the installation is ensuring that magnets are connected to power supplies with the correct polarity [1–4]. Magnetic polarity checkout has typically been performed in under administrative controls with magnets energised [5]. We consider that procedures which require workers to approach energised magnets potentially presents an unacceptable electrical safety hazard.

In the present work, we summarise a technique for performing magnet polarity checks using the remnant magnetic field from prior excitation using the connected power supply. Measuring the remnant field with the power supply off obviates the principal safety concern of needing to work adjacent to energised electrical conductors.

BACKGROUND

In many accelerators, the main magnets are powered by unipolar power supplies. Hence, a quality assurance task associated with the installation of a magnet and power supply system is to confirm that the installed magnet polarities match the design polarities of the lattice [6–9]. When powered, electromagnets have the opportunity to present both electrical and magnetic hazards to personnel approaching them [10]. There are different ways of mitigating these hazards, for instance by implementing electrically insulating shielding or shielding that restricts personnel from approaching the magnetic field that the magnet generates. Another way is to switch off the magnet power supply, and Lock-Out-Tag-Out (LOTO) the source of hazardous energy.

* Work supported by the U.S. Department of Energy, Office of Science, Office of Basic Energy Sciences, under Contract No. DE-AC02-06CH11357.

[†] kwootton@anl.gov

METHOD

We tested this procedure using the bending magnets of the booster bypass vertical ramp and the Linac Extension Area (LEA). The steps in the procedure are outlined below.

1. Accelerator enclosure secured.
2. Accelerator magnets energised at its nominal current setpoint for 10 minutes using its connected power supply. This puts the magnet on its hysteresis curve.
3. Accelerator magnets de-energised, leaving only the remnant field in the magnet.
4. Lock-Out-Tag-Out (LOTO) accelerator magnets, and verify zero energy state by Zero Voltage Verification (ZVV). At this point, all LOTO requirements should be complete to enable authorised access to the accelerator enclosure.
5. Lower the accelerator access control system level to authorised access.
6. Enter the accelerator enclosure and approach the un-powered electromagnet.
7. Measure the polarity of the remnant field (without any electrical hazard) using a permanent magnet probe.

RESULTS

Initial Measurement

On the 22nd of August, 2022, Kent Wootton performed magnet polarity checks on booster bypass and LEA magnets. A magnet polarity checker Magnaprobe MKII was used. The north pole of the bar magnet on the magnet probe is coloured red, and the south pole of the magnet is coloured blue. The polarity checker is illustrated in Fig. 1.

The polarity of quadrupoles and vertical bending magnets (skew dipoles) along the booster bypass transport line was measured. We measured the ‘top-left’ most pole of quadrupoles, and the ‘left’ pole of skew dipoles. This pole convention is illustrated in Fig. 2.

The probe was held near the poles of the magnets. Photographs illustrating polarity measurements are given in Fig. 3 and Fig. 4. One can see that the experimenter’s hand is quite close to the magnet while performing the measurement.

Results of polarity measurements are summarised in Table 1. Magnet polarity measured from remnant field on the 22nd of August, 2022. Magnet types Q_1 correspond to upright quadrupole, and B_2 to skew dipole (vertically deflecting). We deliberately included a couple of quadrupoles from

SYNCHROTRON LIGHT MONITOR FOR THE ADVANCED PHOTON SOURCE BOOSTER SYNCHROTRON*

K. P. Wootton[†], W. J. Berg, W. P. Burns III, J. R. Calvey, J. C. Dooling, L. Erwin, A. H. Lumpkin,
N. S. Sereno, S. Shoaf, S. G. Wang, Argonne National Laboratory, Lemont, IL, USA

Abstract

A new synchrotron light monitor has been tested for the booster synchrotron of the Advanced Photon Source. Visible light synchrotron radiation is collected by a mirror on a path tangential to the electron beam orbit, and directed to an optical imaging system and camera. This is planned to be a non-intercepting, transverse beam-size monitor even with the higher stored beam charges (~17 nC) needed for the Advanced Photon Source Upgrade. In the present work, we describe the present synchrotron radiation diagnostic layout. An analysis of the synchrotron radiation power on the mirror, the optical layout with components, and features of the control system will be presented.

INTRODUCTION

Synchrotron radiation (SR) presents a significant thermal load on components in electron storage rings. As such, typically absorbers are designed with an inclined profile, and composed of a metallic material such as copper, to conduct heat away from the surface.

The motivation for the present work is to enable accurate measurement of beam properties during high-charge studies of the booster synchrotron for the Advanced Photon Source Upgrade (APS-U) [1, 2]. During those studies, it appears that the support for the mirror that reflects SR out of the vacuum deflects under thermal load from SR [3].

In the present work, we calculate the heat load on the mirror of the booster synchrotron photon monitor at the Advanced Photon Source (APS). We present the details of the mirror design. We summarise stability results using the diagnostic.

BACKGROUND

The beam profile monitors are required to support beam size measurements of the electron beam in the booster. Three photon ports are available for use as synchrotron light photon monitors in the booster [4–7]. Previously, only two ports had been instrumented. Under thermal loading, components of the assembly supporting the mirror in these ports expanded under thermal loading. The expansion was so significant that the image of the beam was deflected off sensors used to measure the beam transverse and longitudinal dimensions [3, 8]. Subsequently, this makes it difficult to routinely measure some properties of the electron beam such as emittance and energy spread.

* Work supported by the U.S. Department of Energy, Office of Science, Office of Basic Energy Sciences, under Contract No. DE-AC02-06CH11357.

[†] kwootton@anl.gov

To support physics goals of measuring the emittance in the booster, we propose to instrument all three photon monitors. The position of the beam image on the beam profile monitors needs to remain within a small enough displacement from nominal that it does not move off laterally the imaging and diagnostic devices.

SR POWER ON THE MIRROR

For an electron beam, the vertical distribution of SR power $\frac{dP}{d\Omega}$ in units of [W mrad⁻²] is calculated by [9]:

$$\frac{dP}{d\Omega} = 5.42E^4BI_b \frac{1}{(1 + \gamma^2\psi^2)^{5/2}} \left[1 + \frac{5\gamma^2\psi^2}{7(1 + \gamma^2\psi^2)} \right], \quad (1)$$

where E is in units of [GeV], B is in units of [T], I_b is in units of [A], γ is the Lorentz factor, and ψ is the vertical angle in units of [rad].

The peak power density (on-axis) $\frac{dP}{d\Omega}$ in units of [W mrad⁻²] is given by [9]:

$$\frac{dP}{d\Omega} = 5.42E^4BI_b. \quad (2)$$

Integrating over the vertical angle, the power density in the horizontal direction $\frac{dP}{d\Omega}$ in units of [W mrad⁻¹] is given by [9]:

$$\frac{dP}{d\Omega} = 4.22E^3BI_b. \quad (3)$$

Calculation

We propose to perform a piecewise integration of the SR power, at intervals of 1 ms. Parameters used in the present calculation are summarised in Table 1. These parameters are approximate, and close to the nominal booster ramp [10–12].

Table 1: Booster and Electron Beam Parameters

Parameter	Symbol	Value	Ref.
Booster circumference	C	368 m	[1]
Charge	q	17 nC	[2]
Beam current	I_b	13.9 mA	...
SR source to mirror	d	2.85 m	...
Bending radius	ρ	33.3 m	[13]
Energy at injection	E_i	425 MeV	...
Energy at extraction	E_e	7.1 GeV	...
Ramp time (E_i - E_e)	t_r	0.25 s	...
Booster period	T_B	1.0 s	...
Photon port width	w	60 mm	...
Photon port height	h	37 mm	...

BEAMLINE FOR TIME DOMAIN PHOTON DIAGNOSTICS AT THE ADVANCED PHOTON SOURCE UPGRADE*

K. P. Wootton[†], W. Cheng, G. Decker, N. S. Sereno, F. Westferro
 Argonne National Laboratory, Lemont, IL, USA

Abstract

Time domain photon diagnostics are proposed for electron beam characterisation and operation of the Advanced Photon Source Upgrade storage ring. In the present work, we present updated status on the time-domain X-ray and visible photon diagnostic beamline for the Advanced Photon Source Upgrade. We outline design influences leading to the proposed beamline layout, in particular long-term maintenance and commonality with other beamlines at the Advanced Photon Source.

INTRODUCTION

The Advanced Photon Source Upgrade (APS-U) project is presently underway, with the goal of increasing the brilliance of photon beams to user beamlines at the Advanced Photon Source (APS) [1–3]. A number of user programs take advantage of the fill pattern for time-resolved X-ray techniques. As these user programs are anticipated to continue during APS-U operations, we are providing temporal photon beam diagnostics for the optimisation and diagnostics of accelerator operations.

In the present work, we present updated status on the time-domain X-ray and visible photon diagnostic beamline at 35-BM for the APS-U. We outline design influences leading to the proposed beamline layout, in particular long-term maintenance and commonality with other beamlines at the APS.

DESIGN INFLUENCES

The beamline layout has matured through the design process, with subtle but notable changes since our previous work on this beamline [4]. In particular, we have made a concerted effort to utilise components standardised across APS-U bending magnet front ends and beamlines to the greatest extent possible.

For the APS, the 35-BM front-end and beamline employed a geometry optimised for providing multiple independent photon beams for diagnostics [5, 6]. The beamline featured three branch lines (X-ray, visible, X-ray) separated horizontally in angle from the bending magnet source. The visible light beamline passed a large vertical angular acceptance of ± 2.9 mrad (Fig. 1). Several practical constraints steered us away from adopting the existing 35-BM geometry directly for APS-U.

* Work supported by the U.S. Department of Energy, Office of Science, Office of Basic Energy Sciences, under Contract No. DE-AC02-06CH11357.

[†] kwootton@anl.gov

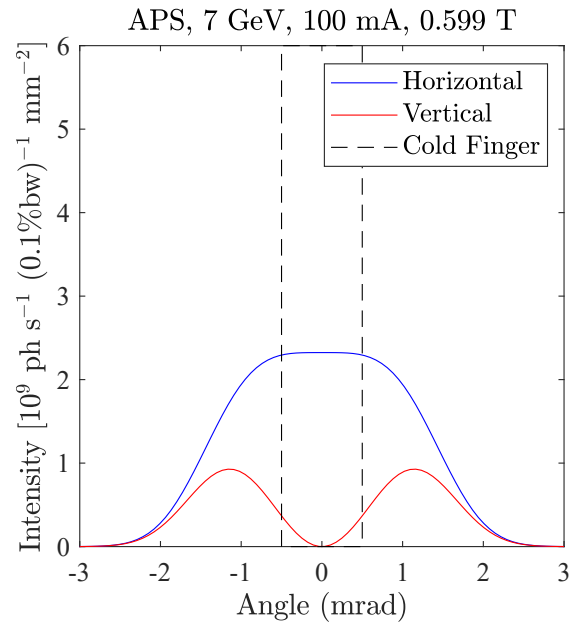


Figure 1: Vertical profile of bending magnet synchrotron radiation accepted by 35-BM for APS storage ring. The cold finger masks synchrotron radiation over the central ± 0.5 mrad.

It is envisaged that two diagnostic beamlines will be operated for routine beam diagnostics measurements for APS-U. Transverse beam sizes and emittances will be observed using the 38-AM bending magnet beamline [7–10]. Bunch length and bunch purity will be observed using visible light and X-ray diagnostics at the 35-BM beamline [4]. To meet the long-term need for time-domain diagnostics at 35-BM, a large vertical aperture is not strictly required for either the X-ray or visible light photon diagnostics. Hence rather than creating large vertical opening apertures in many components of the 35-BM front end, we instead start our design from the new bending magnet front end (BMFE) for user APS-U bending magnet beamlines [1]. The opening angle of visible synchrotron radiation and beamline apertures are illustrated in Fig. 2.

The choice to start from the standard user BMFE design affords us opportunities to standardise many beamline components and control equipment. We anticipate that this will be beneficial for long-term maintenance of the beamline.

FRONT END

35-BM has been operational as a diagnostic beamline at APS for many years [5, 6]. We summarise features of the

ELECTRON BEAM AT THE ADVANCED PHOTON SOURCE LINAC EXTENSION AREA BEAMLINE*

K. P. Wootton[†], W. J. Berg, M. Borland, A. Brill, J. M. Byrd, S. Chitra, J. Collins, J. C. Dooling, J. Edwards, L. Erwin, G. Fystro, T. Grabinski, M. Henry, E. Heyeck, J. Hoyt, R. Keane, S.-H. Lee, J. Lenner, I. Lobach, A. H. Lumpkin, A. Puttkammer, V. Sajaev, N. S. Sereno, Y. Sun, J. Wang, S. G. Wang, A. A. Zholents, Argonne National Laboratory, Lemont, IL, USA

Abstract

The Linac Extension Area has been developed into a beamline area for testing accelerator components and techniques. Beginning commissioning activities in February 2023, we have delivered the first electron beam to the Linac Extension Area at the Advanced Photon Source at 425 MeV. In the present work, we outline the stages of re-commissioning the electron beamline. We summarise measurements of the electron beam transport through the accelerator. We outline scenarios used to verify the adequacy of radiation shielding of the beamline, and measured shielding performance.

INTRODUCTION

The Linac Extension Area (LEA) at the Advanced Photon Source (APS) is a flexible beamline for accelerator component and technique development [1–4]. Hardware installation was completed in 2023, and activities to commission the electron beamline began in 2023.

In the present work, we summarise the progress to date in commissioning the LEA beamline. We outline the features of the LEA beamline. We summarise the stages of re-commissioning. We present measurements of the electron beam using beam diagnostics in the LEA enclosure during stages of commissioning. We outline the beam loss scenarios to be performed for qualifying the enclosure shielding.

LEA BEAMLINE

The LEA beamline lattice is configured to support ‘interleaving’ operation [5, 6]. Interleaving describes switching between a thermionic cathode radiofrequency electron gun (TCGun) as an electron source for APS storage ring operations, and a photocathode radiofrequency electron gun (PCGun) for LEA operations. We denote the LEA beamline as the section of beamline physically located within the LEA enclosure. The LEA beamline is illustrated in Fig. 1.

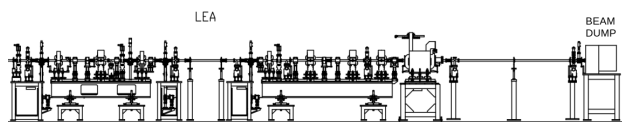


Figure 1: LEA beamline. In this figure the beam direction is from left to right.

As presently installed, the LEA beamline itself occupies ~15 m length within the LEA enclosure, terminating with an electron beam dump. A photograph of the LEA beamline is illustrated in Fig. 2.



Figure 2: Photograph of the LEA beamline within the LEA enclosure. In this figure the beam direction is from right to left.

The electron beam source for LEA is the APS linac. At present, the APS linac is capable of providing electron beams with energies up to ~450 MeV. The electron beam is transported from the APS linac to the LEA enclosure by several sections of beamline, denoted as the Particle Accumulator Ring bypass (PB), the PAR-to-Booster (PTB), and the Booster Bypass (BB) transport lines. The PAR bypass and PTB have been previously used for electron beam transport, and so for commissioning the LEA beamline, the main activity needed was to establish electron beam transport through the BB and LEA beamlines. The lattice of the booster bypass and LEA beamline for 425 MeV electrons is summarised in Table 1. The magnet types XX:QX correspond to upright quadrupoles, and XX:BX to skew dipoles (vertically deflecting). Numerous horizontal and vertical correctors are also included in the beamlines, but omitted from Table 1 for readability.

STAGES OF COMMISSIONING

The principal consideration in commissioning with the electron beam is that the LEA beamline is located within the LEA enclosure. This enclosure had previously been used for the Low-Energy Undulator Test Line (LEUTL) [7–9], but it

* Work supported by the U.S. Department of Energy, Office of Science, Office of Basic Energy Sciences, under Contract No. DE-AC02-06CH11357.

[†] kwootton@anl.gov

SIMULATION OF OSCILLATING ARM WIRE MONITOR MECHANICS DRIVEN BY A STEPPER MOTOR

R. Dölling[†], Paul Scherrer Institut, Villigen, Switzerland

Abstract

The present oscillating arm wire monitors at HIPA operate with wire speeds of 0.75 m/s. Based on basic dynamic simulations of mechanics and motor, we discuss possible variants of this design using stepper motors in open loop control. The results suggest that 4 m/s can be reached with sufficient position resolution, when using a predefined step sequence customized to the mechanics. This speed should be sufficient to measure the full proton beam current in the injection line.

INTRODUCTION

The majority of profile monitors presently operating in the 0.87 MeV, 72 MeV and 590 MeV beam lines of HIPA are wire monitors using an oscillating monitor arm (MA). A fork at the MA holds the wire, foil, or finger, which is moved transversely through the beam (Fig. 1) [1, 2]. The MA is driven via a con-rod (CR) from a crank wheel (CW), which again is driven via a gear (MG) connected to a brushed DC motor. A bellows at the MA axis of rotation separates the vacuum from the in-air mechanics. Since the bellows needs to bend only $\pm 10^\circ$, its lifetime is practically unlimited at the given maximum wire speed of 0.75 m/s. The wire position is determined by a potentiometer attached to the MA, while the home position is indicated by a home switch (HS) actuated by a cam on the CW.

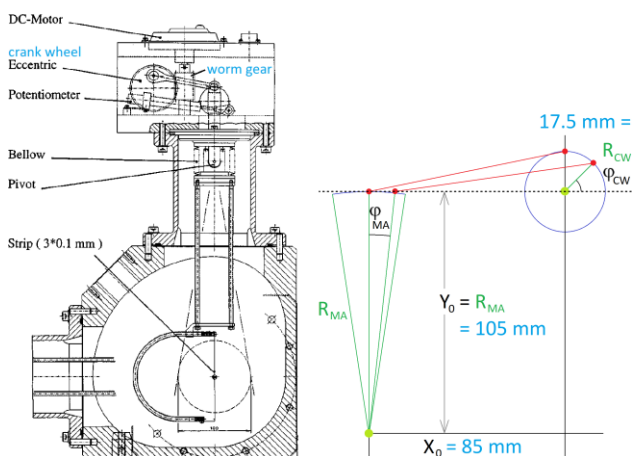


Figure 1: Present MA wire monitor. Wire crosses beam axis at $\phi_{CW} = 90^\circ$ and 270° . HS not shown. The monitor needs little space in beam direction. Horizontal and vertical MA are only 20 mm apart.

In the 0.87 MeV beam line and a few locations in the 72 MeV beam line, the power density at full proton beam current is too high to let the wire or foil survive at the given speed. Beam induced fluorescence monitors installed in 10 of 32 monitor locations in the 0.87 MeV line allow to

measure at full beam current of 10 mA, however, with limited dynamic range. Wire monitors with at least approximately four times higher speed could be an alternative. By using a stepper motor instead of the DC motor, the potentiometer can be eliminated, and the control of the movement is simplified.

In the following we simulate the movement of variants of the present mechanics driven by stepper motors and conclude to wire speed and error of wire position caused by the motor characteristics.

MECHANICS

With the present monitor, the inertia of the 20:1 worm gear and the DC motor is high. We look at three alternatives with stepper motor and the same dimensions of CW-CR-MA connection (Fig. 1, right):

1. Only motor replaced. Worm gear reduction 20:1. The range of unidirectional CW movement is $\phi_{CW} = 151.2^\circ$ to 568.8° . The long travel allows a softer acceleration. Wire speed 0.75 m/s unchanged.
2. Whole mechanics replaced by a moderately less-inertia variant (Fig. 2c). No potentiometer. Spur gear reduction 3:1. Range $\phi_{CW} = 151.2^\circ$ to 568.8° . Wire speed 4 m/s.
3. Ditto, but gear reduction 1:1 (direct drive, Fig. 2a) and Range $\phi_{CW} = 180^\circ$ to 540° .

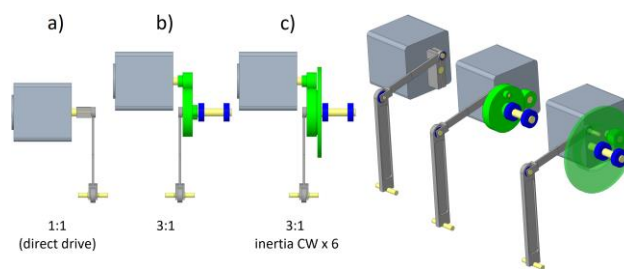


Figure 2: Lower-inertia setups (schematic).

In cases 2, 3, the wire position is determined by counting steps with respect to the HS switching positions. We assume a Baumer precision switch [3], pressed face on by the upper part of the MA. In order not to exceed the specification for the maximum approaching speed, the HS must be positioned not too far from the axis of rotation of the MA. Together with the play of the mechanism, this introduces a wire position error at beam axis of the order of 100 μm . Alternatively, the wire position can be determined by counting steps between the centres of the forward and backward measured beam profiles (if the beam has not shifted in between).

A brake is not needed. The MA is kept in the parking position against gravity by the CR, then in one line with the CW axis. Even the small holding torque of the currentless motor is sufficient for this.

[†] doelling@protonmail.com, rudolf.doelling@psi.ch

STUDY OF SINGLE WIRE SCANNER MONITOR FOR FETS-FFA TEST RING

E. Yamakawa*, D. W. Posthuma de Boer, S. Machida, A. Pertica, A. Letchford
 Rutherford Appleton Laboratory, Didcot, United Kingdom

Y. Ishi, T. Uesugi

Kyoto University Institute for Integrated Radiation and Nuclear Science, Osaka, Japan

Abstract

To confirm the use of Fixed Field Alternating gradient accelerator (FFA) as a high power pulsed neutron spallation source, a prototype called FETS-FFA is studied at Rutherford Laboratory (RAL). A single Wire Scanner Monitor (WSM) is planned to be used to measure beam position and beam profile in the ring. One of the concerns of this monitor is the thermal damage on the Carbon Nano Tube (CNT) wire due to high energy deposition of low energy proton beam in FETS-FFA (3–12 MeV). Furthermore, to measure a beam profile during beam acceleration in the ring, a diameter of CNT wire needs to be smaller than the orbit displacements in turns. To confirm whether a single WSM is suitable for FETS-FFA ring, two different beam tests were performed at RAL and at the Institute for Integrated Radiation and Nuclear Science, Kyoto University (KURNS). Both measurements demonstrated that the single WSM is applicable for FETS-FFA ring if the diameter of CNT is smaller than the orbit separation between two consecutive turns. In this paper, the detail of the design study of single WSM as well as the performance tests are presented.

INTRODUCTION

The ISIS-II project [1] is currently considering a 1.25 MW proton driver for a new pulsed spallation neutron source in Europe. A Fixed Field Alternating Gradient (FFA) ring [2, 3] is one option for the main ring of ISIS-II. In order to demonstrate that FFAs can provide the reliability required for user operations in ISIS-II, the small-scale Front End Test Stand and Fixed Field Alternating gradient (FETS-FFA) ring will be built by 2029. The baseline optics of the horizontal excursion FETS-FFA (hFFA) ring were recently finalised, and its main parameters are presented in Table 1.

Based on the planned commissioning scenario, a single WSM will be used to identify the beam profile and the beam position of the injected beam to optimize any injection mismatch with the design orbit and the Twiss parameters. Destructive monitors are extremely useful when a non-destructive monitor cannot detect the beam induced signal in the case of low intensity beam at the beginning of the beam commissioning. According to the measurement of the accelerating multi-turn beam profile in the FETS-FFA ring, the single WSM will be placed on the orbit of a certain beam energy. As the orbit radius changes with beam energy, a single stationary wire can measure the profile by intercepting the beam over several turns during an acceleration cycle.

* emi.yamakawa@stfc.ac.uk

Table 1: Parameters of 4-fold Symmetry FD-spiral FETS-FFA Ring in 2023

Parameter	Value
Beam energy range	3–12 MeV
Bunch intensity	3×10^{11} ppp
Repetition rate	100 Hz (50 pps)
Injection rate	50 Hz
RF frequency bandwidth	2–4 MHz
Harmonic number	2
Normalised Beam Core	10 π mm mrad
Beam Size	± 20 mm
Orbit Excursion	600 mm
Vertical Physical Acceptance	± 32 mm

As the beam energy changes during a profile measurement, adiabatic damping will cause the transverse beam size to reduce on each successive turn. Furthermore, beam loss due to scattering at the wire might distort the profile during a measurement. To investigate whether the monitor can measure the beam profile in the FETS-FFA ring, a feasibility study of the single WSM is performed in this paper. This will include the relationship between wire thickness and turn separation, as well as predictions for wire heating. Profile measurements made at the FETS Linac and KURNS hFFA ring will then be shown and used to inform conclusions.

FEASIBILITY STUDY

Carbon Nano Tube (CNT) [4–6] wires are used for the single WSM in the FETS-FFA ring owing to their high melting temperature (3000 °C) and high tensile strength (1 GPa).

Wire Thickness

For the case of profile measurement of an accelerating beam over several turns in the FETS-FFA, separation between subsequent transverse profile samples will be fixed by the change in orbit displacement, as illustrated in Fig. 1. This will depend on the RF program and is not expected to be constant throughout an acceleration cycle. To investigate the impact of wire thickness on the measured beam profile, a computer simulation was performed with the vertical excursion FFA (vFFA) lattice [7, 8]¹. In the simulation,

¹ The lattice design of the FETS-FFA ring (Table 1) was changed from the vFFA to the horizontal excursion FFA (hFFA) in 2022. The lattice design of hFFA is different from that of vFFA, however the orbit displacements and the RF program are similar

PERFORMANCE EVALUATION OF GAGG+ AND TUNGSTEN CARBIDE BLADES IN AN X-RAY PINHOLE CAMERA

S. Burholt*¹, L. Bobb, N. Vitoratou, Diamond Light Source, Didcot, UK

Abstract

At Diamond Light Source two X-ray pinhole cameras are used to measure the transverse profile of the 3 GeV electron beam. The current pinhole assembly is formed using tungsten blades with chemically etched shims to produce a 25 μm x 25 μm aperture and the imager incorporates a 0.2 mm LuAG:Ce scintillator. Tungsten carbide is a machinable high-Z material which at millimetre thicknesses is opaque to X-rays. With a slight change in pinhole design, similar to that already in place at the ESRF, tungsten carbide blades could offer a well-controlled aperture size for the pinhole camera with simpler assembly. Further to this, improvements to the photon yield of scintillators mean that the new scintillator GAGG+ has an almost two-fold increase in yield compared to the current LuAG:Ce scintillator. An evaluation of the tungsten carbide blades and GAGG+ scintillator is presented.

INTRODUCTION

X-ray pinhole cameras are important diagnostic systems used for beam emittance monitoring at synchrotron light sources. Diamond currently uses two X-ray pinhole cameras downstream of two different bending magnets to provide non-invasive transverse beam profile measurements. These two pinhole cameras are referred to as pinhole camera 1 (P1), and pinhole camera 2 (P2). A schematic layout can be seen in Fig. 1. There is another pinhole camera (P3) set up in a similar way to the other pinhole cameras where research and development projects are carried out.

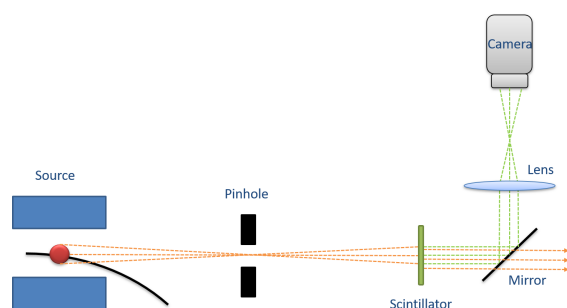


Figure 1: Diamond X-ray pinhole camera layout, including source, pinhole aperture, scintillator, mirror, lens, and camera.

The synchrotron radiation with an energy range of 15 keV to above 60 keV, with a peak around 26 keV, exits vacuum to air through a 1 mm aluminum window. The X-rays then pass through a tungsten pinhole assembly which is formed

of 25 μm x 25 μm apertures [1]. This X-ray beam then interacts with a 0.2 mm thick Lutetium aluminium garnet doped with cerium (LuAG:Ce) scintillator screen and is imaged by a CCD camera (Flea 2), allowing for beam profile measurement and fitting.

The 25 μm pinhole aperture is formed from stacks of 25 mm(h) x 1 mm(v) x 5 mm(d) tungsten blades separated by chemically etched shims of the required thickness [2, 3]. There is one stack vertically and one horizontally so that an aperture of 25 μm in both planes is presented to the X-ray beam. This also forms a 10 mm long tunnel, fully attenuating the beam outside of the aperture. A low flow of nitrogen gas is used to reduce metal oxide growth inside the pinhole assembly.

The spatial resolution of a pinhole camera system can be described by the point spread function (PSF). The PSF is assumed to be constant on relatively long timescales for a given system. For a pinhole camera imaging system the overall PSF may be represented as

$$\sigma_{PSF}^2 = \sigma_{pinhole}^2 + \sigma_{camera}^2 \quad (1)$$

with

$$\sigma_{pinhole}^2 = \sigma_{diffraction}^2 + \sigma_{aperture}^2 \quad (2)$$

and

$$\sigma_{camera}^2 = \sigma_{screen}^2 + \sigma_{lens}^2 + \sigma_{CCD}^2 \quad (3)$$

where the subscripts denote the sources of the PSF contributions [1]. It is well known that there are many contributions to the point spread function. A significant contribution arises from the pinhole aperture [1].

The pinhole aperture material must be opaque to X-rays. A tungsten blade and shim assembly is currently used due to the opacity of tungsten being a high-z material. Shims are required because tungsten is not readily machinable. Therefore the pinhole apertures must be formed using chemically etched shims between the tungsten blades. Due to this the absolute size of the pinhole aperture differs from the shim thickness and is thus unknown. A few factors can cause this discrepancy including; the deformation from cutting or handling the chemically etched shims, misalignment during assembly, and the pressure of the blade-shim-blade assembly. It is also not trivial to measure the pinhole aperture size due to the 5 mm depth of the tungsten blades and three-dimensional structure of the pinhole assembly.

In order to minimise the PSF contribution from the pinhole aperture it is necessary to be able to control the pinhole aperture size and ensure it is matched to the spectrum of the incident synchrotron radiation. Previously machined molybdenum blades were investigated as an alternative to the tungsten/shim design, however the 5 mm molybdenum

* sam.burholt@diamond.ac.uk

100 Hz X-RAY BEAM PROFILE MEASUREMENTS FROM A TRANSMISSIVE CVD DIAMOND DETECTOR

C. Bloomer*¹, L. Bobb, Diamond Light Source, Oxfordshire, UK
 M.E. Newton, University of Warwick, Coventry, UK
¹also at University of Warwick, Coventry, UK

Abstract

A non-destructive CVD diamond X-ray beam imaging monitor has been developed for synchrotron beamlines. The device can be permanently installed in the X-ray beam path and is capable of transmissively imaging the beam profile at 100 frames per second. The response of this transmissive detector at this imaging rate is compared to synchronously acquired images using a destructive fluorescent screen. It is shown that beam position, size, and intensity measurements can be obtained with minimal disturbance to the transmitted X-ray beam. This functionality is beneficial to synchrotron beamlines as it enables them to monitor the X-ray beam focal size and position in real-time, during user experiments. This is a key enabling technology that would enable live beam size feedback, keeping the beamline's focusing optics optimised at all times. Ground vibrations (10 Hz - 20 Hz) can cause movement of focusing optics and beamline mirrors, which disturb the X-ray beam and reduce the ultimate quality of the sample-point beam. This instrument can detect this beam motion, enabling the source to be more easily determined and mitigations to be put in place.

INTRODUCTION

Diamond detectors for synchrotron X-ray beamlines are advantageous for a number of reasons. Firstly, diamond is highly transparent to X-rays compared to other detector materials, which enables it to be installed permanently on the beamline in the beam path. Secondly, diamond has favourable thermal properties such high melting point and heat conduction, that enable it to withstand intense X-ray beams from synchrotrons and XFELs. Thirdly, the strong diamond lattice is both physically robust and resistant to mechanical damage, and it is radiation tolerant. Finally, and of particular use for this form of detector, the diamond structure can be modified by fast laser pulses, to 'write' laser conductive wires and electrodes within the bulk diamond [1]. The results presented in this contribution are from a pixellated single-crystal CVD diamond with laser written electrodes. The design of the 10 x 11 pixel detector and initial results from synchrotrons and XFELs are presented in Refs. [2-5], along with discussion of the advantages and disadvantages of diamond for this application.

To briefly summarise the design and operation of this prototype pixellated diamond detector, it builds upon a concept first presented in Ref. [6]. A pattern of 'strip electrodes' on one face of a diamond plate could be sequentially biased,

while the subsequent charge reaching a pattern of orthogonal electrodes on the opposite face of the diamond is read out using electrometers or other sensitive ammeters. Sequentially biasing the 'strip electrodes' enables one row of pixels to be read out at a time. The graphitic wire detector improves upon this design in two respects: firstly, through the use of laser-written graphitic electrodes which are buried under the surface of the diamond plate, protecting them from damage and resulting in a more physically robust detector; and secondly, through a novel lock-in modulated bias technique, illustrated in Fig. 1, whereby all 'bias' electrodes simultaneously have an AC bias applied to them at different frequencies using a programmable multi-channel DAC. The resulting signal currents from each 'measurement' electrode are simultaneously acquired using a multi-channel 20 kS/s acquisition system. A Fourier transform of the signal currents from each measurement electrode is carried out. The Fourier amplitude of the measured signal at a given frequency is proportional to the flux passing through the detector at the intersection between the measurement electrode and the bias electrode modulated by that frequency.

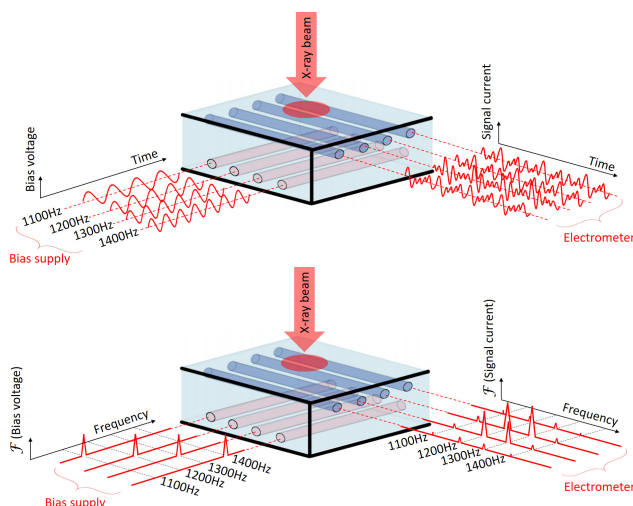


Figure 1: A sketch of the pixel readout scheme, utilising a different modulation frequency applied to each graphitic 'bias' electrode. Top: A time-domain view of the modulation scheme. Bottom: A frequency-domain view, showing how the individual modulation frequencies measured by the electrometer build up a picture of the X-ray beam profile.

* chris.bloomer@diamond.ac.uk

TARGET MULTIWIRE FOR THE FERMILAB BOOSTER NEUTRINO BEAMLINE

R. Prokop[†], Fermi National Accelerator Laboratory, Batavia, IL, USA

Abstract

The Booster Neutrino Beamline experiment requested a new secondary electron emission multiwire profile monitor installation. The device had to be durable in high radiation conditions and mounted within a large 10-foot airtight steel fixture for installation near the beam target. Previous iterations of multiwire suffered radiation damage to both the connectors and wires. To ensure accurate horizontal and vertical beam profile measurements, an updated design was proposed, designed, and constructed. The new BNB multiwire utilizes 3 mil diameter gold-plated tungsten sense wires soldered to vertical and horizontal Alumina-96 ceramic planes, 50 wires per plane. Radiation hard Kapton insulated 30-gauge wires carry the output signals. Profiles are readout through charge integrator scanner electronics. This paper will detail the design and functionality of the BNB target multiwire and present relevant beam profile data.

FUNCTION AND APPLICATION

The Booster Neutrino Beamline Multiwire for Horn 5 is a unique secondary emission monitor design at Fermilab utilized specifically for profile measurements of high intensity beam, up close to the experimental target [1]. This specialization calls for high durability and several modifications from the typical multiwire. The goal is to get clean gaussian profile measurements from small diameter wire, using wire/cable that can withstand high radiation environments. Previous iterations of this design used the classic multiwire flat Kapton ribbon cables with zero insertion force connectors glued to the ceramic frames. This is not ideal, as the intense environment of this device causes damage to the connectors. To remedy this problem, small gauge (30-40 AWG) Kapton insulated wire are individually cut to length and wrapped in bundles, soldered to both the frame and readout connectors. This presents many engineering challenges, but also opportunities to improve and craft a very durable and effective multiwire. This project has been a joint effort between the Fermilab Accelerator Directorate Instrumentation, External Beams & Target Systems groups.

The BNB multiwire operates on the principle of secondary electron emission, much the same as all other SEM profile monitors at Fermilab. The particle beam made up of protons strikes the sense wires and knocks off surface electrons from the metal material. This phenomenon leaves a resultant net positive charge on the wires which can be readout as a current through the signal cables. This current is integrated through transimpedance amplifiers in the front-end electronics and digitized as a voltage value to be plotted as a final beam profile measurement. The resultant

* This work was supported by the U.S. Department of Energy under contract DE-AC02-07CH11359

[†] rprokop@fnal.gov

signal is expected to be proportional to the amount of beam particles striking the wires [2].

Bias planes are comprised of titanium foils, and act to enhance the secondary emission effect by collecting stray electrons. The bias operates at +200 VDC.

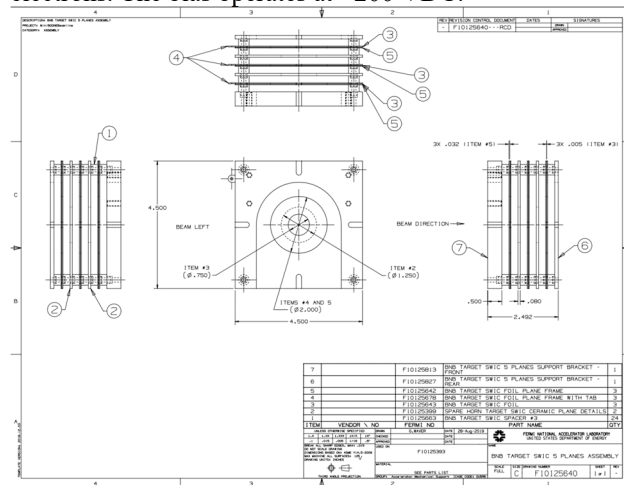


Figure 1: Multiwire assembly drawing.

DESIGN

The BNB Target multiwire is an open air mounted secondary emission monitor designed for the high intensity beam readout. The multiwire assembly as shown in Fig. 1, consists of two ceramic planes, one of vertical orientation and one horizontal. The ceramics are 4.5 x 4.5 inch with a center hole of diameter 1.25 inch. They have 50 pads at 1mm spacing for signal wires, and 100 pads at 0.5 mm spacing for sense wires across the center hole. There are three titanium foils of .005-inch thickness, which act as bias planes to assist in maintaining an electric field for charge deposition on the sense wires. The multiwire assembly is held together by front and back support brackets as well as spacers between the planes. The multiwire mounting assembly is slid into a larger horn mechanical enclosure for insertion close to the target. Discussion of the entire mechanical mounting assembly is beyond the scope of this document.

The signal carrying conductors are fashioned in a similar way to previous the MiniBooNE target multiwire, but without the zero insertion force connectors or Kapton ribbon cables. This new design instead utilizes 100 individual Kapton insulated wires of 0.25 mm diameter for the signal wires, terminated at one end at the pads of the ceramic and at two 50 pin D-Sub connectors on the other end. The use of connectors and epoxy was not ideal for this application, as in previous designs the epoxy wore down and connectors became damaged due to heat and radiation. 0.003-inch diameter AuW wires are soldered pad to pad for the center beam sense wires. AuW wires provide acceptable signal integrity through collected charge, as well as having excel-

Content from this work may be used under the terms of the CC-BY-4.0 licence (© 2023). Any distribution of this work must maintain attribution to the author(s), title of the work, publisher, and DOI

PROGRESS ON AN ELECTRON BEAM PROFILE MONITOR AT THE FERMILAB MAIN INJECTOR*

R. Thurman-Keup†, T. Folan, M. Mwaniki, S. Sas-Pawlik
Fermi National Accelerator Laboratory, Batavia, IL, USA

Abstract

The current program at Fermilab involves the construction of a new superconducting linear accelerator (LINAC) to replace the existing warm version. The new LINAC, together with other planned improvements, is in support of proton beam intensities in the Main Injector (MI) that will exceed 2 MW. Measuring the transverse profiles of these high intensity beams in a ring requires non-invasive techniques. The MI uses ionization profile monitors as its only profile system. An alternative technique involves measuring the deflection of a probe beam of electrons with a trajectory perpendicular to the proton beam. This type of device was installed in MI and initial studies of it have been previously presented. This paper will present the status and recent studies of the device utilizing different techniques.

INTRODUCTION

Measuring the transverse profile of circulating beam in a proton synchrotron is a challenging endeavor. Historically, thin wires were rapidly swept through the beam and downstream losses recorded as a function of the position of the wire to construct the profile. These were called flying wires [1]. In the Main Injector (MI) at Fermilab, they were removed around 2012 due to wire breakage which was not understood. Since it was already known that wires in the circulating beam might pose a problem at the even higher planned intensities, work had begun on building an electron beam profiler (EBP) to complement the ionization profile monitors that were already installed.

The concept of a probe beam of charged particles to determine a charge distribution has been around since at least the early 1970's [2-4]. Several conceptual and experimental devices have been associated with accelerators around the world [5-9]. An operational device is presently in the accumulator ring at the Spallation Neutron Source at Oak Ridge National Lab [10]. The EBP was constructed and installed in the Main Injector (MI) in 2014 and initial results have been presented previously [11]. This paper presents an update on the status of the EBP.

THEORY

The principle behind the EBP is electromagnetic deflection of the probe beam by the target beam under study (Fig. 1). If one assumes a target beam with $\gamma \gg 1$, no magnetic field, and $\rho \neq f(z)$, then the force on a probe particle is [12]

$$\vec{F}(\vec{r}) \propto \int d^2\vec{r}' \rho(\vec{r}') \frac{(\vec{r} - \vec{r}')}{|\vec{r} - \vec{r}'|^2} \quad (1)$$

and the change in momentum is

$$\Delta\vec{p} = \int_{-\infty}^{\infty} dt \vec{F}(\vec{r}(t)) \quad (2).$$

For small deflections, $\vec{r} \approx \{b, vt\}$, and the change in momentum is

$$\Delta\vec{p} \propto \int_{-\infty}^{\infty} dx' \int_{-\infty}^{\infty} dy' \rho(x', y') \cdot \int_{-\infty}^{\infty} dt \frac{\{b - x', vt - y'\}}{(b - x')^2 + (vt - y')^2} \quad (3)$$

where $\{\}$ indicates a vector. For small deflections, $\vec{p} \approx \{0, p\}$ and the deflection is $\theta \approx \frac{|\Delta\vec{p}|}{|p|}$. The integral over time can be written as $\text{sgn}(b - x')$ leading to an equation for the deflection

$$\theta(b) \propto \int_{-\infty}^{\infty} dx' \int_{-\infty}^{\infty} dy' \rho(x', y') \text{sgn}(b - x'), \quad (4)$$

where $\text{sgn}(x) = -1$ for $x < 0$ and $+1$ for $x \geq 0$.

If one takes the derivative of $\theta(b)$ with respect to b , the sgn function becomes $\delta(b - x')$ leading to

$$\frac{d\theta(b)}{db} \propto \int_{-\infty}^{\infty} dy' \rho(b, y') \quad (5)$$

which is the profile of the charge distribution of the beam. Thus, for a Gaussian beam, this would be a gaussian distribution and the original deflection angle would be the error function, $\text{erf}(b)$.

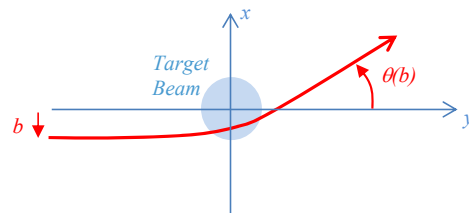


Figure 1: Probe beam deflection (red) for some impact parameter b .

EXPERIMENTAL TECHNIQUE

To obtain $\theta(b)$, one needs to measure the deflection for a range of impact parameters. This can be accomplished by stepping the electron beam through the protons and recording the deflection at each step, or by rapidly sweeping the electron beam through the proton beam (Fig. 2). The latter works without issue provided the sweep time is much smaller than the rms bunch length of the proton beam to

* This manuscript has been authored by Fermi Research Alliance, LLC under Contract No. DE-AC02-07CH11359 with the U.S. Department of Energy, Office of Science, Office of High Energy Physics.
† keup@fnal.gov

A SIMULATION OF THE PHOTOIONIZATION OF H- TOGETHER WITH THE SUBSEQUENT TRACKING OF THE LIBERATED ELECTRONS*

R. Thurman-Keup[†], M. El Baz, V. Scarpine
Fermi National Accelerator Laboratory, Batavia, USA

Abstract

The Proton Improvement Plan - II (PIP-II) is a new linear accelerator (LINAC) complex being built at Fermilab. It is based on superconducting radiofrequency cavities and will accelerate H⁻ ions to 800 MeV kinetic energy before injection into the existing Booster ring. Measurements of the profile of the beam along the LINAC must be done by non-intercepting methods due to the superconducting cavities. The method chosen is photoionization of a small number of H⁻ by a focused infrared laser, aka laserwire. The number of ionized electrons is measured as a function of laser position within the H⁻ beam. To aid in the design of the collection mechanism, a simulation was written in MATLAB with input from the commercial electromagnetic simulation, CST. This simulation calculates the number and positions of the liberated electrons and tracks them through the magnetic collection and H⁻ beam fields to the collection point. Results from this simulation for various points along the LINAC will be shown.

INTRODUCTION

Fermilab is in the process of constructing a new superconducting (SC) linear accelerator to replace the existing normal conducting LINAC. This project is called the Proton Improvement Plan - II (PIP-II) [1] and is being built to increase the deliverable beam intensity to the Deep Underground Neutrino Experiment being constructed in South Dakota. Since the LINAC is mostly superconducting, the use of physical wire scanners as beam profilers is not allowed in much of the LINAC due to the risk of a broken wire contaminating the SC cavities. As the beam is composed of H⁻ ions, laserwires [2, 3] were chosen as the profiler. A laserwire functions by photoionization of the extra electron on the H⁻ ion using a focused laser. The binding energy of the extra electron is only 0.7542 eV and can be ionized by a 1064 nm YAG laser. The ionized electrons, which are proportional in number to the local density of H⁻ ions, are collected as the laser is moved through the H⁻ beam, enabling reconstruction of the profile of the beam. Due to the complexity of the system, a simulation was developed to aid in the planning of the laser optics and the electron collection and is presented in this paper.

EXPERIMENTAL DEVICE

The laserwire system for PIP-II is comprised of a source laser that is transported through a pipe from the laser room to the H⁻ beamline (Fig. 1). The pipe is under vacuum to

both reduce distortions from air currents and to serve as a safety interlock system. At each measurement location (station), there is an insertable mirror to direct the laser down to the beamline.

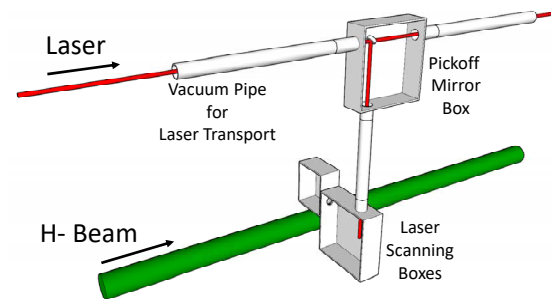


Figure 1: Diagram of laser transport. The laser originates in the laser room and is transported through a vacuum line to the end of the LINAC. At each laserwire, a vertical pipe can direct the laser to the H⁻ beamline.

The optical system at the beamline is comprised of movable stages to scan the laser across the H⁻ beam and to select vertical or horizontal scan mode (Fig. 2).

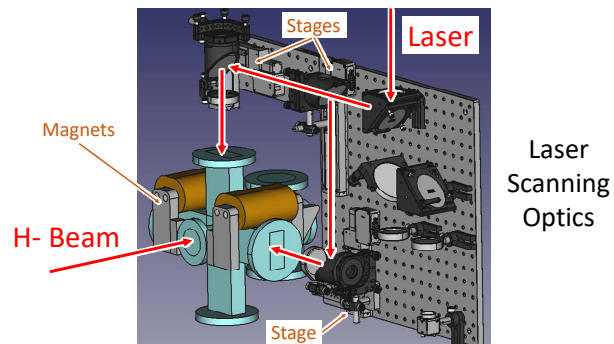


Figure 2: Optics inside the laser scanning box. There are linear stages to pick horizontal or vertical scan, and to do the scans.

There are 12 beamline stations with the locations and beam parameters summarized in Table 1 (plus an additional emittance measuring one after the LINAC). The laserwires are installed just downstream of the location column entry which specifies the cryomodule section and the cryomodule number within that section. The optics within the beamline stations focus the laser from a large incoming rms size of ~ 5 mm to a focused rms size of < 100 μm . The focusing distance will be approximately 300 mm. Once the laser has ionized the H⁻ beam, the electrons are bent vertically upward to a detector which will nominally be a faraday cup (Fig. 3).

* This manuscript has been authored by Fermi Research Alliance, LLC under Contract No. DE-AC02-07CH11359 with the U.S. Department of Energy, Office of Science, Office of High Energy Physics.

[†] keup@fnal.gov

A STUDY OF THE GAIN OF MICROCHANNEL PLATES IN THE IONIZATION PROFILE MONITORS AT FERMILAB*

R. Thurman-Keup†, D. Slimmer, C. Lundberg, J.R. Zigel
 Fermi National Accelerator Laboratory, Batavia, USA

Abstract

One of the on-going issues with the use of microchannel plates (MCP) in the ionization profile monitors (IPM) at Fermilab is the significant decrease in gain over time. There are several possible issues that can cause this. Historically, the assumption has been that this is aging, where the secondary emission yield (SEY) of the pore surface changes after some amount of extracted charge. Recent literature searches have brought to light the possibility that this is an initial ‘scrubbing’ effect whereby adsorbed gasses are removed from the MCP pores by the removal of charge from the MCP. This paper discusses the results of studies conducted on the IPMs in the Main Injector at Fermilab.

INTRODUCTION

Ionization profile monitors (IPM) are used in many accelerator laboratories around the world [1-7]. They have been used in nearly all the synchrotrons built at Fermilab, and presently are used in the Main Injector (MI), Recycler Ring (RR), and Booster synchrotron [8], with another one being planned for the Integral Optics Test Accelerator (IOTA). All Fermilab IPMs, as well as many of those at other laboratories, utilize one or more microchannel plates (MCP) for signal amplification. Historically we have found that the gain of the MCP decreases over time (Fig. 1) and have attributed it to the well-known fact that they age with current extracted from them [9]. Thus, we have periodically replaced them.

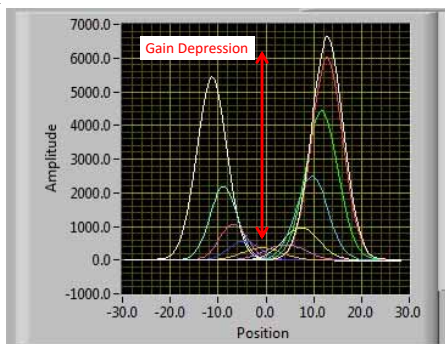


Figure 1: Scan of MCP plate across beam showing gain depression where beam is normally positioned.

Recently, more in-depth investigations have revealed that the decrease in the gain is much more consistent with conditioning, or ‘scrubbing’, of the MCPs, and not aging. Literature searches have rediscovered the fact that a decrease in gain with conditioning is a known property of

* This manuscript has been authored by Fermi Research Alliance, LLC under Contract No. DE-AC02-07CH11359 with the U.S. Department of Energy, Office of Science, Office of High Energy Physics.
 † keup@fnal.gov

MCPs [10,11]. Our own historical IPM data and a recent dedicated test show results which are much more consistent with what one expects from conditioning. In this paper, we summarize our current understanding of the behavior of the MCPs in our IPMs.

EXPERIMENTAL DEVICE

IPMs are devices which utilize the ionization of residual gas to measure the transverse profile of the beam. Figure 2 is a diagram of the present Fermilab IPMs. When the beam passes through the IPM, it ionizes the residual gas. The IPM collects the ionization products using an electrostatic field to accelerate them to the MCP.

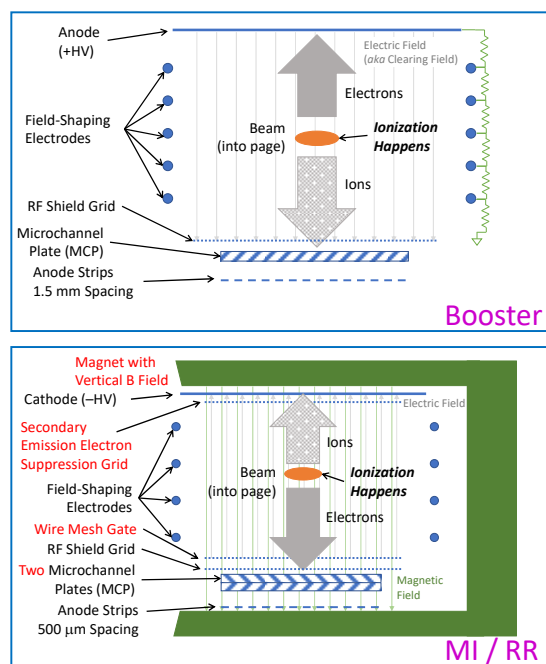


Figure 2: Diagrams of Booster and MI/RR IPMs.

The MCP is a thin plate with microscopic holes (aka pores) through it, each of which acts as a charge multiplier, much like a photomultiplier tube (PMT) (Fig. 3) [12,13].

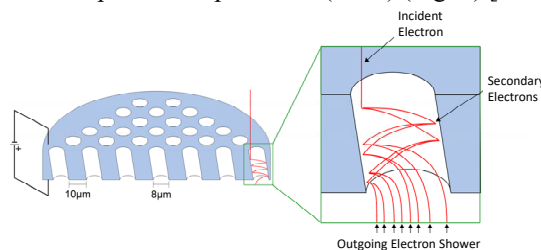


Figure 3: Schematic of MCP functional behavior showing amplification by electron avalanche.

STATUS OF GAS SHEET MONITOR FOR PROFILE MEASUREMENTS AT FRIB*

A. Lokey†, S. Lidia

Facility for Rare Isotope Beams, Michigan State University, East Lansing, MI, USA

Abstract

We report on the status of work on a non-invasive profile monitor under development for use at the Facility for Rare Isotope Beams (FRIB), a heavy-ion LINAC which produces high-intensity, multi-charge state beams. The measurement will be made by collecting photons generated at the interaction point of the beam and a collimated molecular gas curtain. These photons will be collected with an intensified camera system, generating a two-dimensional image and allowing for measurements of profile, beam halo, and other properties more prevalent at specific locations of interest, such as charge state spread after folding segment bends. Included will be ongoing design specifications, simulation results, and discussion of measurement techniques for acquiring signal from the device.

INTRODUCTION

A non-invasive profile measurement device using nitrogen gas fluorescence is in development for use in the Facility for Rare Isotope Beams (FRIB), a high-intensity heavy ion facility which can provide beams of a variety of different ion species and charge states.

By using a non-interceptive method, it is possible to sample the state of the beam during operation, providing information about the spread of the charge states at points of interest, such as after bending magnets in the folding LINAC sections of FRIB. This method also allows the state of the beam to be measured in both transverse directions at once [1].

One way to accomplish this is by creating an ultra-thin, rarefied gas curtain and collecting the photons released in the interaction between the beam and the working gas. This is known as beam-induced fluorescence (BIF) and has the advantage of being a simpler system design than similar ionization-based monitors, which require an electrode to sweep the electrons or ions into the detector and a magnet to steer them to the correct location to be collected. Additionally, BIF monitors have greater time resolution, since the time for the interaction particles to travel to the detector is negligible [2]. By introducing only a small amount of gas to the system, both pumping requirements and interaction effects like scattering and charge stripping are reduced [3].

Assuming the gas sheet is uniform and thin, photons collected can then be correlated to the profile of the beam with some degree of accuracy. This technique has been used successfully with protons and lighter ions at other facilities [1,3-5].

* This material is based upon work supported by the U.S Department of Energy, Office of Science, Office of Nuclear Physics and used resources of the Facility for Rare Isotope Beams (FRIB), which is a DOE Office of Science User Facility, under Award Number DE-SC0000661

† lokey@frib.msu.edu

SYSTEM OVERVIEW AND REQUIREMENTS

The beamline device is divided into three sections: (i) the gas generating chamber; (ii) the main interaction chamber; and (iii) the optics system. Within the gas generating section, nitrogen gas is pumped into a reservoir which feeds into a thin rectangular cavity. Molecules of nitrogen are emitted from a slit at the front of the cavity and are further collimated into sheet by a slit placed between the generating and main chambers as shown in Figure 1.

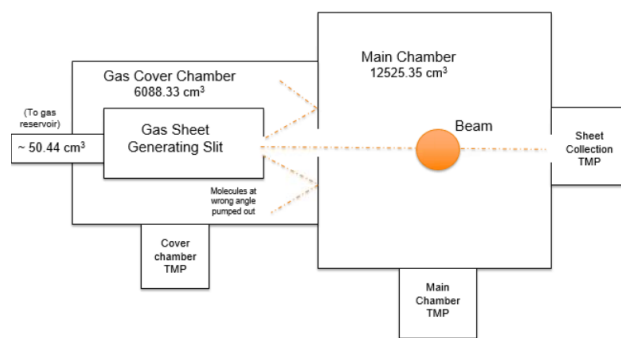


Figure 1: Overview of device layout.

Considerations

Although rarefied, gas generated from the monitor will require significant pumping to prevent contamination and protect the rest of the high vacuum system and this must be accounted for in appropriately sizing of the pumps.

For the measurement to correlate with the beam profile, the sheet must be thin and uniform, positioned at a 45-degree angle to the incident beam with the detector perpendicular to the point of interaction. Careful alignment must be performed to ensure that the angle of interaction is correct [6].

Signals generated by the interaction will be of relatively low intensity. The fluorescence interaction generates a small signal compared to ionization monitors due to fluorescence cross sections being lower than ionization cross sections. To assist with collection and reduce scattering from reflection, the interior of the main chamber will be blackened and an intensified camera array will be used to amplify the incoming signal. Light is gathered by the camera system at a small solid angle, and relatively few photons, are released in the interaction. For example, using a residual-type BIF, Tsang et al. noted a production of 7 photons per 3×10^8 ion Uranium bunch with hydrogen as the working gas [7]. Photon production is expected to be higher with use of a collimated sheet, as well as nitrogen as the working gas since it has a greater fluorescence cross

LANSCE HIGH DENSITY EMITTANCE INSTRUMENTATION SYSTEM*

L. Montoya†, S. Baily, S. Johnson, H. Leffler, H. Watkins, D. Zimmermann
 Los Alamos National Laboratory, Los Alamos, NM, USA

Abstract

The Los Alamos Neutron Science Center (LANSCE) is currently upgrading the existing emittance stations with a high-density instrumentation system for emittance measurements in the low energy beam transport region. Emittance measurements were obtained using obsolete legacy equipment. For motion control a switching station with a mechanical mux to switch actuators was used. This caused a single point of failure for all emittance stations and is becoming increasingly unreliable. For data acquisition, two sets of signal conditioning and digitizers were employed and had to be shared between 7 emittance stations. Physical cable swapping was necessary when taking measurements from station to station. A system was developed using dedicated Quad Actuator Controller (QAC) chassis, capable of driving four (4) actuators, and dedicated data acquisition (DAQ) chassis capable of signal conditioning and digitizing up to 80 channels simultaneously. Details of the system development are presented.

INTRODUCTION

Emittance diagnostics have long been operating using aging instrumentation with limited spares available with the need to be upgraded with modern electronics to avoid obsolescence and increase reliability of measurements.

The emittance instrumentation upgrade aims to extend the lifetime and capability of beam diagnostic equipment by replacing antiquated systems that are now in obsolescence with modern equipment and to improve operational efficiency and performance with the ability to automate previously labor-intensive tasks to initialize measurements on the legacy system. The reliability of the equipment would be greatly improved as the National Instruments (NI) compact Reconfigurable Input/Output (cRIO) controllers are inherently more robust than the legacy equipment and reduces the amount of potential failure and is more easily maintained as components in each chassis are readily available off the shelf.

SYSTEM LOCATION AND OVERVIEW

Locations

There are 11 emittance stations in the H- dome, Low Energy Beam Transport (LEBT), and Transition Region (TR) which corresponds to 44 unique devices associated with the upgrade. Locations upgraded during the 2023 outage are shown in green, and planned upgrades to be completed during the 2024 outage are shown in yellow in Fig. 1.

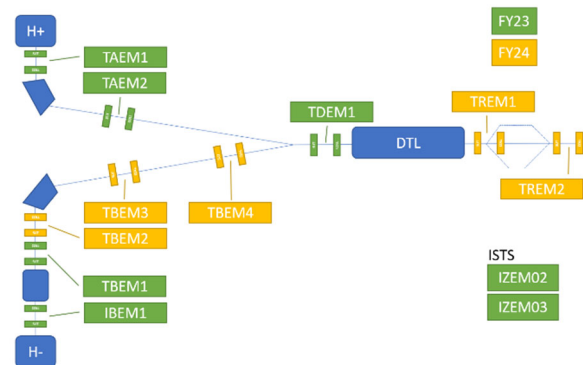


Figure 1: Emittance location map.

System Overview

Emittance stations are beam interceptive devices, thus are comprised of actuators in both horizontal and vertical axes with sensor payloads at the head of each device. Emittance measurements provide necessary information to tune the beam by providing beam parameters such as beam position, shape, angle, and intensity in both transverse and longitudinal planes through the beam pulse.

CONTROLLER HARDWARE

Using recently developed Quad Actuator Controllers (QAC) and Data Acquisition (DAQ) instrumentation chassis, the existing system is to be completely replaced and condensed with increased density of electronics [1]. The hardware diagram of the emittance system is shown on Fig. 2.

The QAC chassis will provide actuator control for a single emittance station, driving vertical and horizontal slits and collectors. In doing so, the legacy actuator switching station will be retired, removing it as a single point of failure in the system. Each emittance station was deployed a dedicated DAQ chassis removing the need to rely on the Sample and Hold chassis and shared digitizers used for all emittance measurements [2]. Both horizontal and vertical collectors in the emittance station are wired in parallel such that excitation of one axis can be read at a time and allow for a single 80 channel DAQ to read in 76 sensor inputs from the collector.

* This work was supported by the U.S. Department of Energy through the Los Alamos National Laboratory. Los Alamos National Laboratory is operated by Triad National Security, LLC, for the National Nuclear Security Administration of U.S. Department of Energy (Contract No. 89233218CNA000001).

† lucasm@lanl.gov. LA-UR-23-30153

LANSCE QAC/DAQ WIRE SCANNER INSTRUMENTATION UPGRADE*

L. Montoya†, S. Johnson, H. Watkins, D. Zimmermann
 Los Alamos National Laboratory, Los Alamos, NM, USA

Abstract

High density instrumentation has been developed to upgrade wire scanner beam diagnostic capability in all areas downstream of the Coupled Cavity (CCL) LINAC (Linear Accelerator). Transverse beam profile measurements were originally obtained using legacy electronics known as Computer Automated Measurement and Control (CAMAC) crates. CAMAC has become obsolete, and a new wire scanner diagnostic system was developed as a replacement. With high wire scanner device density located in each area, instrumentation was developed to meet that need along with the ability to interface with legacy open-loop controlled actuators and be forward compatible with upgraded closed-loop systems. A high-density system was developed using a Quad Actuator Controller (QAC) and Data Acquisition (DAQ) chassis that pair together using a sequencer when taking measurements. Software improvements were also made, allowing for full waveform functionality that was previously unavailable. Deployment of 52 wire scanner locations in 2022 increased device availability and functionality across the facility. Hardware and software design details along with results from accelerator beam measurements are presented.

INTRODUCTION

Legacy diagnostic instrumentation used at the Los Alamos Neutron Science Center (LANSCE) have become obsolete with no readily available spares for CAMAC systems. Because of the density of devices downstream of the CCL a high-density solution was needed.

A new wire scanner instrumentation system has been developed and implemented by the LANSCE controls hardware team to replace CAMAC and interface with legacy devices. Software was developed to interface the old devices with the new hardware, primarily the embedded and client software.

SYSTEM OVERVIEW

Wire scanners are electro-mechanical beam interceptive devices that provide cross-sectional beam profile measurements that describe beam shape and position. A wire scanner system consists of an actuator to drive the sense wires across the beam, and data acquisition to obtain the waveform data from the current induced by the proton beam impinging on the wire. The wire scanner hardware architecture diagram is shown in Fig. 1.

* This work was supported by the U.S. Department of Energy through the Los Alamos National Laboratory. Los Alamos National Laboratory is operated by Triad National Security, LLC, for the National Nuclear Security Administration of U.S. Department of Energy (Contract No. 89233218CNA000001).

† lucasm@lanl.gov. LA-UR-23-30151

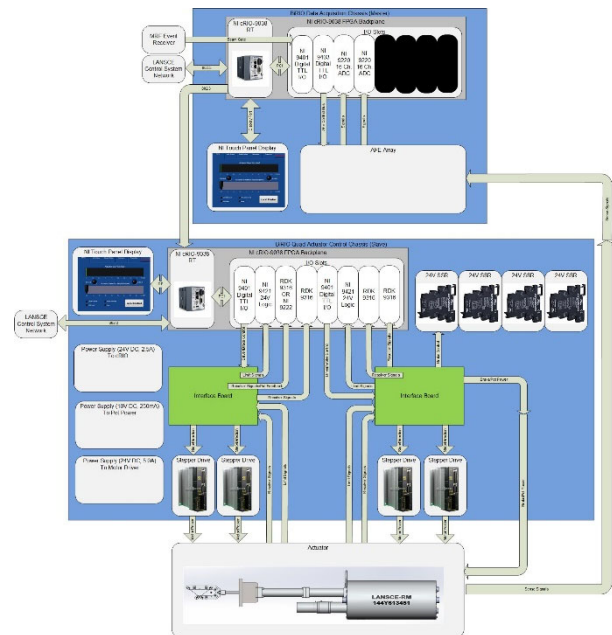


Figure 1: Wire scanner hardware diagram.

CONTROLLER HARDWARE

The electronic hardware consists primarily of two separate chassis, each controlled using a National Instruments (NI) 9038 compact Reconfigurable Input/Output (cRIO) packaged in 4U rack mountable enclosures configured as input output controllers (IOC). The QAC chassis controls the wire scanner actuators, and the DAQ chassis is used for data acquisition from the beam induced current on the wire.

Quad Actuator Controller

The QAC chassis was designed to control up to four stepper motor actuators, two actuators simultaneous. The chassis is compatible with both open loop and closed loop motion control to be forward compatible with potential actuator upgrades to resolver position closed loop control as was done on the LANSCE risk mitigation project [1].

Within the cRIO controller on the QAC is housed NI I/O modules, and serve as the interface between the wire scanner actuator and the cRIO and perform the functions as follows:

- NI 9401 digital I/O for stepper motor and brake control
- NI 9421 sinking digital input for limit switch indication
- NI 9222 voltage input potentiometer position feedback, for open loop control
- RDK 9316 resolver to digital converter, for closed loop only

FIRST RESULTS FOR A 50 MeV BEAM INDUCED FLUORESCENCE MONITOR FOR BEAM PROFILE MEASUREMENTS

G. Rosenthal, J.I. Anderson, A. Cao, E. Cramer, T. Gordon, K. Kuhn, O. Vazquez, J. Lopez S. Lynam, J. Ringuette, L. Szeto, J. Zhou, Nusano, Salt Lake City, UT, USA
E. Dorman, R. Emery, B. Smith, University of Washington Medical Center, Seattle, WA, USA

Abstract

Nusano is developing a 50 MeV alpha ($^4\text{He}^{++}$) particle accelerator (The Nusano accelerator can also accelerate $^2\text{H}^+$, $^3\text{He}^{++}$, $^6\text{Li}^{3+}$, $^7\text{Li}^{3+}$, and a few other heavier ions), primarily to produce medical radionuclides. The accelerator produces an average current of 3 mA_e with 20 mA_e average macro pulse current. This results in an average beam power of 75 kW, and an average beam power within the macro pulse of 500 kW. The beam profile at the exit of the DTL is approximately Gaussian with a radius (FWHM) of about 3 mm. Designing diagnostics for this beam is challenging, as diagnostics that intercept beam will receive a very high heat load. A BIFM (Beam Induced Fluorescence Monitor) is being developed to measure beam profiles. Nitrogen gas is leaked into the beamline. Excitation of the nitrogen by beam particles is captured using an image intensifier. The signal generated is directly proportional to the beam current. A prototype system has been constructed and tested on a lower intensity alpha beam. First results indicate we can measure beam profile to a 100 μm accuracy. Production system is currently being designed.

EXPERIMENTAL SYSTEM

The 50 MeV alpha particle accelerator Nusano is developing will be commissioned in 2025. The 47.3 MeV at the University of Washington Medical Cyclotron Facility was used as a test facility to evaluate the BIFM (Beam Induced Fluorescence Monitor) intended to be installed on the beamline. The cyclotron provides 20-40 μA_e alpha beam, which is a good model for the Nusano beam.

The experimental apparatus is shown in Figure 1, consists of a vacuum chamber that the beam passes through. In the chamber the beam particles interact with nitrogen leaked into the chamber and photons are generated by decay in excited nitrogen. The light exits the chamber through a window and is directed by lenses and mirrors into an image intensified camera (Photonis iNocturn HI-QE Blue). Since the light emitted is directly proportional to the density of nitrogen and the beam current, by analyzing the images generated the beam distribution can be measured. A calibrated PMT is also provided to measure light intensity received by the camera.

Control of the nitrogen pressure is critical to correct operation of the BIFM. The experimental system allowed for both pulse and CW nitrogen flow, but the data presented here is entirely based on CW flow. One of the key goals of the project was to determine the ideal nitrogen pressure for the system. The system also includes vacuum chokes that allow the pressure in the measurement chamber to be about

an order of magnitude higher than the pressure in the surrounding vacuum system.

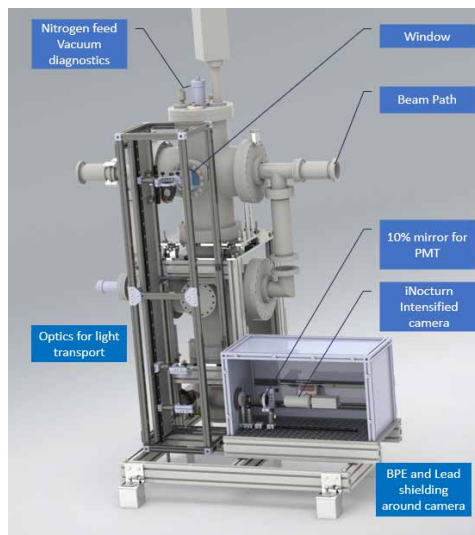


Figure 1: CAD drawing of experimental system.

RESULTS

A basic raw data image is shown in Figure 2. The beam is the horizontal strip shown in the blue outline. The crescent shape, and the three dots (red outline), are compound reflections of light generated by ionization of background gas in the cold cathode pressure gauge.

In order to understand the resolution of the BIFM a picture was taken with a test pattern located at the beam position. Combining this with the data averaged across the beam part of the image indicates a spatial resolution on the order of 100 μm (see Figure 3).



Figure 2: Basic image show the beam induced fluorescence (show in the blue box). The crescent shape, and the three dots (red box), are a compound reflection from the cold cathode pressure gauge.

IMAGE ACQUISITION SYSTEM FOR THE INJECTION DUMP AT THE SPALLATION NEUTRON SOURCE*

W. Blokland[†], N. Evans, A. Oguz, and D. Willis
 Oak Ridge National Laboratory, Oak Ridge, TN, USA

Abstract

We describe the Image Acquisition system for the Injection Dump. This system visualizes the different beamlets, on the vacuum window after the H⁻ beam is stripped of its electrons by two stripper foils. One beamlet is from H⁻ with its electrons stripped by the first foil and the second beamlet has its final electron stripped by the second foil. We used the PXI platform to implement the data-acquisition including timing decoder. We describe the hardware and software for the system. We use a standard non-radhard GigE camera to acquire the image from the luminescent coating on the dump vacuum window. To lower the radiation damage to the camera, we shield it with stainless steel blocks. We present radiation measurements before and after shielding. We also show the radiation damage over time to estimate the camera's lifetime.

INTRODUCTION

The Ring Injection Dump (RID) needs diagnostics to properly steer two waste beam species, leftover from the charge exchanging injection scheme, to the dump. The Proton Power Upgrade (PPU) upgrades the magnets in the injection region and confirmation is needed of the new trajectories.

The two waste species are referred to as “H⁰ beam” (partially stripped H⁻ beam) and “H⁻ beam” (the beam that misses the primary foil) see Fig. 1. The width of the beam is up to 20 cm with vertical size slightly smaller. Both species end up as H⁺ after passing through a secondary stripping foil.

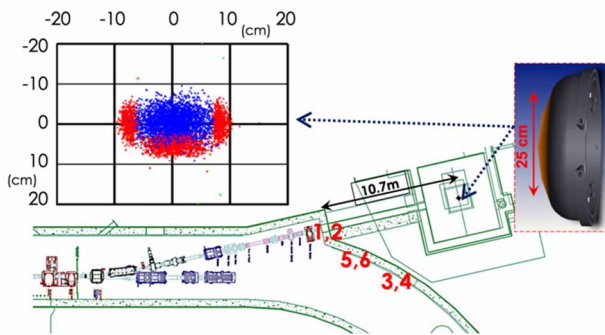


Figure 1: The Ring Injection Dump line along with the calculated projection of beam particles on dump window.

To visualize the waste species on the injection dump window, it has been coated with a luminescent coating made of Al₂O₃:Cr, similar to the SNS target. An optical

system transfers the light to a camera, see Ref. [1]. The requirements include an absolute position accuracy of 10 mm, both horizontal and vertical, and to survive an 16-hour study period to confirm the particles' trajectories. The intention was to install the window with the coating right before the measurement but changes in schedule resulted in installing the coating window but not the optical system. Hence no results with actual beam will be presented in this paper. The coating luminescence will have been reduced due to radiation damage while running beam without the having an optical system but experience with the SNS target coatings indicates that enough luminescence remains to perform the required measurements once the optical system has been installed. The optics are described in Ref. [1].

CAMERA SETUP

The system is based on non-radhard GigE cameras because radhard cameras are expensive or do not have the right features. To use non-radhard cameras we tested the radiation doses during full power beam conditions at different locations, see also Ref. [2]. The results are repeated in Table 1. The odd locations are at ground level and the even locations at about 1.5 m (above the beam plane). Location ES (Electron Scanner) is in a straight section of the ring and is listed as a control reference. Cameras in those locations easily survive multiple years of beam runtime (5000 Hrs/year). We used CERN HiRadMat results from Ref. [3] to convert from dose to Time-to-Death and Time-to-Significant-Event (crash). The calculation confirms that cameras at the ES location can survive for a long time. The results in the table show that locations further from the injection dump beamline have lower doses. However, locations 1 and 2 simplify the optical system and location 1 allows for the system to be installed on the floor. Unfortunately, this location has the highest dose rates, thus we will use shielding to reduce the dose.

Table 1: Camera Locations, Doses, and Expected Time to Death and Significant Event (SE) at 1.4 MW Beam Power

Location	Total (Gy/MW hr)	Time to Death (Hrs)	Time to SE (Hrs)
1	0.29	285	0.91
2	0.24	339	1.09
3	0.04	2246	7.20
4	0.05	1797	5.76
5	0.08	998	3.20
6	0.08	998	3.20
ES	0.0032	25674	82.29

* SNS is managed by UT-Battelle, LLC, under contract DE-AC05-00OR22725 for the U.S. Department of Energy

[†] blokland@ornl.gov

A Schottky Tune Meter for the Fermilab Mu2E Delivery Ring*

V. Scarpine[†], B. Fellenz, A. Semenov, D. Slimmer
 Fermi National Accelerator Laboratory, Batavia, IL, USA

Abstract

The Mu2E experiment will measure the ratio of the rate of the neutrinoless, coherent conversion of muons into electrons as a measure of Charged Lepton Flavor Violation. As part of the Mu2E experiment, a proton storage ring, called the Delivery Ring, will utilize resonant extraction to slow-spill protons to the experiment. To regulate and optimize the Delivery Ring resonant extraction process, a fast tune measurement scheme will be required. This Mu2E tune meter will measure the average tune and the tune spectrum, in multiple time slices, through the entire resonant extraction cycle of nominally 43 msec. The Mu2E tune meter system utilizes vertical and horizontal 21.4 MHz Schottky detector resonant pickups, taken from the decommissioned Tevatron, high-gain amplifiers and digital down-conversion FPGA logic for its signal processing. This paper will present the design of this Schottky tune meter as well as tune measurements from the Mu2E delivery ring.

MU2E SLOW SPILL

The Mu2E experiment will search for the charged-lepton flavor violating process $\mu^- N \rightarrow e^- N$ [1]. Mu2E proposes to measure the ratio of the rate of the neutrino-less, coherent conversion of muons into electrons in the field of a nucleus, relative to the rate of ordinary muon capture on the nucleus. This requires the resonant extraction of a stream of pulsed beam, comprised of short micro-bunches (pulses) from the Delivery Ring (DR) to the Mu2e target [2].

Mu2e uses 8 kW of 8 GeV protons extracted from the Fermilab Booster. Figure 1 show a table of key DR beam parameters. Once $1e12$ protons are injected into the DR, beam is then slow extracted to the Muon proton target at the DR revolution frequency of 590.08 kHz over a nominally 43 ms spill period. Between each spill period, there is 5 ms reset period, in which there is no extraction. After the 8th spill, there is no beam in DR for 1.02 s. Figure 2 shows the Mu2E DR intensity timeline for eight slow spills.

By exciting two families of the harmonic sextupoles in the DR, the third integer slow-spill resonant extraction condition is established [3]. Figure 3 shows the modelled change in the DR tune along a single slow spill along with expected data points from this tune meter system.

MU2E TUNE METER SYSTEM

The Mu2E tune meter system, shown in figure 4, consists of 21.4 MHz inductively resonated stripline pickups,

low noise RF amplifiers, bandpass filters and a high-speed FPGA-based DAQ board.

Parameter	Value	Units
MI Cycle time	1.333	sec
Number of spills per MI cycle	8	
Duration of each spill	34-54	msec
Number of protons per micro-pulse	$(3.0-5.0) \times 10^7$	protons
Maximum DR Beam Intensity	1.0×10^{12}	protons
Reset Time Gap between spills	5	msec
Operation point (Qx/Qy)	9.650/9.735	
DR revolution frequency	590.018	kHz

Figure 1: Mu2E delivery ring beam parameters.

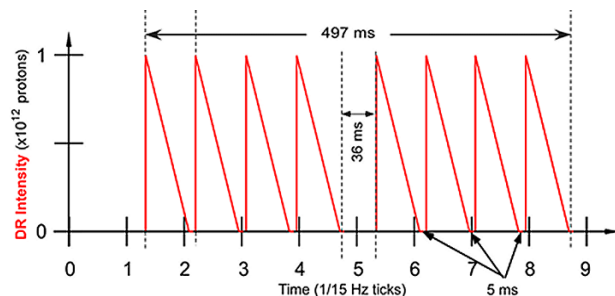


Figure 2: Mu2E slow spill beam timeline.

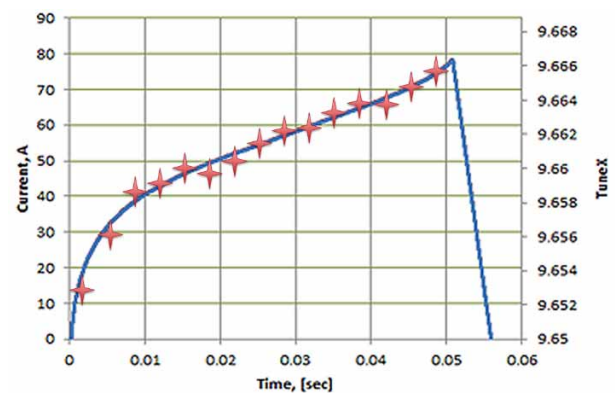


Figure 3: Expected tune along slow spill.

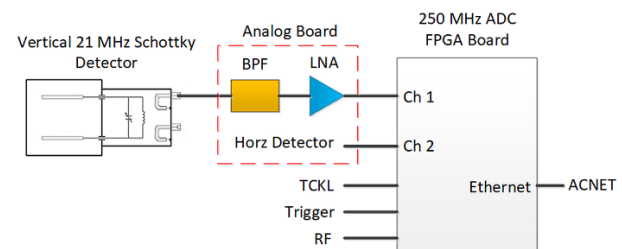


Figure 4: Mu2E tune meter system.

* This work was supported by the U.S. Department of Energy under contract No. DE-AC02-07CH11359.

[†] Scarpine@fnal.gov

EFFECT OF LONGITUDINAL BEAM-COUPLING IMPEDANCE ON THE SCHOTTKY SPECTRUM OF BUNCHED BEAMS

C. Lannoy^{1,*}, D. Alves, K. Lasocha, N. Mounet, CERN, Geneva, Switzerland
T. Pieloni, EPFL, Lausanne, Switzerland
¹also at EPFL, Lausanne, Switzerland

Abstract

Schottky spectra can be strongly affected by collective effects, in particular those arising from beam-coupling impedance when a large number of bunch charges are involved. In such conditions, the direct interpretation of the measured spectra becomes difficult, which prevents the extraction of beam and machine parameters in the same way as is usually done for lower bunch charges. Since no theory is yet directly applicable to predict the impact of impedance on such spectra, we use here time-domain, macro-particle simulations and apply a semi-analytical method to compute the Schottky spectrum for various machine and beam conditions, such as the ones found at the Large Hadron Collider. A simple longitudinal resonator-like impedance model is introduced in the simulations and its effect studied in different configurations, allowing preliminary interpretations of the impact of longitudinal impedance on Schottky spectra.

INTRODUCTION

Theoretical reconstructions of Schottky spectra, such as the matrix formalism proposed in [1, 2], or the Monte Carlo approach used in [3, 4], are based on the assumption that the synchrotron frequency distribution is known. Under certain conditions, one can derive an analytical relation between the amplitude of the synchrotron oscillation and its frequency (see below) allowing these methods to reconstruct the Schottky spectrum from the synchrotron amplitude distribution. However, this relation has to be modified when external forces, such as the one coming from beam-coupling impedance, affect the longitudinal dynamics.

This study will briefly present the available theory relating the amplitude of the synchrotron oscillation to its frequency, as well as a commonly adopted approximation. The second section will deal with the additional external forces coming from impedance, extending the theory presented in [5] to the case of a non-linear radio frequency (RF) bucket. Finally, we will apply the developed theory to the particular case of a longitudinal broad-band resonator, and will benchmark it against macro-particle simulations performed with PyHEADTAIL [4, 6, 7], in the case of a proton bunch in the Large Hadron Collider (LHC).

Synchrotron Oscillation

For an impedance-free environment, the equation of motion for the RF phase ϕ ¹ of a given particle is [8, Eq. (9.51)]:

$$\frac{d^2\phi}{dt^2} + \Omega_0^2 \sin \phi = 0, \quad (1)$$

assuming that the synchronous phase ϕ_s is such that $\sin \phi_s$ is small enough to be neglected (i.e. no acceleration or energy loss compensation). The nominal synchrotron frequency² reads

$$\Omega_0^2 = \omega_0^2 \frac{-\eta h e \hat{V}}{2\pi E_0 \beta^2} \cos \phi_s, \quad (2)$$

where e is the elementary charge, and where the relevant machine parameters are: the revolution frequency ω_0 , the slippage factor η , the amplitude of the RF voltage \hat{V} , the rf harmonic number h , the relativistic factor β , and the reference energy E_0 . Note that by convention η is positive above transition, such that η and $\cos \phi_s$ always have opposite sign.

Equation (1) is similar to the non-linear pendulum equation, hence the synchrotron frequency Ω_s of the particle can be written [9]

$$\Omega_s(\hat{\phi}) = \frac{\pi}{2\mathcal{K}\left[\sin\left(\frac{\hat{\phi}}{2}\right)\right]} \Omega_0, \quad (3)$$

where $\hat{\phi}$ is the RF phase amplitude of the synchrotron oscillation and \mathcal{K} is the complete elliptic integral of the first kind [10, Eq. (8.112.1)].

Equation (1) can also be approximated by replacing the sine function with its Maclaurin series expansion up to the third order, which yields

$$\frac{d^2\phi}{dt^2} + \Omega_0^2 \left(\phi - \frac{\phi^3}{6}\right) + \mathcal{O}(\phi^5) = 0. \quad (4)$$

This last equation has been studied in [9], and an approximation of the oscillation frequency is given by

$$\Omega_s(\hat{\phi}) = \Omega_0 \left(1 - \frac{\hat{\phi}^2}{16}\right). \quad (5)$$

Figure 1 illustrates how the exact solution from Eq. (3) compares with the approximation from Eq. (5). The amplitude distribution corresponding to a Gaussian bunch profile of standard deviation $\sigma = 31$ ns is also shown in order to compare the most populated region with the zone where the

¹ Above transition ϕ has to be taken as the difference between the RF phase of the particle and π .

² By nominal synchrotron frequency, we mean the limit of the synchrotron frequency for synchrotron amplitudes approaching zero.

* christophe.lannoy@cern.ch

STATISTICAL PROPERTIES OF SCHOTTKY SPECTRA

C. Lannoy^{1,*}, D. Alves, K. Lasocha, N. Mounet, CERN, Geneva, Switzerland
T. Pieloni, EPFL, Lausanne, Switzerland
¹also at EPFL, Lausanne, Switzerland

Abstract

Schottky signals are used for non-invasive beam diagnostics as they contain information on various beam and machine parameters. The instantaneous Schottky signal is, however, only a single realisation of a random process, implicitly depending on the discrete distribution of synchrotron and betatron amplitudes and phases among the particles. To estimate the expected value of the Schottky power spectrum, and reveal the inner structure of the Bessel satellites described by the theory, the averaging of instantaneous Schottky spectra is required. This study describes this procedure quantitatively by analysing the statistical properties of the Schottky signals, including the expected value and variance of Schottky power spectra. Furthermore, we investigate how these quantities evolve with the number of particles in the bunch, the observed harmonic of the revolution frequency, the distribution of synchrotron oscillation amplitudes, and the bunch profile. The theoretical findings are compared against macro-particle simulations as well as Monte Carlo computations.

INTRODUCTION

The Large Hadron Collider (LHC) Schottky system provides a single spectrum every second, based on the signal acquired over approximately the last 16 000 revolutions. Notably, consecutive spectra exhibit significant dissimilarity, requiring the aggregation of numerous spectra to attain the mean value. This study aims at exploring the inherent variability of consecutive instantaneous Schottky spectra and at characterising their statistical properties.

The LHC Schottky monitors measure the power spectral density (PSD) of a signal (intensity for the longitudinal spectrum, or dipole moment for the transverse one). For a random process $X(t)$, the PSD is defined in general by [1, Eq. (10.9)]

$$P(\omega) = \lim_{T \rightarrow \infty} \frac{1}{2T} |X_T(\omega)|^2, \quad (1)$$

where $X_T(\omega)$ is the Fourier transform of the truncated process

$$X_T(\omega) = \int_{-T}^T X(t) e^{-j\omega t} dt.$$

In these proceeding we will first investigate the statistical properties of the longitudinal spectrum, before elaborating on the transverse one. Then we will compare our results with simulations and the available measurements, and finally present our conclusions.

* christophe.lannoy@cern.ch

LONGITUDINAL SCHOTTKY SPECTRA

As shown in the literature [2–5], the intensity signal $i(t)$ of a bunch consisting of N particles can be written

$$i(t) = qf_0 \sum_{i=1}^N \sum_{n,p=-\infty}^{\infty} J_p(n\omega_0 \widehat{\tau}_i) e^{j(n\omega_0 t + p\Omega_{s_i} t + p\varphi_{s_i})}, \quad (2)$$

where J_p is the Bessel function of the first kind of order p , q the charge of the particle, $f_0 = \omega_0/2\pi$ the revolution frequency, and $\widehat{\tau}_i$, Ω_{s_i} , and φ_{s_i} , respectively, the synchrotron time amplitude¹, frequency, and initial phase of particle i . The summations over n and p are related to the revolution frequency harmonic and the Bessel satellite number p .

Equation (2) is a deterministic signal entirely defined by a set of N amplitudes $\widehat{\tau}_i$ and N phases φ_{s_i} (the synchrotron frequencies Ω_{s_i} can be determined from the synchrotron amplitudes as in [6, 7]). To examine the statistical properties of the Schottky spectra, we define the corresponding random process $I(t)$ of the intensity signal $i(t)$

$$I(t) = qf_0 \sum_{i,n,p} J_p(n\omega_0 \widehat{T}_i) e^{j(n\omega_0 t + p\Omega_{s_i} t + p\Phi_{s_i})}, \quad (3)$$

where the summation bounds have been omitted for readability. The random variables \widehat{T}_i and Φ_{s_i} describe respectively, the synchrotron time amplitude and initial phase for particle i . Equation (2) can be seen as one realisation of the random process defined by Eq. (3).

In the following, Φ_{s_i} is assumed to follow a uniform distribution on $[0, 2\pi]$, while \widehat{T}_i is described by various probability density functions $g(\widehat{\tau})$, such as the Rice distribution as in [7]

$$g(\widehat{\tau}) = \frac{\widehat{\tau}}{\sigma^2} e^{-\frac{\widehat{\tau}^2}{2\sigma^2} - \frac{b^2}{2}} I_0(\widehat{\tau}b/\sigma),$$

or a distribution corresponding to a Gaussian bunch profile

$$g(\widehat{\tau}) = \frac{\widehat{\tau}}{\sigma^2} e^{-\frac{\widehat{\tau}^2}{2\sigma^2}},$$

in order to assess the impact of different bunch profiles.

Applying the PSD definition from Eq. (1) to Eq. (3) yields [8]

$$P(\omega) = q^2 f_0^2 \sum_{\substack{i,n,p \\ i',p'}} J_p(n\omega_0 \widehat{T}_i) J_{p'}(n\omega_0 \widehat{T}_{i'}) e^{j(p\Phi_{s_i} - p'\Phi_{s_{i'}})} \\ \times 2\pi \delta(n\omega_0 + p\Omega_{s_i} - \omega) \delta_K(p\Omega_{s_i} - p'\Omega_{s_{i'}}), \quad (4)$$

¹ By time amplitude, we mean the maximum time arrival difference between a given particle and the synchronous particle

STUDY OF NON-DESTRUCTIVE BPM-BASED ENERGY MEASUREMENT OF THE CANADIAN LIGHT SOURCE LINAC

H. Shaker*, D. Bertwistle, E.J. Ericson¹, Y. Sigari¹, E. Soltan²
 Canadian Light Source, Saskatoon, Canada

¹also at the University of Saskatchewan, Department of Physics and Engineering Physics

²also at the University of Saskatchewan, Department of Computer Science

Abstract

There is a plan in the Canadian Light Source (CLS) to replace the current Linac with a new one from Research Instruments GmbH in mid-2024. The first straight section of LTB (Linac-To-Booster) was upgraded to have two BPMs (Beam Position Monitors) with a 4.75 m drift between them and two phosphor screens were replaced by YAG screens. A new BPM and a YAG-based screen station upgraded the following 90-degree achromat beamline. These upgrades help us to measure the current and future Linac beam parameters, including the beam twiss parameters, energy, and energy spread. In this paper, we discussed how we could use these three BPMs for non-destructive energy measurement, which will be a part of the active energy correction system.

INTRODUCTION

Canadian Light Source's current electron linear accelerator will be replaced with a new one by Research Instruments GmbH in mid-2024 [1, 2]. As part of the project, the beam diagnostic systems in the LTB were upgraded. Figure 1 shows the layout of LTB and where the current diagnostic components were upgraded or new components added. A new BPM, BPM2, added by pairing with the BPM1, measures the transversal position and momentum of the electron beam in the BPM2 location. There is a long drift between these two BPMs and one Steerer (ST0003-05), just 26.22 cm before that, and its effect is negligible compared to a pure drift as calculated. VSC0003-01 and VSC0003-03 phosphor screens were replaced by one inch round YAG screens, and the camera was upgraded to a digital one. This helps us to measure twiss parameters. Also, they can be used to calibrate BPMs. A new VSC0003-06 screen was installed in the achromat beamline to measure energy and energy spread destructively and be used as a reference to calibrate the BPM3. An online non-destructive method for the energy measurement is required for the energy monitoring by operators and potentially to use in an active energy correction system, which uses a script which implement a negative feedback system to change the phase of the Linac accelerating section to keep the energy constant. For this purpose, a new BPM, SLM0003-03 (BPM3), was installed in the achromat beamline just before the new screen station and after the slit. The slit will be upgraded, as part of the project, for the beam profile scanning and energy filtering. When we combine these three BPMs together, as we suggest, we can

measure the energy non-destructively. The first two are to measure the transverse position and momentum of the beam just before entering the achromat beamline in the location of the BPM2. Then, using the transfer matrix between the BPM2 and the BPM3 and the location of the beam read by the BPM3, we can find the energy of the electron beam.

TRANSFER MATRIX & NORMALIZED X

The position of the beam at BPM3, SLM0003-03, is a function of the beam energy and the beam position and momentum at the BPM2 location. Here we defined a new parameter, normalized horizontal position, or normalized x , which is just a function of energy. To calculate that, we should know the transversal position and momentum of the beam in the BPM2 location. We can measure x_1 and x_2 and Eq. (1) shows how we can calculate x'_2 by knowing the drift length between them, which is 4.7518 m.

$$\begin{Bmatrix} x_2 \\ x'_2 \end{Bmatrix} = \begin{Bmatrix} 1 & D \\ 0 & 1 \end{Bmatrix} \begin{Bmatrix} x_1 \\ x'_1 \end{Bmatrix} \Rightarrow x'_2 = (x_2 - x_1)/D \quad (1)$$

Equation (2) shows the position and momentum at the BPM3 location, knowing the transfer matrix and the position and momentum at the BPM2 location. We used a 3x3 transfer matrix which included the horizontal information and dispersion. Because of using linear elements, the vertical components are decoupled.

$$\begin{Bmatrix} x_3 \\ x'_3 \\ \Delta p/p \end{Bmatrix} = M \begin{Bmatrix} x_2 \\ x'_2 \\ \Delta p/p \end{Bmatrix} \quad (2)$$

Now we can define the normalized x which is equal to $\Delta p/p$ as you can see in Eq. (3) and it is a function of horizontal beam position in three BPMs, the drift length between BPM1 and BPM2 and the first row of the transfer matrix between the BPM2 and BPM3.

$$\begin{aligned} x_3 &= M_{11} * x_2 + M_{12} * x'_2 + M_{13} * \Delta p/p = \\ &M_{11} * x_2 + M_{12} * (x_2 - x_1)/D + M_{13} * \Delta p/p \Rightarrow \\ x_n &\equiv [x_3 - M_{11} * x_2 - M_{12} * (x_2 - x_1)/D] / M_{13} = \Delta p/p \end{aligned} \quad (3)$$

The BPM2 to BPM3 transfer matrix can be calculated by knowing the elements between two BPMs.

$$M = M_{D4} * M_{QF2} * M_{D3} * M_B * M_{D2} * M_{QF1} * M_{D1} \quad (4)$$

* hamed.shaker@lightsources.ca

IMPLEMENTATION OF TRANSIMPEDANCE ANALOG FRONT – END CARD FOR LOS ALAMOS NEUTRON SCIENCE CENTER ACCELERATOR WIRE SCANNERS *

D. Rai†, H. Leffler, S.A. Baily, D. Zimmermann, L. Montoya, L. Kennel, D. Martinez, J. Duran, A. Braidó
Los Alamos National Laboratory, Los Alamos, NM, USA

Abstract

The Los Alamos Neutron Science Center’s (LANSCe) Accelerator Operations and Technology division - Instrumentation and Controls (AOT-IC) team executed a project that implemented a new Analog Front-End (AFE) card for their wire scanner’s Data Acquisition (DAQ) system. The AFE accommodates the signal amplification and noise reduction needed to acquire essential measurement data required for beam diagnostics for LANSCe accelerator. Wire Scanners are electro-mechanical beam interceptive devices that provide cross-sectional beam profile measurement data fitted to a Gaussian distribution that is then extrapolated to provide beam shape and position. The beam shape and position information allow the operator to adjust parameters such as acceleration, steering, and focus to provide optimized beam delivery to targets. The project included software and hardware implementation that eliminated the dependency on legacy systems and consolidated various AFE designs for diagnostics systems into a single design with 11 gain settings ranging from 100 nA to 40 mA at 10 V full scale to accommodate its future applications on other diagnostics systems.

BACKGROUND

The LANSCe facility utilizes various beam diagnostics devices for operators to adjust beam parameters such as acceleration, steering, and focus to provide efficient and effective beams to all five experimental areas. Wire scanners are interceptive beam diagnostics devices with a mechanical actuator assembly and a single or pair of Silicon Carbide (SiC) or Tungsten (W) wires (sensor) mounted vertically and/or horizontally to the sensor fork mount as shown in Fig. 1.

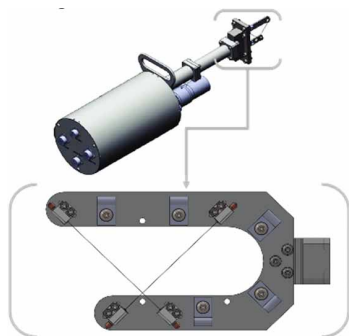


Figure 1: Wire Scanner and Sensor Fork Assembly.

* This work was supported by the U.S. Department of Energy through the Los Alamos National Laboratory. Los Alamos National Laboratory is operated by Triad National Security, LLC, for the National Nuclear Security Administration of U.S. Department of Energy (Contract No. 89233218CNA000001). † drai@lanl.gov, LA-UR-23-30149

When the beam impinges on the wires, current resulting from the emitted secondary emission yield is deposited on the wire; this current is proportional to the beam current [1]. Since the wire’s position is scanned in the beam pipe, the wire scanner provides the transverse vertical and horizontal profile measurements with a Gaussian fit, as shown in Fig. 2.

The data from the wire scanner is obtained by hardware and software implementation of the QAC (Quad Actuator Controller) DAQ, National Instruments – CompactRIO (cRIO) Systems. The QAC DAQ cRIO system controls movement and acquires data. The user interface JAVA program analyzes and displays the result of the received scan data [2]. The AFE card is the component of the DAQ that acquires beam-impinged secondary electron current flow from the wires. The AFE is a compact Peripheral Component Interconnect (cPCI) form factor card supporting 16 channels, assuming one channel for each axis, supporting eight wire scanners per card.

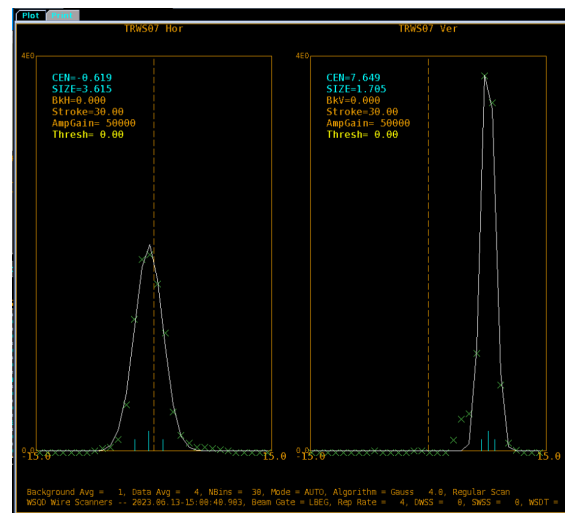


Figure 2: LBEG (Long Bunch Enabled Gate) Beam scan of TRWS07 Wire Scanners.

During the implementation of the QACDAQ system for wire scanner systems in the transition region and downstream areas, the LANSCe Harp AFE was used. The LANSCe Harp AFE full scale range is from 3 μ A to 270 μ A and was not sensitive enough for typical Wire scanner application [3]. As shown in Table 1, LBEG is a higher current beam with 50 times greater macro pulse average current and 100 times greater charge per pulse than MPEG (Micro Pulse Enabled Gate) [4]. Therefore, the LANSCe Harp AFE was adequate in performing wire scanner scans of the LBEG beam but not for MPEG.

Content from this work may be used under the terms of the CC-BY-4.0 licence (© 2023). Any distribution of this work must maintain attribution to the author(s), title of the work, publisher, and DOI

UPGRADE OF THE ELBE TIMING SYSTEM

M. Kuntzsch, A. Schwarz, K. Zenker, M. Justus
Helmholtz-Zentrum Dresden-Rossendorf, Dresden, Germany
Z. Oven, L. Perusko, L. Krmpotic, U. Legat, U. Rojec, Cosylab, Ljubljana, Slovenia

Abstract

The ELBE center for high power radiation sources is operating an electron linear accelerator to generate various secondary radiation like neutrons, positrons, intense THz and IR pulses and Bremsstrahlung. The legacy timing system has been modified and extend over the past two decades to enable new experiments. Part of this system is using obsolete parts which makes the maintenance more complex and the heterogenous structure requires a major revision of the timing signal generation and distribution at ELBE.

A new timing system based on the Micro Research Finland hardware platform is being adapted to be used at ELBE. It will enable parallel operation of two electron sources and subsequent kickers to serve multiple end stations at a time. The hardware enables low jitter emission of timing patterns and a long term drift compensation of the distribution network. In spring 2023 the development of the software has been accomplished, which included the mapping of operation modes and different complex beam patterns onto the capabilities of the commercial MRF platform. The system generates complex beam patterns from single pulse, to macro pulse and 26 MHz continuous wave (CW) operation, including special triggers for diagnostics and machine subsystems.

REQUIREMENTS

The requirements for the new timing system have been derived mainly from the features of the old timing system and feature requests from the ELBE user community. Timing signal receivers as well as operators expect a particular composition of different signals, that have to be delivered by the new timing system.

Even though ELBE is a CW machine, a macro pulser is used to generate pulsed, low current beams. This mode is mainly used for beam tuning in order to allow a safe operation of destructive diagnostics like view screens. The macro pulser setting defines in turn also the timing for diagnostic triggers for the low level radio frequency (LLRF) controllers, cameras and loss monitors. If in operation, the macro pulser chops the beam into short bursts using magnetic steerer coils. The inductance of the coils combined with the capabilities of the driver unit define the rising and falling slope of the macro pulse train. At ELBE slew rates are on the 10 μ s scale and define the shortest opening time of 100 μ s. The minimal period is derived from the maximum camera sampling time of 10 ms. So, the period can be set to multiples of 10 ms up to many minutes period.

Biological experiments at ELBE require a very complex trigger pattern in order to adjust the applied dose and its structure to a sample with high accuracy. At the same time

the background radiation needs to be reduced which means to suppress dark current from the injector section.

For this application a dedicated single pulser system needs to be in place, which allows for patterns with single bunch resolution, periods up to minutes and a possibility to combine the gun pulse emission with a macro pulse gate to suppress dark current. These features are required for both thermionic injector and superconducting radiofrequency (SRF) gun that are available at ELBE.

Table 1 summarizes the main pulser modes of the timing system and their parameter range. In detail, the requirements are much more complex, the edge cases and error handling makes the implementation a complex development. The complete specification has been written into a design documents which serves as a reference for the implementation process.

Table 1: Main Pulser Modes and Their Parameter Ranges

	Unit	Min	Max
Electron Bunch Rate	Hz	0.03	26e6
Macro Pulser Period	s	10e-3	33864
Macro Pulser Duty Cycle	s	100e-6	33864
Single Pulser Period	s	115.5e-9	33864
Single Pulser Duration	s	38.5e-9	33864

SYSTEM DESCRIPTION

Hardware

For the implementation at ELBE different systems have been evaluated and after a comprehensive feasibility study a European Tender has been awarded to COSYLAB to set up the new ELBE timing system. As hardware platform the Micro Research Finland Oy (MRF) timing modules have been selected [1].

The latest revision of the MRF hardware is available for MicroTCA standard, which is becoming more and more popular in accelerator community and found its application for new beam diagnostic systems and LLRF systems at ELBE.

The system consists of event master modules (EVM) that are generating and send a continuous stream of events which are received by event receiver modules (EVR). EVRs are located in different sections around the accelerator and generate physical trigger signals based on the event stream. EVMs and EVRs are connected over optical fibers, forming a hierarchic structure which allows for a high flexibility and the possibility to extend the system with ease.

Each EVR has four fixed TTL outputs on the front panel and provides two slots for universal IO modules, each housing two physical outputs. There are universal IO modules for different logic levels, electrical and optical outputs

PROGRESS ON DISTRIBUTED IMAGE ANALYSIS FROM DIGITAL CAMERAS AT ELSA USING THE RABBITMQ MESSAGE BROKER

M. Switka*, K. Desch, T. Gereons, S. Kronenberg, D. Proft, A. Spreitzer
 Physikalisches Institut, University of Bonn, Germany

Abstract

In the course of modernization of camera based imaging and image analysis for accelerator hardware and beam control at the ELSA facility, a distributed image processing approach was implemented, called FGrabbit. We utilize the RabbitMQ message broker to share the high data throughput from image acquisition, processing, analysis (e.g. profile fit), display and storage between different work stations to achieve an optimum efficacy of the involved hardware. Re-calibration of already deployed beam profile monitors using machine vision algorithms allow us to perform qualitative beam photometry measurements to obtain beam sizes and dynamics with good precision. We describe the robustness of the calibration, image acquisition and processing and present the architecture and applications, such as the programming- and web-interface for machine operators and developers.

INTRODUCTION

The ELSA facility [1] deploys around 50 optical beam monitors based on luminescence screens (Chromox or OTR) and synchrotron radiation. The previous installation of cameras with analogue video signal output provided mediocre beam analysis capability due to limited signal quality and the lack of comprehensive camera control. To obtain qualitative beam data from photometry we modernize hardware and software of the optical monitors, primarily utilizing Ethernet-capable digital cameras controlled with non-commercial camera drivers and open source machine vision libraries for image calibration. The FGrabbit framework was created [2] to provide resource-optimized camera control, data handling and computing power based on the RabbitMQ message broker for distributed analysis. A Gigabit Ethernet (GigE) network between PoE-capable switches links processing computers and image generating devices, such as GenIcam [3] compatible digital cameras, other digitizers or image generating programs. A graphical user interface allows access to the FGrabbit framework from the accelerator control system or the facility website and provides comprehensive device and image control.

ARCHITECTURE

The architecture of the FGrabbit framework is depicted in Fig. 1. All peripheral devices (cameras, computers) participating in the FGrabbit framework communicate through a GigE network, separated from the ELSA control system, but accessible through a gateway computer. As camera control and readout can be achieved through various

drivers. We favor the Aravis [4] driver in combination with GenICam [3] compatible digital cameras. Streams from other drivers (e.g. Video4linux¹), VNC² servers or image generating programs may also be used as input for the FGrabbit framework. Comprehensive image calibration can be applied via the OpenCV computer vision library [5] to account for beam profile distortions resulting from tilted screens (extrinsic properties) or lens imperfections of the imaging system (intrinsic properties). Calibrated images are typically cropped to a useful area of interest (AOI) and ideally visualize an undistorted transverse cross section of an observed beam with correct pixel to millimeter scaling. The calibrated images are typically reduced in size, allowing to economically stream images from multiple cameras through the GigE network. The data load from imaging and image analysis is handled by the RabbitMQ message broker. Computing power (e.g. for computational expensive 2D profile fits) is distributed to multiple standard computers within the network. A QT-based [6] graphical user interface

¹ <https://www.kernel.org/doc/html/v4.8/media/v4l-drivers/>

² virtual network computing

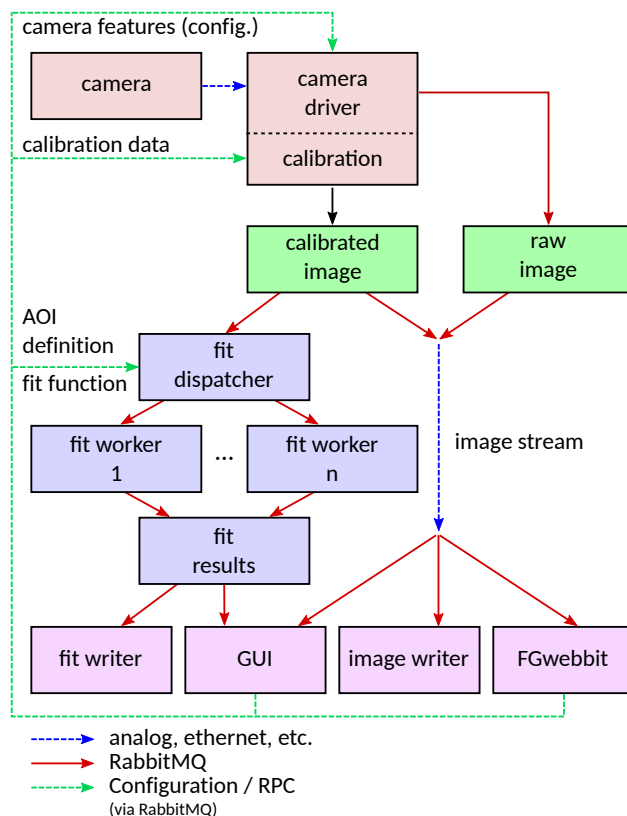


Figure 1: Architecture of the FGrabbit framework.

* switka@physik.uni-bonn.de

LCLS-II TIMING SYSTEM AND SYNCHRONOUS BUNCH DATA ACQUISITION*

C.B. Mattison, K. Kim, P. Krejcik, M. Weaver, M. Zelazny
SLAC National Laboratory, CA USA

Abstract

The new timing system for the LCLS-II SC linac and FEL meets the challenging requirements for delivering multiple interleaved timing patterns to several different destinations at rates up to 1 MHz. The timing patterns also carry information on bunch charge and beam energy to prevent inadvertent selection of beam dumps beyond their rated beam power. Beamline instruments are equipped with a timing receiver that performs bunch-by-bunch synchronous data acquisition based on the timing pattern for that location. Data is buffered in on-board memory for up to 10^6 machine pulses (1 s at 1 MHz). The large data volume can be locally processed and analysed before transmission to clients on the network. Commissioning and experience with the new system will be presented

INTRODUCTION

The LCLS-II Timing System developed at SLAC is the first timing system able to provide programmable timing patterns with variable rates from 1 Hz to 1 MHz with interleaved bunches to multiple destinations. The LCLS-II Timing System provides the triggers for the timing receivers along the 4 km beamline that are used to trigger hardware pulsed devices (kickers, Klystrons) and diagnostic devices (BPMS, cameras, wire scanners etc) as well as providing soft triggers for the data acquisition.

The LCLS-I and LCLS-II timing systems are physically decoupled: two separate dedicated fiber networks. The Timing pattern is generated upstream in the LINAC with a Timing Pattern Generator (TPG) and is then distributed to the Timing Pattern Receivers (TPR) at the device level. In shared areas, between LCLS-I and LCLS-II, the TPRs are capable to select the timing source to trigger on.

The SLAC accelerator complex provides multiple sources and destinations options to the machine operators.

The complexity of programming the LCLS-II timing pattern is ultimately resolved in the Timing Pattern Generator Graphical User Interface (TPGGUI). The LCLS-II project is currently under commissioning and it is the scope of this paper to describe the components that made the LCLS-II Timing System successful as well as discuss the commissioning experience with this new cutting-edge system.

TIMING PATTERN GENERATOR

The LCLS-II Timing System is composed of the master source, phase reference distribution, timing pattern generator, and timing pattern receiver units.

* Work supported by the U.S. Department of Energy under contract number DE-AC02-76SF00515.

The LCLS-II master source generates the 1300 MHz and 185.7 MHz (1300 MHz/7) phase reference signals with small jitters, phase locked together. The transmission of the 1300 MHz phase reference to LLRF has tight requirements on the stability and jitter of the timing signal over a large distance.

The LCLS-II Requirements parameters are listed in Table 1 below:

Table 1: LCLS-II Timing System Parameters

Timing Attribute	Value
Phase Reference (Linac RF)	1300 MHz
Clock (Gun RF = Linac RF/7)	185.71 MHz
Nominal Beam Rate (Clock/200)	0.92857 MHz
Fiducial Resync Freq (Clock/2600)	0.07143 MHz
Fiducial (Power Line Phase)	360 Hz
Stability - Standard (fiber)	0.4 ns
Stability - Phase reference line (PRL)	1 fs/sec, 1 ps/day
Jitter - Standard (fiber)	30 ps
Jitter - PRL (50 Hz to 5 kHz)	0.005° or 10.7 fs

The Timing Pattern Generator (TPG) runs on an FPGA in an ATCA crate. The TPG publishes the timing pattern over a dedicated fiber network. A timing pattern is a collection of timing frames and contains unique information about a beam pulse (Table 2). The timing frame is time stamped by the TPG and tagged with a unique pulse ID for post-data acquisition processing, allowing cross-correlation of signals between multiple devices.

The timing pattern frame in Fig. 1 shows how the timing pattern frame is encapsulated within control characters that allow additional data streams to be serialized onto the link. This configuration allows control transmissions of differing domains that firmware outside of that domain are not required to parse. The entire 1 MHz frame is validated by 32-bit CRC calculation [1].

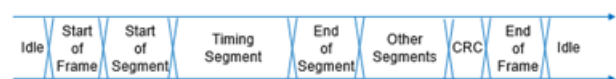


Figure 1: Timing pattern frame (visual).

The timing frame is manipulated by the firmware and software. The software, hosted on the EPICS control system, can send information to the firmware by programming the sequence engines, which can then update the pulse timing frame content providing useful information such as the beam destination.

NOVEL CAVITY BPM ELECTRONICS FOR SHINE BASED ON RF DIRECT SAMPLING AND PROCESSING*

L.W. Lai†, R. Meng, Y.M. Zhou, S.S. Cao, J. Chen, X.Q. Liu
SSRF, Shanghai Advanced Research Institute, Chinese Academy of Sciences,
Shanghai, China

Abstract

A RF direct sampling beam signal processor has been developed in SSRF. It mainly consists of four channels RF direct sampling ADCs and a SoC FPGA. The ADC is 9 GHz bandwidth and 2.6 GHz sampling rate. A prototype of RF module contains band pass filter, low noise amplifier and step attenuator has been designed for SHINE cavity BPM system. Then a novel cavity BPM electronic including the processor and the RF module has been built for SHINE. The performance of the electronic has been analyzed and evaluated in lab. The amplitude relative error is 2.0×10^{-4} which is better than the required 1×10^{-3} on cavity BPM system. The phase error is 14 fs, also better than the requirement of RF BAM system. The algorithm and implementation in FPGA have been introduced.

INTRODUCTION

Shanghai High repetition rate XFEL and Extreme light facility (SHINE) is a 3 km long hard X-ray FEL facility built 30 m underground in Shanghai. The designed beam repetition rate is 1 MHz. The project was initiated at the end of 2018, and to be completed at 2027. The SHINE was built adjacent to the campus of Shanghai Synchrotron Radiation Facility (SSRF) and Shanghai Soft X-ray FEL (SXFEL). Three types of BPMs are used in different sections: stripline BPMs are used in injector and sections between cryomodules, cold button BPMs are installed inside the cryomodules of the super conducting LINAC, and cavity BPMs are used in beam distribution lines and FEL sections.

Two types of cavity BPMs are designed for SHINE. A $\Phi 35$ mm cavity BPM is designed for the distribution lines, which center frequency is 3520.87 MHz, and the required resolution $1 \mu\text{m}$ at 100 pC, and the dynamic range is ± 1 mm. While a $\Phi 8$ mm cavity BPM is designed for the FEL sections, which center frequency is 5254.2 MHz, and the required resolution 200 nm at 100 pC, and the dynamic range is $\pm 100 \mu\text{m}$. It means the relative resolution of the cavity BPM electronics should be better than 0.1%.

The cavity BPM generates signals with different modes when electron beam passing through. The amplitude of TM_{010} mode signal is proportional to beam charge, and the TM_{110} mode signal is proportional to both beam charge and beam position. The signals are narrow bandwidth at high

frequency with high Signal to Noise Ratio (SNR), normally at several GHz.

BPM electronics use independent RF front-end modules and digital signal processors. Different RF front-end modules will be designed to meet the signal characteristics requirements of different BPM types. A generic beam signal processor platform has been developed for beam diagnostic system. Three types of electronic structures can be used to process the high frequency cavity BPM signal. First is the heterodyne, it down converts the signal to intermediate frequency (always at tens of MHz) for digitizing. It is proven trusted and high performance, and widely used, like LCLS I, LCLS-II, SXFEL, *et al.* But it is complicated and large physical size. The long chain RF components, especially Local Oscillator (LO) synthesizer and mixing modules introduce extra noise, and fragile to environment temperature humidity. Second is direct sampling the high frequency signal with ADC. The hardware is the simplest, most flexible, it is practical at L, S, C band right now. Because of the limitation of ADC bandwidth and effective number of bits, no large-scale application now exists. Third is direct-convert the signal to base band, or we say zero intermediate frequency in two quadrature channels. This structure lowers the requirement to low-pass filters and ADCs, simplifies the digital signal processing. European XFEL made excellent work with this structure. The challenges of this structure including I/Q balance, local oscillator leakage, the interference from low frequency noise, also need one more ADC.

In SXFEL, the cavity BPM signal is down converted from about 4680 MHz to 30 MHz, and then digitized and processed with a self-developed signal processor (DBPM) [1]. The DBPM in a one stand-alone processor with a FPGA carrier board, an ADCs board and an ARM board. The ADC board has four input channels, the maximum sampling rate is 125 MHz, resolution is 16 bits, and bandwidth is 650 MHz. The ADC running at 119 MHz external clock synchronizing to RF. A XILINX Virtex5 FPGA is used as the core component on the carrier board. Except for the DBPM, a RF front-end is installed besides the pickup in tunnel, a LO synthesizer and a down-conversion module are installed in the cabinet of electronic hall with DBPM. Obviously, the install space is quite large and cost is high.

In SHINE, the cavity BPM electronic cabinets are near the pickups in tunnel. The RF module integrates RF front-end module, LO synthesizer, and down conversion module into a 1U chassis. The signal is down-converted to 54 MHz, then sampled and processed with a generic beam diagnostic processor. The processor is stand-alone 1U height, including a XILINX Soc FPGA carrier board, a high-speed

*Work supported by The National Science Foundation of China (Grant No.12175293), Youth Innovation Promotion Association, CAS (Grant No. 2019290)

†Corresponding author: lailw@sari.ac.cn

ANALYSIS OF THE TRANSVERSE SCHOTTKY SIGNALS IN THE LHC

K. Lasocha*, D. Alves, CERN, Geneva, Switzerland

Abstract

Schottky-based diagnostics are remarkably useful tools for the non-invasive monitoring of hadron beam and machine characteristics such as the betatron tune and the chromaticity. In this contribution recent developments in the analysis of the transverse Schottky signals measured at the Large Hadron Collider will be reported. A fitting-based technique, where the measured spectra are iteratively compared with theoretical predictions, will be presented and benchmarked with respect to the previously known methods and alternative diagnostic.

INTRODUCTION

Schottky signals are the fluctuations of macroscopic beam characteristics, such as intensity or dipole moment, due to the discrete nature of the particle ensemble. They were first measured at the CERN's Intersecting Storage Ring in the early 1970s [1] and immediately used to provide information on momentum spread and betatron tune, as well as the rate of growth of betatron amplitudes at tune values close to resonant lines. Notably, it was the observation of Schottky signals what convinced Simon van der Meer to pursue the implementation of his eminent concept of stochastic cooling [2].

Since then, the Schottky signal analysis has become a standard diagnostic technique for both coasting and bunched hadron beams, used among others in Tevatron [3], RHIC [4], SIS18 [5], CSR [6], ELENA [7] and LHC [8]. The basic theory of Schottky signals of coasting beams [9] has been enriched by studies on the Schottky spectrum deformation due to space charge, impedance and collective effects present in dense cooled beams [10, 11].

The case of Schottky signals of bunched beams is much less understood. The theory describing such signals is more complex, as it also has to take into account the particles' synchrotron motion. Some main principles can be found in Refs. [12, 13], as well as the effect of space-charge [14], but the knowledge on the impact of impedance, octupole magnets or beam-beam effects on Schottky spectra is so far very limited.

In addition, bunching introduces a finite degree of correlation in the motion of individual particles. In steady-state conditions, thanks to the filamentation associated with the betatron and synchrotron motion of particles, this correlation (also known as coherent motion) has a limited impact on the observed Schottky spectrum. Nevertheless, in certain conditions coherent effects are not negligible, yet very difficult to describe quantitatively.

* kacper.lasocha@cern.ch

In this contribution we shall recall the theory of the transverse Schottky spectra of bunched beams. Using experimental Schottky spectra measured during the ongoing LHC Run3 (2022-2026), we will address the issues of how and when the theory can be used to derive parameters such as the betatron tune and chromaticity. We shall also apply a fitting-based technique, proposed in [15, 16], which can be used to derive transverse beam characteristics from the spectrum, even in the presence of coherent components.

THEORY

Let us consider first the Power Spectral Density (PSD) of a transverse Schottky signal originating from a single particle. Around every harmonic h of the revolution frequency ω_0 , the PSD consists of two bands, described by the following expression

$$P_T^\pm(\omega, \hat{\tau}, \Omega_{s_0}, Q, Q_\xi) = \hat{a} \sum_{p=-\infty}^{\infty} J_p^2 \left(\chi_{\hat{\tau}, h \mp Q_I}^\pm \right) \delta[\omega - (h \pm Q_F) \omega_0 - p \Omega_s(\hat{\tau})], \quad (1)$$

where Q_I and Q_F denote respectively the integer and fractional part of the betatron tune Q , Q_ξ is the chromaticity, $\hat{\tau}$ is the time amplitude of synchrotron motion, $\Omega_s(\hat{\tau})$ is the amplitude-dependent synchrotron frequency and \hat{a} is a constant proportional to the squared amplitude of the betatron motion at the pick-up location. The argument of the Bessel function is given by

$$\chi_{\hat{\tau}, n}^\pm = \left(n \hat{\tau}_i \pm \frac{\hat{Q}_i}{\Omega_{s_i}} \right) \omega_0 = (n \eta \pm Q_\xi) \frac{\omega_0 \hat{p}}{\Omega_{s_i} p_0}, \quad (2)$$

with η denoting the slip factor and \hat{p} the amplitude of momentum oscillations around the nominal value p_0 . We assume that particles perform harmonic synchrotron motion, with the synchrotron frequency given by the theory of the mathematical pendulum [17]:

$$\Omega_s = \frac{\pi}{2 \mathcal{K} \left[\sin \left(\frac{h_{RF} \omega_0 \hat{\tau}}{2} \right) \right]} \Omega_{s_0}, \quad (3)$$

where Ω_{s_0} is the nominal, limit synchrotron frequency, $h_{RF} \omega_0 \hat{\tau}$ is the the RF phase amplitude of synchrotron oscillations and $\mathcal{K}([0, 1]) \rightarrow [\pi/2, \infty]$ denotes the complete elliptic integral of the first kind [18, p. 590].

In the absence of coherent components which, in the case of the transverse Schottky spectrum is equivalent to having a uniform distribution of both betatron and synchrotron oscillation phases, the total multiparticle PSD is given simply